

# Crosslinkable low bandgap polymers for organic solar cells

Dissertation

zur Erlangung des akademischen Grades

Doktor der Naturwissenschaften (Dr. rer. nat.)

im Promotionsprogramm

Photophysik synthetischer und biologischer multichromophorer Systeme  
der Bayreuther Graduiertenschule für Mathematik und Naturwissenschaften

vorgelegt von

**Philipp Sebastian Knauer**

geboren in Coburg

Bayreuth 2016



Die vorliegende Arbeit wurde in der Zeit von April 2012 bis März 2016 am Lehrstuhl für Makromolekulare Chemie I der Universität Bayreuth unter der Betreuung von Prof. Dr. Peter Strohrigl angefertigt.

Vollständiger Abdruck der von der Bayreuther Graduiertenschule für Mathematik und Naturwissenschaften (BayNat) der Universität Bayreuth genehmigten Dissertation zur Erlangung des akademischen Grades eines Doktors der Naturwissenschaften (Dr. rer. nat.).

Datum der Einreichung:	24. März 2016
Zulassung durch das Leitungsgremium:	04. April 2016
Datum des wissenschaftlichen Kolloquiums:	22. Juli 2016

Amtierender Direktor der Graduiertenschule:	Prof. Dr. Stephan Kümmel
---	--------------------------

Prüfungsausschuss:

Prof. Dr. Peter Strohrigl	Erstgutachter
Prof. Dr. Anna Köhler	Zweitgutachterin
Prof. Dr. Georg Papastavrou	Vorsitzender
Prof. Dr. Carlo Unverzagt	



## Abbreviations

### Molecules and polymers

APFO	alternating polyfluorene
Ar	aromatic group
Bu	butyl group
C <sub>60</sub>	C <sub>60</sub> buckminster fullerene
CB	chlorobenzene
CuPc	copper phthalocyanine
Cy	cyclohexyl group
DCB	dichlorobenzene
DIO	1,8-diiodooctane
DMAc	dimethylacetamide
DMF	dimethylformamide
DMSO	dimethylsulfoxide
Et	ethyl group
ITO	indium tin oxide
L	ligand
MEH-CN-PPV	poly(2-methoxy-5-(2'-ethylhexyloxy)-1,4-(1-cyanovinylene phenylene)
MEH-PPV	poly(2-methoxy-5-(2'-ethylhexyloxy)-1,4-phenylene vinylene)
<i>n</i> -	linear alkyl chain
OAc	acetate group
ODT	1,8-octanedithiol
Otf	triflate group (CF <sub>3</sub> SO <sub>3</sub> R)
Ots	tosyl (CH <sub>3</sub> C <sub>6</sub> H <sub>4</sub> SO <sub>3</sub> R)
<i>p</i>	para
P3HT	poly(3-hexylthiophene)
PCBM	phenyl-C <sub>61</sub> -butyric acid methyl ester
PCDTBT	poly( <i>N</i> -9'-heptadecanyl-2,7-carbazole- <i>alt</i> -5,5-(4',7'-di-2-thienyl-2',1',3'-benzothiadiazole]
PDMS	poly(dimethylsiloxane)
PEDOT:PSS	poly(3,4-ethylenedioxythiophene) polystyrene sulfonate
PEN	poly(ethylene naphthalate)
PET	poly(ethylene terephthalate)
PFDTBT	poly(2,7-(9,9-dialkylfluorene)- <i>alt</i> -(5,5-(4',7'-di-2-thienyl-2',1',3'-benzothiadiazole)
Ph	phenyl group
PivOH	pivalic acid
PPV	poly( <i>p</i> -phenylenevinylene)
PV	perylene tetracarboxylic dianhydride
PVC	poly(vinylchloride)
<i>t</i>	tertiary
TFA	trifluoroacetic acid
THF	tetrahydrofuran

## Physical quantities and units

$\overline{M}_n$	number average molecular weight
$\overline{M}_w$	weight average molecular weight
°C	degree Celsius
μm	micrometer
a.u.	arbitrary units
$c$	concentration
cm <sup>-1</sup>	reciprocal centimeter
cm <sup>2</sup>	square centimeter
$D$	diffusion coefficient
D	polydispersity index
d	day
$E_g$	bandgap energy
$E_{opt}$	optical gap
EQE	external quantum efficiency
eV	electron volt
FF	fill factor
g	gram
GWh	gigawatt hour
h	hour
IPCE	incident photon-to-electron conversion efficiency
$J$	current density
J	joule
$J_{max}$	current density at maximum power
$J_{SC}$	short circuit current
K	Kelvin
$L_D$	exciton diffusion length
m	meter
mA	milliampere
mg	milligram
min	minute
ml	milliliter
mol	mole
mmol	mollimol
$N_0$	initial number of monomers
nm	nanometer
ns	nanosecond
$N_t$	number of monomers at a given time $t$
$P$	power
$p$	conversion
PCE	power conversion efficiency
PDI	polydispersity index
$P_{in}$	power of incident light
$P_{max}$	maximum power
$P_n$	number average degree of polymerization
ppm	parts per million
$R_S$	series resistance

$R_{SH}$	shunt resistance
$S_0$	singlet electronic ground state
$S_1$	first excited singlet state
$T$	temperature
$t$	time
$T_g$	glass transition temperature
V	volt
V	voltage
$V_{max}$	voltage at maximum power
$V_{OC}$	open circuit voltage
W	watt
wt%	weight percent
$\delta$	chemical shift
$\eta$	efficiency
$\lambda$	wavelength
$\nu$	frequency
$\tau$	exciton lifetime

### Constants

$c$	speed of light ( $299,792,458 \text{ ms}^{-1}$ )
$h$	Planck's constant ( $6.626 \times 10^{-34} \text{ Js}$ )
$q$	elementary charge ( $1.602 \times 10^{-19} \text{ C}$ )

### Miscellaneous

alt.	alternating
AM	air mass
aq	aqueous solution
BHJ	bulk heterojunction
BIPV	building integrated photovoltaics
BLA	bond length alternation
cat	catalytic
CROP	cationic ring-opening polymerization
d	doublet (NMR)
D-A	donor-acceptor
DSSC	dye-sensitized solar cell
e.g.	for example ( <i>exempli gratia</i> )
EBL	electron blocking layer
<i>et al.</i>	and others ( <i>et alii</i> )
ETL	electron transporting layer
HBL	hole blocking layer
HOMO	highest occupied molecular orbital
HTL	hole transporting layer
i.e.	that is ( <i>id est</i> )
IR	infrared

LUMO	lowest unoccupied molecular orbital
m	multiplet (NMR)
<i>n</i> -	linear alkyl chain
NIL	nanoimprint lithography
NMR	nuclear magnetic resonance spectroscopy
OD	optical density
OLED	organic light emitting diode
OPV	organic photovoltaics
OSC	organic solar cell
<i>p</i>	para
PAG	photoacid generator
PL	photoluminescence
PLQE	photoluminescence quantum efficiency
q	quartet (NMR)
qui	quintet (NMR)
ref.	reference
RF	reflux
s	singlet (NMR)
SANIL	solvent assisted nanoimprint lithography
SEC	size exclusion chromatography
SEM	scanning electron microscopy
SPC	Suzuki polycondensation
<i>t</i> -	tertiary
t	triplet (NMR)
TAG	thermal acid generator
TGA	thermogravimetric analysis
UV	ultraviolet
UV/Vis	ultraviolet-visible spectroscopy





# Table of Contents

1	Introduction .....	1
1.1	Organic Photovoltaics .....	1
1.2	Organic photovoltaic devices and materials .....	9
1.3	Low bandgap materials .....	16
1.4	Crosslinking of organic semiconductors.....	33
1.5	Stabilization of the morphology of BHJ solar cells by crosslinking .....	42
1.6	Patterning of organic semiconductors .....	46
2	Aim of the thesis .....	49
3	Synthesis and crosslinking of oxetane functionalized low bandgap polymers .....	51
3.1	Synthesis of the monomers .....	52
3.2	Polymer synthesis and characterization .....	57
3.3	Crosslinking experiments .....	64
4	Stabilization of bulk heterojunction solar cells by crosslinking .....	77
4.1	Preliminary experiments .....	80
4.2	Accelerated aging tests .....	85
5	Patterning of low bandgap polymers by imprinting .....	97
6	Summary .....	107
7	Zusammenfassung .....	111
8	Experimental .....	117
8.1	Materials and methods .....	117
8.2	Syntheses of the monomers .....	120
8.3	Syntheses of the polymers .....	129
8.4	Crosslinking experiments .....	137
8.5	Fabrication and characterization of organic solar cells .....	138
8.6	Imprinting.....	139
9	Appendix .....	141
10	References.....	161
11	List of publications and presentations .....	173







# 1 Introduction

One major challenge of the 21st century is the transition from limited fossil to more sustainable energy sources. Particularly in Germany this development was propelled by a governmental decision from 2011, the so-called *Energiewende*. In this program the prevalent sources of energy - oil, coal, gas, and nuclear energy – are set to be more and more replaced in favor of what is now called *renewable energies*. The last of the German nuclear power plants will be decommissioned by the year 2022, so alternative strategies for the generation of electricity are of particular interest. Main focus is on wind and water power, biogas plants, and photovoltaics. In 2014 about 18.9 billion euros were invested in such projects, enabling Germany already to cover 27% of its gross electric power demand via *clean energies*. Photovoltaics alone contributed 6%, more than 35,000 GWh, of all electric power generated in this year.<sup>[1]</sup>

## 1.1 Organic Photovoltaics

Photovoltaics are expected to play a major role in the future's electricity supply: Utilizing the ubiquitous energy provided by the sun for the generation of electricity is deemed highly suitable.<sup>[2]</sup> Today, the vast majority of commercially available photovoltaic devices is based on silicon. Devices made of monocrystalline silicon have record efficiencies of over 25% in the lab and up to 22% in modules.<sup>[3]</sup> Reportedly, they have lifespans of about 20 years.<sup>[4]</sup> A less expensive alternative are polycrystalline cells. The efficiencies of commercially available modules range from 12 to 17% with comparable lifetimes.<sup>[5]</sup> Thin-layer devices from amorphous silicon have the lowest price of this class. Their overall efficiencies barely reach up to 10%.<sup>[6]</sup> Since the late 1990's organic photovoltaics (OPV) have attained much interest in academia, offering entirely new perspectives for processing and application of photovoltaic devices.<sup>[7]</sup> Here, instead of silicon, organic semiconductors, i.e., small molecules and polymers based on carbon, are utilized as functional material.<sup>[8]</sup> Properties, such as solubility, absorption, and charge carrier transport, can be tuned by synthesis. With particular respect to OPV, these materials offer the perspective for low-energy, low-cost manufacturing of large-area devices by solution processing, for example roll-to-roll production.<sup>[4]</sup> The lower production costs result in short energy payback times. Less than six months of operation are sufficient to harvest the amount of energy invested in the fabrication process.<sup>[9]</sup> However, fabrication from solution is not the only way for manufacturing commercial OPV devices. Heliatek GmbH is among the leaders in the fabrication of OPV by physical vapor deposition.

In 2012 they launched a pilot facility for the production of OPV films by a roll-to-roll vacuum process at low temperatures.<sup>[10]</sup> Furthermore, semitransparent OPV devices can be fabricated. They can be integrated into the (glass) facade of buildings (BIPV, building integrated photovoltaics) and are considered for automotive applications.<sup>[11]</sup> Figure 1 illustrates some applications of OPV. All projects shown are in the prototype stage.

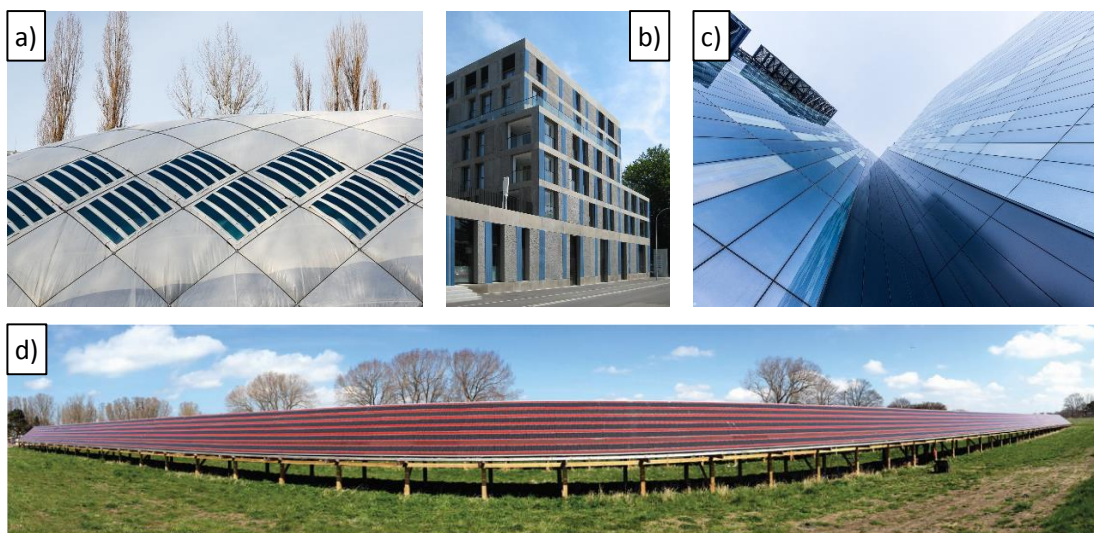


**Figure 1.** Top: Building integrated OPV concepts from Heliatek GmbH: **a)** ultra-light OPV foil on a PVC air dome,<sup>[12]</sup> **b)** concrete facades with solar films,<sup>[13]</sup> **c)** transparent solar films for windows (©AGC Glass Europe).<sup>[14]</sup> Bottom: **d)** OPV park at the Technical University of Denmark.<sup>[15]</sup>

These photographs show the unique properties of OPV. Devices are very light and flexible. This makes them suitable for installation on air domes (Figure 1a) or any other kind of building, where no heavy Si-based devices could be mounted.<sup>[12]</sup> Also in the first OPV based solar park (Figure 1d) the 100 m long and 2.5 m high panels are held by simple wood constructions.<sup>[15]</sup> Even though the overall efficiency is rather low (1.53%), the time it takes to gain the energy consumed during fabrication – the energy payback time – is only six months.<sup>[15]</sup> Another interesting aspect is the integration of OPV into buildings. In a concrete facade (Figure 1b) OPV devices do not only generate clean energy but also serve as design elements.<sup>[13]</sup> Semitransparent OPV panels can also be installed on windows (Figure 1c), utilizing the areas of glass facades for generating electricity.<sup>[14]</sup>

In this chapter, an overview of the device principles and fundamental processes in organic photovoltaics will be given, alongside with device characterization. Also, materials for OPV will be introduced with special attention to low bandgap polymers, their properties and synthesis.

The term organic photovoltaics describes several types of solar cells containing at least one organic semiconductor in the active area.<sup>[8]</sup> Devices whose active layers are made up by both, organic and inorganic materials, are often referred to as hybrid solar cells. The following section will describe the fundamental photophysical processes in an organic

solar cell and address the methods for measuring overall efficiency as well as other characteristic parameters.

A first report on an organic solar cell was published by Tang in 1986. Here, copper phthalocyanine (CuPc) was used as a donor and a derivative of perylene tetracarboxylic dianhydride (PV) was used as an acceptor.<sup>[16]</sup> Tang vacuum evaporated both materials into two separate layers between a transparent, conducting substrate of indium tin oxide (ITO) coated on glass and a metal cathode, here silver. Figure 2 shows the basic set-up of an organic solar cell and the materials used in the first reported cell by Tang.

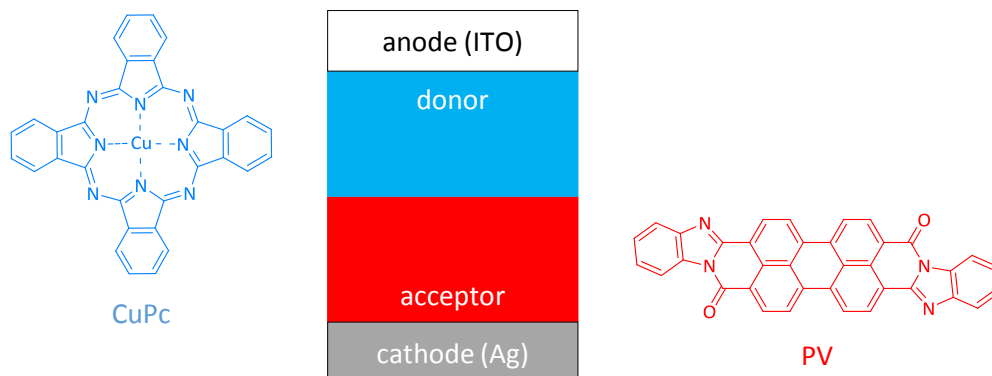


**Figure 2.** Bilayer device by C. Tang.<sup>[16]</sup> Between a transparent electrode (ITO) and a metal cathode (silver) is the active layer. The hole transporting copper phthalocyanine (CuPc) and an electron conducting perylene derivative (PV) were used in the first bilayer device.

### 1.1.1 Fundamental processes in organic solar cells

Based on this, academia started revealing the fundamental processes in organic solar cells. Several articles address these processes, the following section is mainly based on a review by Deibel and Dyakonov.<sup>[17]</sup> Basically, the following six steps are required for the generation of electrical power in an OSC:

- i) Absorption of a photon and formation of an exciton
- ii) Exciton migration towards an interface between donor and acceptor material
- iii) Exciton dissociation into free charge carriers
- iv) Separation of the charge carriers
- v) Transport of the free carriers towards the corresponding electrodes
- vi) Extraction of the charges.

These fundamental processes in an organic solar cell are schematically drawn in Figure 3.

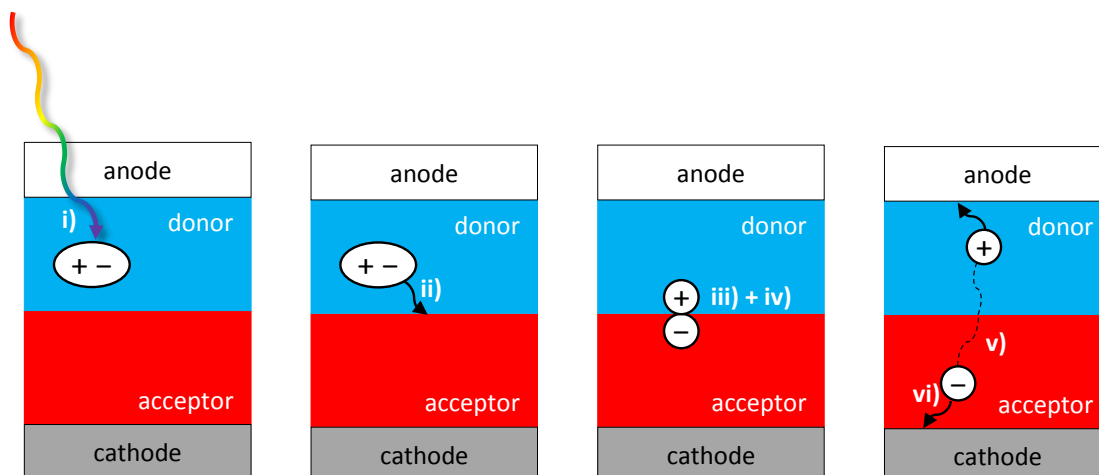


**Figure 3.** Fundamental processes in an organic solar cell. **i)** Exciton formation from an absorbed photon, **ii)** diffusion of the exciton towards the donor-acceptor interface, **iii)** excitation dissociation, electron transfer from the donor to the acceptor material, **iv)** separation of the free charge carriers, **v)** transport of electron and hole by hopping, **vi)** extraction of charges through the electrodes. Adapted from reference<sup>[17]</sup>.

In organic semiconductors incident photons cause the formation of excited states. This bound electron-hole pair is referred to as an exciton.<sup>[18]</sup> The low dielectric constant of organic semiconductors leads to high Coulomb forces between the hole and electron formed.<sup>[19]</sup> In contrast to inorganic semiconductors in organic matter the binding energy between an electron and a hole is much larger than the thermal energy at room temperature.<sup>[20]</sup> Thus, for charge separation an additional driving force has to be implemented. This is achieved by the addition of an electronegative organic semiconductor as an acceptor material. The driving force for the electron transfer from the donor to the acceptor material is the energy difference of both materials' LUMO (lowest unoccupied molecular orbital).<sup>[19]</sup> Thus, exciton dissociation is efficient only at an interface between the electron donor and the electron acceptor material. This is the reason why single layer devices, as they are standard for silicon based photovoltaic cells, are not very efficient in organic solar cells.

Furthermore, lifetimes of excitons in organic semiconductors are distinctly short, below 1 ns. So, for charge separation to be efficient, an exciton has to reach a donor-acceptor interface within its lifetime. The distance an exciton can migrate is expressed by the exciton diffusion length  $L_D$ , as in equation 1, where  $D$  is the diffusion coefficient and  $\tau$  is the exciton lifetime.

$$L_D = \sqrt{D\tau} \quad \text{Equation 1}$$

Assuming a lifetime of less than 1 ns, the diffusion length is limited to 20 nm in conjugated polymers. Consequently, only those excitons generated in immediate vicinity of an interface between donor and acceptor material can dissociate and contribute to the photocurrent.<sup>[21]</sup> This explains why bilayer devices with their planar heterojunction between donor and acceptor are limited in their efficiency. Most of the excitons generated

will rather decompose – by photoluminescence or by radiationless decay – than reach an interface.<sup>[17]</sup> When it comes to exciton harvesting the concept of the bulk heterojunction (BHJ) proved to be much more effective. A scheme of a BHJ is shown in Figure 6. In a blend of donor and acceptor materials a bicontinuous interpenetrating network is formed, resulting in a huge interface and short exciton diffusion paths.<sup>[22,23]</sup> The BHJ is described in detail in its own section below.

An exciton that reaches an interface can transfer its electron to the acceptor very rapidly. The rates for this charge transfer are in the range of hundreds of femtoseconds.<sup>[24,25]</sup> However, both carriers, even though now on different materials, still remain bound by Coulomb forces.<sup>[26,27]</sup> This so-called polaron pair has to be separated to finally generate free carriers.<sup>[28]</sup> For a description of the polaron pair dissociation the Onsager-Brown model is most commonly used. It deals with the separation of Coulomb bound charges under the assistance of an external electric field and describes the odds for charge carriers to overcome the Coulomb attractive forces and move on as free charges.<sup>[29–31]</sup> If electrons and holes recombine at this stage, this is referred to as *geminate recombination*. This recombination is a monomolecular process and thus proportional to the concentration of polaron pairs.<sup>[17]</sup>

After separation, the charges are transported towards the electrodes by hopping. The holes are transported through the donor material, while the acceptor material functions as the electron conductor. Hopping implies that the charges are transferred from one localized state to another. In crystalline organic semiconductors, which provide more long-range order, also band-like transport can be found.<sup>[17]</sup> Still during transport recombination of the charge carriers can occur. In this – now called *non-geminate recombination* – the charge carriers recombine with their opposites. In bilayer OSCs the non-geminate recombination is minimal.<sup>[32]</sup>

In the final step towards the generation of a photocurrent the charge carriers are extracted via the electrodes. Holes are extracted by the anode, while electrons are extracted by the cathode. For this step the interface between the (metal) electrodes and the organic layers is important. Also the mobilities of holes and electrons in the respective transport materials have to be balanced for efficient photocurrent generation.<sup>[33]</sup>

## 1.1.2 Characterization of organic solar cells

Organic solar cells are mainly characterized by two methods: the external quantum efficiency (EQE) and the current density-voltage ( $J$ - $V$ ) characteristics. An exemplary  $J$ - $V$  curve is shown in Figure 4.

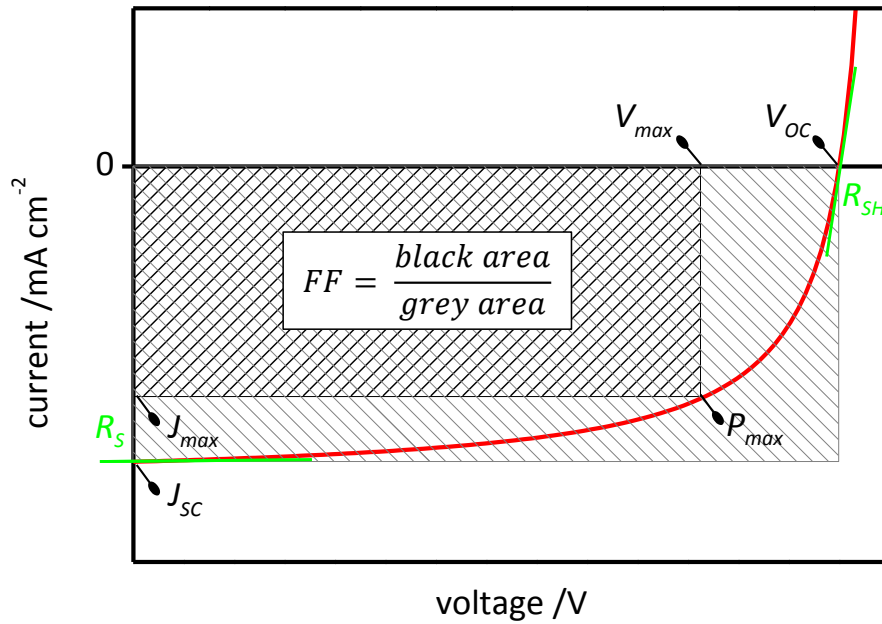


**Figure 4.** Illustration of a generic  $J$ - $V$  curve under illumination.  $V_{OC}$  is the open circuit voltage,  $J_{SC}$  the short circuit current density,  $P_{max}$  is the maximum power density,  $V_{max}$  and  $J_{max}$  are the voltage and the current density at the maximum power density, and  $FF$  is the fill factor. Series ( $R_s$ ) and shunt resistance ( $R_{SH}$ ) are calculated from the inverse slopes of the  $J$ - $V$  curve near  $J_{SC}$  and  $V_{OC}$ , respectively.

An  $J$ - $V$  curve is recorded in dark and under illumination. There are standard conditions for the measurement under illumination: Measurements are conducted at 25 °C in a solar simulator.<sup>[34]</sup> Here, a solar-like spectrum is generated. As a global reference an air mass 1.5 solar spectrum (1.5 AM) is used.<sup>[35]</sup> This simulates the yearly average spectrum of the sun that reaches the mid-latitudes of northern hemisphere.<sup>[32,36]</sup> The standard intensity of irradiation is set to 1000 W m<sup>-2</sup>, known as 1 sun.<sup>[34]</sup>

From the  $J$ - $V$  curve a number of characteristic device parameters can be determined. Firstly, the short circuit current density  $J_{SC}$ , the open circuit voltage  $V_{OC}$ , and the fill factor  $FF$ . By the help of these parameters the power conversion efficiency (PCE,  $\eta$ ) is calculated according to equation 2.

$$\eta = \frac{P_{max}}{P_{in}} = \frac{J_{SC} \times V_{OC} \times FF}{P_{in}} \times 100\% \quad \text{Equation 2}$$

The PCE is the quotient of the maximum power ( $P_{max}$ ) produced by the solar cell and the power of the incident light ( $P_{in}$ ).  $J_{sc}$  and  $V_{oc}$  determine the power production of the solar cell. However, the power delivered by the cell is zero at  $J_{sc}$  and it is also zero at  $V_{oc}$ . The maximum power of a device is determined by the product of  $J_{max}$  and  $V_{max}$ . Due to losses to resistance and recombination as well as the diode behavior, the maxima of current density and voltage is lower than the product of  $J_{sc}$  and  $V_{oc}$ .<sup>[37]</sup> This relation is expressed by the FF in equation 3.

$$FF = \frac{P_{max}}{J_{sc} \times V_{oc}} = \frac{J_{max} \times V_{max}}{J_{sc} \times V_{oc}} \quad \text{Equation 3}$$

In Figure 4 the FF is illustrated by the ratio of the areas of the black square ( $J_{max} \times V_{max}$ ) and the grey square ( $J_{sc} \times V_{oc}$ ). For an efficient solar cell a high FF is desired. Series resistance ( $R_s$ ) and shunt resistance ( $R_{SH}$ ) have a strong impact on the FF. Both parameters are calculated by the inverse slope of the  $J$ - $V$  curve. From the slope near to  $J_{sc}$  the series resistance is determined. The shunt resistance is derived from the slope around  $V_{oc}$ . To end up with a high fill factor,  $R_s$  should be close to zero, while  $R_{SH}$  is desired to be very high.

The EQE, also referred to as incident photon-to-current conversion efficiency (IPCE), gives another measure for the efficiency of photovoltaic devices. It is calculated according to equation 4, where  $J_{sc}(\lambda)$  is the short-circuit current density at a specific wavelength  $\lambda$ ,  $P(\lambda)$  is the monochromatic incident optical power,  $\lambda$  is the wavelength,  $h$  is the Planck's constant,  $c$  is the speed of light, and  $q$  is the elementary charge.

$$EQE = \frac{\text{charges generated}}{\text{incident photons}} = \frac{J_{sc}(\lambda)}{P(\lambda) \times \lambda} \times \frac{h \times c}{q} \quad \text{Equation 4}$$

Here, the number of charge carriers generated at a specific wavelength is compared to the number of incident photons of this specific wavelength. The EQE is closely connected to the absorption behavior of the materials used in the active layer of the solar cell. An EQE spectrum is illustrated in Figure 5. This example shows an almost ideal EQE spectrum. In reality a much narrower absorption is achieved which is an issue for OSC efficiency.

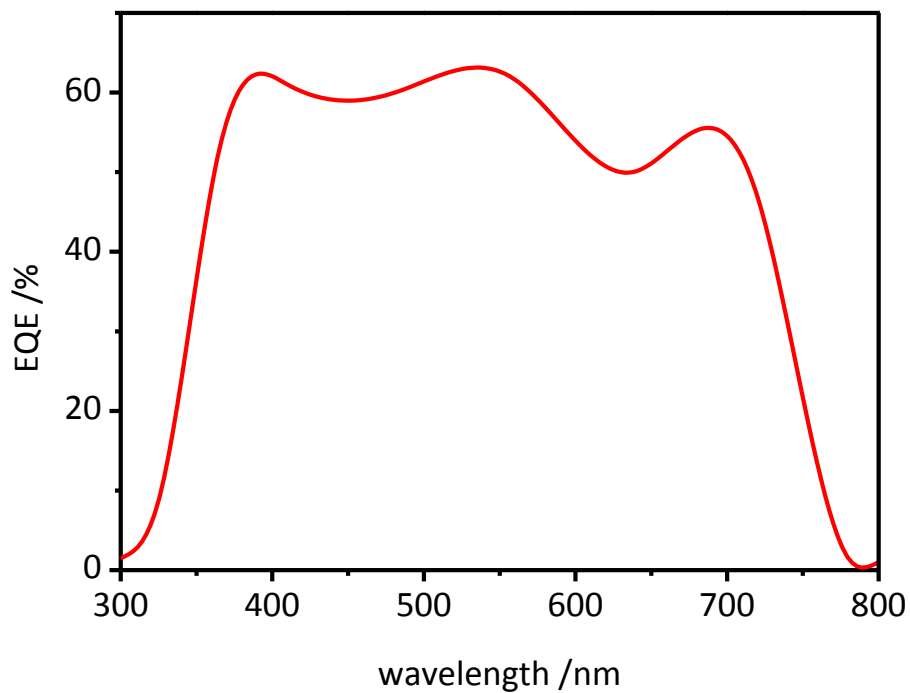


**Figure 5.** Idealized external quantum efficiency (EQE) spectrum with a very broad spectral coverage.

The following section will summarize the most prominent classes of OPV devices and describe the concept of the bulk heterojunction, the most relevant type of OPV devices for this work.

## 1.2 Organic photovoltaic devices and materials

Bilayer OSCs are still interesting for researchers. Due to their simple architecture and well-defined interfaces they are very helpful for gaining deeper insight into the fundamental phenomena, such as exciton diffusion.<sup>[38,39]</sup>

Grätzel *et al.* reported the dye-sensitized solar cell (DSSC), a first hybrid solar cell, in 1991. The active layer comprised a porous network of titanium dioxide, an inorganic semiconductor. As absorbing material a ruthenium dye was chemisorbed to the TiO<sub>2</sub> and the pores of the dye-sensitized TiO<sub>2</sub> network were filled with a hole conducting material. Initially, a liquid electrolyte (I<sup>-</sup>/I<sub>3</sub><sup>-</sup> in acetonitrile) was used as hole conductor.<sup>[40]</sup> These so-called Grätzel cells reached remarkably high efficiencies of up to 12.3%.<sup>[41]</sup> The drawback of this concept is the liquid electrolyte that limits the long term stability. Bringing in solid hole conductors helps fixing this stability issue, but only on expense of efficiency.<sup>[42]</sup> The best solid state dye-sensitized solar cells reach efficiencies of 7.2%.<sup>[43]</sup>

In this decade another class of hybrid solar cells emerged as one of the hottest developments in recent OPV research: Perovskite solar cells were first reported by Miyasaka *et al.* in 2009.<sup>[44]</sup> Here, the light harvesting material is an inorganic-organic hybrid material with the generic structure CH<sub>3</sub>NH<sub>3</sub>PbX<sub>3</sub>, where X stands for either I, Cl, Br.<sup>[45]</sup> These compounds crystallize in a cubic ABX<sub>3</sub> lattice, known as perovskite structure.<sup>[46]</sup> As hole-transporting material organic semiconductors, such as spirobifluorene derivatives are commonly used.<sup>[45]</sup> Since the report by Miyasaka, this field has taken an unprecedented development. Between 2009 and 2015 the PCE of perovskite solar cells of several architectures rose from 3.8%<sup>[44]</sup> to over 20%.<sup>[47-49]</sup>

### 1.2.1 Bulk heterojunction OSCs

The bulk heterojunction (BHJ) is probably the most popular concept for the active layer of an all-organic solar cell. In contrast to the planar heterojunction set-up, the donor and acceptor material are mixed rather than in two discrete layers. This results in an increased interface area between donor and acceptor. Ideally, both materials form an interpenetrating, bicontinuous network with domain sizes in the range of 20 to 30 nm, roughly twice the exciton diffusion length. Thus, most of the excitons are able to reach a donor-acceptor interface within their lifetime. The incident photon to electron conversion efficiency of a BHJ exceeds that of a bilayer by a factor of 10.<sup>[19]</sup>

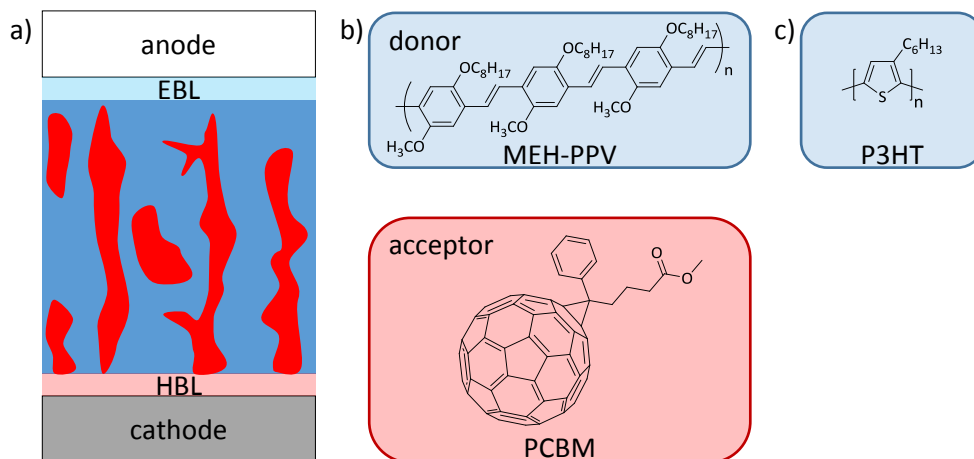


**Figure 6.** a) Schematic drawing of an idealized bicontinuous interpenetrating network formed by blending a conjugated polymer (donor, blue) with a low-molecular weight fullerene derivative (acceptor, red) in a BHJ device. Between the transparent anode and the BHJ material an electron-blocking layer (EBL) and between the metal cathode and the BHJ material a hole-blocking layer (HBL) is introduced. b) Materials of the first BHJ solar cell by Heeger *et al.*, poly(2-methoxy-5-(2'-ethyl-hexyloxy)-1,4-phenylene vinylene) (MEH-PPV) as donor and phenyl-C<sub>61</sub>-butyric acid methyl ester (PCBM) as acceptor.<sup>[22]</sup> c) Poly(3-hexylthiophene) (P3HT), the combination with PCBM is one of the most studied BHJ systems.

The fundamental idea for this concept was the discovery of the ultrafast electron transfer from a conjugated polymer to a fullerene.<sup>[24,50]</sup> In 1995 Heeger *et al.* reported the first “bulk donor-acceptor heterojunction material”.<sup>[22]</sup> This consisted of the polymer poly(2-methoxy-5-(2'-ethyl-hexyloxy)-1,4-phenylene vinylene) (MEH-PPV) and the soluble fullerene derivative phenyl-C<sub>61</sub>-butyric acid methyl ester (PCBM).<sup>[51,52]</sup> An illustration of a donor-acceptor blend and the chemical structures are shown in Figure 6a and b. Typically, these blends are achieved by mixing solutions of both components and subsequent spin coating.

Basically, these types of materials are still chosen for contemporary BHJ devices. Only instead of MEH-PPV novel conjugated polymers are commonly used. The combination of poly-(3-hexylthiophene) (Figure 6c) and PCBM became one of the most intensely studied BHJ materials.<sup>[53]</sup> Conjugated polymers with enhanced absorption properties, so-called low bandgap polymers are also very popular donor materials.<sup>[54]</sup> They will be addressed in detail in chapter 1.4.

The key point of the bulk heterojunction concept is the nature of the donor acceptor blend.<sup>[55]</sup> In a review article the inventor Alan Heeger summarizes the requirements: “A bulk heterojunction (BHJ) material is a solid state *mixture* of two components (donor and acceptor) with *nanostructured morphology* formed by spontaneous *phase separation*: these donor and acceptor components self-assemble to form *bicontinuous interpenetrating networks*.”<sup>[56]</sup>

Phase separation is triggered by an intrinsic tendency of polymers: Their low entropy of mixing favors the formation of pure domains. This effect can be enhanced if one or both components tend to crystallize.<sup>[57]</sup> In the literature there are two mechanisms for phase

separation reported: nucleation and growth or spinodal demixing.<sup>[58]</sup> However, phase separation alone is not sufficient for an efficiently working BHJ material. It is important to be aware of the domain sizes and the degree of interpenetration between the donor and acceptor phases. On the one hand, the formation of an interpenetrating network is required. This guarantees that the surface area between donor and acceptor material is as large as possible. Also, percolated, continuous paths for charge transport to the electrodes are necessary. This means that the amount of domains of electron and hole transporting material, which are not connected to their respective electrode, has to be kept to a minimum. Otherwise charges generated on one of these “island” have no chance of being extracted and increase the probability for non-geminate recombination, resulting in lower device efficiency. On the other side, the size of the domains in the donor acceptor blend is another important aspect. Ideally, lateral domain sizes should be in the range of twice the exciton diffusion length. In this case all excitons could reach a donor-acceptor interface and be dissociated during their lifetime. Thus, domain sizes below 20 nm are desired. However, arbitrarily small domains are not favorable, either. In this case the transport of the free charge carriers towards the electrodes is hampered, with non-geminate recombination becoming more dominant. Thus, control over the blend morphology is utterly important. An idealized schematic drawing of a donor acceptor blend morphology is shown in Figure 6a. Several factors play an important role in the formation of efficient bulk heterojunctions: choice of solvent, solvent vapor annealing, thermal annealing, and solvent additives.<sup>[59]</sup>

The solvent from which a BHJ film is cast has significant influence on the morphology. The prerequisite for any solvent is to provide good solubility for the polymer as well as the fullerene derivative. By tendency solvents with high boiling points, such as chlorobenzene (CB) and dichlorobenzene (DCB) lead to a better PCE than low boiling solvents.<sup>[60]</sup> High boiling solvents lead to the formation of considerably smaller domains and influence the degree of crystallinity.<sup>[59,60]</sup> The choice of solvent can also influence the vertical distribution of the materials.<sup>[59]</sup> By the concept of vertical phase separation ideally donor material is accumulated at the anode, while acceptor material is accumulated around the cathode.<sup>[61]</sup> In between interpenetrating domains of both materials are formed with lateral dimensions of around 20 nm.<sup>[62]</sup> An illustration of a vertically phase separated blend is shown in Figure 7. Vertical phase separation is deemed beneficial for charge transport.<sup>[63]</sup>

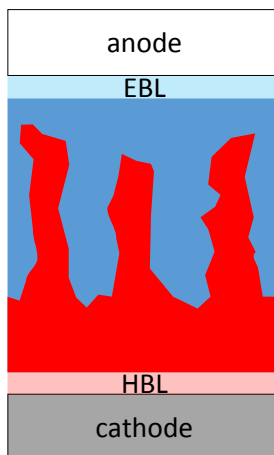


**Figure 7.** Schematic illustration of a vertically phase separated BHJ blend (not to the scale).

Solvent vapor annealing is another strategy for the control of the BHJ morphology. Here, the drying process of cast films is slowed down. Storing the films right after coating in a sealed case with solvent or solvent vapor reduces the evaporation rate of the solvent.<sup>[59]</sup>

Thermal annealing is widely applied in the field of organic electronics. In the literature thermal treatment of cast BHJ films is considered to enhance crystallinity, leading to an improved charge carrier transport.<sup>[59,64]</sup> In several works also a shift of absorption to longer wavelengths is observed.<sup>[59]</sup> This is explained by enhanced interchain interactions in the more ordered structures.<sup>[65]</sup> The effect of thermal annealing on the morphology of P3HT/PCBM blends is very well known. Upon annealing the photocurrent can be increased. This is explained by two aspects: a red shift in the absorption spectrum caused by diffusion of PCBM out of the P3HT matrix allowing for enhanced interaction between the polymer chains and the growth of PCBM crystals leading to the formation of percolation paths for charge transport.<sup>[66]</sup>

The use of solvent additives became a very popular approach for controlling the blend morphology.<sup>[59]</sup> Common additives are 1,8-octanedithiol (ODT) and 1,8-diiodooctane (DIO). The impact of both additives on the morphology is similar. Both selectively dissolve the PCBM and break up aggregates of the fullerenes in solution.<sup>[67]</sup> In combination with their high boiling points (ODT 269 °C, DIO 170 °C) compared to the main solvent (chlorobenzene 131 °C), this causes the PCBM to remain in solution longer than the polymer.<sup>[68]</sup> The results are higher crystallinity of the donor polymer, smaller domains, and enhanced interpenetration of the donor and acceptor phases.<sup>[59,69]</sup>

The effect of any of these concepts on the morphology cannot be predicted in general for a given polymer-PCBM combination. However, a trend toward smaller domain sizes is observed when using solvent additives.<sup>[59]</sup>

Furthermore, the model of entirely phase-separated systems with only pure domains of donor or acceptor material has been extended.<sup>[70]</sup> There are indications that also kind of a third phase is present. This is regarded as an amorphous mixture of both materials, also

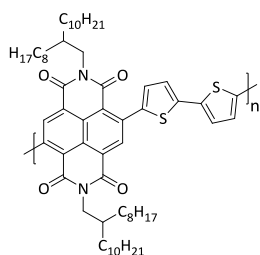
in some studies the “pure” phases are denoted as donor-rich and acceptor-rich domains.<sup>[71]</sup> In these phases where fullerenes are intercalated between polymer chains excitons are formed within angstroms of donor-acceptor interfaces.<sup>[72]</sup> Instead of having to diffuse, these excitons can be separated directly. Additionally, it was also found that free charges can be transported through these molecularly mixed domains.<sup>[71]</sup>

### 1.2.2 Materials for bulk heterojunction solar cells

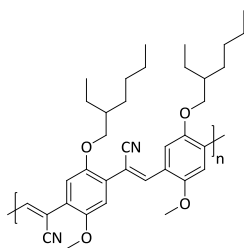
So far mainly polymer:fullerene BHJs were discussed. Besides them all-polymer bulk heterojunction cells were reported shortly after Heeger’s first publication.<sup>[23]</sup> Until now the efficiencies of these devices are still behind the efficiencies of the best polymer:fullerene blend devices.<sup>[73]</sup> However, they are attractive because of their superior film forming properties compared to fullerene based blends.<sup>[73]</sup> Furthermore, polymer acceptors show better absorption in the visible range of the solar spectrum compared to fullerenes.<sup>[73]</sup> Figure 8a shows two examples for acceptor polymers: P(NDI2OD-T2),<sup>[74]</sup> a copolymer based on naphthalene bisimide and thiophene, and the poly(*p*-phenylene vinylene) derivative MEH-CN-PPV.<sup>[73]</sup> On the other hand, there is also some effort in molecular bulk heterojunctions, consisting of low-molar mass donor and acceptor materials.<sup>[75,76]</sup> A record efficiency for a solution processed small-molecule BHJ of 7.9% was reported by Heeger and Bazan *et al.*<sup>[77]</sup> The donor and acceptor materials from this work are illustrated in Figure 8b. They used PC<sub>70</sub>BM as an acceptor, which shows enhanced absorption compared with PC<sub>60</sub>BM.<sup>[78]</sup> In contrast to polymers small molecules can also be processed by thermal evaporation techniques.<sup>[79]</sup> Solar cells with up to 5.2% efficiency fabricated by co-evaporation of the donor and acceptor materials are known.<sup>[80]</sup> As examples an oligo-thiophene (DCV5T, donor) and C<sub>60</sub> are shown in Figure 8c.

Furthermore, tandem OSCs have been proposed.<sup>[81]</sup> Here, two or more BHJ cells are stacked above each other, which greatly increases the absorption efficiency. Devices made up by several layers of organic and inorganic low-molar mass compounds are fabricated with a world record efficiency of 12% by Heliatek GmbH.<sup>[82]</sup>

## a) Acceptor polymers

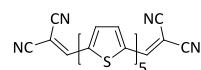


P(NDI2OD-T2)



MEH-CN-PPV

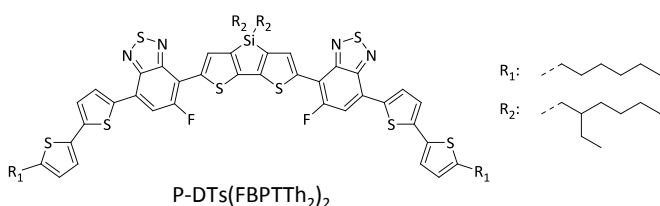
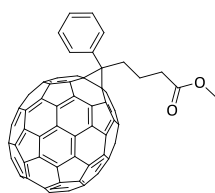
## c) Co-evaporated small molecule BHJ



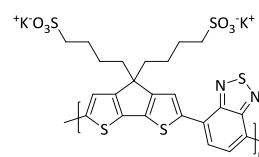
DCV5T

C<sub>60</sub>

## b) Solution processed small molecule BHJ

P-DTs(FBPTTh<sub>2</sub>)<sub>2</sub>PC<sub>70</sub>BM

## d) Hole conducting layer

PCPDTBT-SO<sub>3</sub>-K

**Figure 8.** Materials for bulk heterojunction solar cells. **a)** Acceptor polymers P(NDI2OD-T2)<sup>[74]</sup> and MEH-CN-PPV.<sup>[73]</sup> **b)** Solution processable small molecules P-DTs(FBPTTh<sub>2</sub>)<sub>2</sub> and PC<sub>70</sub>BM.<sup>[77]</sup> **c)** Small molecules for co-evaporation DCV5T and C<sub>60</sub>.<sup>[80]</sup> **d)** Conjugated polyelectrolyte PCPDTBT-SO<sub>3</sub>-K as hole transporting interlayer.<sup>[83]</sup>

Despite the still lower efficiencies, small molecule BHJ surpass the polymer based BHJ concept at one certain point: Batch-to-batch variation is basically not a factor when working with small molecules. The chemical structure of small molecules is perfectly defined whereas polymers always show molecular weight distributions. An important issue is the purity of organic semiconductors. Small molecules can be obtained in excellent purity by train sublimation.<sup>[84]</sup> In the case of polymers it is difficult to obtain highly pure materials. From a rather limited pool of methods precipitation is the commonly used technique. However, the potential of this method is not even close to the purities achieved from sublimation. All of this can have implications on the solubility, and thus processability, of polymers and on their performance. Molecular weight, polydispersity, conjugation length, and impurities have been demonstrated to significantly influence the performance of polymer solar cells.<sup>[85]</sup>

Besides the steady improvement of active layer materials and morphology, also advances concerning device set-up lead to significant improvements in BHJ solar cell performance, pushing the PCE of the best devices up to 10%.<sup>[86]</sup>

One important step was the introduction of additional functional layers between the electrodes and the BHJ material (Figure 6a).<sup>[87]</sup> This is required because of the blend morphology. Commonly donor and acceptor material are randomly mixed and thus contact both electrodes. To prevent short-circuit, an electron transporting layer (ETL), which is also referred to as hole-blocking layer (HBL), is inserted between the metal cathode and the active organic layer.<sup>[83]</sup> Analogously, a hole transporting layer (HTL), which is also electron-blocking (EBL), is added between the BHJ layer and the transparent anode. Electron- and hole transporting layers also enhance the selectivity of charge collection at the electrodes and reduce the energy barrier for charge extraction.<sup>[88]</sup> As an interlayer material between the ITO anode and the active layer PEDOT:PSS is commonly used.<sup>[89]</sup> However, it has been shown that the acidic PEDOT:PSS might etch the ITO and cause instabilities over the lifetime of a device.<sup>[90]</sup> Alternatives for PEDOT:PSS are, for instance, transition metal oxides, such as MoO<sub>3</sub>, V<sub>2</sub>O<sub>5</sub>, and WO<sub>3</sub><sup>[91]</sup> or conjugated polyelectrolytes.<sup>[92]</sup> As an example for a conjugated polyelectrolyte as hole transporting interlayer PCPDTBT-SO<sub>3</sub>-K is shown in Figure 8d.<sup>[83]</sup> The metal oxides mentioned are highly transparent and conductive.<sup>[89]</sup> An interlayer of MoO<sub>3</sub> was reported to improve the device performance of BHJ solar cells.<sup>[93]</sup> In this work MoO<sub>3</sub> was chosen as material for the anodic interlayer.

Standard cathode materials are thermally deposited low-work function metals, for instance aluminium or calcium.<sup>[94]</sup> A first interlayer material facilitating the electron collection was LiF.<sup>[95]</sup> Besides, water/alcohol soluble conjugated polymers known as electron injection layers in OLEDs can be used for better electron transport at the cathode interface.<sup>[96,97]</sup> A new strategy was the formation of buffer layers by self-organisation.<sup>[96]</sup> Small amounts of a fluorinated fullerene derivative are mixed into the BHJ blend. The fluorocarbon spontaneously migrates to the film surface during spin coating and provides better alignment between the Al cathode and the energy level of the acceptor material.<sup>[96,98]</sup> Introducing an cathodic interlayer of titanium oxide (TiO<sub>x</sub>) turned out as a very successful concept. In addition to its electron transporting properties, this material also serves as an oxygen barrier, improving the device stability.<sup>[96]</sup> Furthermore, TiO<sub>x</sub> serves as an optical spacer: The effect of an optical spacer is a spatial redistribution of the light intensity in a device.<sup>[99]</sup> As a consequence, a larger area of the active layer can be used for the generation of charges.<sup>[100]</sup> This leads to an increase of power conversion efficiency of up to 50% compared to devices without an optical spacer.<sup>[99]</sup> Apart from TiO<sub>x</sub> also zinc oxide (ZnO) is used with similar success.<sup>[101]</sup>

### 1.3 Low bandgap materials

The early success of bulk heterojunction organic solar cells propelled the development of organic semiconducting materials with improved absorption and transport properties. While fullerene derivatives are still the materials of choice as electron acceptors, the field of donor materials remains a work in progress. Since this thesis focusses on donor polymers, the development of these materials will be central in the following section. Appropriate donor polymers are expected to fulfill certain criteria: First, and most important, such materials should absorb in a broad range of the solar spectrum for an efficient collection of photons. Furthermore, the hole mobility should be similar to the electron mobility of the acceptor material to allow a balanced charge carrier transport. Finally, compatibility of the energy states of the donor material and the acceptor and electrode materials is required to reduce energy barriers within the device and provide efficient charge transport.<sup>[102]</sup>

In the first works on BHJ devices poly(*p*-phenylenevinylene) (PPV) derivatives were used as donor materials. Later, poly-(3-hexylthiophene) (P3HT) emerged to become one of the most commonly used donor polymers. Besides them, low bandgap polymers have become more and more important.<sup>[103]</sup>

#### 1.3.1 Concepts for lowering the bandgap

The term band gap originates from the band structure model established for inorganic solids. By this theory materials are classified as conductors, semiconductors, and insulators.<sup>[104]</sup> In the early years of organic semiconductor research concepts and terminology from solid state physics were adapted (Figure 9a). As a consequence, the energy difference between HOMO (highest occupied molecular orbital) and LUMO (lowest unoccupied molecular orbital) levels of organic semiconductors became known as bandgap. However, this should be regarded as a simplification and the term bandgap has to be used cautiously in context with conjugated polymers.<sup>[105]</sup>

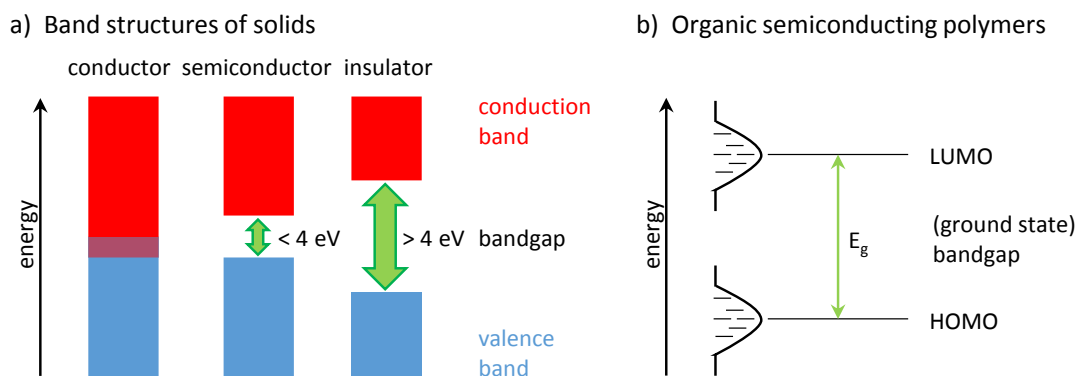


**Figure 9. a)** Band structures of a solid: The valence band (blue) is filled with electrons, the conduction band (red) is empty. Valence and conduction band overlap in a conductor. In a semiconductor a small bandgap between valence and conduction band exists. The energy of the bandgap can be overcome by thermal or optical excitation. In an insulator the bandgap is that large so it cannot be overcome. Adapted from reference<sup>[104]</sup>. **b)** Bandgap in a semiconducting polymer in the ground state. HOMO and LUMO levels are broadened to a Gaussian distribution. The ground state bandgap  $E_g$  is the energy difference of the HOMO and LUMO level. Adapted from reference<sup>[106]</sup>.

In an organic semiconducting polymer the molecular energy levels are present as Gaussian distributions.<sup>[106]</sup> They are not sharply defined as known from inorganic materials due to energetic and structural disorder as well as intermolecular interactions. Figure 9b shows a scheme of the energy levels in a ground state polymer. In addition, the ground state bandgap and the ground state HOMO and LUMO levels cannot be measured directly.<sup>[106]</sup> From optical absorption measurements the optical gap ( $E_{opt}$ ) can be obtained. This is the energy difference between the electronic ground state ( $S_0$ ) and the lowest excited state ( $S_1$ ).<sup>[107]</sup> Within this work the experimentally accessible  $E_{opt}$  is used as a rough estimation for the bandgap of the polymers synthesized. A measure for the HOMO energies of the polymers was obtained from photoelectron spectroscopy.

Within the field of low bandgap polymers the versatility of organic semiconductors becomes obvious. By smart synthesis the optical and electronic properties can be tuned. Key parameters for donor polymers for organic solar cells are the energy levels of their HOMO and LUMO (lowest unoccupied molecular orbital) and the optical gap  $E_{opt}$ .<sup>[108]</sup> Several strategies for achieving a lower bandgap are known, and controlling the polymer structure turned out to be the key.<sup>[109]</sup> Figure 10 summarizes the main parameters for a low bandgap energy.

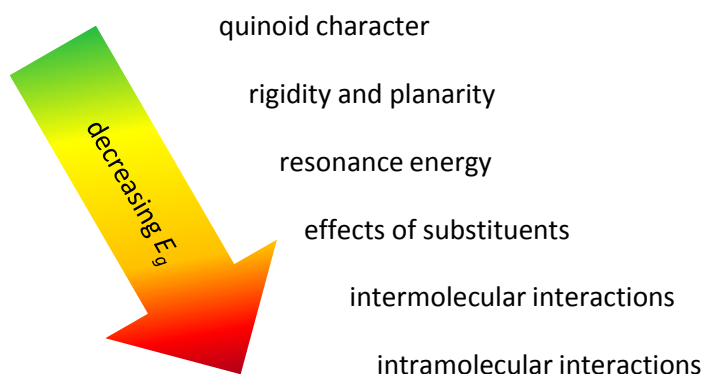


**Figure 10.** Strategies for a lower bandgap.<sup>[109–111]</sup>

The bond length alternation (BLA) was described as one factor for lowering the bandgap.<sup>[109]</sup> It is a geometric parameter representing the average length difference of neighboring carbon-carbon bonds in a polyene chain. In a conjugated polyaromatic system two resonance forms exist: the aromatic and the quinoid form. The BLA can be regarded as the ratio of both forms.<sup>[109]</sup> With an increased occurrence of the quinoid form the double bond character of the carbon-carbon bonds between two rings increases and the BLA decreases simultaneously.<sup>[109]</sup> Due to the loss of aromaticity the quinoid form is less stable, which leads to a lower bandgap.<sup>[109]</sup>

Another approach is the extension of the conjugated system. Introducing rigidity and planarity helps increasing the delocalization of  $\pi$ -electrons along the polymer backbone.<sup>[110]</sup> Furthermore, the inductive and mesomeric effects of substituents and intermolecular as well as intramolecular interactions influence the bandgap energy.<sup>[111]</sup> The concept most often used in practice is the alignment of electron-rich (referred to as *donor*) and electron-poor (referred to as *acceptor*) units in the polymer backbone in an alternating fashion.<sup>[112]</sup> This leads to strong push-pull forces within the molecule resulting in enhanced electron delocalization. In this donor-acceptor (D-A) approach the interaction between donor and acceptor units leads to a lowered optical gap. A schematic drawing of this D-A concept is illustrated in Figure 11a.

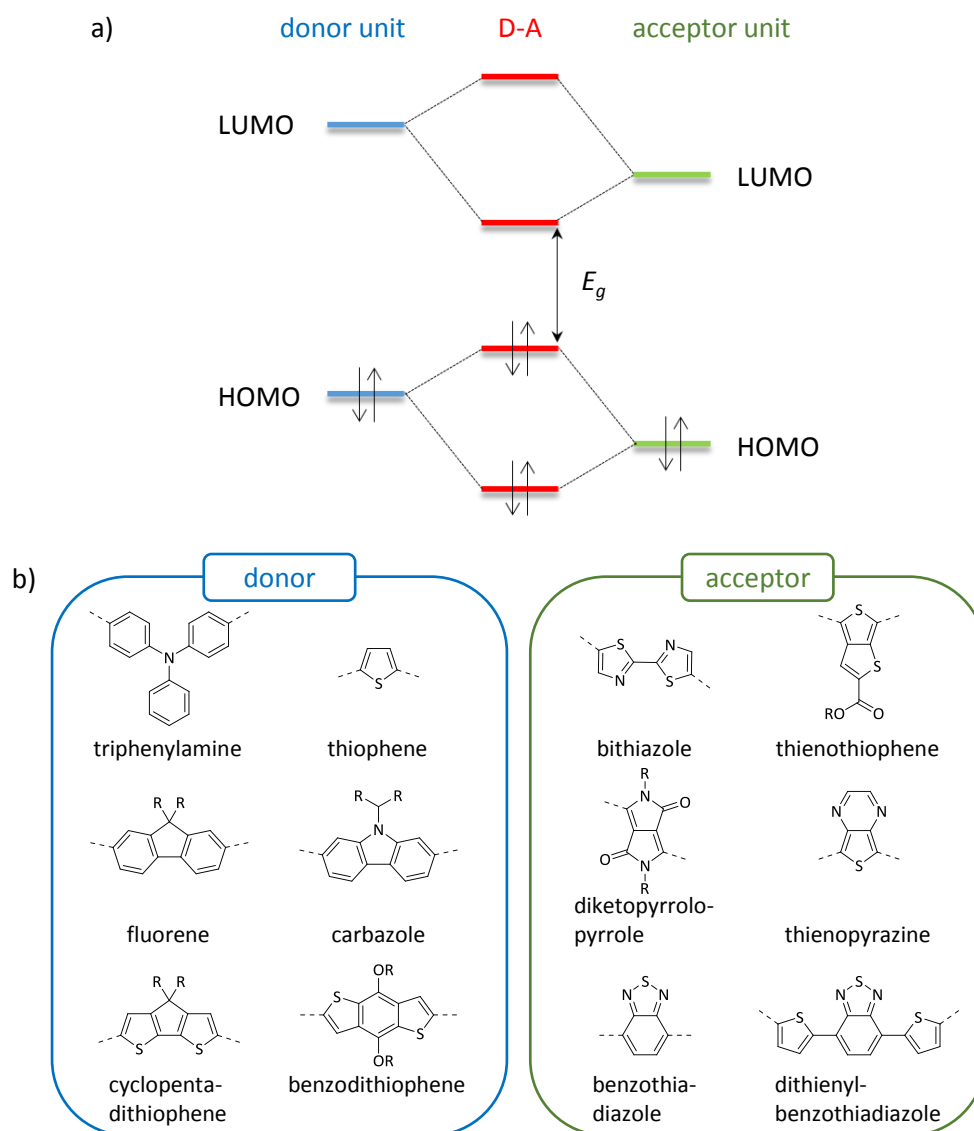


**Figure 11. a)** Lowered bandgap by interaction of donor and acceptor units.<sup>[103]</sup> **b)** Selected examples of donor and acceptor building blocks for low bandgap polymers.<sup>[107]</sup>

On the basis of the D-A concept a vast variety of low bandgap materials have emerged in the last years. This approach is very versatile, leaving plenty of choice of donor and acceptor building blocks. Examples for moieties frequently used in low bandgap materials are shown in Figure 11b. The synthesis of donor-acceptor polymers is presented in the following section.

### 1.3.2 Synthesis of low bandgap polymers

The established methods for the synthesis of low bandgap polymers following the donor-acceptor concept, and conjugated polymers in general, are metal-catalyzed carbon-carbon coupling reactions. Very popular are palladium-catalyzed cross-coupling reactions between an organic electrophile and an organometallic nucleophile.<sup>[113]</sup> Among them are, for instance, Negishi, Sonogashira, Stille, and Suzuki reactions. Another important approach for Pd-catalyzed C-C cross-coupling is the Heck reaction. Some selected reactions from this class commonly used for the formation of aryl-aryl bonds are summarized in Figure 12.

In a Heck reaction an alkenyl or aryl halide or triflate is coupled with an alkene. Conjugated acetylenic materials can be synthesized by a Sonogashira reaction. Here, vinyl or aryl halides are coupled with terminal alkynes. A copper(I) salt is employed as co-catalyst. In a Negishi reaction organozinc compounds act as the nucleophile. These are highly reactive in Pd-catalyzed cross-coupling reactions and at the same time exhibit low toxicity. However, the most commonly used techniques for the synthesis of low bandgap polymers are Stille and Suzuki reactions. Stille reactions are known as mild and versatile with tolerance to a variety of functional groups. The drawback, however, are the highly toxic organotin compounds used as nucleophiles. In Suzuki reactions the nucleophiles are organoborane derivatives.<sup>[114]</sup> The Suzuki cross-coupling was chosen for the synthesis of all low bandgap polymers within this thesis. The following section will give more details about this reaction.

## Negishi reaction



R<sup>1</sup>= alkyl, aryl, vinyl; X = Cl, Br, I, OTf

R<sup>2</sup>= aryl, benzyl, vinyl

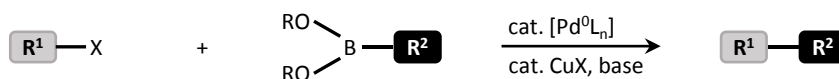
## Stille reaction



R<sup>1</sup>= alkyl, alkynyl, aryl, vinyl; X = Br, Cl, I, OAc, OP(=O)(OR)<sub>2</sub>, OTf

R<sup>2</sup>= acyl, alkynyl, allyl, aryl, benzyl, vinyl

## Suzuki reaction



R<sup>1</sup>= alkyl, alkynyl, aryl, vinyl; X = Br, Cl, I, OP(=O)(OR)<sub>2</sub>, OTf, OTs

R<sup>2</sup>= alkyl, alkynyl, aryl, benzyl, vinyl

**Figure 12.** Reaction schemes of selected palladium-catalyzed carbon-carbon cross-coupling reactions.<sup>[115]</sup>

### 1.3.3 Suzuki cross-coupling

Palladium-catalyzed cross-coupling of alkenyl and aryl halides with organoborane derivatives was first described by Suzuki and coworkers in the late 1970's.<sup>[116]</sup> In Suzuki reactions carbon-carbon bonds are formed under mild conditions with regioselectivity and stereoselectivity.<sup>[117]</sup> One major advantage of the Suzuki reaction is the stability of the monomers concerning air and moisture as well as their low toxicity, especially when compared with the organotin compounds for Stille coupling.<sup>[118]</sup> Figure 13 shows a schematic drawing of the mechanism of a Suzuki reaction.<sup>[119]</sup> As an example the coupling reaction between two aryl building blocks is illustrated.

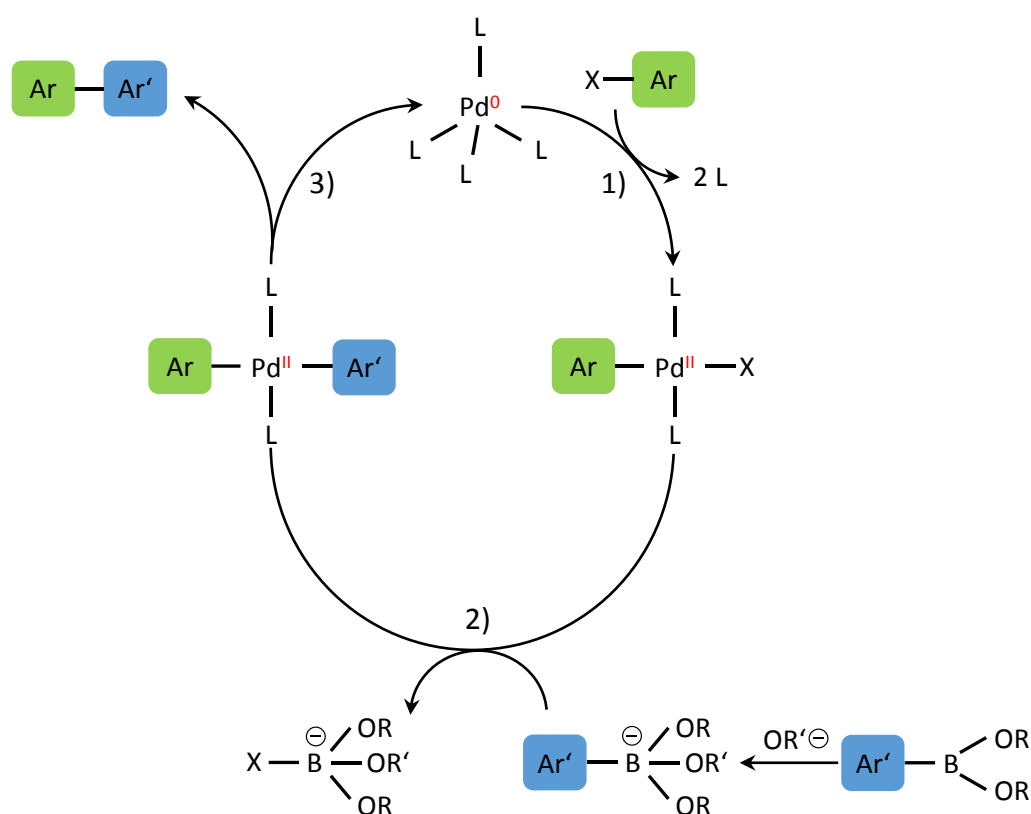


**Figure 13.** Scheme of the catalytic cycle of a Suzuki coupling reaction. The steps are 1) oxidative addition, 2) transmetalation, and 3) reductive elimination. Ar and Ar' represent aryl compounds, L represents a ligand, X a halide (I, Br, Cl).<sup>[119]</sup>

The catalytic cycle of a Suzuki cross-coupling is made up by three fundamental steps: oxidative addition, transmetalation, and reductive elimination. Initially, the palladium inserts into the aryl-halide bond to form a palladium(II) complex. This step is reported to be rate-limiting.<sup>[120]</sup> A weaker, and thus more reactive, aryl-halide bond accelerates this step. The reactivity of the halides in the oxidative addition decreases from iodide to bromide, chloride is by far the least reactive in this sequence. Also, strong electron-donating ligands are assigned to assist this step, as they stabilize higher oxidation states of the palladium.<sup>[121]</sup> Prior to the transmetalation step, the boron reactant undergoes a reaction with the base to form a much more nucleophilic tetravalent borate. This significantly facilitates the transmetalation. In the final step, the reductive elimination, the aryl-aryl bond is formed to yield the coupled product, and the Pd(0) complex is regenerated.

A reaction system for Suzuki couplings typically consists of a biphasic solvent mixture. Within the organic phase (commonly toluene, DMF, dioxane) the reactants, the catalyst and optional ligands are dissolved. The second phase is an aqueous solution of a base. Commonly applied bases are Et<sub>3</sub>N, K<sub>2</sub>CO<sub>3</sub>, and Na<sub>2</sub>CO<sub>3</sub>. In some cases a phase-transfer catalyst is added. An example is Aliquat 336 (*N*-methyl-*N,N,N*-triethylammonium chloride). Two strategies for the palladium catalyst are known. The catalyst can be added

as a complex, such as  $\text{Pd}(\text{PPh}_3)_4$  or  $\text{Pd}_2(\text{dba})_3$ , with the palladium already in the active zerovalent state.<sup>[122]</sup> In the alternative approach a Pd(II) precatalyst is used. Compounds such as  $\text{PdCl}_2$  or  $\text{Pd}(\text{OAc})_2$  are easier to store and less sensitive to oxygen than the Pd(0) species.<sup>[122]</sup> The active catalyst is formed *in situ* upon reaction with a reducing agent.<sup>[123]</sup> Commonly phosphines are used as reducing agents, with triphenylphosphine ( $\text{PPh}_3$ ) as one of the most frequently applied<sup>[122]</sup>. Triphenylphosphine is also a very common ligand. Besides, biaryl based phosphine ligands<sup>[124,125]</sup> and bulky phosphine ligands ( $\text{PCy}_3$ ,  $\text{P}(t\text{-Bu})_3$ )<sup>[126,127]</sup> are frequently used.

### 1.3.4 Suzuki Polycondensation

Several years after the first report on the Suzuki cross-coupling reaction this concept was extended successfully to the synthesis of polyarylenes.<sup>[128]</sup> Until today Suzuki polycondensation (SPC) is an often applied technique for the synthesis of conjugated polymers.<sup>[129]</sup> In general, SPC is considered a step-growth polymerization.<sup>[130]</sup> The two possible approaches are illustrated in Figure 14.

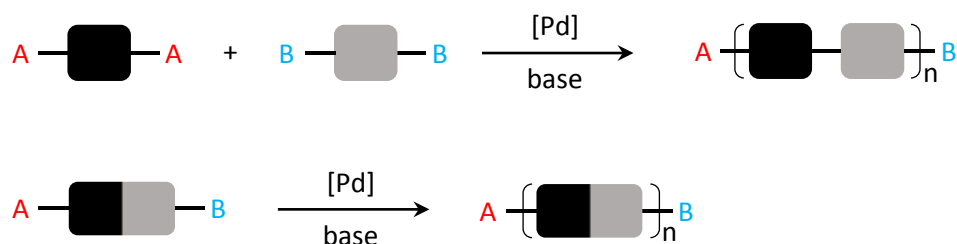


**Figure 14.** Two approaches for Suzuki polycondensation. Top: AA/BB approach, bottom: AB approach. For typical Suzuki polycondensations A stands for a halide (Br, sometimes I, Cl) or triflate, B for a boronic acid derivative.

In the AA/BB approach two types of monomers are coupled, resulting in an alternating sequence of both monomers in the polymer. Here, one monomer carries two halide or triflate functionalities, while the second monomer is equipped with two boronic acid derivatives. This approach is very popular for the synthesis of low bandgap polymers using the donor-acceptor concept. However, also from the AB approach low bandgap polymers with alternating donor and acceptor moieties can be obtained. The asymmetric AB monomers, which carry both functional groups, usually require more synthetic efforts than the synthesis of the symmetric monomers for the AA/BB approach. Another important difference between both approaches comes from Carothers' equation (equation 5).<sup>[131]</sup> It describes the influence of the monomer conversion  $p$  on the number average degree of polymerization  $P_n$  in a step-growth polymerization.<sup>[132]</sup>

$$P_n = \frac{1}{1-p} \quad \text{with } p = \frac{N_0 - N_t}{N_0} \quad \text{Equation 5}$$

This equation is valid if the numbers of both functional groups are equal. Using AB type monomers the stoichiometry is guaranteed. Then  $N_0$  is the initial number of monomers and  $N_t$  is the number of monomers at a given time  $t$ .<sup>[132]</sup> The correlation of the number average degree of polymerization and the conversion is illustrated in Figure 15.

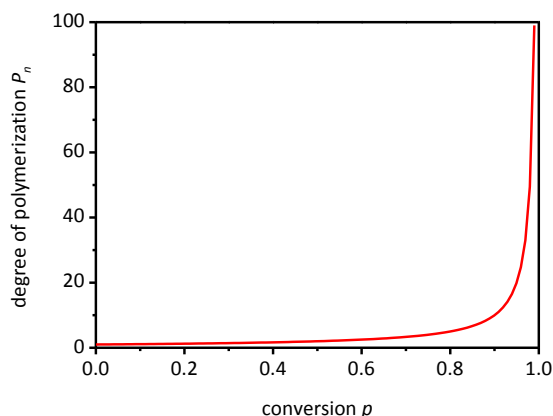


**Figure 15.** Carothers' equation. Correlation of the number average degree of polymerization  $P_n$  and the conversion  $p$ .

In general, in a step-growth polymerization oligomers are formed first, and the  $P_n$  remains low. Only if high conversions of more than 90% are reached, the degree of polymerization increases significantly. Here, oligomers are coupled and polymers are finally formed. From equation 5 can be calculated that a conversion of 90% results in a  $P_n$  of only 10. A  $P_n$  of 50 requires 98% conversion. In theory, a conversion of 100% leads to an infinite  $P_n$ .<sup>[132]</sup> The bottom line is that high molar mass polymers can only be achieved from a very high conversion. In practice this leads to the relatively long reaction times of several days for most of the SPCs reported. To reach high conversions, it is absolutely essential that both functional groups are in an equimolar ratio at any time during the polymerization. Thus, side reactions have to be eliminated, and particular attention has to be paid to purity, weighing, and transferring of the monomers to the reaction flask. These are major concerns especially if the AA/BB approach is used.

Besides the stoichiometry of the functional groups, factors like residual oxygen, side reactions, and the solvent mixture influence the SPC. Especially oxygen traces in the reaction mixture have severe implications. On the one hand, phosphine ligands are prone to oxidation. This also leads to the precipitation of colloidal Pd.<sup>[133]</sup> Moreover, homocoupling reactions are reported to be triggered by oxygen.<sup>[134]</sup> Homocoupling not only leads to defects in the monomer sequence, but also hampers the stoichiometric ratio of both reactive groups.<sup>[135]</sup> This directly leads to a lower degree of polymerization. Besides coupling of two boron functionalized monomers, also the cleavage of the B-C bond is reported.<sup>[136]</sup> Another side reaction is the dehalogenation of organic halides in the presence of a Pd catalyst.<sup>[137]</sup> Also, the mixing of both phases of the biphasic solvent mixture is not to be neglected. The effect of phase-transfer catalysts, like quarternary

ammonium salts, is still discussed controversially. It was assumed that phase-transfer catalysts improve the transfer of the boronate anion from the aqueous to the organic phase.<sup>[138,139]</sup> Other reports claim disadvantages like slowing the reaction, decomposition of the catalyst, poor reproducibility, and foaming.<sup>[138,140]</sup>

Removal of the reactive endgroups is an important step concerning the quality of the polymer obtained. Usually, this is achieved by endcapping with monofunctional reagents. Utilizing bromobenzene and phenylboronic acid the polymers are equipped with stable phenyl endgroups. Residual boron groups can affect the solubility of the polymers. Boronic acids tend to condensate, resulting in broader PDIs or in the worst case insoluble fractions.<sup>[138]</sup> Another prerequisite for materials to be used in organic electronic devices is the removal of traces of the catalyst, especially Pd and P contamination has to be kept to a minimum. Residual Pd is reported to interfere with excited states of the polymers.<sup>[138,141]</sup> Precipitation helps to significantly reduce the Pd content.<sup>[138]</sup> Even lower amounts (< 0.5 ppm) can be reached by treatment with aqueous NaCN<sup>[142]</sup> or by Pd scavengers.<sup>[143]</sup> Scavengers form intensively colored complexes with Pd residues. These complexes can easily be separated from the polymer due to their different solubility.<sup>[143]</sup> However, chemically bound Pd cannot be eliminated by scavengers. Besides Pd also P contamination is a concern. This can occur by aryl-aryl scrambling between the phosphine ligands (e.g. PPh<sub>3</sub>) and the growing polymer.<sup>[129]</sup> Thus, the aryl rest from the ligand can act as an endcapper, and also P atoms can be found in the polymer chain.<sup>[129,144]</sup> Phosphorus can act as chain terminus or as insulating defect within a conjugated polymer.<sup>[129,144]</sup>

In the last years some works on chain-growth Suzuki polycondensations were reported.<sup>[145]</sup> For instance, several strategies for controlled polymerization yielding well-defined polyfluorenes were developed.<sup>[146]</sup> Fischer *et al.* used AB type monomers (bromide/boronic acid pinacol ester) and an arylpalladium(II) catalyst.<sup>[147]</sup> The narrow polydispersities of 1.2 and below – the PDI of step-growth polycondensation products is typically 2 – can be achieved if the catalyst is not released into the reaction mixture after every coupling cycle, but rather stays on the molecule.<sup>[148,149]</sup> The catalyst then “slides” along the  $\pi$ -electron system towards the chain end where the next coupling cycle is initiated.<sup>[150,151]</sup> This concept is particularly appealing for AB type Suzuki polycondensations, even though conventional SPC is by far more understood and chain-growth SPC still suffers from less reproducibility and lower molecular weights.

## 1.3.5 PFDTBT – a fluorene based low bandgap polymer

The work for this thesis is built around fluorene based low bandgap polymers. Polyfluorenes are widely studied as materials for organic light emitting diodes and organic field effect transistors. Fluorenes are rigid, planar molecules and combine good charge-transporting and film-forming properties.<sup>[152]</sup> However, due to their large bandgap energy, fluorene homopolymers are not suitable for application in organic solar cells. By the incorporation of electron deficient units according to the D-A concept fluorene based low bandgap polymers for organic solar cells were achieved. A very popular version was published by Svensson *et al.* as PFDTBT (**poly(2,7-(9-(2'-ethylhexyl)-9-hexyl-fluorene)-*alt*-5,5-(4',7'-di-2-thienyl-2',1',3'-benzothiadiazole)**) in 2003.<sup>[153]</sup> Here, fluorene serves as the electron-rich donor unit, while dithienylbenzothiadiazole is the acceptor. Introduction of the flanking thienyl groups to the strong acceptor benzothiadiazole reduces the steric hindrance between the donor and acceptor parts and leads to a more planar structure.<sup>[110]</sup> The synthesis and the structure of PFDTBT are shown in Figure 16. In the literature this polymer is sometimes also referred to as APFO (alternating polyfluorene).

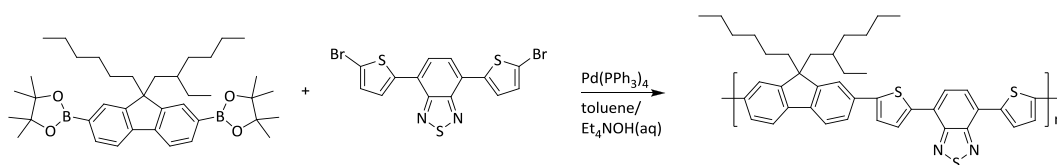
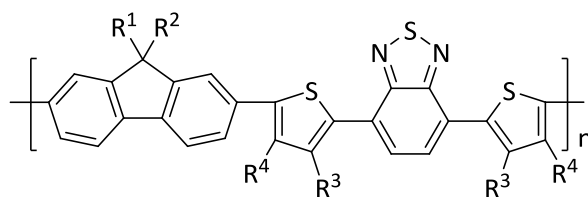


**Figure 16.** Synthesis of PFDTBT as reported by Svensson *et al.*<sup>[153]</sup>

The polymer was synthesized by Suzuki polycondensation. Svensson *et al.* used a 10% excess of the fluorene monomer to limit the molecular weight. With this strategy they achieved a soluble polymer with  $\overline{M}_n$  4,000 g mol<sup>-1</sup> and  $\overline{M}_w$  14,000 g mol<sup>-1</sup>.<sup>[154]</sup> They fabricated BHJ solar cells with a blend of PFDTBT and PCBM (ratio 1:4) on top of ITO coated with PEDOT:PSS. As interlayer between the blend and the aluminium cathode they used LiF. Power conversion efficiencies of 2.2% and a fill factor of 0.46 were reported.<sup>[154]</sup> Based on this structure several variations in the periphery of the  $\pi$ -conjugated backbone and their influence on the polymers' properties were investigated. The following section gives an overview of selected examples of polyfluorene-*alt*-dithienyl-dibenzothiadiazoles.

### 1.3.6 Influences of substituents

A great concern for the first PFDTBT was the solubility of high molecular weight fractions. Svensson *et al.* used non-stoichiometric amounts of both monomers to keep the molecular weight low ( $\overline{M}_n$  4,900 g mol<sup>-1</sup> and  $\overline{M}_w$  12,600 g mol<sup>-1</sup>).<sup>[153]</sup> The low solubility is explained by the high number of unsubstituted aromatic rings in the polymer backbone.<sup>[154]</sup> Significant influence on the solubility is attributed to the choice of substituents. Commonly, alkyl substituents are employed. Flexible and bulky alkyl chains hinder the tendency of the aromatic units to aggregate. However, the number and size of substituents have to be chosen wisely, since there is a trade-off between processability and deterioration of the optical and electronic properties of the polymer.<sup>[155]</sup> Alkyl groups intrinsically do not contribute to absorption and charge transport. In PFDTBT, substituents are most often applied at the C-9 atom of the fluorene and at the C-3 or C-4 atom of the thiophene. A generic structure of PFDTBT with the sites for substitution is shown in Figure 17. The names of the PFDTBT derivatives in the following were adapted from the references cited.



name <sup>a</sup>	ref.	R <sup>1</sup>	R <sup>2</sup>	R <sup>3</sup>	R <sup>4</sup>
HEH-PFDTBT	[153]			H	H
DiH-PFDTBT	[156]			H	H
DiO-PFDTBT	[156]			H	H
PFDTBT-C12	[168]			H	H
BisEH-PFDTBT	[165]			H	H
BisDMO-PFDTBT	[165]			H	H
PF10TBT	[167]			H	H
PF-co-DTB	[172]				H
PFO-DHTBT50	[171]			H	

**Figure 17.** Generic structure of PFDTBT. R<sup>1</sup> to R<sup>4</sup> denote the sites for substitution with alkyl substituents. <sup>a</sup> Nomenclature of the polymers was adapted from the reference cited.

Shortly after their first report on PFDTBT the group of Svensson published a series of PFDTBT derivatives with varying side chains attached to the fluorene unit. The new polymers were no longer asymmetrically substituted as was the original PFDTBT (referred to as HEH-PFDTBT). Svensson *et al.* synthesized dihexyl (DiH-PFDTBT), dioctyl (DiO-PFDTBT), and didodecyl (DiD-PFDTBT) substituted polymers.<sup>[156]</sup> Table 1 summarizes the molecular weights and the characteristic values of this PFDTBT series in BHJ solar cells.

**Table 1.** Summary of the molecular weights and the solar cell parameters of a series of PFDTBT derivatives with different alkyl chains attached to the fluorene. All values from this table were gathered from reference [156].

	molecular weight <sup>a</sup>		solar cell parameters <sup>b</sup>			
	$\overline{M}_n$ [g mol <sup>-1</sup> ]	$\overline{M}_w$ [g mol <sup>-1</sup> ]	$J_{sc}$ [mA cm <sup>-2</sup> ]	$V_{oc}$ [V]	FF	PCE [%]
<b>DiH-PFDTBT</b>	3,500	8,500	3.74	1.02	0.36	1.4
<b>HEH-PFDTBT</b>	4,900	12,500	3.65	1.05	0.44	1.7
<b>DiO-PFDTBT</b>	4,900	11,800	3.55	1.01	0.58	2.1
<b>DiD-PFDTBT</b>	12,000	31,000	2.40	0.98	0.60	1.4

<sup>a</sup> From SEC in 1,2,4-trichlorobenzene at 135 °C using a polystyrene calibration.

<sup>b</sup> BHJ solar cells with a blend ratio of PFDTBT/PCBM 1:4; device set-up: ITO/PEDOT:PSS/PFDTBT:PCBM/LiF/Al, measured under 1.5 AM illumination with an intensity of 100 mW cm<sup>-2</sup>.

They found that under the same conditions of polymerization the molecular weight of the polymers increases when longer alkyl chains are employed. On the other hand, the solar cell experiments reveal that the highest PCE values can be attained by attaching two octyl chains to the fluorene.<sup>[156]</sup> Based on DiO-PFDTBT studies the morphology of blend solar cells were conducted. Changing the solvent for spin coating of the active layer from chloroform to chlorobenzene resulted in a slightly increased PCE of 2.45%.<sup>[157]</sup> The same group also reported a PCE of 3.46% from spontaneously formed multilayers of PCBM rich and DiO-PFDTBT rich layers.<sup>[157,158]</sup> Andersson *et al.* worked on the optimization of the ratio of PFDTBT:PCBM in BHJ blends. They conclude that in the DiO-PFDTBT:PCBM system the electron mobility is lower than the hole mobility.<sup>[159]</sup> Thus, a high acceptor loading of around 80% is necessary to achieve a balanced charge transport.<sup>[159]</sup> With a DiO-PFDTBT:PCBM ratio of 1:4 they reached a PCE of 3.5% in a device of the composition ITO/PEDOT:PSS/DiO-PFDTBT:PCBM/LiF/Al.<sup>[159]</sup>

During the last ten years DiO-PFDTBT was intensely studied as material as well as in devices. For instance, in-depth studies were conducted on the electrochemical and optical properties. Thus, the HOMO (5.4 eV) and LUMO (3.3 eV) levels are well described from cyclic voltammetry measurements.<sup>[160]</sup> The optical band gap was determined from the onset of the absorption spectrum ( $\lambda_{onset} = 657$  nm,  $E_{opt} = 1.8$  eV).<sup>[160]</sup> DiO-PFDTBT was also useful to gain insights into fundamental processes in a BHJ solar cell.<sup>[161]</sup> It helped revealing that geminate recombination has a much stronger impact on the overall efficiency than non-geminate recombination.<sup>[162]</sup> Thus, two approaches for optimization were suggested: optimization of the blend morphology and enhancement of the charge carrier mobility.<sup>[162]</sup> Furthermore, DiO-PFDTBT was used in studies aiming to clarify the origin of the  $V_{oc}$  in polymer/fullerene solar cells.<sup>[163]</sup>

However, the molecular weights of the DiO-PFDTBT types reported are still not very high. Mostly non-equimolar amounts of monomers were used to limit the molecular weight to a range in which the polymers are still soluble.<sup>[164]</sup> Aiming for higher molecular weights several groups tested some other side chains as substituents to the fluorene. Chen *et al.*

investigated the influence of sterically demanding 2-ethylhexyl (BisEH-PFDTBT) substituents compared to the less bulky 3,7-dimethyloctyl (BisDMO-PFDTBT) side chains.<sup>[165]</sup> Once again, they emphasize the interplay of more bulky alkyl chains assisting processability and sterically less demanding substituents increasing the probability of  $\pi$ - $\pi$  stacking and thus enhancing the charge carrier transport.<sup>[165]</sup> Using the same synthetic protocol as Svensson *et al.* they achieved much higher molecular weights with a  $\overline{M}_n$  of 20,000 g mol<sup>-1</sup>.<sup>[165]</sup> Their BisDMO-PFDTBT reaches a PCE of 4.5% in a solar cell of ITO/PEDOT:PSS/BisDMO-PFDTBT:PC<sub>70</sub>BM (1:3)/Ca/Al. Even the cell with BisEH-PFDTBT attains a PCE of 3.5%.<sup>[165]</sup> In both devices the active layers are rather thin (49 nm with BisEH-PFDTBT and 47 nm with BisDMO-PFDTBT).<sup>[165]</sup> However, not only due to the differences in molecular weights these values are not entirely comparable to the PCEs previously reported for PFDTBT based BHJ solar cells, since they used PC<sub>70</sub>BM instead of the less absorbing PCBM.

As a point of reference serves a work by Calabrese *et al.* Here, they used a Bis-EH-PFDTBT with a  $\overline{M}_n$  of 13,600 g mol<sup>-1</sup> and a PDI of 2.5.<sup>[166]</sup> Using a blend ratio of Bis-EH-PFDTBT:PCBM of 1:3 they achieved a PCE of 1.84%.<sup>[166]</sup> With a blend ratio of 1:4 Calabrese *et al.* could improve the PCE to 2.57%.<sup>[166]</sup> The solar cell was composed of ITO/PEDOT:PSS/Bis-EH-PFDTBT:PCBM/LiF/Al and the thickness of the active layer was 100 nm.<sup>[166]</sup>

Slooff *et al.* attached decyl chains to the fluorene. Their PF10TBT has a  $\overline{M}_w$  of 36,900 g mol<sup>-1</sup> with a rather broad PDI of 3.6.<sup>[167]</sup> With a blend ratio of PF10TBT/PCBM 1:4 and a thickness of the active layer of 186 nm the PCE was 4.2%.<sup>[167]</sup> The set-up of the solar cell was ITO/PEDOT:PSS/PF10TBT:PCBM/LiF/Al.<sup>[167]</sup>

Recently, Yu *et al.* reported a PFDTBT synthesized by Stille coupling. They obtained the didodecyl substituted PFDTBT-C12 with a  $\overline{M}_n$  of 10,000 g mol<sup>-1</sup> and a PDI of 2.1.<sup>[168]</sup> Except for the somewhat lower PDI the PFDTBT synthesized by this method does not surpass the DiD-PFDTBT by Svensson *et al.* Furthermore, Yu *et al.* report a PCE of the PFDTBT-C12:PCBM (1:3) blend of 0.62%.<sup>[168]</sup>

Table 2 summarizes the molecular weights and solar cell parameters of the exemplarily mentioned PFDTBTs from this section.

**Table 2.** Summary of the molecular weights and the solar cell parameters of selected PFDTBT derivatives.

	molecular weight		solar cell parameters <sup>c</sup>			
	$\overline{M}_n$ [g mol <sup>-1</sup> ]	$\overline{M}_w$ [g mol <sup>-1</sup> ]	$J_{sc}$ [mA cm <sup>-2</sup> ]	$V_{oc}$ [V]	FF	PCE [%]
<b>BisEH- PFDTBT</b> <sup>[165]</sup>	21,000	31,500 <sup>a</sup>	8.40	0.95	0.44	3.5 <sup>d</sup>
<b>DiEH- PFDTBT</b> <sup>[166]</sup>	13,600	34,000 <sup>a</sup>	4.99 5.16	0.98 1.07	0.38 0.46	1.8 <sup>e</sup> 2.6 <sup>f</sup>
<b>BisDMO- PFDTBT</b> <sup>[165]</sup>	20,000	26,000 <sup>a</sup>	9.10	0.97	0.51	4.5 <sup>d</sup>
<b>PF10TBT</b> <sup>[167]</sup>	9,700	34,900 <sup>a</sup>	7.70	0.99	0.54	4.2 <sup>g</sup>
<b>PFDTBT- C12</b> <sup>[168]</sup>	10,100	21,200 <sup>b</sup>	2.48	0.77	0.32	0.6 <sup>h</sup>

<sup>a</sup> Method not specified.<sup>b</sup> From SEC using a polystyrene calibration.<sup>c</sup> BHJ solar cells, measured under 1.5 AM illumination with an intensity of 100 mW cm<sup>-2</sup>.<sup>d</sup> Blend ratio of PFDTBT/PC<sub>70</sub>BM 1:3; device set-up: ITO/PEDOT:PSS/PFDTBT:PC<sub>70</sub>BM/LiF/Al.<sup>e</sup> Blend ratio of PFDTBT/PCBM 1:3; device set-up: ITO/PEDOT:PSS/PFDTBT:PCBM(130nm)/LiF/Al.<sup>f</sup> Blend ratio of PFDTBT/PCBM 1:4; device set-up: ITO/PEDOT:PSS/PFDTBT:PCBM(100nm)/LiF/Al.<sup>g</sup> Blend ratio of PFDTBT/PCBM 1:4; device set-up: ITO/PEDOT:PSS/PFDTBT:PCBM(186nm)/LiF/Al.<sup>h</sup> Blend ratio of PFDTBT/PCBM 1:3; device set-up: ITO/PEDOT:PSS/PFDTBT:PCBM/Ca/Al.

Beyond alkyl chains at the fluorene unit of PFDTBT also the introduction of side chains to the aromatic rings of the acceptor moiety is an important aspect. Additional solubilizing groups can help improving the molecular weight and at the same time help retaining solubility and processability.<sup>[110]</sup> Considering the DTBT unit, substituents can be introduced at the 5- and 6-position of the benzothiadiazole as well as at the 3- or 4-position of the thiophene. A drastic increase of steric hindrance is observed when alkyl chains are attached to the benzothiadiazole.<sup>[169]</sup> This significantly hampers the conjugation between the donor and acceptor units, resulting in an increased bandgap.<sup>[110]</sup> Thus, in the following only the influence of substitution at the thiophene will be discussed. Again, the effect of the steric hindrance of the substituents on the dihedral angle between thiophene and benzothiadiazole and between thiophene and fluorene is crucial.<sup>[107]</sup> Zhou *et al.* found that the steric hindrance of substituents at the 4-position causes just a small increase of the dihedral angles compared to the non-substituted DTBT.<sup>[169]</sup> Substitution at the 3-position of the thiophene results in a sterically more hindered conformation and thus a larger bandgap.<sup>[169]</sup> Furthermore, the additional solubilizing side chains can also influence the performance of polymer:PCBM BHJ solar cells. Polymers without side chains have a tendency to aggregate in a solution at room temperature.<sup>[110]</sup> This also leads to a smaller surface area between donor and acceptor phases in the blend which negatively impacts the overall efficiency of a BHJ solar cell.<sup>[110]</sup> Concerning the length and shape of the side chains, the same trend is valid as discussed for the substituents at the fluorene. Size and branching strongly influence the solid state organization of the polymers: Straight and short chains enable stronger intermolecular interactions than branched and long side

chains.<sup>[170]</sup> By choosing the appropriate side chain not only solubility and molecular weight can be influenced, but also absorption and charge transport.<sup>[110]</sup> The influence of the length and shape of alkyl chains on intermolecular interactions and solubility is schematically illustrated in Figure 18.

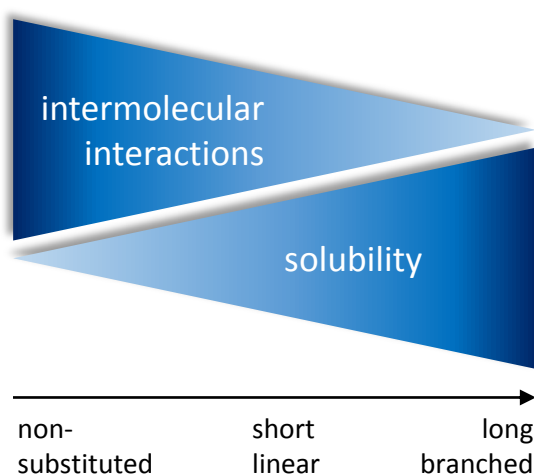


**Figure 18.** Influence of length and shape of the alkyl side chains on intermolecular interactions and solubility. Intermolecular interactions are in close relation with important material properties, for instance, absorption and charge carrier transport.<sup>[110]</sup>

Hou *et al.* reported a PFDTBT with hexyl groups at the 4-position of the thiophenes. Due to the more soluble DTBT monomer they obtained a soluble polymer with a number average molecular weight  $\overline{M}_n$  of 40,000 g mol<sup>-1</sup> *via* Suzuki polycondensation.<sup>[171]</sup> Back then, this PFDTBT was tested as red emitter in organic light emitting diodes. As a material for organic solar cells it was first mentioned by Shi *et al.* They introduced oxydecyl groups at the 3-position of the thiophenes and reached very high molecular weights of  $\overline{M}_n$  68,000 g mol<sup>-1</sup>.<sup>[172]</sup> In a blend ratio of Polymer:PCBM 1:4 the PCE was 1.60%.<sup>[172]</sup>

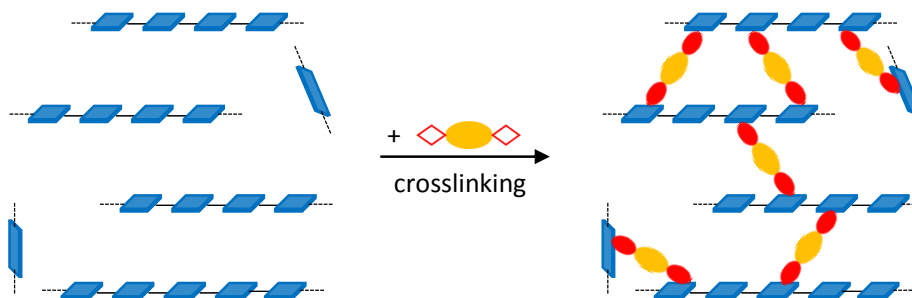
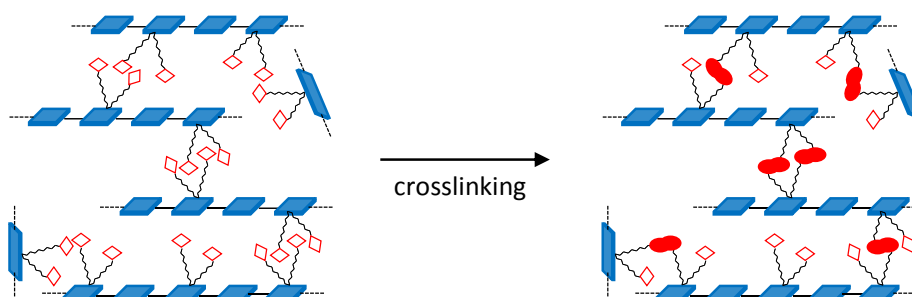
Besides the common application of PFDTBT as electron donor material McNeill *et al.* used a PFDTBT derivative as an acceptor polymer in a BHJ solar cell with P3HT as donor.<sup>[173]</sup> They took advantage of the ambipolar transport ability of PFDTBT.<sup>[174,175]</sup> Solar cells of a blend with equal amounts of P3HT and PFDTBT reached efficiencies of 1.20% after annealing.<sup>[173]</sup> Mori *et al.* pointed out that thermal annealing of a P3HT:PFDTBT blend induces crystallization of P3HT domains and simultaneously leads to more pure areas of the amorphous PFDTBT.<sup>[176]</sup> Both processes are deemed beneficial for suppressing recombination.<sup>[176]</sup> Sommer *et al.* extended this concept and synthesized PFDTBT-*block*-P3HT block copolymers.<sup>[177]</sup>

## 1.4 Crosslinking of organic semiconductors

Crosslinking is a well-established concept for the processing of organic semiconductors. This section will summarize the potential and discuss the different approaches to crosslinking of conjugated polymers. The crosslinking of conjugated polymers *via* reactive oxetane groups will be presented in detail.

Usually, crosslinking is applied to a film after it was cast from solution. The key point of crosslinking is the transformation of a soluble material into an insoluble network. Taking advantage of this, a number of applications were developed: fabrication of multilayers from solution and patterning of organic semiconductors via photolithography. In recent years crosslinking emerged as a concept for stabilization of bulk heterojunction blends in organic solar cells. Each of these concepts will be addressed within this chapter.

In general, two approaches to the crosslinking of organic semiconductors are known. They are illustrated in Figure 19. Crosslinking can be achieved by bi- or multivalent crosslinking agents. In Figure 19a this is schematically shown for the crosslinking of polymer chains with a bivalent crosslinking agent. Another concept is the introduction of functional groups. Upon reaction between the functional groups a network is formed. This is depicted in Figure 19b.

a) Crosslinking *via* a crosslinking agentb) Crosslinking *via* functional groups

soluble polymer

insoluble polymer network

**Figure 19.** General approaches for crosslinking of conjugated polymers: **a)** Crosslinking *via* a bivalent crosslinking agent, **b)** crosslinking *via* reactive functional groups.

Using a crosslinking agent is a rather straightforward concept. A compound bearing two or more reactive groups is added to the polymer solution before a film is cast. As an example, a bisazide crosslinker and its activation reaction are shown in Figure 20a. In this particular case the crosslinking reaction is triggered by UV irradiation. Cleavage of nitrogen leads to a highly reactive bisnitrene species. The reactive nitrene inserts to C-H bonds of the surrounding polymer and the polymer chains are thus linked to each other. By the amount of crosslinker the crosslinking density can be controlled. With this approach Tan *et al.* fabricated multilayer solar cells from polymer solutions. Usually, two layers of organic material cannot be cast on top of each other, since the solvent of the second layer would redissolve the previously cast film. In only a few cases this can be circumvented by the use of orthogonal solvents. Crosslinking provides a tool to render a cast film insoluble, enabling the next layer to be applied from the same or a similar solvent. The polymers and the device are illustrated in Figure 20b and Figure 20c. Tan *et al.* applied P3HT as the donor and P(NDI2OD-T2) as acceptor, a thin interlayer of PCDTBT was introduced to suppress recombination.<sup>[178]</sup>

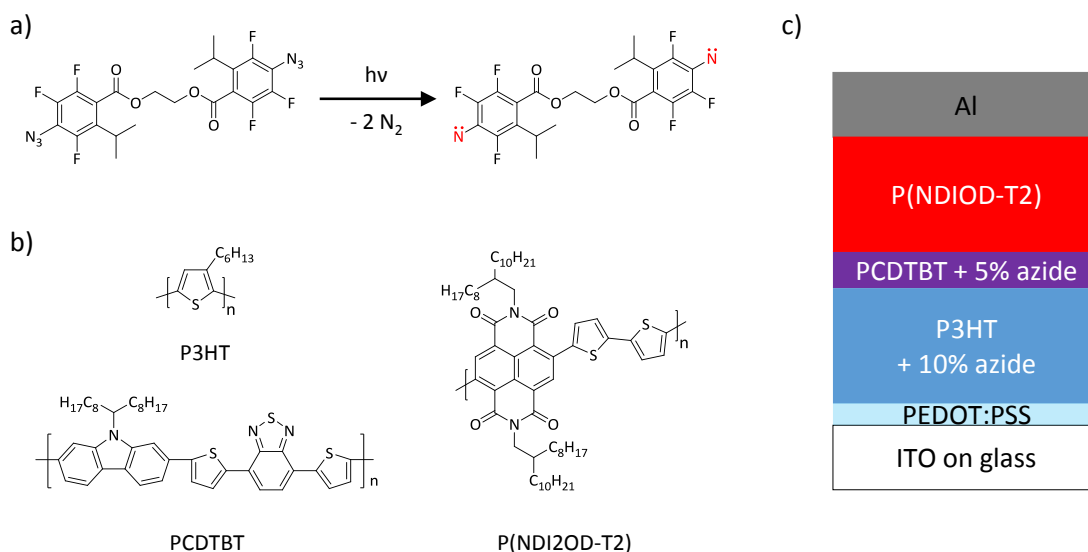


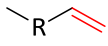
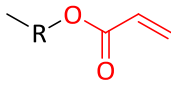
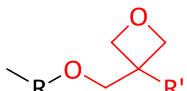
**Figure 20.** Multilayer organic solar cell fabricated from solution by crosslinking. **a)** Sterically substituted bis(fluorophenyl azide) and the formation of the crosslinking bisazide. **b)** The polymers P3HT (electron donor), PCDTBT (interlayer), and P(NDI2OD-T2) (electron acceptor). **c)** Schematic drawing of the stack of materials of the multilayer solar cell.<sup>[178]</sup>

The device was built by sequential spin coating, crosslinking and rinsing steps.<sup>[178]</sup> On top of the ITO/glass substrate coated with PEDOT:PSS first the P3HT layer was applied by spin coating. To the P3HT solution 10% of the crosslinking agent were added. Photocrosslinking rendered the P3HT film insoluble.<sup>[178]</sup> The non-crosslinked fractions were washed off with solvent and the thickness of the crosslinked P3HT film was 13 nm.<sup>[178]</sup> Then a layer of PCDTBT was cast from a solution containing 5% of bisazide. This layer was photocrosslinked, again, and rinsed as described for the first one before a 36 nm thick layer of P(NDI2OD-T2) was cast on top.<sup>[178]</sup> The most efficient device of this series with a 3 nm thick interlayer of PCDTBT reached a PCE of only 0.45%.<sup>[178]</sup>

Crosslinking agents proved to be a viable method for crosslinking conjugated polymers. It is also very versatile, since compounds like the mentioned bisazide can easily be added to any polymer solution. A drawback of this concept arises from the high reactivity, and thus low selectivity, of the bisnitrene formed. Tang *et al.* point out that crosslinking mainly takes place between the alkyl side chains.<sup>[179]</sup> However, nitrene might also add into a C-H bond of the conjugated backbone. This would be detrimental for the optic and electronic properties.

The alternative approach is crosslinking *via* functional groups. When it comes to conjugated polymers, crosslinkable groups are usually attached to the ends of the solubilizing alkyl chains. This requires more synthetic effort, since the functional groups have to be introduced during monomer synthesis or after the polymerization. Common functional groups for crosslinking are alkyl bromide,<sup>[180]</sup> azide,<sup>[181]</sup> acrylate,<sup>[182]</sup> vinyl,<sup>[183]</sup> and oxetane.<sup>[184]</sup> Table 3 summarizes the functional groups and compares them concerning their crosslinking mechanism, initiation, and selectivity.

**Table 3.** Selection of functional groups for crosslinking of conjugated polymers.

functional group	crosslinking mechanism	initiation	additional initiator	selectivity
	radical	hν	no	no
	radical	hν ΔT	no	no
	radical	hν ΔT	no	yes
	radical	hν ΔT hν + initiator	no no yes	yes
	cationic	hν + PAG ΔT + TAG acid vapor	yes yes no	yes

PAG: photoacid generator, TAG: thermal acid generator.

These functional groups can further be classified into two groups: Bromide and azide functionalities lead to non-selective radical species, while vinyl, acrylate, and oxetane groups undergo bimolecular reactions with functionalities of their kind.<sup>[181]</sup>

Upon UV irradiation the C-Br bond of the bromide functionalized side chain is cleaved homolytically.<sup>[185]</sup> For this cleavage no additional initiator is required. The radicals formed non-selectively react with neighboring molecules.<sup>[102]</sup> Also bromine radicals might have negative effects on the optic and electrical properties of the conjugated materials.<sup>[102]</sup>

Similar to the azide based crosslinker molecule described above, azide groups in the periphery of a conjugated polymer are activated by UV or heat treatment.<sup>[186]</sup> Cleavage of nitrogen results in extremely reactive nitrenes. The crosslinking proceeds through insertion of the nitrene into C-H bonds.<sup>[181]</sup> An advantage of this system is that no initiator has to be added. However, the high reactivity of the nitrene results in poor selectivity. Thus, unwanted reactions with the conjugated system cannot be ruled out.<sup>[187]</sup>

Introducing vinyl groups as crosslinking units is particularly interesting for crystalline materials.<sup>[183]</sup> The structure and the steric demands of a terminal vinyl group is very close to that of a linear alkyl group.<sup>[183]</sup> Large functional groups are expected to decrease the crystallinity of the polymer. In the case of P3HT, for instance, this leads to a lower hole mobility.<sup>[183]</sup> For vinyl groups the crosslinking is initiated by UV light or thermal activation.<sup>[102,183]</sup> The crosslinking reaction itself is highly selective.<sup>[102]</sup> Furthermore, no initiator has to be added and no side products occur during the crosslinking process.<sup>[102]</sup>

The crosslinking mechanism of acrylate is similar to vinyl. Acrylates can be crosslinked by UV or thermal treatment.<sup>[187,188]</sup> In numerous works, though, crosslinking of acrylate

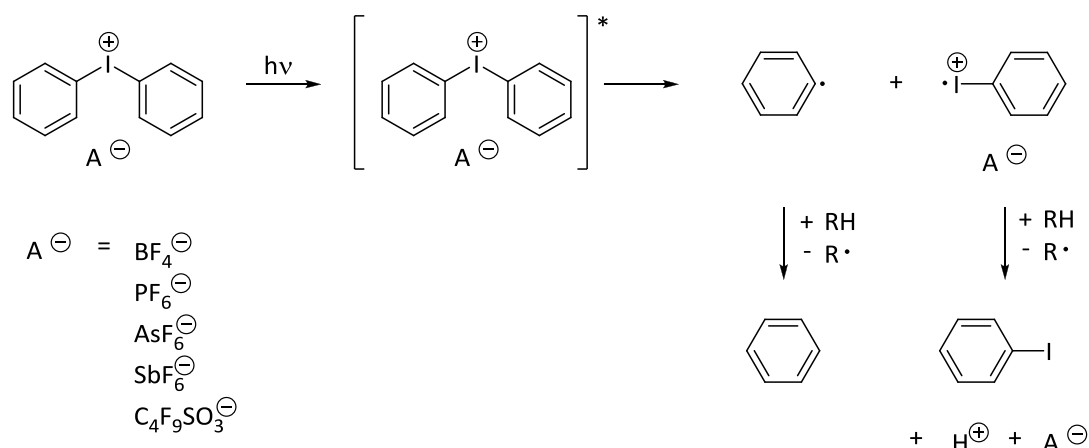
groups is achieved by a combination of UV irradiation and a photo labile initiator.<sup>[189]</sup> Such a system can, for instance, be used for patterning of oligofluorenes via photolithography.<sup>[190]</sup> This topic will be addressed in section 1.6 Patterning of organic semiconductors.

#### 1.4.1 Oxetane as crosslinkable group

In contrast to the crosslinkable groups previously mentioned, oxetanes are not crosslinked by a radical mechanism. Instead, crosslinking takes place by cationic ring-opening polymerization (CROP). Usually, the protons for the initiation of the CROP originate from acid generating molecules. Frequently used are arylodonium and arylsulfonium salts. These compounds are activated either by UV irradiation (photoacid generator, PAG) or by thermal treatment (thermal acid generator, TAG). They are added to the polymer solution prior to film preparation. The activation mechanism of a diphenyliodonium based PAG, which was used in this work, and a scheme of the CROP of oxetanes are shown in Figure 21.

Upon light exposure the diphenyliodonium salt is excited. The major decay path of this species proceeds *via* a homolytic decay of a C-I bond.<sup>[191]</sup> Resulting iodobenzene radical cations further react to form the desired protons and iodobenzene.<sup>[191]</sup> Typically, diaryliodonium salts absorb at wavelengths below 350 nm.<sup>[193]</sup> In combination with a  $\pi$ -conjugated material the decay reaction can be sensitized.<sup>[194]</sup> Considering organic semiconductors, the material which has to be crosslinked can serve as sensitizer. This process, called photoinduced electron transfer, utilizes the excitation of the conjugated material, which usually absorbs at longer wavelengths compared to the PAG.<sup>[193]</sup> By an electron transfer from the excited conjugated molecule to the PAG the decay reaction is induced and a proton is generated.<sup>[194]</sup> Since the material that has to be crosslinked is present in large excess, an efficient transfer to the PAG is provided.<sup>[194]</sup>

## a) Generation of a proton from a diphenyliodonium salt



## b) Cationic ring-opening polymerization of oxetane

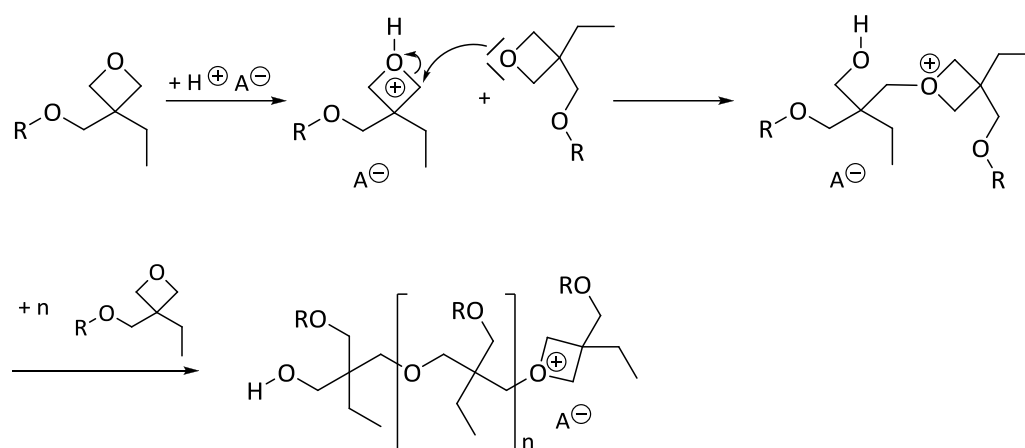


**Figure 21.** a) Formation of protons from a photolabile diphenyliodonium salt. Reproduced from references<sup>[191,192]</sup>.  
 b) Cationic ring-opening polymerization of oxetane. Reproduced from reference<sup>[193]</sup>.

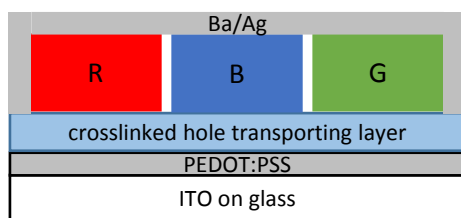
In the first step of the cationic ring-opening polymerization (Figure 21b) a proton adds to the oxygen atom of the oxetane ring forming an oxonium cation.<sup>[132]</sup> Upon reaction with another oxetane the ring is opened and the positive charge is transferred to the oxygen of the still closed ring of the dimer. The polymerization proceeds in the same way and a poly(ether) is formed.<sup>[132]</sup>

Commonly, crosslinking of oxetanes induced by PAGs is executed in two steps: illumination and curing. During the illumination step protons are generated. In the subsequent curing the sample is heated. This helps protons to reach oxetane groups to initiate the CROP. Also the molecules to be crosslinked are more mobile. This increases the probability of an activated oxetane group to find a reaction partner. However, with every crosslink formed the system becomes more and more immobile. Crosslinking is terminated when the network hinders oxetane groups from coming into contact in order to react.<sup>[195]</sup>

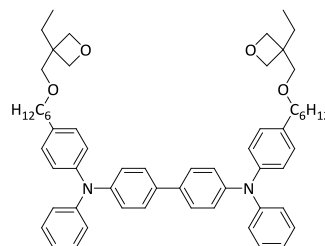
Oxetane was chosen as the crosslinkable group for the low bandgap polymers in this work because of several reasons. First, it is stable and manageable during synthesis and workup. Other than acrylate or vinyl groups, oxetane tolerates the conditions of Suzuki polycondensation and does not undergo side reactions.<sup>[195]</sup> Thus, protective groups and subsequent deprotection of the polymer are not needed. Furthermore, the polymers should be able to efficiently crosslink in a blend with PCBM. If the crosslinking proceeds via a radical mechanism, as it is the case, for instance, with acrylates, the strong electron accepting fullerene derivatives would react with these radicals. The chances are slim that a single PCBM molecule quenches two or more radicals to form a crosslink.<sup>[181]</sup> With oxetanes the network formation is based on cations and thus is not affected by the presence of fullerenes.<sup>[196]</sup> Further advantages of oxetane as crosslinkable group are the fast cationic polymerization in bulk with a high conversion and only a small impact on the optoelectronic properties of the crosslinked materials.<sup>[196]</sup>

Small molecules and polymer organic semiconductors with oxetane groups attached to their side chains were used as crosslinkable materials in organic light emitting diodes. Usually, an OLED is composed of a stack of organic layers. Crosslinking is a key strategy for aligning layers of organic material on top of each other from solution. Multilayer devices can be fabricated by repetitive steps of casting and crosslinking. Owing to the sequence of functional layers in an OLED, most of the crosslinkable materials known are hole transport materials and emitters.<sup>[193]</sup> Based on this concept the group of Meerholz fabricated multicolor polymer OLED displays with red, blue, and green pixels from solution.<sup>[195]</sup> A schematic drawing of the device set-up is shown in Figure 22a. Such a device was fabricated by a sequence of selective crosslinking steps of oxetane functionalized materials. As first organic layer the hole transporting triphenylamine derivative<sup>[197]</sup> (Figure 22b) was applied on top of the glass substrate coated with ITO and PEDOT:PSS. The photoacid generator for crosslinking the hole transport material and the following emitter materials was a diphenyliodonium salt. It was added in concentrations of 0.2 wt% to 0.5 wt%.<sup>[195]</sup> On top of the crosslinked and insoluble hole transport layer the first electroluminescent polymer was coated.<sup>[195]</sup> As an example the blue emitting polymer is shown in Figure 22c. For crosslinking the emitter polymers UV illumination was conducted using a shadow mask. This resulted in the formation of crosslinked and non-crosslinked areas. The non-crosslinked parts of the film remained soluble and were rinsed off with THF.<sup>[195]</sup> This procedure was repeated for the other polymers. Finally, the electrode consisting of barium and silver was evaporated on top.<sup>[195]</sup>

a) Scheme of the three color OLED



b) Crosslinkable hole transporting material



c) Crosslinkable blue emitting polymer

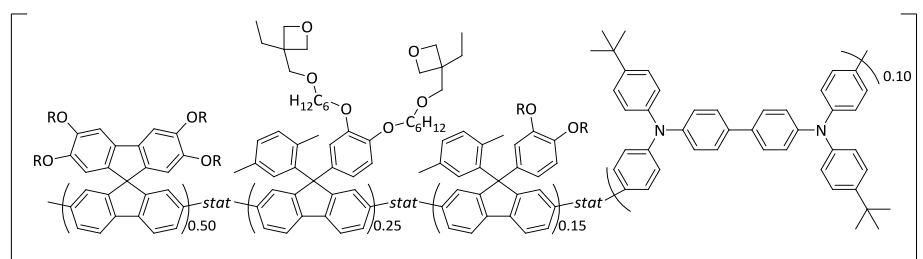


**Figure 22.** Full-color OLED display fabricated by solution processing and crosslinking. **a)** Schematic drawing of the device. R, B, G represent a red, blue, and a green pixel. **b)** Crosslinkable triphenylamine derivative used as hole transporting layer. **c)** Crosslinkable blue emitting polymer, R = 2-methylbutyl. Reproduced from references<sup>[195,197]</sup>

Charas *et al.* published several works on oxetane functionalized organic semiconducting polymers.<sup>[198]</sup> They first focused on fluorene based polymers with a crosslinkable monomer (F8Ox, Figure 23).<sup>[198]</sup> Later they attached oxetane groups to the side chains of the fluorene moiety to achieve crosslinkable fluorene based low bandgap polymers (F8T2Ox2, F8T2Ox1, Figure 23).<sup>[199]</sup> With these crosslinkable low bandgap polymers Charas *et al.* investigated oxetane crosslinking in organic solar cells. In their first concept they coated blends of F8T2Ox1 or F8T2Ox2, respectively, with the inert polystyrene on top of ITO/PEDOT:PSS.<sup>[200,201]</sup> Before coating, a PAG (4.6 wt% with respect to P8FT2Ox1) was added to the solution.<sup>[201]</sup> Crosslinking of P8FT2Ox1 was conducted by illumination with UV-light (254 nm) at 100 °C for one minute and curing for five minutes.<sup>[201]</sup> Subsequently, polystyrene was washed away with THF, leaving behind the crosslinked polyfluorene.<sup>[201]</sup> The voids in the polyfluorene film are then filled with PCBM from solution.<sup>[201]</sup> Charas *et al.* first proposed that for a BHJ blend the phase separation is better assisted by an inert polymer than by PCBM itself<sup>[201]</sup> and a well-defined morphology is achieved.<sup>[202]</sup> However, they investigated blends of P8FT2Ox1:PCBM where the polymer was crosslinked after spin coating and ended up with significantly more efficient solar cells.<sup>[201]</sup> Besides the crosslinkable fluorene based polymers the group of Charas also synthesized an oxetane functionalized P3HT derivative (P3HT-Ox), which is also shown in Figure 23.<sup>[202]</sup>

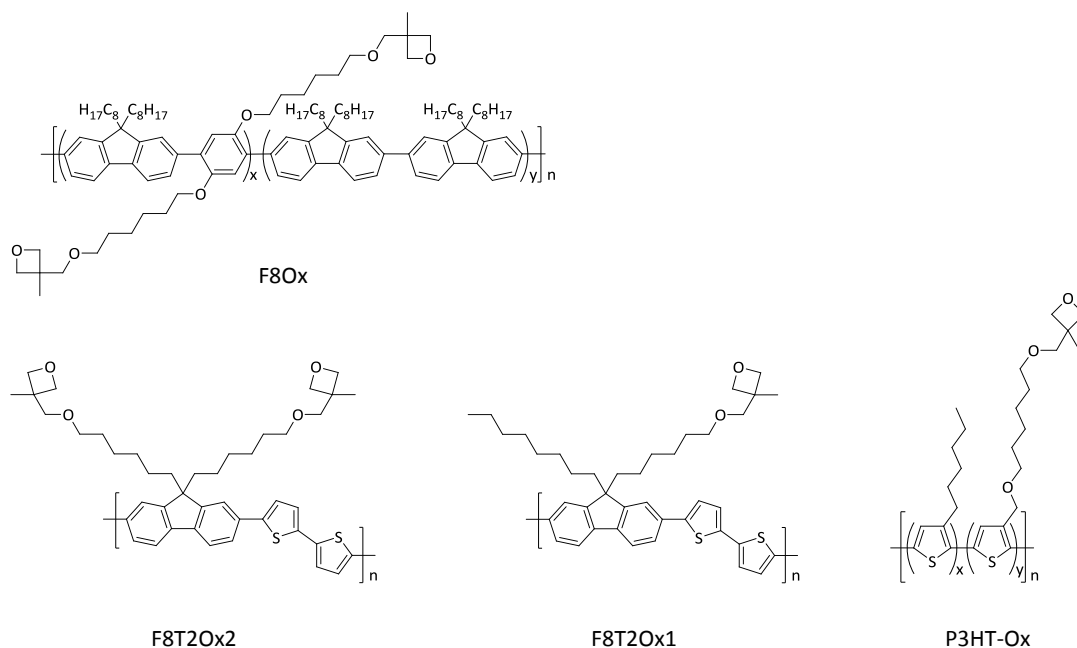


**Figure 23.** Conjugated polymers with crosslinkable oxetane groups: Poly(fluorene) (F8Ox) with a crosslinkable comonomer,<sup>[198]</sup> fluorene-based low bandgap polymers with two oxetane groups (F8T2Ox2)<sup>[200]</sup> and one oxetane group (F8T2Ox1),<sup>[199]</sup> poly(3-hexylthiophene) derivative (P3HT-Ox)<sup>[202]</sup> containing oxetane functionalized comonomers.

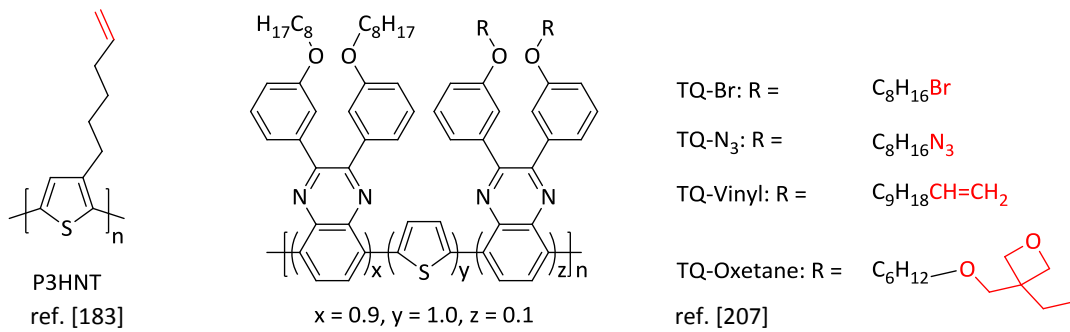
However, some drawbacks arise from the use of oxetane as crosslinkable group. A great concern is the photoacid generator. Residual photoacid and side products from the decay reaction remain in the active material and might negatively influence properties such as molecular order, charge transport, and stability.<sup>[102]</sup> Another issue might be the cationic character of the active centers of the ring-opening reaction.<sup>[102]</sup> Meerholz *et al.* suggest neutralization of the films after crosslinking by rinsing with base or nucleophiles such as THF.<sup>[193]</sup> Thermal treatment is assumed to achieve the same effect.<sup>[193]</sup>

An approach to initiate the CROP of oxetanes without adding a photoacid generator was described by Yau *et al.* They reported crosslinking of an oxetane functionalized low bandgap polymer by exposing it to trifluoroacetic acid (TFA) vapor.<sup>[203]</sup> The acid can permeate through the film and act as ring-opening catalyst. After the crosslinking process, excess TFA can be removed from the sample by a vacuum step.<sup>[203]</sup>

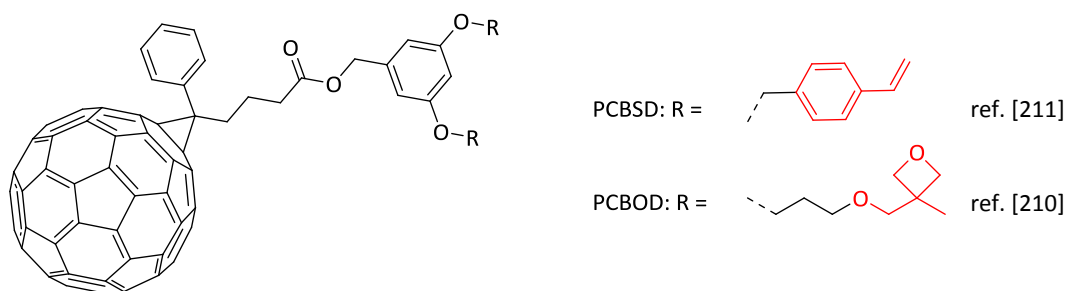
### 1.5 Stabilization of the morphology of BHJ solar cells by crosslinking

Crosslinking emerged as a promising concept for the stabilization of the morphology of bulk heterojunction solar cells.<sup>[102]</sup> As discussed earlier, the nanostructure of BHJ blends has significant influence on the device performance. There are several ways for achieving such a beneficial morphology.<sup>[204]</sup> However, nanophase separation of polymers and fullerenes is a non-equilibrium state and prone to degradation.<sup>[205]</sup> Crosslinking provides a tool for locking the morphology by hindering detrimental diffusion processes in the blend, resulting in macrophase separation or aggregation of the fullerenes.<sup>[102]</sup> In the literature different approaches are described: crosslinking donor to donor, crosslinking acceptor to acceptor, crosslinking donor to acceptor, and crosslinking a donor-acceptor blend by a reactive additive.<sup>[187]</sup> Examples for materials used in the different concepts are shown in Figure 24. The focus of the following section is on the donor to donor crosslinking concept which is also applied within this work.

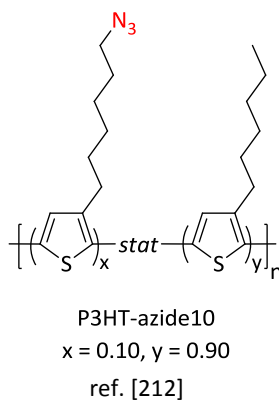
## a) Crosslinking donor to donor



## b) Crosslinking acceptor to acceptor



## c) Crosslinking donor to acceptor



## d) Crosslinking of blends via crosslinking agents

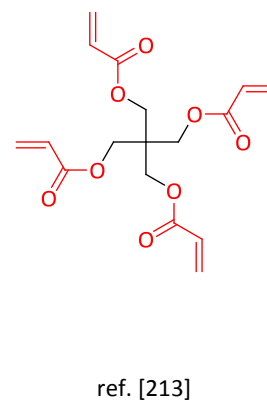


**Figure 24.** Selection of crosslinkable materials for the stabilization of BHJ solar cells.

In the donor to donor crosslinking approach crosslinkable groups are attached to the side chains of the donor material.<sup>[187]</sup> The basic idea is that the polymer network formed by crosslinking hinders the diffusion of PCBM. It was shown first by Miyanishi *et al.* on a poly(thiophene) (P3HNT) bearing vinyl groups (Figure 24a).<sup>[183]</sup> Commonly, crosslinked and non-crosslinked reference cells are compared in accelerated aging experiments. Here, both types of solar cells are exposed to thermal treatment for several hours. During this experiment, the change of the device parameters is monitored. Miyanishi *et al.* annealed their P3HNT in a blend with PCBM (polymer:PCBM 1:0.8) for 10 hours at 150 °C and compared it with a P3HT:PCBM blend of the same composition.<sup>[183]</sup> The initial efficiencies

of both devices were comparable (P3HNT:PCBM 3.03%, P3HT:PCBM 3.11%).<sup>[183]</sup> After thermal annealing, the efficiency of P3HT:PCBM dropped to 1.00%, while P3HNT:PCBM retained an efficiency of 1.74%.<sup>[183]</sup> They ascribe the smaller decrease in efficiency to the slowed formation of large PCBM aggregates.<sup>[183]</sup> However, the formation of PCBM aggregates could not be suppressed entirely.<sup>[183]</sup>

Carlé *et al.* compared in their study the influence of different crosslinkable groups. They investigated the low bandgap polymer TQ1 (poly[2,3-bis-(3-octyloxyphenyl)quinoxaline-5,8-diyl-*alt*-thiophene-2,5-diyl])<sup>[206]</sup> bearing bromo, azide, vinyl, or oxetane groups. As a reference material they synthesized the non-crosslinkable TQ1 (Figure 24a).<sup>[207]</sup> Films were fabricated by spin coating of polymer:PCBM (1:1) solutions. To the TQ-Oxetane:PCBM solution 5 wt% of a photoacid generator were added. The blends of TQ-Br, TQ-N<sub>3</sub>, TQ-Vinyl, and TQ-Oxetane were crosslinked by irradiation at a wavelength of 254 nm for 10 minutes.<sup>[207]</sup> In this article Carlé *et al.* used optical micrographs to monitor the formation of PCBM aggregates in annealed polymer:PCBM films. After annealing at 150 °C for 13 hours, large PCBM crystallites were observed in the non-crosslinked TQ1 blend.<sup>[207]</sup> Also in the crosslinked TQ-Br blend PCBM aggregates were visible. In TQ-N<sub>3</sub>, TQ-Vinyl, and TQ-Oxetane no PCBM aggregates were observed.<sup>[207]</sup> Furthermore, they compared the power conversion efficiencies of organic solar cells from this set of polymer:PCBM blends. The cells were annealed at 100 °C for a total of 50 hours.<sup>[207]</sup> From this accelerated aging experiment the study only provides normalized PCE values. In the cases of TQ1, TQ-Br, and TQ-Oxetane the PCE dropped to 20% of the initial efficiency after 20 hours. At this point TQ-N<sub>3</sub> retained 40% of its efficiency and TQ-Vinyl about 50%.<sup>[207]</sup> From 20 hours to 50 hours only marginal changes of the PCE were observed.<sup>[207]</sup>

These two examples show, along with similar studies,<sup>[185,208,209]</sup> that crosslinking of the donor material can indeed help to improve the long term stability of BHJ solar cells. However, it was not shown that PCBM aggregation can be prevented completely.<sup>[187]</sup> Thus, the obvious approach to prevent crystallization of PCBM is crosslinking the acceptor.<sup>[187]</sup> To achieve crosslinkable acceptor materials, several functionalized PCBM derivatives were investigated.<sup>[210]</sup> As crosslinkable moieties acetylene, styrene, epoxy, oxetane, and silyl groups are known.<sup>[187]</sup> Examples for crosslinkable PCBM derivatives are illustrated in Figure 24b. The oxetane functionalized PCBM is crosslinked by catalytic amounts of a photoacid generator und UV irradiation.<sup>[187]</sup> Crosslinking of the styrene functionalized PCBM is thermally induced.<sup>[187]</sup> Cheng *et al.* used a styrene functionalized PCBM (PCBSD) in ternary blends with the composition P3HT:PCBM:PCBSD 6:5:1.<sup>[211]</sup> The films were annealed for 10 minutes at 110 °C for morphology optimization. A second annealing step for 10 minutes at 150 °C induced the polymerization of the styrene groups, resulting in fixation of the morphology.<sup>[211]</sup> The initial power conversion efficiency of BHJ solar cells was 3.32%.<sup>[211]</sup> In an accelerated aging experiment the PCE increased upon further annealing at 150 °C.<sup>[211]</sup> The highest efficiency (4.01%) was achieved after 10 hours at 150 °C. After 25 hours, a PCE of 3.70% was attained.<sup>[211]</sup> A reference device of P3HT:PCBM

in a 1:1 ratio during the same experiment suffered a drastic loss in efficiency, dropping from 4.08% in the beginning to 0.69% after 25 hours at 150 °C.<sup>[211]</sup>

Another approach to prevent PCBM crystallization is crosslinking the donor material with the acceptor. In this context Kim *et al.* worked on azide functionalized polythiophenes (Figure 24c).<sup>[212]</sup> They found that azide can crosslink in two ways: Upon photoexcitation nitrene radicals are formed. Without any selectivity these radicals react with donor as well as acceptor molecules.<sup>[212]</sup> Aside from that, azides can react in a thermally induced, selective cycloaddition with PCBM.<sup>[212]</sup> As donor material in their crosslinked BHJ solar cells they used a blend of 85% P3HT and 15% P3HT-azide10. This blend was mixed with PCBM in a 1:1 ratio. As reference device they used a P3HT:PCBM (1:1) BHJ cell. Kim *et al.* ran an accelerated aging experiment to compare the stability of the crosslinked and the reference device. The initial PCE of the reference was 3.44%. For the crosslinked device the PCE was 3.32%.<sup>[212]</sup> After 40 hours at 150 °C the P3HT:PCBM device exhibited an efficiency of 1.92%, while the crosslinked P3HT/P3HT-azide10:PCBM solar cell retained its efficiency of over 3.3%.<sup>[212]</sup> Kim *et al.* claim the formation of a stabilizing fullerene attached P3HT graft polymer at the P3HT/PCBM interface.<sup>[212]</sup> This interlayer significantly inhibits macrophase separation.<sup>[187]</sup>

The approach of adding crosslinking agents to a donor-acceptor blend has one advantage over the three concepts mentioned above: Here, no crosslinkable groups have to be attached to the materials, which in some cases can be challenging.<sup>[187]</sup> In this approach readily available materials can be used. However, only a few works utilizing this concept are known in the literature.<sup>[213,214]</sup> Examples for crosslinking agents are a tetravalent acrylate<sup>[213]</sup> (Figure 24d), a diene derivative<sup>[214]</sup> and the bisazide introduced in Figure 20a.

## 1.6 Patterning of organic semiconductors

Crosslinking of BHJ materials is only one concept for controlling and stabilizing the morphology in organic solar cells. Alternative concepts for stable and defined morphologies exploit phase separation of block copolymers<sup>[215]</sup> or self-organization of nanocrystals in polymer brushes.<sup>[187,216]</sup> Another approach towards a defined interface between donor and acceptor materials are patterning techniques. Applying such methods to crosslinkable materials is interesting, since the structures gained can be stabilized by crosslinking and a second material can be added from solution.

A classical approach towards patterned structures of organic semiconductors is using shadow masks during vapor deposition. Again, this method is viable only for small molecule organic semiconductors. Patterns of conjugated polymers or other materials restricted to solution processing can be achieved by photolithography. In this process a film is irradiated through a shadow mask. This results in the formation of defined areas in the film, where a light induced reaction such as crosslinking takes places. Commonly, such reactions lead to a change in solubility of the exposed material. Feature sizes smaller than 1  $\mu\text{m}$  were attained by Scheler *et al.* from photo-crosslinkable fluorene based oligomers.<sup>[217]</sup> Even smaller patterns of crosslinkable oligofluorenes were achieved by electron beam lithography.<sup>[218]</sup>

Looking at bulk heterojunction organic solar cells, domain sizes of some 10 nm are considered ideal for efficient exciton separation. To achieve features in the nanometer range, alternative concepts like nanoimprinting can be applied.<sup>[219]</sup> Nanoimprint techniques are frequently used for structuring polymers.<sup>[220]</sup> The working principle of nanoimprint lithography (NIL), also referred to as mechanical lithography, is schematically drawn in Figure 25.

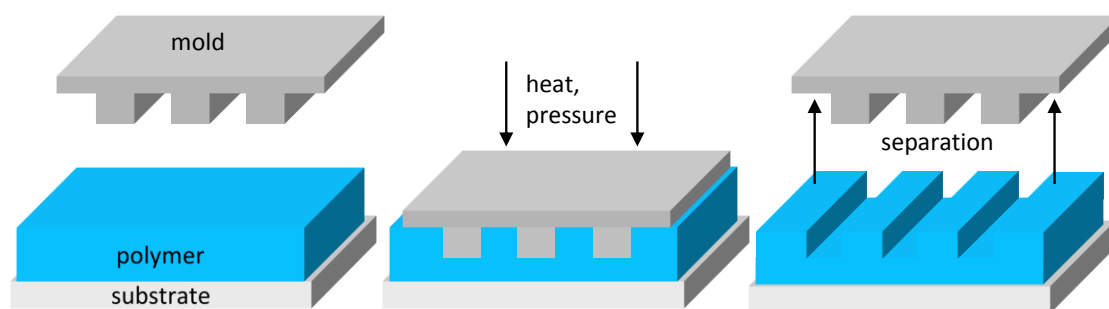


**Figure 25.** Fundamental steps of nanoimprint lithography. Reproduced after reference<sup>[219]</sup>.

A polymer film is cast on top of a substrate. The mold, in this example the mold is bar-shaped, is pressed into the polymer. This step can be assisted by heating the array above the glass transition temperature of the polymer (hot embossing) or by exposing the film and the mold to solvent vapor (SANIL, solvent assisted nanoimprint lithography).<sup>[219]</sup> After separation, a negative of the pattern of the mold is imprinted into the polymer film.<sup>[219]</sup>

The mold can be made from hard materials, for instance silicon or quartz. Also soft stamps from polydimethylsiloxane (PDMS) are frequently used.<sup>[220]</sup>

For an application in organic solar cells the imprinted structures are required to possess a high aspect ratio.<sup>[221]</sup> In other words, very thin and high structures are desired, offering a large donor-acceptor interface area.<sup>[219]</sup> Several reports on nanostructured P3HT have been published.<sup>[221]</sup> One example is by Ayril *et al.*, who used an anodic aluminium oxide membrane as a stamp for imprinting of a P3HT film.<sup>[222]</sup> Using this mold, hexagonal pillars (65 nm in width and 200 nm in height) were transferred into the P3HT film.<sup>[223]</sup> A layer of PCBM was cast on top of the P3HT from an orthogonal solvent.<sup>[219]</sup> However, this was found to lead to a diffuse and intermixed donor-acceptor interface.<sup>[219,224]</sup> To circumvent this intermixing caused by applying the acceptor from solution, evaporation of a layer of C<sub>60</sub> on top of P3HT nanostructures was tested.<sup>[219]</sup>

Another approach towards heterojunctions with defined structures in the range of the exciton diffusion length was reported by He *et al.* Interpenetrating columns with feature sizes as small as 25 nm were achieved by a combination of SANIL and double imprinting.<sup>[225,226]</sup> Their first report was on a polymer solar cell with P3HT as donor and PFDTBT as acceptor polymer. In the first step they used a patterned silicon mold to imprint columnar structures into a P3HT film at room temperature in a chloroform atmosphere.<sup>[225]</sup> The P3HT film was cast on top of glass coated with ITO and PEDOT:PSS. After imprinting the nanostructured P3HT film was used as a stamp for imprinting the PFDTBT layer. This PFDTBT film was spin coated on top of aluminium evaporated onto a Kapton foil.<sup>[225]</sup> The second imprinting step was conducted at room temperature in an atmosphere of dichloromethane.<sup>[225]</sup> Devices with an imprinted feature size of 25 nm showed the highest power conversion efficiencies in this study with 1.85%.<sup>[225]</sup> This significantly exceeds the PCE of a planar bilayer (0.36%) and of a P3HT:PFDTBT blend (1.09%).<sup>[225]</sup> After their successful proof of principle, He *et al.* fabricated P3HT:PCBM and PFDTBT:PCBM solar cells following the same procedure.<sup>[226]</sup> The PFDTBT:PCBM device with 25 nm dots showed an PCE of 2.30%, surpassing the blend (1.90%).<sup>[226]</sup>

Some examples from the literature encourage that nanoimprinting can indeed be an helpful approach towards organic solar cells with well-defined donor-acceptor interfaces. Combining NIL and crosslinking could advance this concept even further, since crosslinking might help stabilizing the imprinted structure and retain the sharp donor-acceptor interface after adding the second organic material from solution.



## 2 Aim of the thesis

Organic solar cells are an advancing technology and subject to research for the last two decades. The development of novel functional materials and the evolution of device architecture helped organic solar cells surpassing the barrier of 10% power conversion efficiency. However, long term stability still remains an issue. This work will address the question whether crosslinking can help achieving more stable and defined active layer structures in polymer based organic solar cells.

The central aims of this thesis are the synthesis of crosslinkable low bandgap polymers and their application in organic solar cells. Based on the well-known low bandgap polymer PFDTBT (poly(2,7-(9,9-dialkylfluorene)-*alt*-(5,5-(4',7'-di-2-thienyl-2',1',3'-benzothiadiazole))) a series of crosslinkable low bandgap polymers and the non-crosslinkable reference material should be synthesized. Oxetanes are attached to the alkyl side chains of the fluorene moiety and serve as crosslinkable functional groups. The crosslinkable polymers are targeted to show similar behavior compared to the reference material concerning molecular weight as well as chemical, thermal, optical, and electronic properties.

For an application of the synthesized crosslinkable low bandgap polymers in organic solar cells detailed knowledge about the crosslinking process is essential. With respect to device fabrication a process for crosslinking in thin films has to be developed.

Bulk heterojunction organic solar cells are fabricated with the crosslinkable low bandgap polymer and the reference material. Furthermore, the long term stability of solar cells based on both materials is studied. A major reason for a decreasing efficiency is the instability of the morphology of the donor acceptor blend. Diffusion and aggregation of the low molar mass fullerene in the polymer matrix leads to a loss of the beneficial phase separation with nanometer sized domains. Ultimately, this results in poorly performing macrophase separated donor-acceptor blends. For this purpose, accelerated aging experiments have to be conducted. Crosslinking is expected to result in more stable blends, since the diffusion of the acceptor compound is reduced significantly in a densely crosslinked polymer network.

Creating a large and defined donor acceptor interface is an approach to improve the architecture of the active layer of organic solar cells. A concept for patterning organic semiconductors is nanoimprint lithography. Within this work the strategy of imprinting will be applied to the synthesized low bandgap polymers.



### 3 Synthesis and crosslinking of oxetane functionalized low bandgap polymers

Over the past decades crosslinking has emerged as a powerful tool for the processing of organic semiconductors. It is usually applied to a film which was processed from solution. During the crosslinking procedure the soluble organic semiconducting material is converted into an insoluble network. As a result these materials can be utilized for the fabrication of multilayer stacks from solution. A more advanced application is the formation of patterned structures by photolithography.<sup>[190,195]</sup> Recently, the focus turned to crosslinking of low bandgap polymers in organic bulk heterojunction solar cells.<sup>[187]</sup> Several studies have shown that crosslinking can be beneficial for the long term stability of BHJ cells.<sup>[102,187]</sup>

Crosslinking can be realized by either adding a crosslinking agent or by the incorporation of reactive functional groups. Although it requires some more synthetic effort, the concept of crosslinkable groups was chosen for this thesis. For this purpose several functional groups are known in the literature, for instance, alkyl bromide, azide, acrylate, vinyl, and oxetane. An advantage of oxetane is its selectivity, as it only reacts with other oxetane groups during crosslinking. Also, oxetane is easy to handle during synthesis and work-up. It is not labile to oxygen, light, and heat and tolerates the reaction conditions of Suzuki cross-coupling. With respect to an application in BHJ solar cells the cationic crosslinking mechanism is the key advantage of oxetane. Other than for groups that crosslink *via* a radical mechanism, for instance vinyl and acrylate, the presence of strongly electron accepting fullerenes does not affect the cationic crosslinking of oxetanes.

This work is based on the well-known low bandgap polymer PFDTBT (poly(2,7-(9,9-dialkylfluorene)-*alt*-(5,5-(4',7'-di-2-thienyl-2',1',3'-benzothiadiazole))).<sup>[153]</sup> This structure was modified with crosslinkable oxetane units attached to the side chains of the fluorene moiety. By this a series of low bandgap polymers with varying amounts of crosslinkable groups were synthesized and characterized. The crosslinking process was carefully investigated and optimized to determine the parameters for the formation of insoluble films. As reference material a non-crosslinkable PFDTBT was also synthesized. The structure of PFDTBT equipped with two crosslinkable oxetane groups is shown in Figure 26.

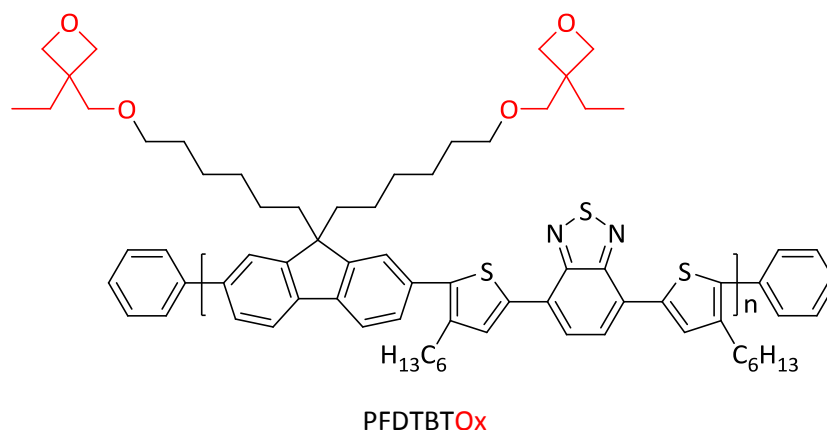
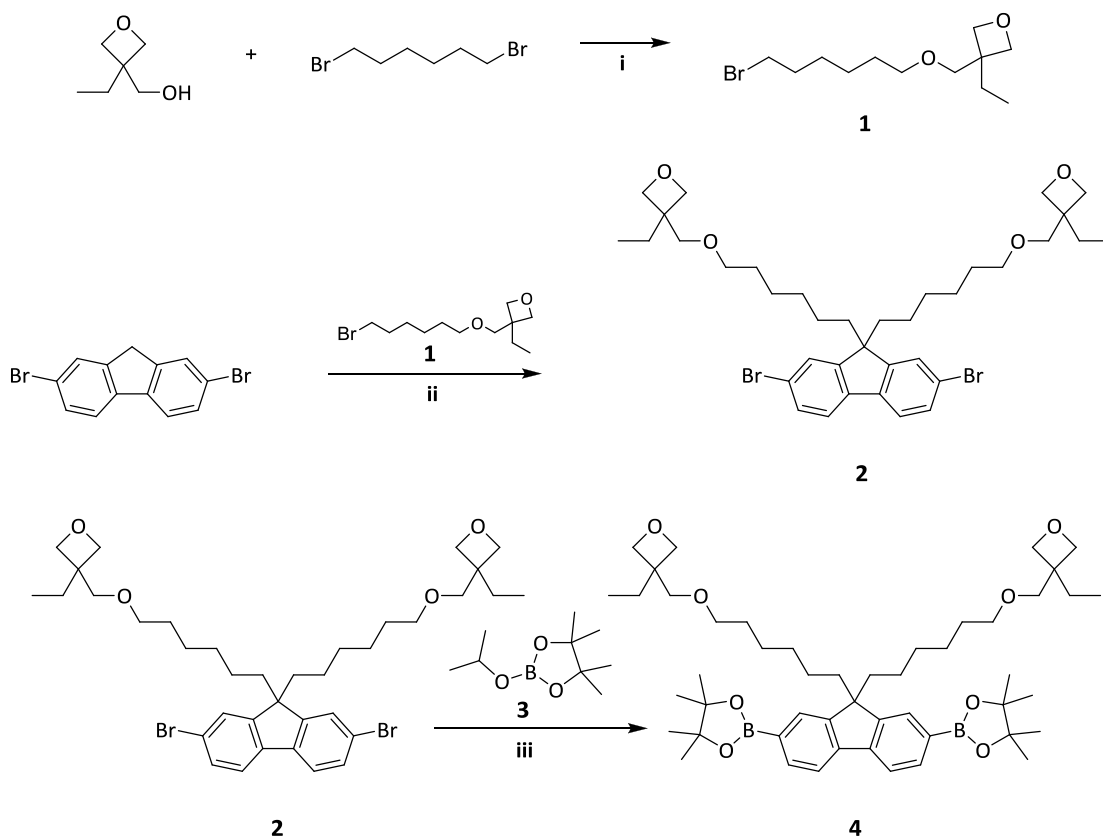


**Figure 26.** Crosslinkable low bandgap polymer PFDTBT Ox.

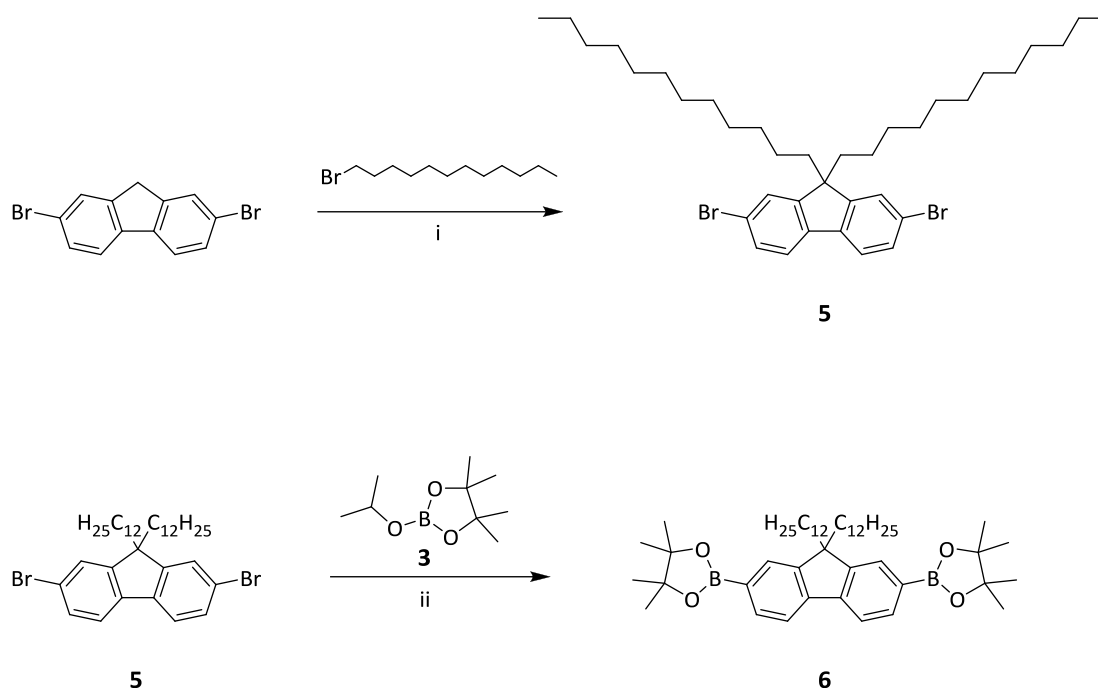
### 3.1 Synthesis of the monomers

Scheme 1 shows the synthetic pathways towards the crosslinkable fluorene monomer. In the first step the crosslinkable alkyl chain (**1**) is synthesized according to the literature.<sup>[227]</sup> Commercially available 3-ethyloxetanemethanol is reacted with a threefold excess of 1,6-dibromohexane under basic conditions in a Williamson etherification. The product 3-(6-bromohexyloxymethyl)-3-ethyloxetane (**1**) is isolated by column chromatography with 80% yield and subsequently used for the alkylation of commercially available 2,7-dibromofluorene.<sup>[190]</sup> By using concentrated NaOH fluorene is selectively deprotonated at the 9-position, making way for the C6-oxetane chains. After column chromatography 2,7-dibromo-9,9-bis(hexyl-6,1-diyl)bis(oxymethyl-3-ethyloxetane)-fluorene (**2**) is isolated in 70% yield. For Suzuki polycondensation boronic acid functionalities have to be introduced. Since boronic acids show tendency to condensate and are prone to interactions with silica during column chromatography, we choose a cyclic ester, namely boronic acid pinacol ester. The conversion is conducted as described in the literature.<sup>[228]</sup> To a solution of the dibromofluorene derivative (**2**) *n*-butyllithium and isopropoxyboronic acid pinacol ester (**3**) are sequentially added at -78 °C. Special attention is paid to purification, since polycondensation requires extremely pure monomers. In several cases the monomers are purified by two or more column chromatography runs and highly pure (**4**) is obtained in yields of up to 57%.



**Scheme 1.** Synthesis of the crosslinkable fluorene monomer. Conditions: **i**: hexane, 45% NaOH, phase-transfer catalyst tetrabutylammonium bromide, 100 °C. **ii**: DMSO, 50% NaOH, phase-transfer catalysts benzyltriethylammonium chloride and tetrabutylammonium chloride, 100 °C. **iii**: THF, *n*-butyllithium, -78 °C.

The synthesis of the non-crosslinkable fluorene monomer proceeds in analogous fashion.<sup>[229]</sup> It is illustrated in Scheme 2. For the alkylation of 2,7-dibromofluorene the commercially available 1-bromododecane is used. A dodecyl chain was chosen because it contains the same number of carbon atoms as the C6-oxetane chain of the crosslinkable fluorene monomer. The product 2,7-dibromo-9,9-didodecylfluorene (**5**) is obtained in 90% yield after purification by column chromatography. Reaction of (**5**) with isopropoxyboronic acid pinacol ester affords the diboronic acid functionalized fluorene (**6**). After purification by column chromatography 2,7-bis(4,4,5,5-tetramethyl-1,3,2-dioxaborolane)-9,9-didodecylfluorene (**6**) is isolated in high purity and with 72% yield.



**Scheme 2.** Synthesis of the non-crosslinkable fluorene monomer 2,7-bis(4,4,5,5-tetramethyl-1,3,2-dioxaborolane)-9,9-didodecylfluorene. i: DMSO, 50% NaOH, 1-bromododecane, phase-transfer catalysts benzyltriethylammonium chloride and tetrabutylammonium chloride; 100 °C. ii: THF, *n*-butyllithium, -78 °C.

As acceptor unit for the low bandgap polymers dithienylbenzothiadiazole (DTBT) is used. Several versions of this unit are known in the literature. Three derivatives are shown in Figure 27. The non-substituted DTBT is rather poorly soluble. Thus, polymers tend to precipitate during synthesis, which limits the molecular weights. Introducing linear hexyl chains to the thiophenes significantly improves the solubility of monomers and polymers. Higher molecular weights can be achieved and the resulting materials can be easily processed from solution. As discussed in section 1.3.6, the shape and position of the solubilizing groups influences the optoelectronic properties of the polymers. Since substitution at the 4-position of thiophene has a rather small impact, D4HTBT was chosen as the acceptor unit in this work.

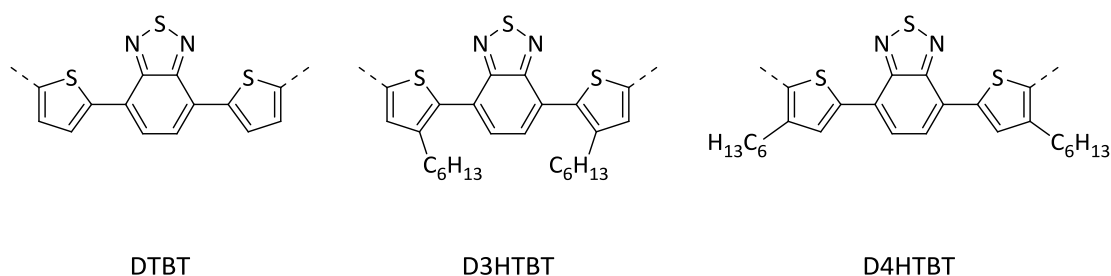
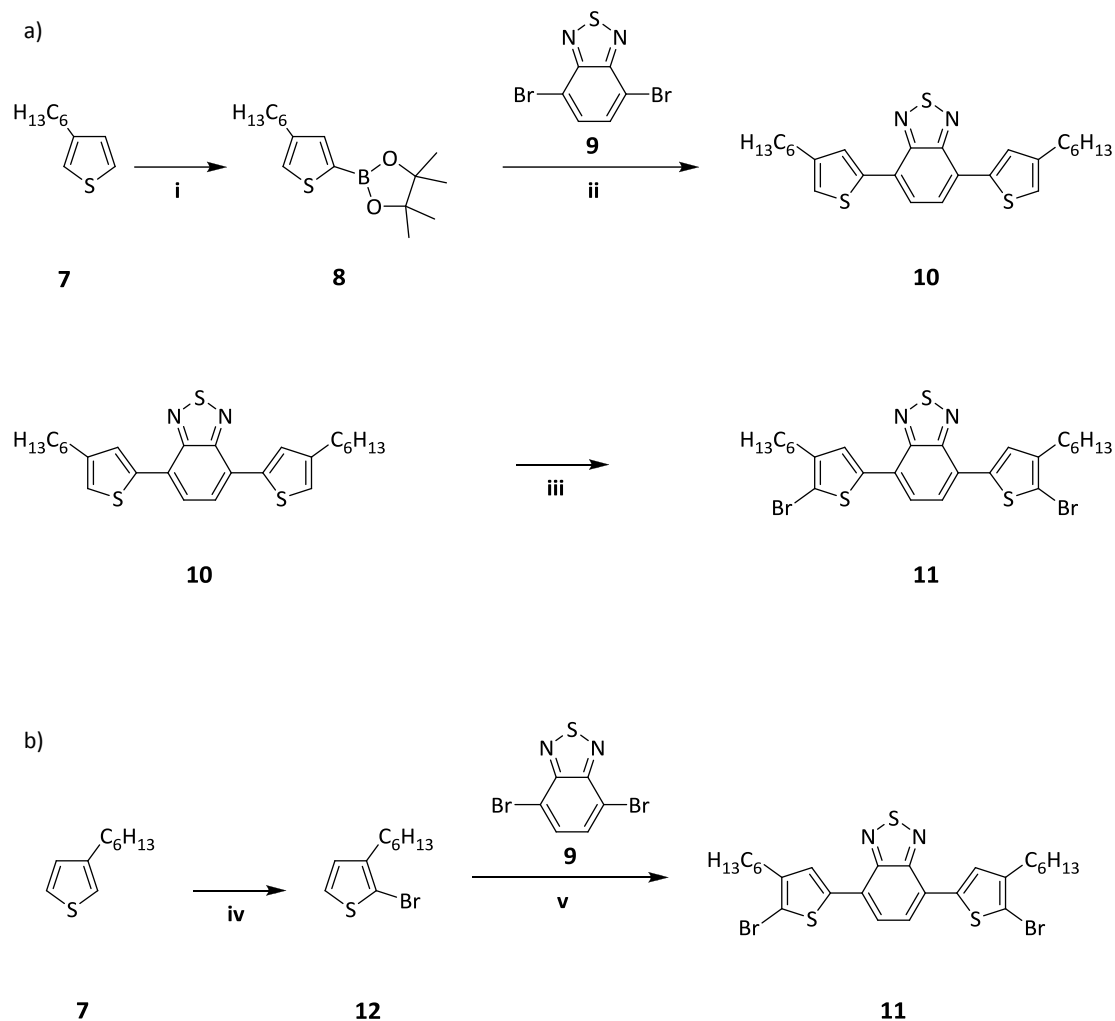


**Figure 27.** Derivatives of dithienylbenzothiadiazole. Left: The non-substituted DTBT. Middle and right: Soluble DTBT derivatives equipped with linear hexyl chains at the 3-position of the thiophene (D3HTBT) and at the 4-position of the thiophenes (D4HTBT).

The monomer 4,7-bis(5-bromo-4-hexyl-2-thienyl)-2,1,3-benzothiadiazole (**11**) can be prepared in a multi-step synthesis. Coupling of 4-hexylthiophenes to the benzothiadiazole

core can be achieved by either Suzuki or Stille reactions.<sup>[230,231]</sup> Scheme 3a presents an overview of the synthetic steps from the Suzuki route. In the first step the boronic acid ester group is attached to the 2-position of 4-hexylthiophene (**7**) by lithiation with *n*-butyllithium and subsequent addition of the boronic acid ester. The yield of 2-(4,4,5,5-tetramethyl-1,3,2-dioxaborolane)-4-hexylthiophene (**8**) is 89%.<sup>[232]</sup> Suzuki coupling of two equivalents of (**8**) with 4,7-dibromo-2,1,3-benzothiadiazole (**9**) affords dithienylbenzothiadiazole (**10**) in 83% yield. In the final step (**10**) is brominated twice with *N*-bromosuccinimide to afford 4,7-bis(5-bromo-4-hexyl-2-thienyl)-2,1,3-benzothiadiazole (**11**) in 85% yield.

Recently, Sommer *et al.* reported an alternative two-step synthesis of (**11**) by direct arylation (Scheme 3b).<sup>[233]</sup> For this synthesis no boronic acid ester compound is required. The educt hexylthiophene (**7**) is brominated with *N*-bromosuccinimide to give 2-bromo-3-hexylthiophene (**12**) in 95% yield. Two equivalents of (**12**) are coupled with 4,7-dibromo-2,1,3-benzothiadiazole (**9**) in a direct arylation. In this step the yield of 4,7-bis(5-bromo-4-hexyl-2-thienyl)-2,1,3-benzothiadiazole (**11**) is 26%.

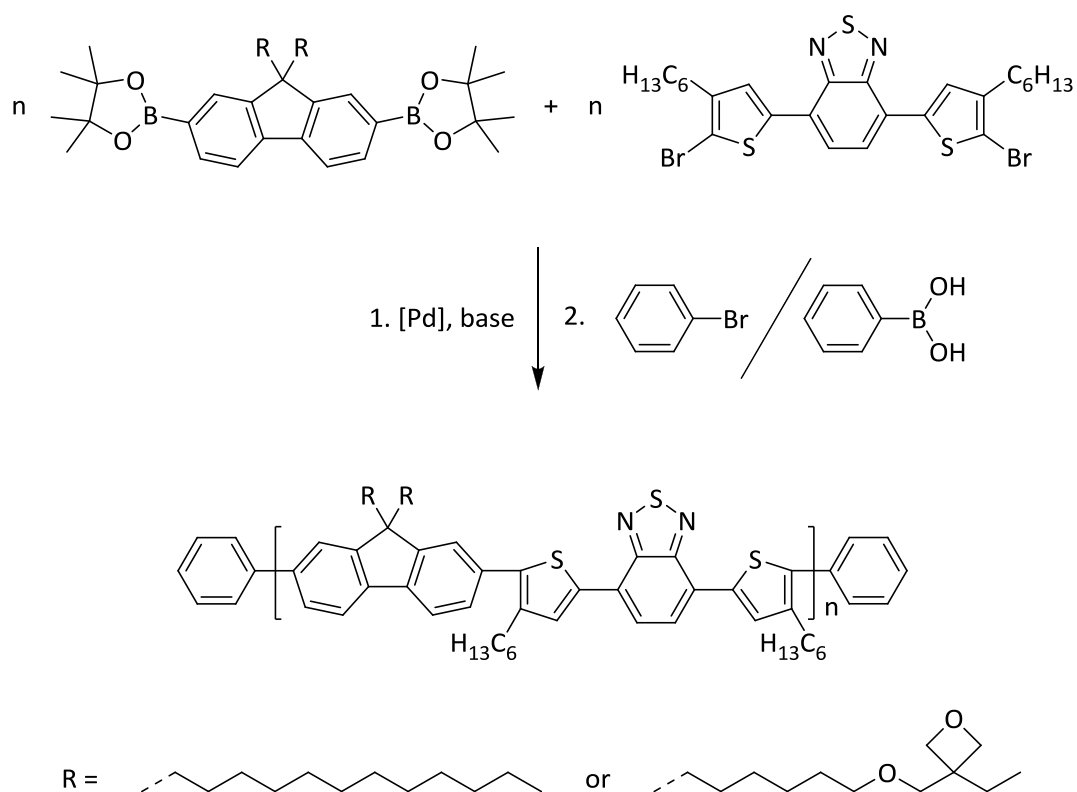


**Scheme 3.** Synthesis of 4,7-bis(5-bromo-4-hexyl-2-thienyl)-2,1,3-benzothiadiazole. **a)** Synthesis *via* Suzuki reaction.<sup>[230]</sup> Conditions: **i:** THF, *n*-butyllithium, isopropoxyboronic acid pinacol ester, -78 °C, 89%; **ii:** toluene:water, Pd(PPh<sub>3</sub>)<sub>4</sub>, K<sub>2</sub>CO<sub>3</sub>, aliquat 336, 90 °C, 83%; **iii:** CHCl<sub>3</sub>/acetic acid, *N*-bromosuccinimide, 50 °C, 85%. **b)** Synthesis *via* direct arylation.<sup>[233]</sup> Conditions: **iv:** CHCl<sub>3</sub>/acetic acid, *N*-bromosuccinimide, 50 °C, 95%; **v:** DMAc, PivOH, K<sub>2</sub>CO<sub>3</sub>, Pd(OAc)<sub>2</sub>, PCy<sub>3</sub>, 60 °C, 26%.

For the low bandgap polymers in this work the acceptor 4,7-bis(5-bromo-4-hexyl-2-thienyl)-2,1,3-benzothiadiazole (**11**) was purchased from SunaTech Inc. in excellent purity. A <sup>1</sup>H NMR spectrum can be found in the appendix.

## 3.2 Polymer synthesis and characterization

The polymerization of the crosslinkable polymers and the non-crosslinkable reference materials was conducted by using Suzuki polycondensation. A generic reaction scheme is depicted in Scheme 4. The biphasic reaction system of toluene and aqueous  $\text{Na}_2\text{CO}_3$  is thoroughly degassed before the catalyst  $\text{Pd}(\text{PPh}_3)_4$  is added. To eliminate boronic acid ester and bromine terminal groups, the polymer is endcapped by bromobenzene and phenylboronic acid. Removal of boronic acid and bromine end groups is important to achieve a good low bandgap polymer. Residual boronic acid groups are prone to condensation. This might cause issues concerning the solubility of the polymer and molar mass determination.<sup>[138]</sup> Bromo endgroups severely influence the electronic properties of a conjugated polymer.



**Scheme 4.** Suzuki polycondensation for the synthesis of PFDTBT based low bandgap polymers. Conditions: toluene:water,  $\text{Pd}(\text{PPh}_3)_4$ ,  $\text{Na}_2\text{CO}_3$ , aliquat 336, RF, 4 d, endcapping with bromobenzene and phenylboronic acid.

In the following section the characterization of a series of fluorene based low-bandgap polymers is described. An important aspect of polymer characterization in this work is the comparison of the crosslinkable PFDTBTOx and the reference material PFDTBT in order to find out if the incorporation of oxetane groups has any detrimental effects on the chemical, thermal, and optical properties of the polymers. Figure 28 compares the SEC traces, TGA, and the absorption and emission spectra for the crosslinkable PFDTBTOx and the reference polymer PFDTBT. The data of both polymers are summarized in Table 5.

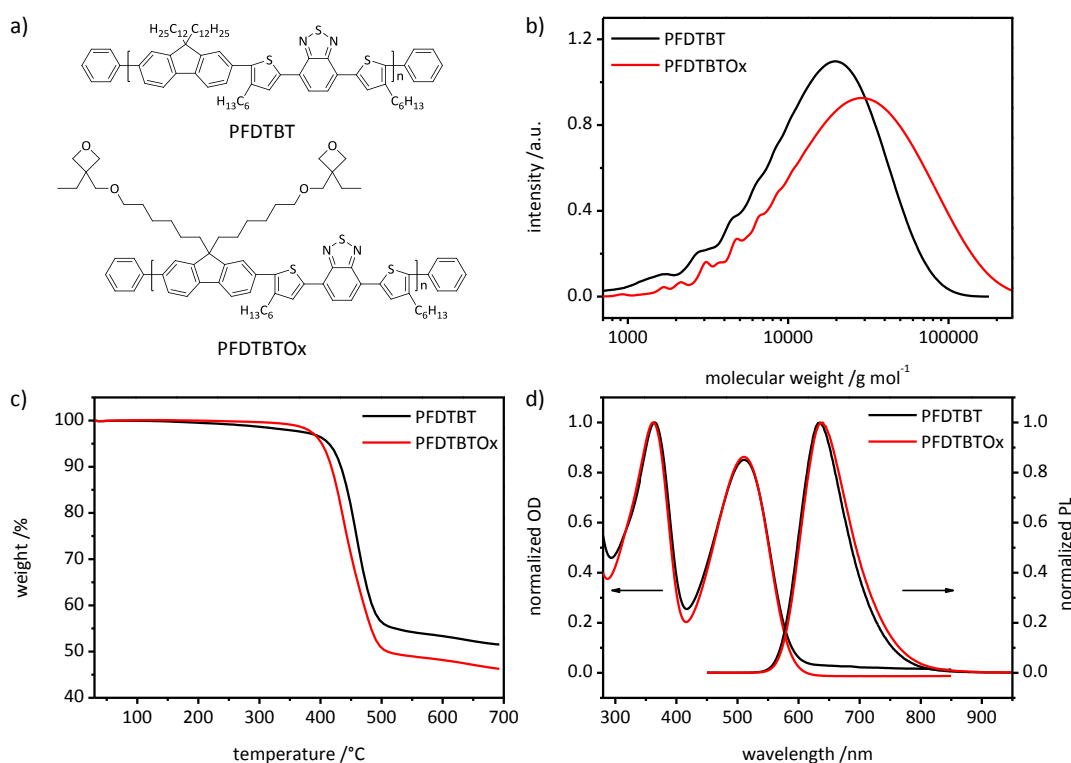
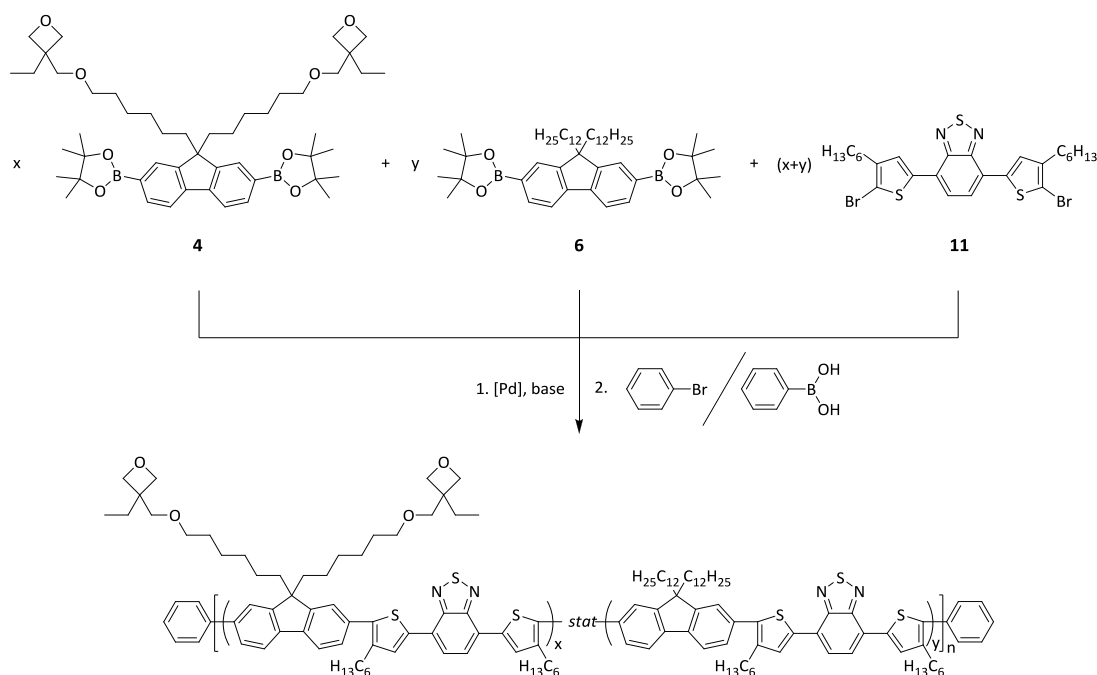


**Figure 28.** Characterization of the reference polymer PFDTBT and the crosslinkable low bandgap polymer PFDTBTx. **a)** Chemical structures of PFDTBT and PFDTBTx; **b)** SEC traces, eluent: THF, polystyrene calibration; **c)** thermogravimetric analysis, 10 K min<sup>-1</sup>, N<sub>2</sub>; **d)** absorption and fluorescence spectra from THF solutions ( $c = 10^{-3}$  g mol<sup>-1</sup>).

SEC measurements (Figure 28b) of the raw polymers before Soxhlet extraction show comparable molecular weights, with number average molecular weights ( $\overline{M}_n$ ) in the range of 15,000 g mol<sup>-1</sup>. This corresponds to a degree of polymerization of about 15. From the SEC there is no hint for any influence on the Suzuki polycondensation caused by the oxetane groups. Also, the steric demands of the dodecyl and the hexyloxy-oxetane chains are comparable, as both consist of twelve carbon atoms. Both materials show more than sufficient thermal stability. In nitrogen atmosphere degradation starts above 400 °C. Oxetane causes no thermal degradation at lower temperatures (Figure 28b). Also the optical spectra look very similar (Figure 28c). Both polymers possess absorption maxima at about 360 nm and 510 nm. The optical bandgaps  $E_g$  are estimated to be 2.1 eV from the onset of the absorption edges of both polymers. Photoluminescence behavior is also very similar, with only a slight red-shift of the maximum of PFDTBTx (639 nm, PFDTBT 635 nm).

Comparing both materials, a crosslinkable low bandgap polymer and its non-crosslinkable equivalent were successfully synthesized. Both materials possess similar molecular weights, thermal, and optical properties. This is important for the following crosslinking experiments and the use of these materials in organic solar cells.

In the case of PFDTBTOx the concentration of crosslinkable groups is very high, with two oxetane groups being present in each repeat unit. To gain polymers with varying amounts of crosslinkable groups, a series of polymers was synthesized by copolymerization of the crosslinkable (**4**) and non-crosslinkable fluorene monomer (**6**) and dithienylbenzothiadiazole (**11**). The synthesis of these polymers is shown in Scheme 5.



**Scheme 5.** Synthesis of polymers with varying amounts of crosslinkable groups. Conditions: toluene:water, Pd(PPh<sub>3</sub>)<sub>4</sub>, Na<sub>2</sub>CO<sub>3</sub>, aliquat 336, RF, 4 d, endcapping with bromobenzene and phenylboronic acid.

The copolymers PFDTBTO<sub>x0.75</sub>, PFDTBTO<sub>x0.50</sub>, PFDTBTO<sub>x0.25</sub>, PFDTBTO<sub>x0.10</sub>, and PFDTBTO<sub>x0.05</sub> were synthesized as described previously for PFDTBT and PFDTBTO<sub>x</sub> by Suzuki polycondensation. Table 4 lists the monomer feed ratios for the polymers of this series.

From <sup>1</sup>H NMR spectra the amount of crosslinkable repeat units in the polymers is calculated. Figure 29 shows a generic structure of the crosslinkable (co-)polymers from this series and the NMR spectra. The relative amount of crosslinkable repeat units is determined by the ratio of the integrals of the singlet caused by the -O-CH<sub>2</sub>-oxetane protons at 3.40 ppm (marked in red in Figure 29) and the multiplet of the aromatic protons between 7.40 and 8.10 ppm (indicated in blue in Figure 29). In Table 4 these values are summarized. The amount of oxetane containing fluorene units found in the copolymers is in all cases very close to the number expected from the feed ratios.

**Table 4.** Series of low bandgap polymers with varying amounts of crosslinkable oxetane groups. The index x represents the crosslinkable fluorene monomer, the index y represents the non-crosslinkable didodecylfluorene monomer.

	feed ratio		found in polymer <sup>a</sup>		molecular weight <sup>b</sup>	
	x	y	x	y	$\overline{M}_n$	$\overline{M}_w$
<b>PFDTBTO<sub>x</sub></b>	1	0	1	0	14,800	37,900
<b>PFDTBTO<sub>x0.75</sub></b>	0.75	0.25	0.76	0.24	14,200	33,400
<b>PFDTBTO<sub>x0.50</sub></b>	0.50	0.50	0.52	0.48	6,200	13,200
<b>PFDTBTO<sub>x0.25</sub></b>	0.25	0.75	0.25	0.75	12,500	22,500
<b>PFDTBTO<sub>x0.10</sub></b>	0.10	0.90	0.10	0.90	11,800	24,000
<b>PFDTBTO<sub>x0.05</sub></b>	0.05	0.95	0.04	0.96	11,000	21,100
<b>PFDTBT</b>	0	1	0	1	11,500	24,400

<sup>a</sup> The ratio of x/y was determined from <sup>1</sup>H NMR spectra based on the integrals of the singlet at 3.40 ppm and the multiplet between 7.40 and 8.10 ppm.

<sup>b</sup> Determined from SEC, eluent: THF,  $\overline{M}_n$  and  $\overline{M}_w$  were calculated from polystyrene calibration.

Apart from PFDTBTO<sub>x0.50</sub> the molecular weights of all polymers from this series are in the same range.

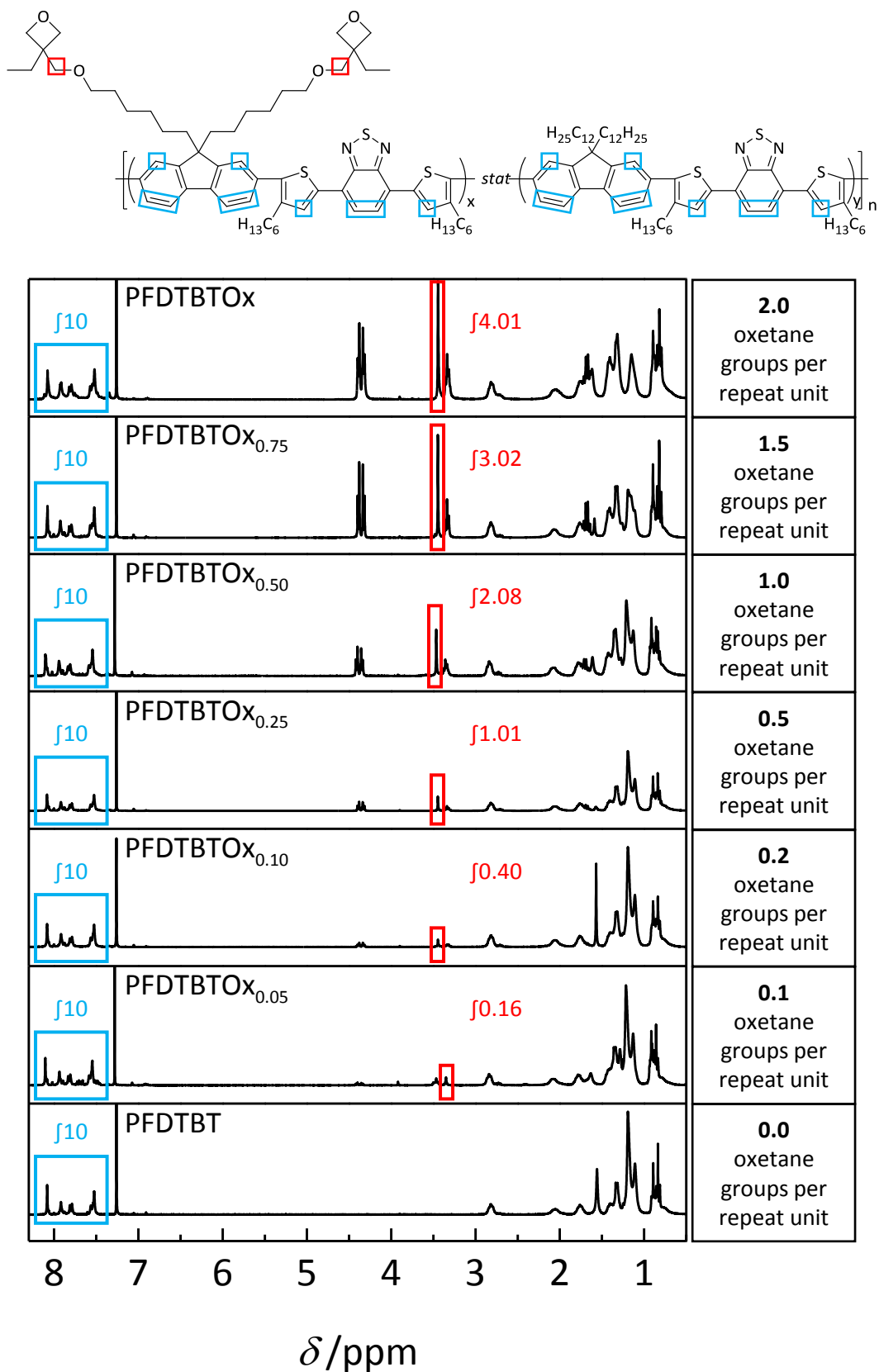
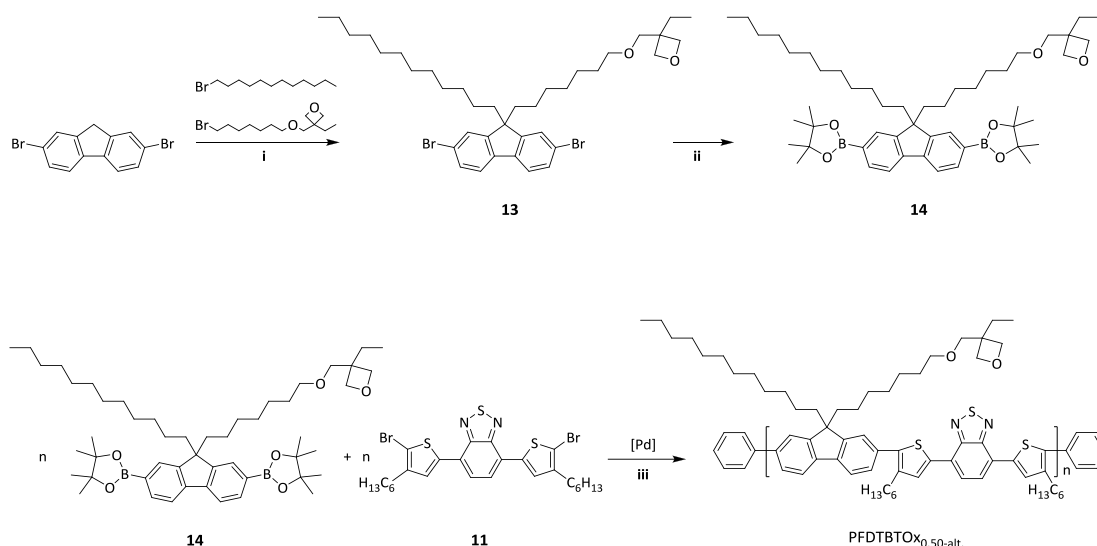


**Figure 29.** Determination of the amount of oxetane groups in the series of crosslinkable polymers by  $^1\text{H}$  NMR spectroscopy.

In addition to the series shown in Table 4, a PFDTBT with one oxetane group per repeat unit is synthesized by a different strategy. Instead of using equimolar amounts of the crosslinkable and non-crosslinkable fluorene monomers, 50% of crosslinkable repeat units were achieved by incorporating one heptyloxy-oxetane and one dodecyl chain to the fluorene monomer. The synthetic route is illustrated in Scheme 6.



**Scheme 6.** Synthetic steps towards PFDTBT<sub>0.50-alt.</sub>. Conditions: **i**: DMSO, 50% NaOH, phase-transfer catalysts benzyltriethylammonium chloride and tetrabutylammonium chloride, 100 °C; **ii**: THF, *n*-butyllithium, isopropoxyboronic acid pinacol ester, -78 °C; **iii**: toluene:water, Pd(PPh<sub>3</sub>)<sub>4</sub>, Na<sub>2</sub>CO<sub>3</sub>, aliquat 336, RF, 4 d, endcapping with bromobenzene and phenylboronic acid.

In the first step 2,7-dibromofluorene is alkylated in 9-position. Here, an equimolar mixture of 1-bromododecane and 3-(7-bromoheptyloxymethyl)-3-ethyloxetane is used. This results in a statistic mixture of the two symmetrically substituted dibromofluorenes, bearing either two dodecyl or two hexyloxy-oxetane chains, and the desired 2,7-dibromo-9-dodecyl-9-(heptyl-7,1-diyl-oxymethyl-3-ethyloxetane)-fluorene (**13**). Due to their differences in polarity, these components can be separated and purified by column chromatography. The yield of (**13**) is 42%. Afterwards the boronic acid pinacol ester groups are introduced. The monomer (**14**) was obtained in high purity after column chromatography in 27% yield. Polymerization was conducted as described above, yielding a PFDTBT<sub>0x</sub> with one oxetane group in each repeating unit. This should result in a comparable density of crosslinkable groups as expected in a copolymer of 50% crosslinkable and 50% non-crosslinkable fluorene monomers as it was described previously. The amount of oxetane groups was checked by <sup>1</sup>H NMR and found to be exactly 1.0 per repeat unit. From SEC the molecular weight of the polymer was determined to  $\overline{M}_n$  11,500 g mol<sup>-1</sup> and  $\overline{M}_w$  23,900 g mol<sup>-1</sup>. This is within the molecular weight range of the other polymers from this series. In the following crosslinking experiments the polymer obtained from this alternative strategy, named PFDTBT<sub>0.50-alt.</sub>, was used as the material with 1.0 oxetane groups per repeat unit. The experimental data of all polymers from this series are summarized in Table 5.

**Table 5.** Data of the crosslinkable polymers and the reference polymer PFDTBT.

	SEC <sup>a</sup>		TGA <sup>b</sup>	UV/Vis <sup>c</sup>			PL <sup>d</sup>
	$\overline{M}_n$	$\overline{M}_w$	$T_d$	$\lambda_{\max}$	$\lambda_{\text{onset}}$	$E_{\text{opt}}$	$\lambda_{\max}$
<b>PFDTBTOx</b>	14,800	37,900	410 °C	362, 510 nm	590 nm	2.1 eV	639 nm
<b>PFDTBTOx<sub>0.75</sub></b>	14,200	33,400	395 °C	365, 510 nm	584 nm	2.1 eV	634 nm
<b>PFDTBTOx<sub>0.50-alt.</sub></b>	11,500	23,900	402 °C	360, 510 nm	590 nm	2.1 eV	640 nm
<b>PFDTBTOx<sub>0.25</sub></b>	12,500	22,500	395 °C	364, 509 nm	584 nm	2.1 eV	633 nm
<b>PFDTBTOx<sub>0.10</sub></b>	11,800	24,000	419 °C	361, 505 nm	584 nm	2.1 eV	633 nm
<b>PFDTBTOx<sub>0.05</sub></b>	11,000	21,100	256 °C	363, 509 nm	586 nm	2.1 eV	634 nm
<b>PFDTBT</b>	11,500	24,400	420 °C	365, 511 nm	587 nm	2.1 eV	635 nm

<sup>a</sup>  $\overline{M}_n$  and  $\overline{M}_w$  were calculated from polystyrene calibration.

<sup>b</sup> Measured under N<sub>2</sub> at 10 K min<sup>-1</sup>.  $T_d$ : decomposition temperature, here: temperature of 5% weight loss.

<sup>c</sup> Spectra from THF solutions ( $c = 10^{-3}$  mg ml<sup>-1</sup>),  $\lambda_{\text{onset}}$ : determined from linear fit of absorption edge.  $E_{\text{opt}} = h \times c / \lambda_{\text{onset}}$ .

<sup>d</sup> Spectra from THF solutions ( $c = 10^{-3}$  mg ml<sup>-1</sup>),  $\lambda_{\text{excitation}} = 360$  nm.

### 3.3 Crosslinking experiments

Polymerization of oxetane takes place *via* a cationic ring-opening polymerization (CROP). The polymerization is initiated by protons, the mechanism is shown in Figure 21b. When oxetanes are used as crosslinkable groups in organic semiconductors the cationic crosslinking can be initiated by either a photoacid generator (PAG) or by acid vapor. The first part of this section describes the crosslinking of PFDTBTOx initiated by a PAG.

Photoacid generators are photolabile materials. Under UV irradiation they release protons, which act as initiators for the ring-opening. Usually, samples are irradiated for rather short times (< 1 min). After irradiation the sample is heated to a temperature above the glass transition of the material that is to be crosslinked. During this post-bake, the crosslinking as such takes place. Above  $T_g$  the polymer chains are sufficiently mobile, enabling oxetane groups of different molecules to react with each other.

This photoacid generator concept was utilized in a first series of experiments to investigate the crosslinking of PFDTBTOx. The goal of this study was to determine the process conditions for the formation of an insoluble polymer film. Subsequently, parameters such as the exposure time, the time and temperature of the postbake step, and the concentration of the PAG were optimized to keep the conditions as mild as possible. Solubility tests were conducted to monitor the crosslinking experiments. A schematic drawing of the sequence of steps in a crosslinking experiment is shown in Figure 30.

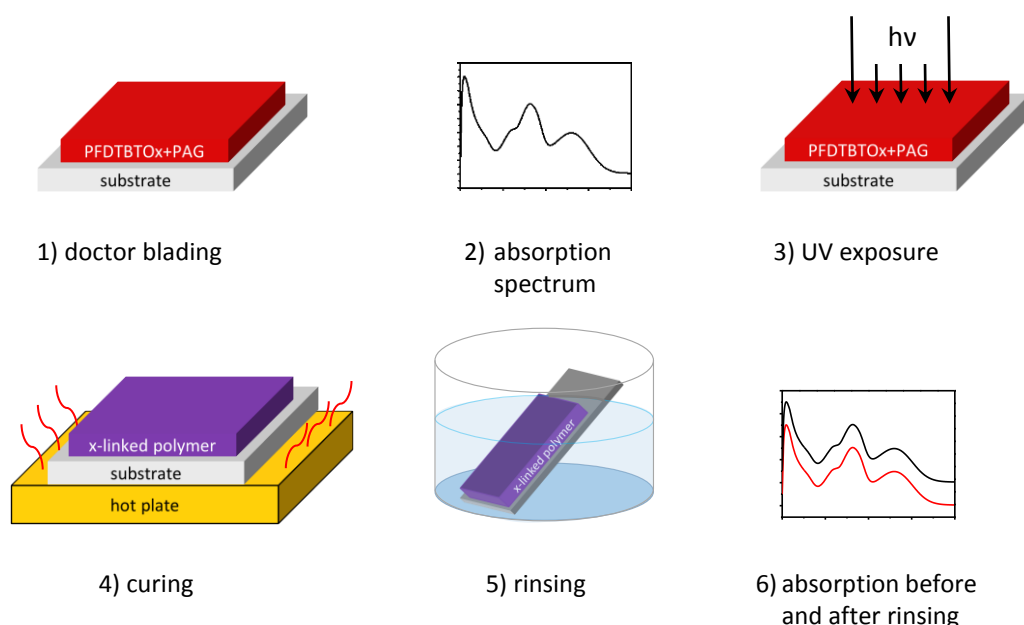


**Figure 30.** Solubility test for the crosslinking of PFDTBTOx with a PAG. Optionally an additional absorption spectrum was recorded after curing.

Films with thicknesses of about 80 nm were cast from a chlorobenzene solution of PFDTBTOx with a photoacid generator (DPI-109, Figure 31a, 5 wt% with respect to the

polymer). The films were dried in vacuum at 80 °C. To prevent oxidation, steps 3 and 4 were conducted under nitrogen in a glovebox. The samples were exposed to the light of a xenon UV lamp for 2 to 15 minutes before a curing step at 150 °C for 5 to 20 minutes was applied. After curing another absorption spectrum was recorded optionally. To gain insight into the efficiency of the crosslinking, the solubility of the crosslinked films was tested. Comparing the optical densities of films before and after rinsing with THF helped us to quantify the progress. Ideally no loss in optical density is observed. Loss in optical density resembles polymer chains that have not been incorporated into the network and thus remain soluble.

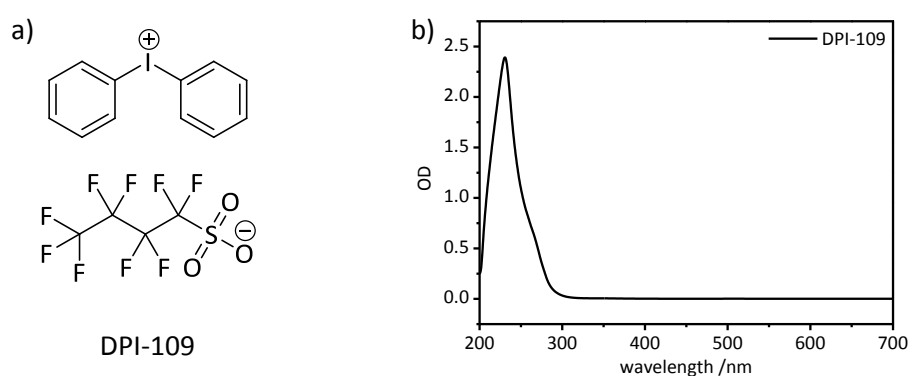


**Figure 31.** Photoacid generator DPI-109. **a)** Chemical structure. **b)** UV/Vis absorption spectrum. The spectrum was recorded in THF solution ( $c = 0.1 \text{ mg ml}^{-1}$ )

With respect to later device fabrication the parameters exposure time, postbake temperature, and postbake time were optimized to find the mildest conditions. Exposure to UV light for 5 minutes and curing at 150 °C for 10 minutes were found as the most convenient parameters for crosslinking. The absorption spectra from this solubility test are shown in Figure 32a. Also, we had to make sure that the backbone of the polymer does not suffer any damage during the crosslinking process. We cautiously conducted UV exposure and curing under inert atmosphere, knowing of the sensitivity of fluorene polymers to (photo-)oxidation. Photoluminescence (PL) can be used as an indicator to see whether the conjugated system is intact. Damages to the chromophore would be visible as a shift of the maximum of emission or as a decay of intensity. Comparing the PL of PFDTBTOx films with 5 wt% DPI-109 before and after crosslinking shows no evidence of any damage to the polymer backbone. The PL spectra are displayed in Figure 32b. A second and very sensitive method is photoluminescence quantum efficiency (PLQE). We determined the PLQE of films of PFDTBTOx with 5 wt% DPI-109 before and after crosslinking to be constant at 5%.

In the next step the aim was reducing the amount of photoacid generator. For an application in organic solar cells the number of “foreign” molecules added to the active

materials is desired to be minimal. A drawback arising from the use of PAGs is that molecules or fragments of them cannot be removed entirely from the active layer.

Based on the previously optimized conditions the same crosslinking experiment was carried out with 1 wt% of the PAG DPI-109. In this case, however, only partially insoluble films were achieved. Even longer postbake times or higher temperatures did not result in any significant improvement. We appointed this to not enough protons being present and thus the CROP is not initiated sufficiently. Another point might be the mobility of the protons formed by the PAG. In our system the corresponding anion (perfluorobutane sulfonate) is rather bulky, presumably impeding efficient diffusion of the protons. A result from the solubility test with 1 wt % PAG is shown in Figure 32c.

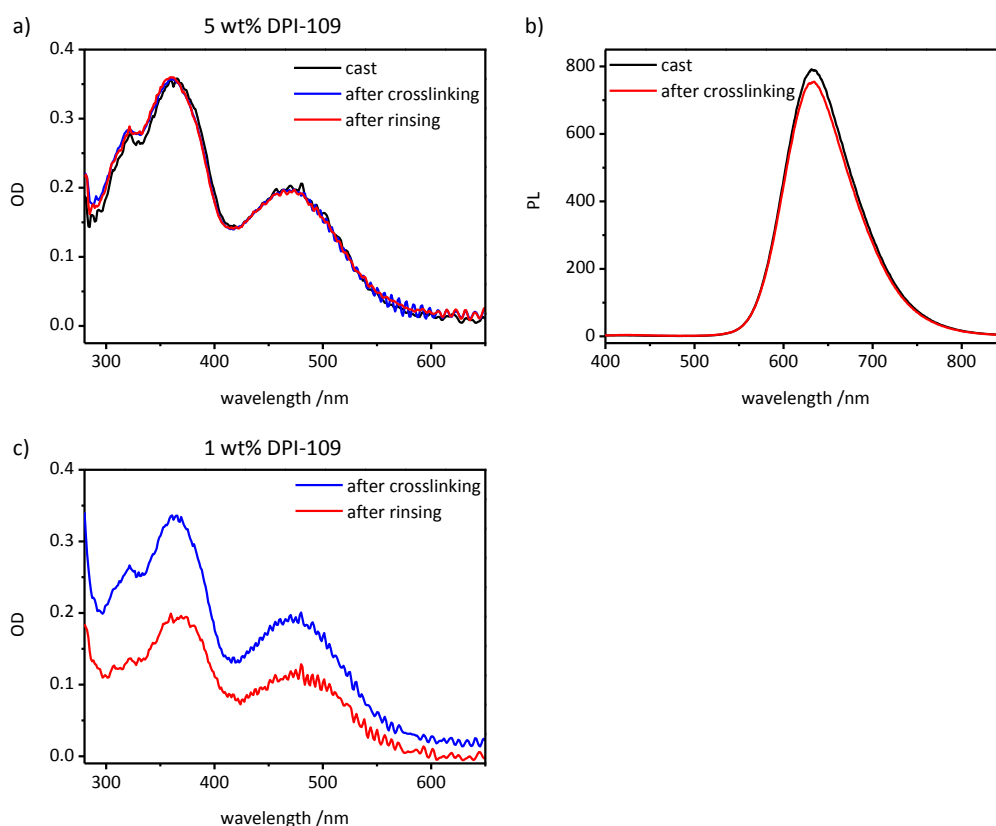


**Figure 32.** Crosslinking initiated by a PAG. **a)** UV/Vis absorption spectra: insoluble films of PFDTBTOx with 5 wt% DPI-109, 5 minutes UV exposure, 10 minutes curing at 150 °C. **b)** Photoluminescence spectra of PFDTBTOx with 5 wt % DPI-109 before and after crosslinking. **c)** UV/Vis absorption spectra: partially insoluble films of PFDTBTOx with 1 wt% DPI-109, 10 minutes UV exposure, 15 minutes curing at 150 °C.

As an alternative to the photoacid generator concept trifluoroacetic acid (TFA,  $\text{CF}_3\text{COOH}$ ) was used as initiator.<sup>[203]</sup> This strategy combines a number of advantages compared to PAGs: The samples are prepared from plain polymer solutions without any photolabile component, which needs to be taken care of during processing. The low boiling point of 78 °C and TFA's high vapor pressure help saturating the thin sample with protons even at comparably mild temperatures. This means that residual TFA can easily be removed from the films by a simple vacuum treatment. With regard to device fabrication we also

investigated if TFA has any influence on the properties of indium tin oxide (ITO) on the substrates of the solar cells. Conductivity measurements of ITO coated glass before and after exposure to TFA vapor at 100 °C for 30 minutes showed no indication of degradation.

The sequence of steps for the crosslinking experiments with TFA is illustrated in Figure 33. After spin coating from chlorobenzene solution (15 mg ml<sup>-1</sup>) and drying, the approximately 80 nm thick films were exposed to TFA and heat under an inert argon atmosphere. Exclusion of oxygen is crucial to avoid degradation. After crosslinking the films were stored in vacuum at 80 °C for 30 minutes. Again, to estimate the crosslinking efficiency, the optical densities before and after rinsing with solvent were compared.

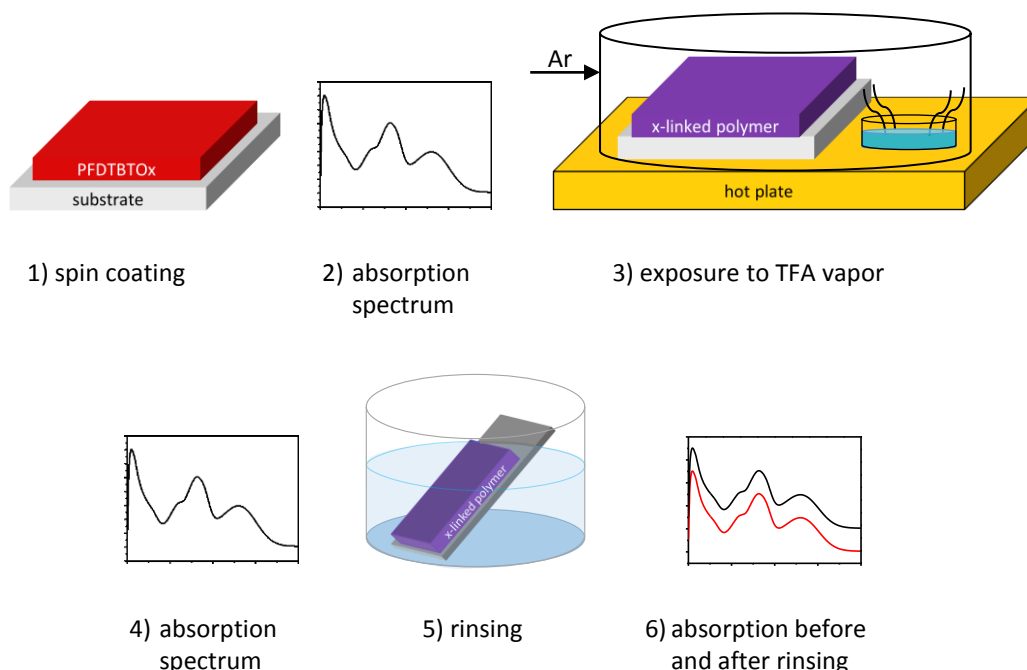


**Figure 33.** Solubility test for the crosslinking of PFDTBTOx initiated by trifluoroacetic acid.

In a first series of experiments films of PFDTBTOx were exposed to TFA vapor at 100 °C for 5 to 60 minutes. This strategy immediately proved to be much more effective compared to the crosslinking induced by PAGs. Insoluble films are obtained already after 5 minutes in TFA atmosphere at 100 °C (Figure 34a). Striving for milder conditions, the same experiments were conducted at 80 °C. Even in this case, exposure to TFA for 5 minutes resulted in entirely insoluble films. The results from the solubility tests are shown in Figure 34b. Only the absorption spectra of the samples that were exposed to TFA for five minutes are shown. Longer crosslinking times (10, 20, 30, and 60 minutes) also resulted in completely insoluble films.

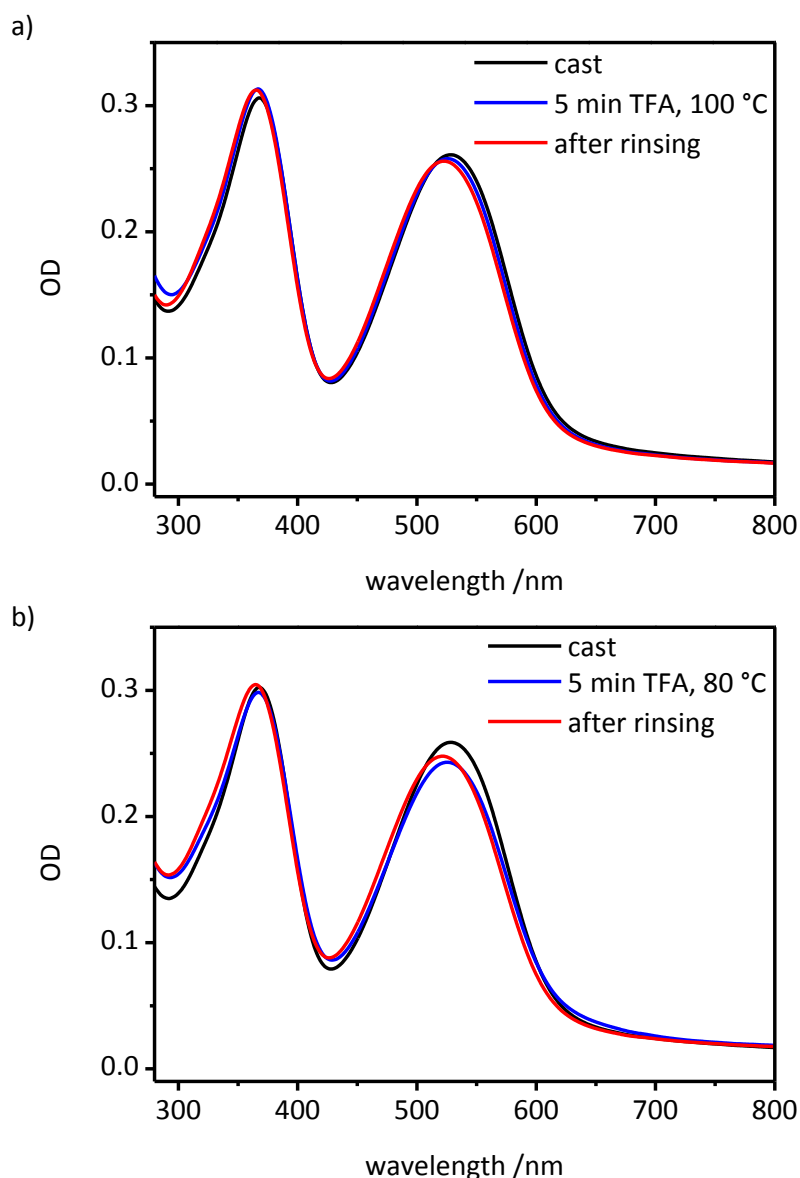


**Figure 34.** Crosslinking initiated by TFA vapor. **a)** Insoluble films of PFDTBTOx after exposure to TFA vapor for five minutes at 100 °C. **b)** Insoluble films of PFDTBTOx after exposure to TFA vapor for five minutes at 80 °C.

Trifluoroacetic acid vapor is assumed to provide an excess of protons, penetrating the entire thin film. In combination with the high density of crosslinkable groups in PFDTBTOx – two oxetanes per repeat unit – a huge density of active sites for the CROP is created. The abundance of reactive groups leads to a rapid formation of an insoluble network even at low temperatures compared to the crosslinking with photoacid generators. From a theoretical point of view it would be sufficient, if two oxetane groups per polymer chain were involved in the network. Thus, in order to form an insoluble network complete conversion of the oxetane groups is not necessary.

As an example the number of crosslinkable groups in a PFDTBTOx chain is estimated. Therefore, the SEC curve of PFDTBTOx is shown in Figure 35. The molecular weights are

calculated using a polystyrene calibration. While the chains of polystyrene are rather flexible, PFDTBTOx is a more rigid polymer. Thus, in a THF solution the hydrodynamic volume of the rigid PFDTBTOx is larger than that of a polystyrene with the same molecular weight. Consequently, the molecular weights measured for PFDTBTOx by SEC with polystyrene calibration are higher than the absolute values. In the literature this issue is addressed for polyfluorene homopolymers.<sup>[152,234]</sup> Based on the values reported by Scherf *et al.* and Scheler *et al.* an overestimation of the  $\overline{M}_n$  by about 60% was assumed. The molecular weight of PFDTBTOx was estimated according to equation 6.

$$\overline{M}_n^{est.} = 0.6 \times \overline{M}_n^{SEC} \quad \text{Equation 6}$$

With this new molecular weight the number of repeat units is calculated. From this value the number of oxetane groups per polymer chain is estimated after equation 7.

$$N_{oxetane/chain} = \frac{\overline{M}_n^{est.}}{M} \times 2 \quad \text{Equation 7}$$

$M$  is the molecular weight of the repeating unit of PFDTBTOx (1027 g mol<sup>-1</sup>), 2 is the number of oxetane groups present in every repeating unit.

This estimation was done for short chains ( $\overline{M}_n^{SEC}$  10,000 g mol<sup>-1</sup>), medium ( $\overline{M}_n^{SEC}$  15,000 g mol<sup>-1</sup>), and long chains ( $\overline{M}_n^{SEC}$  80,000 g mol<sup>-1</sup>).

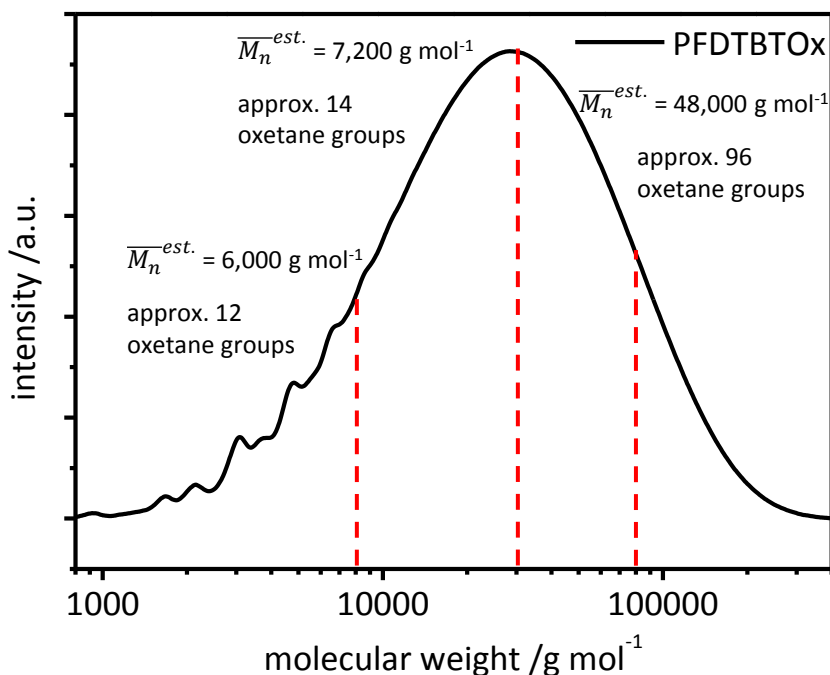


**Figure 35.** Estimation of the number of oxetane groups per polymer chain for the example of PFDTBTOx. The molecular weights and the number of oxetane groups were estimated according to equations 6 and 7.

The estimation shows that the amount of crosslinkable groups exceeds the theoretic number for crosslinking by far. Even short polymer chains possess enough oxetane groups to form a network. However, this entire calculation is to be regarded as an estimation rather than an exact determination.

Additionally, it was confirmed that TFA renders the PFDTBTOx films insoluble by opening the oxetane ring. This was done by IR spectroscopy of dropcast, and thus very thick, films of PFDTBTOx. A part of the IR spectrum of PFDTBTOx before and after crosslinking is shown in Figure 36. The band at  $980 \text{ cm}^{-1}$  is characteristic for the cyclic C-O-C group of the oxetane ring. Upon exposure to TFA vapor this band is reduced significantly. This result indicates that the majority of the oxetane rings are opened by TFA. In the IR spectrum of the crosslinked PFDTBTOx also new bands appear in the range of  $1150 \text{ cm}^{-1}$ . Typically in this region the bands of acyclic esters can be found. These are the products expected from the CROP of oxetanes.

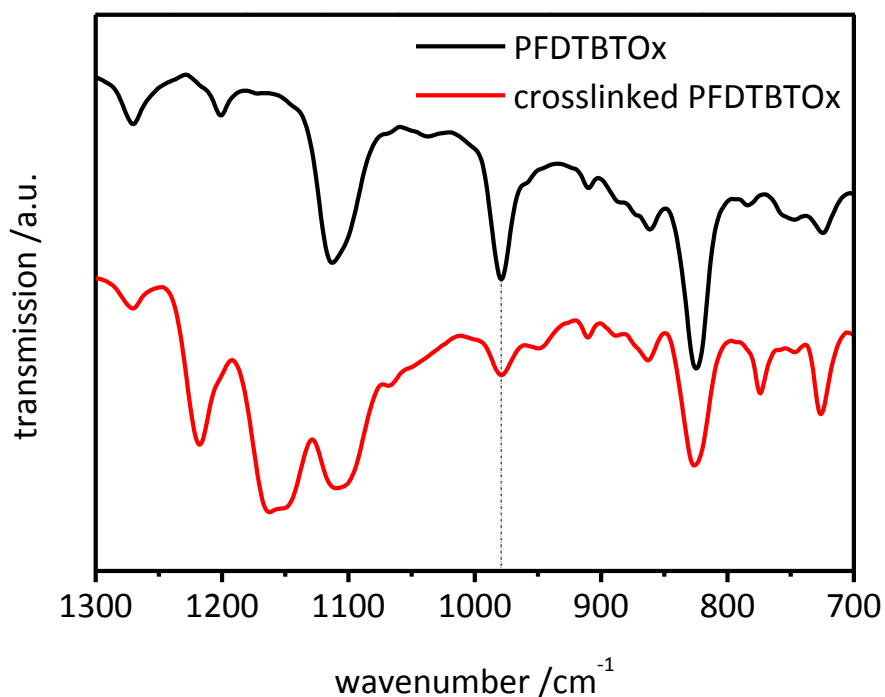


**Figure 36:** IR spectra of PFDTBTOx films before (black) and after exposure (red) to TFA vapor (15 minutes at 80 °C). The dashed vertical line at 980 cm<sup>-1</sup> indicates the characteristic band attributed to the oxetane group.

After experiencing that TFA vapor rapidly leads to the formation of insoluble films of PFDTBTOx, we studied the kinetics of crosslinking in more detail. Therefore, crosslinking experiments with copolymers with varied amounts of crosslinkable groups were performed. As described in Figure 33 the crosslinking efficiency was monitored by solubility tests. Films of PFDTBTOx, PFDTBTO<sub>x0.75</sub>, PFDTBTO<sub>x0.50-alt.</sub>, PFDTBTO<sub>x0.50</sub>, and PFDTBTO<sub>x0.25</sub> were exposed to TFA vapor at 80 °C for 2, 5, 10, 20, and 30 minutes. The kinetics plot of crosslinking is shown in Figure 37. The values of film retention were calculated from the ratio of optical density of the samples after crosslinking and after rinsing. Optical density was taken from the absorption maximum around 530 nm.

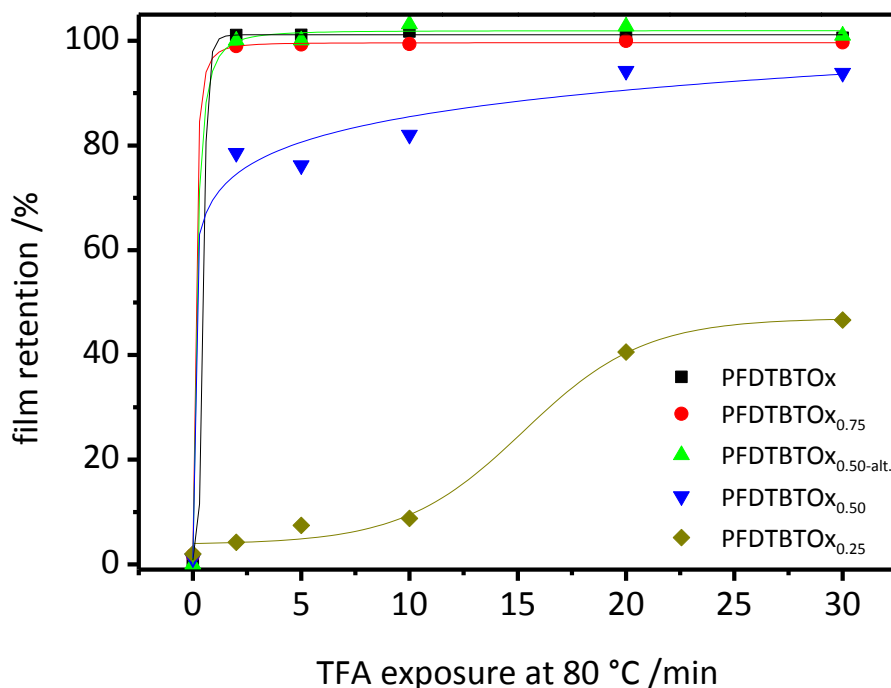


**Figure 37.** Kinetics of crosslinking from solubility tests. Film retention was calculated from the optical density of films before and after rinsing with THF.

Polymers with high density of oxetane groups, PFDTBTOx and PFDTBTOx<sub>0.75</sub>, almost immediately form insoluble networks upon exposure to TFA. Strikingly, PFDTBTOx<sub>0.50-alt.</sub> and PFDTBTOx<sub>0.50</sub> show different crosslinking behavior. PFDTBTOx<sub>0.50-alt.</sub> has exactly one oxetane group in every repeat unit. In this case insoluble films are formed after two minutes as it is known from the polymers with higher amounts of oxetane units. With PFDTBTOx<sub>0.50</sub> 80% film retention is achieved already after short exposure times. After 20 and 30 minutes these samples are more than 90% insoluble. In PFDTBTOx<sub>0.50</sub> crosslinkable and non-crosslinkable repeat units are distributed statistically. NMR spectra showed that the number of crosslinkable groups per repeat unit is also one. However, in this case this is only the average value. Additionally, the molecular weight of PFDTBTOx<sub>0.50</sub> is significantly lower ( $\overline{M}_n$  6,800 g mol<sup>-1</sup>) compared to the other polymers of this series. Consequently, it is very likely that particularly the very short polymer chains do not contain enough crosslinkable groups. In the case of such low molecular weights even the formation of polymers without any crosslinkable groups cannot be ruled out entirely.

In PFDTBTOx<sub>0.25</sub> exposure times of 10 minutes and below do not result in any significant crosslinking. More than 90% of the films remain soluble. In this case a longer exposure time obviously helps to crosslink at least parts of the films, resulting in 50% film retention after 30 minutes. To double-check the results this series of experiments was conducted with the non-crosslinkable PFDTBT. Here, even after 30 minutes exposure to TFA at 80 °C, the films remained completely soluble and were washed from the substrate within a few

seconds. Without crosslinkable oxetane group no crosslinking by any other means takes place. We also checked if the crosslinking can be induced solely by temperature. To do so, we stored samples of PFDTBTOx at 100 °C under argon for 30 minutes. These samples also remained entirely soluble when rinsed with solvent. Annealing of PFDTBTOx for 20 hours at 100 °C did not result in any kind of crosslinking.

With this set of experiments it was shown that crosslinking of our fluorene based low bandgap polymers obviously requires the presence of crosslinkable oxetane groups as well as a source of protons (from a photoacid generator or trifluoroacetic acid vapor). We did not observe any hints for thermal activation of the oxetane groups. Polymers with high amounts of crosslinkable groups form insoluble films very rapidly. With lower concentrations of oxetane longer times for crosslinking are required and partially soluble films are formed after 20 minutes.

Based upon the knowledge about the crosslinking gained in the solubility tests, the focus was put on more device oriented studies. Up to now only the crosslinking of neat polymer films was investigated. These results are, for instance, valuable for the fabrication of bi- or multilayer devices. Onto a crosslinked layer of the low bandgap polymer another layer of the acceptor material can be applied from solution. Due to the crosslinking, the low bandgap polymer layer is insoluble and thus not harmed by the solvent of the subsequently added layer.

In the field of polymer solar cells the bulk heterojunction (BHJ) concept is way more popular compared to layered device architectures. Here, the active layer typically comprises a blend of a low bandgap polymer and an electron accepting compound, for example fullerene and its derivatives. By this approach a large interfacial area between the donor and acceptor material is gained. This significantly enhances exciton separation at the donor-acceptor interface. However, the nanostructure of such an polymer:fullerene blend is in a thermodynamic non-equilibrium and thus prone to macrophase separation. If macrophase separation sets in, the beneficial intermixing of donor and acceptor materials deteriorates. Our goal is to stabilize such a structure by crosslinking the low bandgap polymer. For this purpose it has to be demonstrated that PFDTBTOx can be crosslinked in a blend with fullerenes. Again, the solubility test was the method to monitor the crosslinking. The steps for this experiment are drawn in Figure 38.

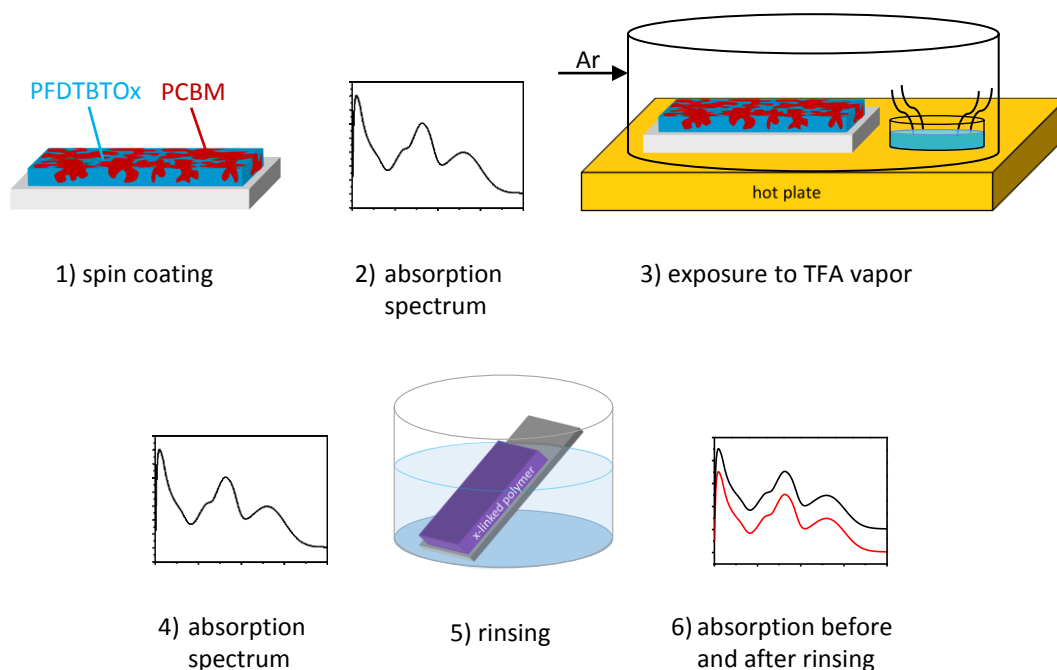


**Figure 38.** Crosslinking of blends of PFDTBTOx and PCBM (1:2) initiated by TFA vapor.

The crosslinkable polymer PFDTBTOx and the fullerene derivative PCBM (1:2 w/w,  $30 \text{ mg ml}^{-1}$ ) were mixed in a solution of chlorobenzene. After spin coating and drying absorption spectra were recorded. In an inert argon atmosphere films were exposed to TFA at  $100 \text{ }^\circ\text{C}$  followed by storage in vacuum at  $60 \text{ }^\circ\text{C}$  for 30 minutes. To estimate the crosslinking efficiency, the optical densities before and after rinsing with solvent were compared.

The absorption spectra are shown in Figure 39. Strikingly, in the range of 280 to 400 nm most of the optical density is lost after rinsing. However, the remaining absorption spectrum matches the spectrum of neat PFDTBTOx. The low bandgap polymer is crosslinked successfully, remaining as insoluble layer. All the loss of optical density during rinsing is assigned to PCBM. The low-molar mass acceptor is not incorporated into the polymer network by chemical bonds. Upon rinsing PCBM is easily washed out of the thin samples, leaving behind the polymer scaffold.

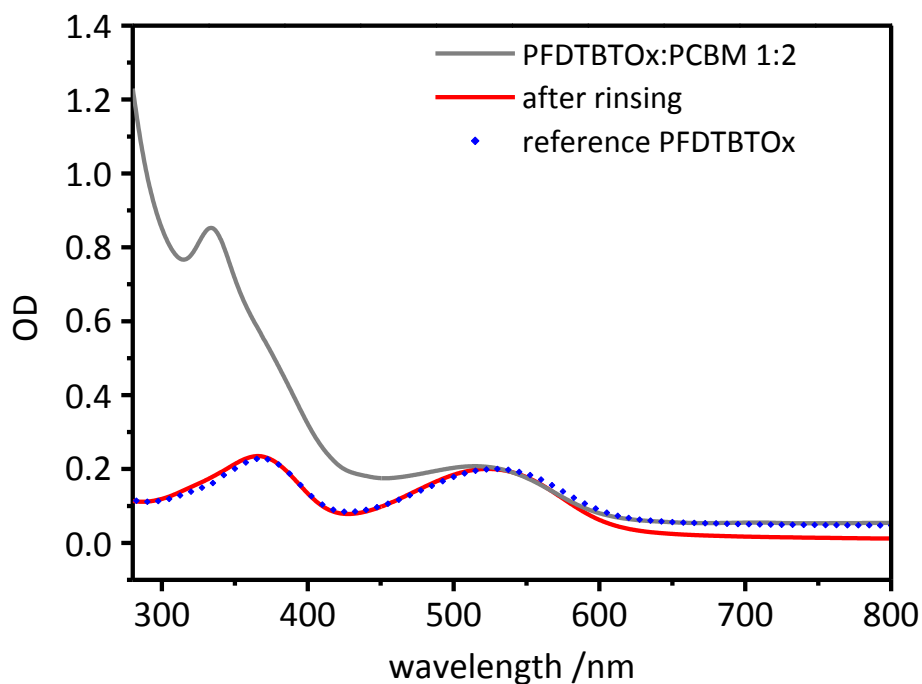


**Figure 39.** Crosslinking of PFDTBTOx in a blend with PCBM. The sample was exposed to TFA vapor at 100 °C for five minutes. The reference spectrum of PFDTBTOx was normalized to the maximum at 530 nm.

In this case the formation of a completely insoluble polymer films is evident from the local absorption maximum at 530 nm. This signal is assigned to PFDTBTOx and no loss in intensity is visible after rinsing the sample with solvent. As a guide to the eye an absorption spectrum of a PFDTBTOx film is shown. The reference spectrum was normalized to the maximum at 530 nm. Crosslinking times of 5, 10, 20, and 30 minutes were tested. Already after 5 minutes PFDTBTOx was insoluble.

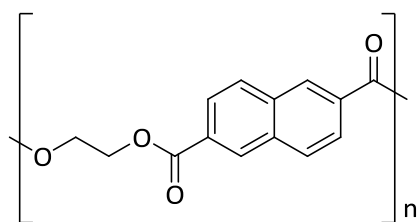


## 4 Stabilization of bulk heterojunction solar cells by crosslinking

The bulk heterojunction (BHJ) emerged as the most popular concept for the active layer of organic solar cells based on conjugated polymers. However, device stability at long operation times still remains an issue. Different mechanisms are responsible for the degradation of OSCs: chemical and especially photochemical instability of the materials as well as the instability of the donor-acceptor blend morphology. These topics will be addressed in the following section starting with chemical stability.

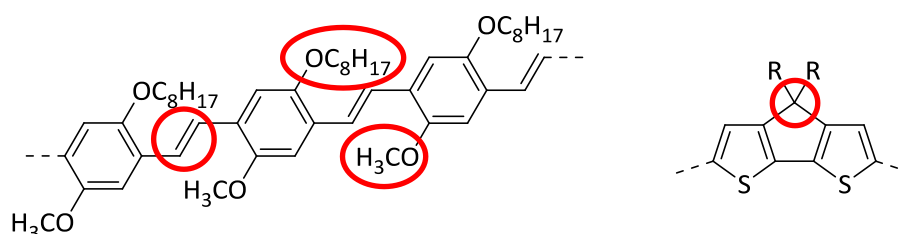
To keep oxygen and water out of OSC devices, they can be sandwiched between glass or between glass and a metal back plate.<sup>[205]</sup> If flexible devices are desired, polymer films can be used for encapsulation. Transparent polyesters like poly(ethylene terephthalate) (PET) are widely applied.<sup>[205,235]</sup> However, the barrier properties still need to be improved. For instance, poly(ethylene naphthalate) (PEN) provides an enhanced barrier against oxygen and water.<sup>[236]</sup> The chemical structure of PEN is shown in Figure 40a. Additionally, the barrier properties of polymer films can be enhanced by the deposition of a thin inorganic blocking layer of, for instance, Al<sub>2</sub>O<sub>3</sub> or SiO<sub>2</sub>.<sup>[237]</sup> Furthermore, photochemical stability of the organic semiconductors has to be considered. The chemical structure significantly influences the stability. Examples for photochemically unstable and stable units are shown in Figure 40b and c. In Figure 40b exemplarily a part of MEH-PPV and a cyclopentadithiophene are shown. The units that induce instability are denoted with circles. Exocyclic double bonds are unstable. Also, C-O single bonds can be cleaved rather easily. For photochemical stability the number of side chains should be kept to a minimum. Quaternary sites should be avoided, since they can be oxidized.<sup>[238]</sup> More stable building blocks are benzene, thiophene, benzothiadiazole, and thienopyrazine. In general, aromatic polycyclic moieties provide good chemical stability.<sup>[238]</sup> Additionally, carefully reducing the amount of impurities in the low bandgap polymers can improve the stability of organic solar cells.<sup>[239]</sup> Organic and metal impurities might arise from polymer synthesis. Furthermore, low molar mass fractions are suspected to lead to degradation of device efficiency over long times.<sup>[239]</sup>

## a) Polymer for flexible encapsulation



poly(ethylene naphthalate)

## b) Photochemically instable units



## c) Photochemically stable units

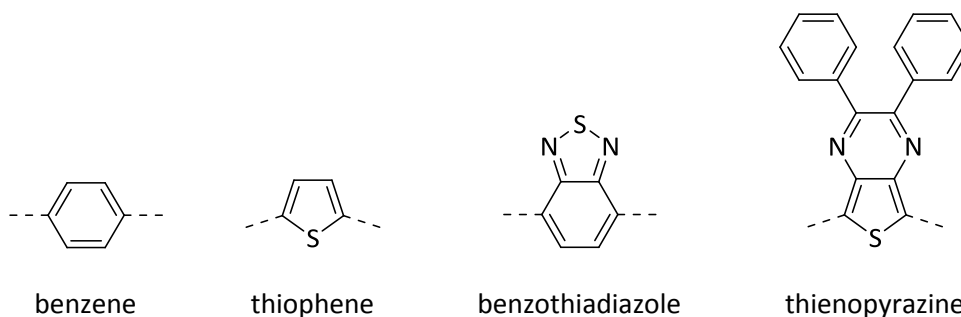


**Figure 40.** Stability of organic solar cells. **a)** Flexible encapsulation: poly(ethylene naphthalene) with enhanced barrier properties.<sup>[236]</sup> **b)** Units that induce photochemical instability are marked with red circles: exocyclic double bonds, easily cleavable C-O bonds, alkyl side chains, and quaternary sites.<sup>[238]</sup> **c)** Units that provide stability against photochemical degradation.<sup>[238]</sup>

Apart from those factors, the stability of the morphology is a special concern for bulk heterojunction devices. In a typical BHJ a low bandgap polymer acts as the electron donor and a low-molar mass fullerene derivative, such as PCBM, serves as the electron acceptor material. However, such a donor acceptor blend only achieves its best solar cell performance if the morphology meets certain requirements: Domains in the size of the exciton diffusion length (< 20 to 30 nm) ensure that excitons can reach a donor-acceptor interface within their lifetime. Nanometer sized domains also result in an increased donor-acceptor interface area. Furthermore, an ideal morphology comprises a bicontinuous

network of donor and acceptor material. This guarantees paths for charge carrier transport towards the electrodes.

Obviously, controlling the morphology is the crucial point of this BHJ approach. Several strategies for controlling the blend morphology during device fabrication are known: The choice of solvent, solvent additives, thermal annealing or solvent vapor annealing can help achieving an optimum morphology. However, such a complex morphology is thermodynamically instable and prone to macrophase separation on a long timescale. This effect is even enhanced if one component tends to crystallize. Once degradation of the nanoscale morphology occurs, the overall performance of an organic solar cell will drop significantly.

In recent years, crosslinking was utilized as an approach to lock in the morphology of a donor-acceptor blend and thus improve its long term stability. Basically, three concepts for crosslinking bulk heterojunction materials are known: Crosslinking the donor, crosslinking the acceptor, and crosslinking the donor with the acceptor. These approaches are discussed in detail in section 1.5.

Within this work the crosslinkable low bandgap polymer PFDTBTOx is tested as donor material in BHJ solar cells, and the influence of crosslinking on the device performance is investigated. Central questions are: Does crosslinking of PFDTBTOx influence the solar cell performance? Can crosslinking of PFDTBTOx help to stabilize the morphology of PFDTBTOx:PCBM blends? Will crosslinking in this case result in BHJ solar cells which retain their efficiency over a prolonged time?

## 4.1 Preliminary experiments

Bulk heterojunction solar cells were fabricated with the crosslinkable low bandgap polymer PFDTBT and the non-crosslinkable reference material PFDTBT. The set-up of the OSC devices in these experiments is shown in Figure 41a. Devices are made of glass/ITO/MoO<sub>3</sub>/active layer/Al. In all experiments the active layer was applied by spin coating and the thickness was adjusted to 80 nm. A first series of devices was fabricated from the PFDTBT reference with three different PCBM ratios. Figure 41c shows the current-voltage characteristics of solar cells with PFDTBT:PCBM ratios of 1:1, 1:2, and 1:3.

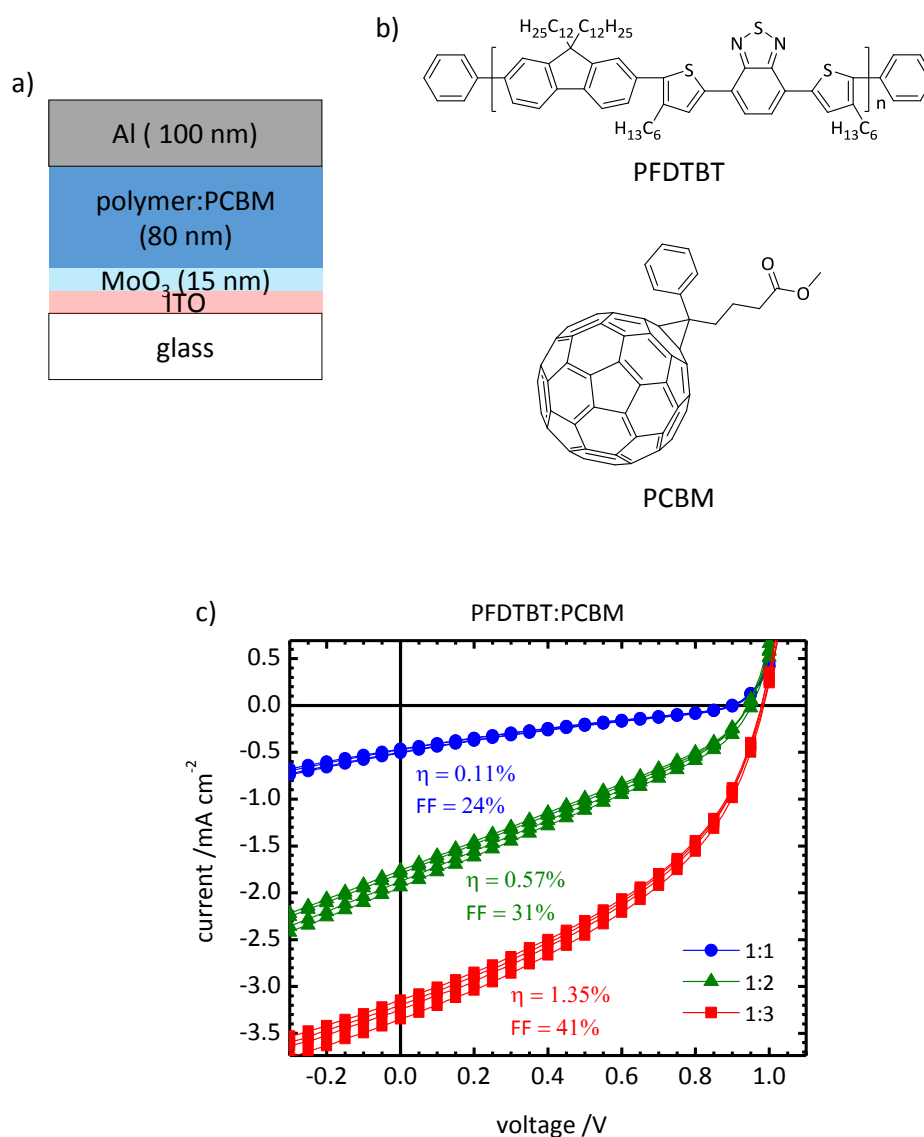


**Figure 41.** Bulk heterojunction organic solar cells from PFDTBT blends with different amounts of PCBM. **a)** Device set-up. **b)** Active layer materials PFDTBT and PCBM. **c)** Current-voltage characteristics of blend solar cells with PFDTBT:PCBM ratios of 1:1, 1:2, and 1:3. For each material combination four solar cells were measured.

Four solar cells were analyzed for each composition. In the current-voltage characteristics a strong influence of the amount of PCBM on the fill factor and efficiency becomes evident. This phenomenon is already mentioned in the literature.<sup>[159]</sup> By changing the blend ratio from 1:1 to 1:3 the efficiency increases significantly from 0.11% to 1.35%. The fill factor is improved from 24% to 41%.

Using high boiling solvent additives for spin coating polymer:PCBM blends is beneficial for the solar cell performance in particular cases. Thus, trying to increase the PCE of the solar cells a second series of devices was fabricated from PFDTBT:PCBM solutions with 5% diiodooctane (DIO). A comparison of the *J-V* curves of PDTBT:PCBM 1:1, 1:2, and 1:3 with and without DIO is shown in Figure 42.

The poorly performing 1:1 blend (Figure 42a) is not improved by adding DIO. A positive effect of DIO is visible for the 1:2 blend (Figure 42b). Here the fill factor is increased from 31% to 47%, and the power conversion efficiency is improved from 0.57% to 0.73%. An opposite effect of DIO is seen for the 1:3 blend (Figure 42c). While the fill factor of both systems remains constant at 41% and 44%, respectively, the short circuit current drops from  $-3.4 \text{ mA cm}^{-2}$  to  $-1.2 \text{ mA cm}^{-2}$ . Additionally, a slight loss in open current voltage is observed. Consequently, the PCE of the PFDTBT:PCBM blend processed with DIO is by a factor of three smaller compared to the efficiency of blend without additive.

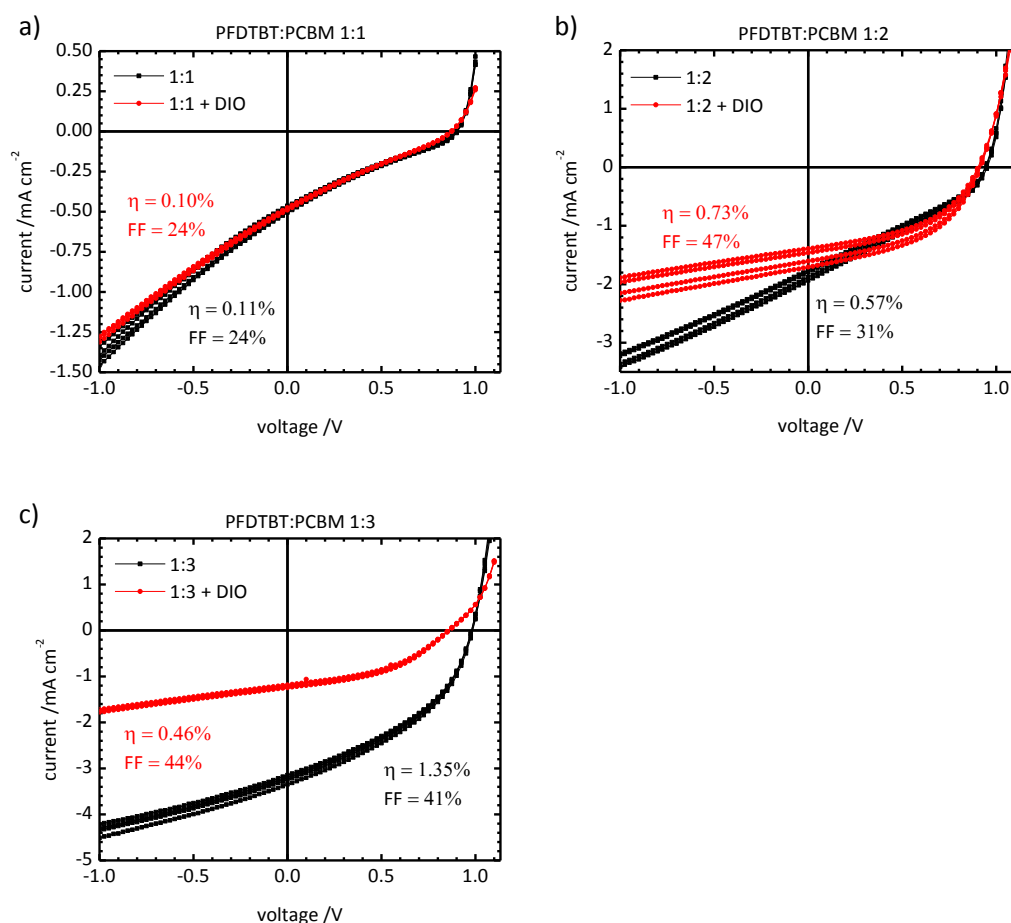


**Figure 42.** Influence of the solvent additive 1,8-diiodooctane (DIO) on the solar cell characteristics. **a)** PFDTBT:PCBM 1:1, **b)** PFDTBT:PCBM 1:2, **c)** PFDTBT:PCBM 1:3. For each material combination four solar cells were measured.

From this first set of experiments with the reference polymer PFDTBT it became obvious that this system is very sensitive to the composition and the use of solvent additives. Increasing the amount of PCBM significantly improves the device performance. A blend of PFDTBT:PCBM with a ratio of 1:3 was found to be the best performing in this experiment. Adding DIO for device fabrication has no effect on PFDTBT:PCBM 1:1 and only slightly improves the performance of the PFDTBT:PCBM 1:2 devices. DIO is even detrimental for the PFDTBT:PCBM 1:3 blend. Thus, in the following experiments with the crosslinkable PFDTBTOx DIO was no longer applied as processing additive.

The next step was applying the processing parameters known from the reference material to the crosslinkable PFDTBTOx. Therefore, BHJ solar cells with PFDTBTOx:PCBM ratios of 1:1, 1:2, and 1:3 were fabricated. The current-voltage characteristics are displayed in Figure 43.

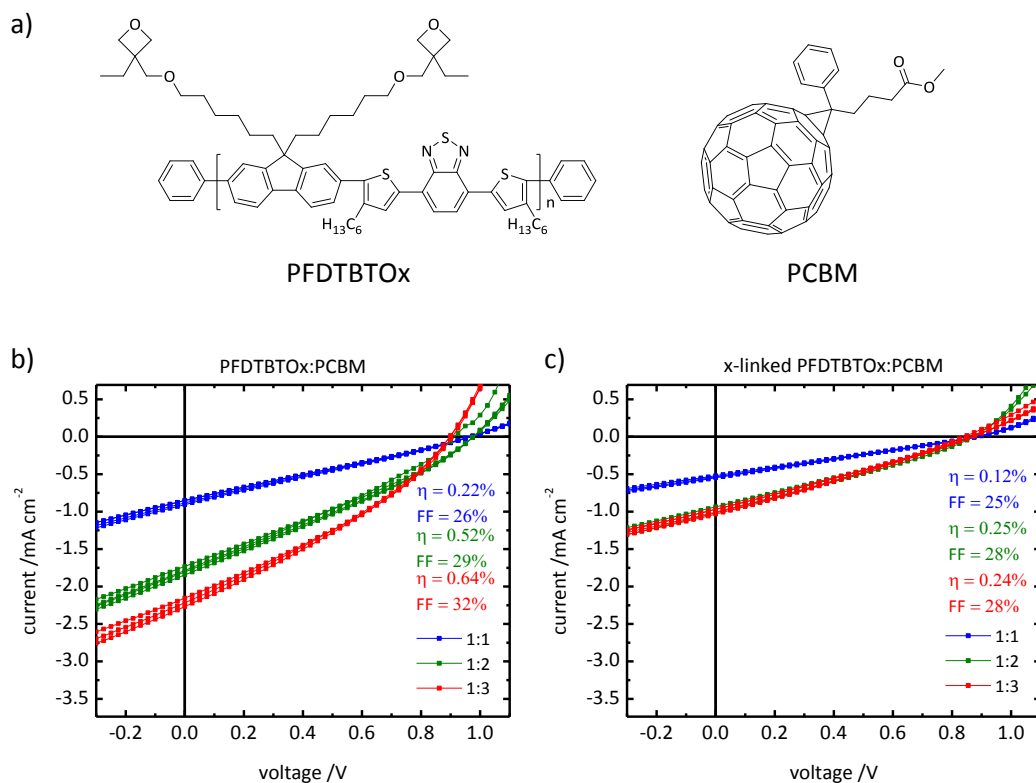


**Figure 43.** Bulk heterojunction organic solar cells from PFDTBTOx blends with different amounts of PCBM. **a)** Active layer materials PFDTBTOx and PCBM. **b)** Current-voltage characteristics of blend solar cells with PFDTBTOx:PCBM ratios of 1:1, 1:2, and 1:3. **c)** Current-voltage characteristics of crosslinked blend solar cells with PFDTBTOx:PCBM ratios of 1:1, 1:2, and 1:3. For each material combination four solar cells were measured.

The solar cell performance of PFDTBTOx does not quite match the parameters of the reference material. Increasing the amount of PCBM does not improve the PCE in such a significant way as it was found with PFDTBT. However, the best efficiency was still achieved with a blend ratio of PFDTBTOx:PCBM 1:3. A question arising was whether the stabilizing effect of crosslinking can still be observed for a relatively low amount of crosslinkable polymer in the 1:3 blend.

Ultimately, BHJ solar cells with crosslinked PFDTBTOx:PCBM blends were tested. Following spin coating of the active layer, the devices were exposed to TFA vapor at 80 °C under an inert atmosphere. Residual TFA was removed in high vacuum prior to the evaporation of the aluminium electrodes. Figure 43c shows the *J-V* curves of crosslinked devices with blend ratios of 1:1, 1:2, and 1:3. The efficiencies and fill factors are lower compared to the non-crosslinked PFDTBTOx devices. In addition, with increasing amount of PCBM almost no improvement of the solar cell performance is observed.

Figure 44 compares the power conversion efficiencies of the investigated BHJ materials. The efficiency of the reference polymer PFDTBT strongly depends on the amount of PCBM. By the solvent additive DIO the efficiency of the PFDTBT:PCBM 1:2 blend is only slightly increased. However, DIO has a negative influence on the performance of the 1:3 blend. For PFDTBTOx the efficiencies are lower compared to PFDTBT. Also the effect of the

polymer:PCBM ratio is less significant. Crosslinking the polymer leads to the lowest efficiencies in this series. The presence of a high number of oxetane groups seems to have a significant influence on the solar cell performance. Compared with the reference polymer PFDTBT the crosslinkable PFDTBTOx leads to lower PCEs in blend ratios of 1:1, 1:2, and 1:3. The efficiency is further decreased if the low bandgap polymer is crosslinked. In PFDTBTOx the amount of oxetanes is very high (two oxetanes per repeat unit). Thus, a very densely crosslinked network is formed by crosslinking. We were aware of reports in the literature that a high crosslinking density might be detrimental for the device performance.<sup>[203,207]</sup> Nevertheless, we chose this material for the following accelerated aging tests. When it comes to stabilizing the blend morphology, the high number of crosslinkable groups should be very helpful for observing an effect on the long term stability.

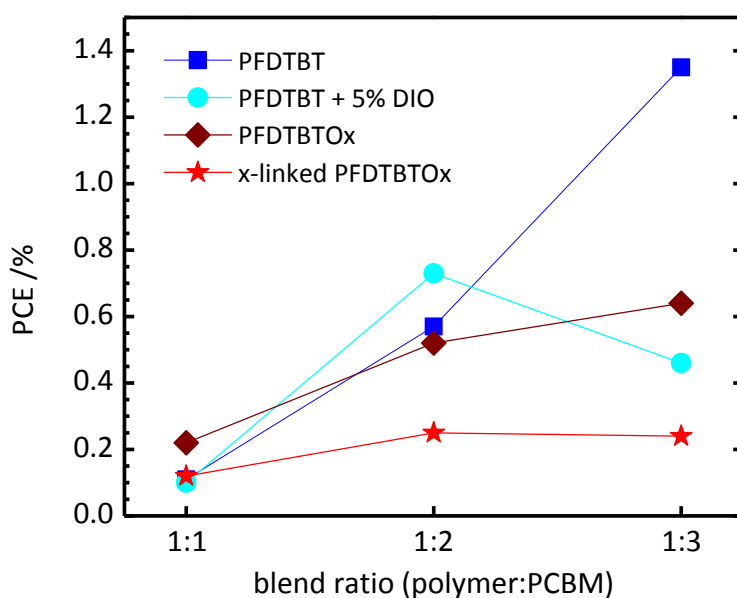


**Figure 44.** Influence of the blend ratio on the power conversion efficiency.

## 4.2 Accelerated aging tests

For investigating the influence of crosslinking on the long term stability of BHJ solar cells accelerated aging tests were performed. In such an experiment the development of devices after long operation times is simulated. As described above, the morphology is the crucial point for BHJ solar cells. For a polymer:PCBM blend the morphology is likely to be hampered by diffusion of the low-molar mass fullerene. This leads to the formation of large aggregates of PCBM. However, PCBM diffusion is rather slow at room temperature. In an accelerated aging experiment diffusion is increased by annealing the samples at elevated temperatures. Thus, the behavior of solar cells at long operation times can be simulated in a reasonable time. In this work, 100 °C was chosen as the temperature for the annealing process. This was deemed a good temperature for accelerating PCBM diffusion on the one hand and not creating detrimental thermal degradation on the other.

Prior to the fabrication of solar cells, the impact of thermal treatment on the blend morphology was tested. Therefore, blends of PFDTBTOx:PCBM and PFDTBT:PCBM were cast on glass slides. The films were annealed at 100 °C under inert atmosphere for 15 minutes, 75 minutes, 8 hours, 30 hours, and 100 hours. After each step, the samples were checked for PCBM aggregates using polarization optical microscopy. In Figure 45 optical micrographs of polymer:PCBM 1:3 blends are shown. The left column shows samples of PFDTBTOx:PCBM 1:3 that were crosslinked at 80 °C in TFA vapor after spin coating. They are compared with non-crosslinked PFDTBTOx:PCBM films and blends of the non-crosslinkable PFDTBT:PCBM. Micrographs of the samples after spin coating are shown in the first line. Using crossed polarizers and a  $\lambda$  plate, the amorphous film appears red. Within the resolution of the optical microscope no aggregates can be observed in the initial state of the three samples. In the crosslinked blend shown in the left column no aggregates can be observed for annealing times of up to 100 hours. After eight hours, occasional small aggregates are visible in the PFDTBT:PCBM blend shown in the right column. More aggregates appear after 30 hours. After annealing for 100 hours, aggregates of PCBM have grown to lengths of more than 10  $\mu\text{m}$ . Strikingly, the other non-crosslinked sample, PFDTBTOx:PCBM shown in the middle, exhibits a different behavior. Similar to the crosslinked PFDTBT no aggregates are observed within the first 30 hours of annealing. Only after 100 hours small aggregates become visible.

The stabilizing effect of crosslinking the donor polymer becomes evident from comparing the crosslinked PFDTBTOx:PCBM with the PFDTBT:PCBM blend. Furthermore, the non-crosslinked PFDTBTOx:PCBM seems to be much more stable than the PFDTBT:PCBM reference. The oxetane groups in PFDTBTOx might be the reason for this stabilization. In previous crosslinking experiments (chapter 3) no thermally activated crosslinking of oxetane was observed. However, in these experiments only shorter times were tested compared to the very long annealing times in this experiment. The established solubility tests were performed to clear whether thermally activated crosslinking is the reason for the surprising stability of the initially non-crosslinked PFDTBTOx:PCBM blends.

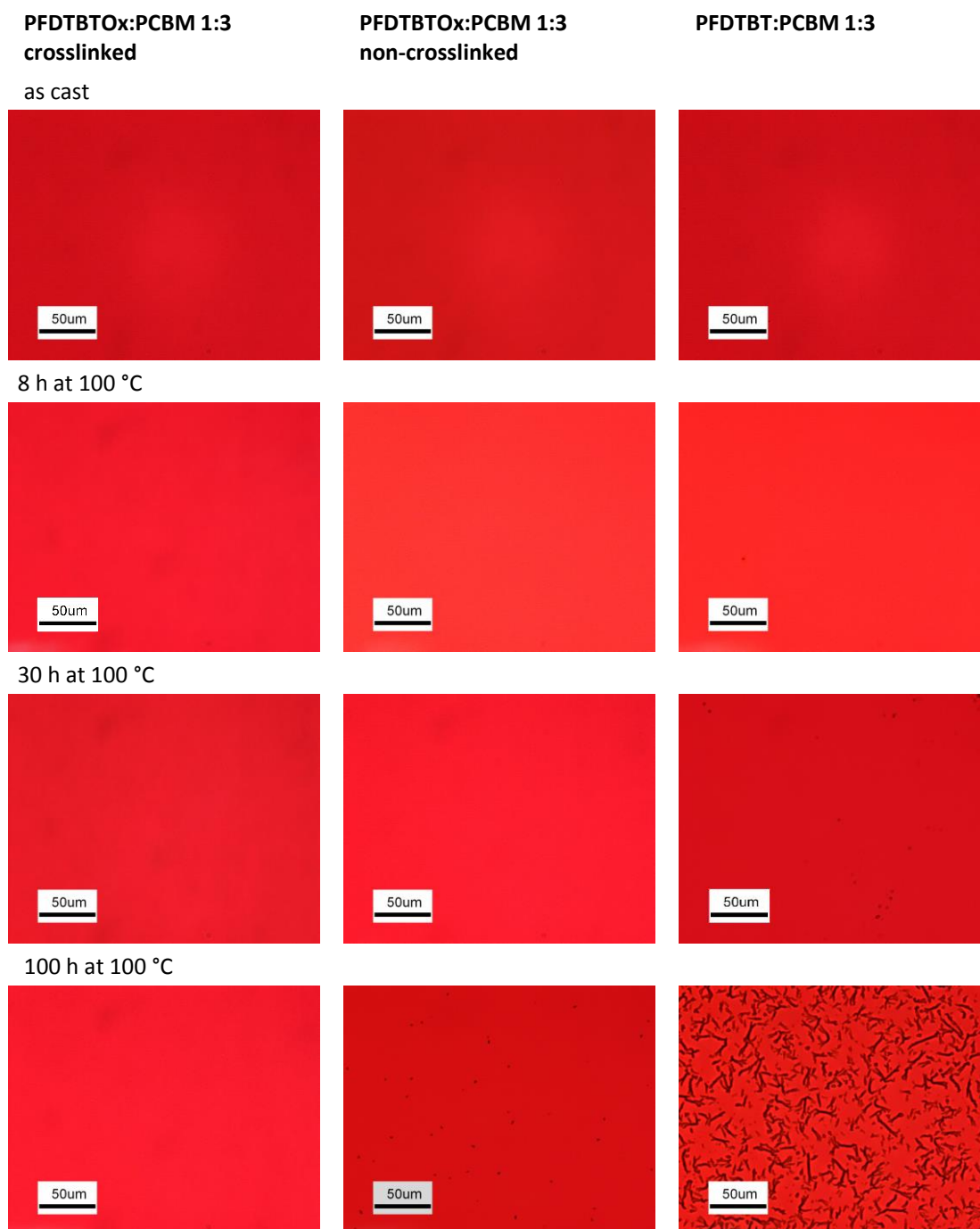


**Figure 45.** Optical micrographs of polymer:PCBM 1:3 blends. Crosslinked PFDTBTOx (left column) is compared with non-crosslinked PFDTBTOx (middle) and the non-crosslinkable PFDTBT (right column).

The stabilizing effect of crosslinking the donor polymer becomes evident from comparing the crosslinked PFDTBTOx:PCBM with the PFDTBT:PCBM blend. Furthermore, the non-crosslinked PFDTBTOx:PCBM seems to be much more stable than the PFDTBT:PCBM reference. The oxetane groups in PFDTBTOx might be the reason for this stabilization. In previous crosslinking experiments (chapter 3) no thermally activated crosslinking of oxetane was observed. However, in these experiments only short times were tested compared to the very long annealing times in this experiment. The established solubility

tests were performed to clear whether thermally activated crosslinking is the reason for the surprising stability of the initially non-crosslinked PFDTBTOx:PCBM blends. Results from the solubility tests are shown in Figure 46.

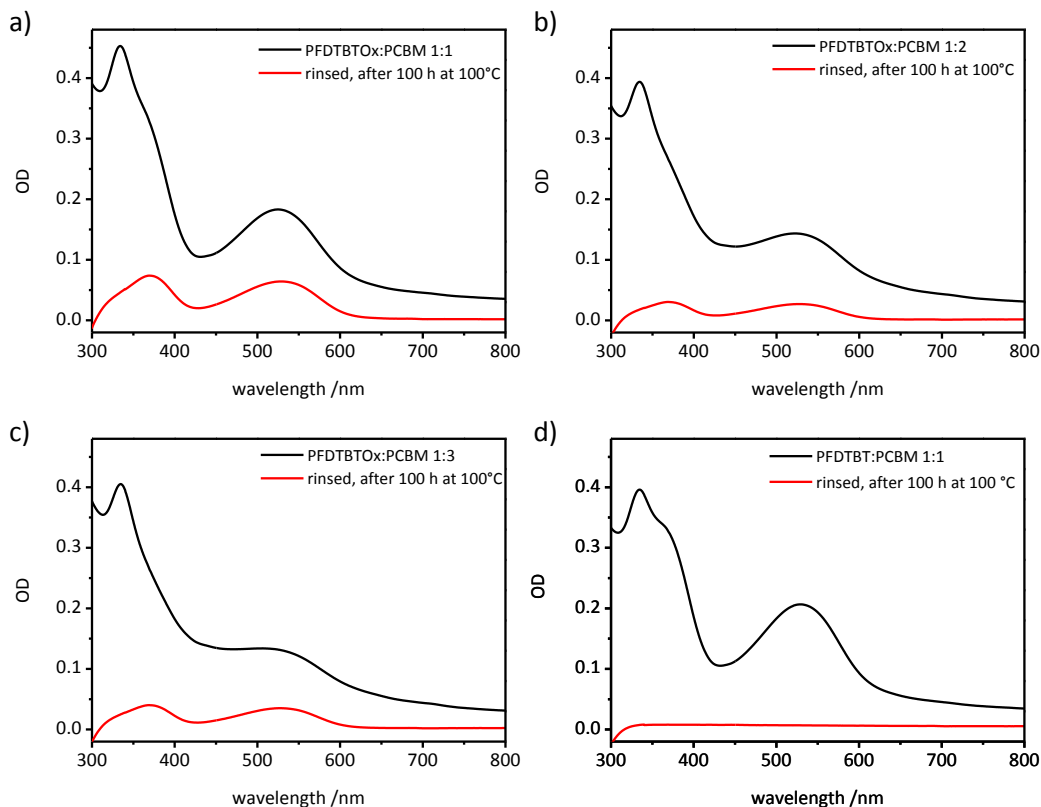


**Figure 46.** Thermally induced crosslinking. Solubility tests of polymer:PCBM films. **a)** PFDTBTOx:PCBM 1:1. **b)** PFDTBTOx:PCBM 1:2. **c)** PFDTBTOx:PCBM 1:3. **d)** The non-crosslinkable reference PFDTBT:PCBM 1:1.

From the solubility tests it becomes obvious that PFDTBTOx becomes partially insoluble after annealing at 100 °C for 100 hours. Approximately 20 to 30% of the optical density of the polymer is retained after rinsing. In the case of the PFDTBT reference without crosslinkable groups, the polymer is completely washed away. We conclude that PFDTBTOx is thermally crosslinked during annealing at 100 °C for very long times. Thus, crosslinking might cause the stabilizing effect of the initially non-crosslinked PFDTBTOx:PCBM blends.

For the accelerated aging experiments BHJ solar cells of the crosslinked PFDTBTOx were compared with the reference polymer PFDTBT and additionally with the non-crosslinked PFDTBTOx. The steps of the accelerated aging experiment are illustrated in Figure 47. The active layer is applied to the solar cell substrates by spin coating from chlorobenzene solutions of PFDTBTOx:PCBM and PFDTBT:PCBM. Polymer:PCBM ratios of 1:1, 1:2, and 1:3 were investigated. In all devices the active layer was 80 nm thick. Crosslinking was executed in trifluoroacetic acid (TFA) vapor at 80 °C under inert atmosphere. The devices were allowed to warm to 80 °C for five minutes prior to the exposure to TFA for 15 minutes. Consequently, the non-crosslinked devices were annealed at 80 °C for 20 minutes

under inert atmosphere. On top of the active layer the Al electrode was evaporated. The devices were allowed to rest for three days at room temperature in inert atmosphere before the initial *J-V* curves are recorded. To monitor the development of the device performance during annealing, they were characterized after 15 minutes, 60 minutes, 8 hours, 30 hours, and 100 hours of thermal treatment at 100 °C. Solar cell characterization was executed under inert atmosphere. For each material combination four solar cells were measured.

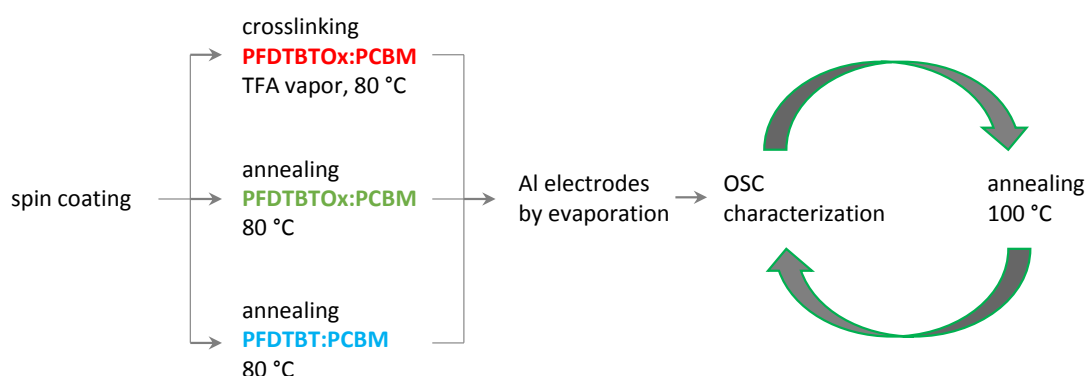


**Figure 47.** Accelerated aging experiment. Sequence of steps for device fabrication, characterization and annealing. For all three material systems the blend ratios polymer:PCBM 1:1, 1:2, and 1:3 were investigated. A scheme of the device set-up is drawn in Figure 41a.

The following discussion of the results from the accelerated aging experiment focusses on the polymer:PCBM 1:2 and 1:3 blends. The 1:1 blends are excluded because of their poor performance.

Following every single interval of annealing, the current-voltage characteristics and EQE spectra of the solar cells were measured. The *J-V* curves are shown in Figure 48.

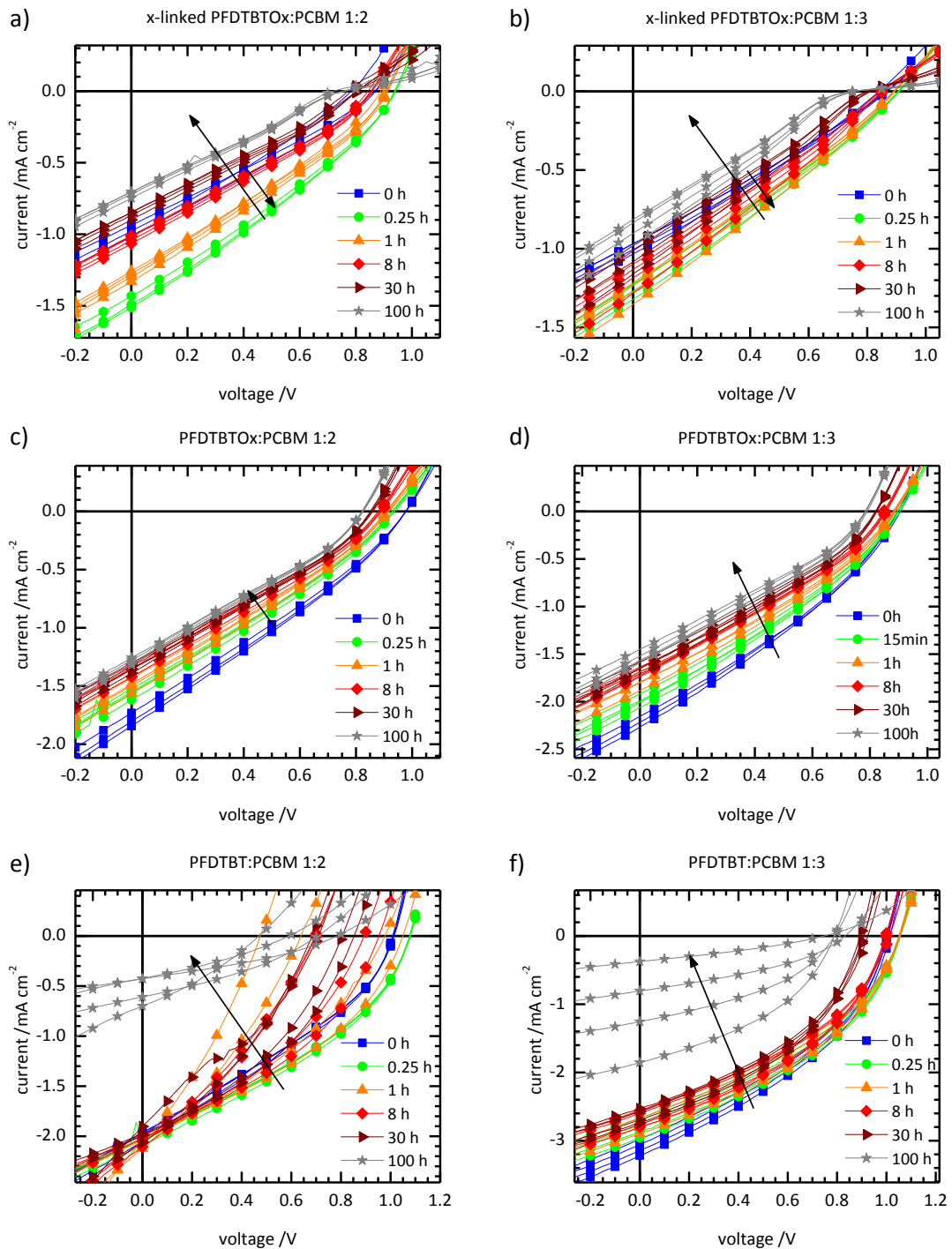


**Figure 48.**  $J$ - $V$  characteristics from accelerated aging tests of the crosslinked PFDTBTOx (a, b), non-crosslinked PFDTBTOx (c, d), and non-crosslinkable PFDTBT (e, f). Polymer:PCBM blends with a 1:2 ratio are shown on the left (a, c, e), polymer:PCBM 1:3 blends on the right (b, d, f). For each material combination four solar cells were measured.

From the  $J$ - $V$  curves similar behavior of the 1:2 and 1:3 blends of the three different systems becomes visible. The crosslinked PFDTBTOx devices show an improved OSC performance after short annealing times of 15 minutes. Even after eight hours at 100 °C the devices show better current-voltage characteristics compared to the devices before

annealing. After long annealing times (30 hours and 100 hours), the performance drops below the initial values. The non-crosslinked PFDTBTOx and the non-crosslinkable reference PFDTBT show a different behavior upon annealing. In the current-voltage characteristics of both materials an immediate downtrend can be seen. Strikingly, the process of the decay looks different for both materials. The devices with the non-crosslinkable PFDTBT diversify upon annealing. After 100 hour of annealing, the device performance is reduced considerably. On the other hand, for the non-crosslinked PFDTBTOx almost no spread is observed. Furthermore, the degradation seems to slow down in the course of this experiment. Similar to the crosslinked PFDTBTOx samples these devices do not decay entirely.

From the current-voltage characteristics shown the PCEs were calculated. Figure 49 shows the development of the efficiencies during the accelerated aging experiment.

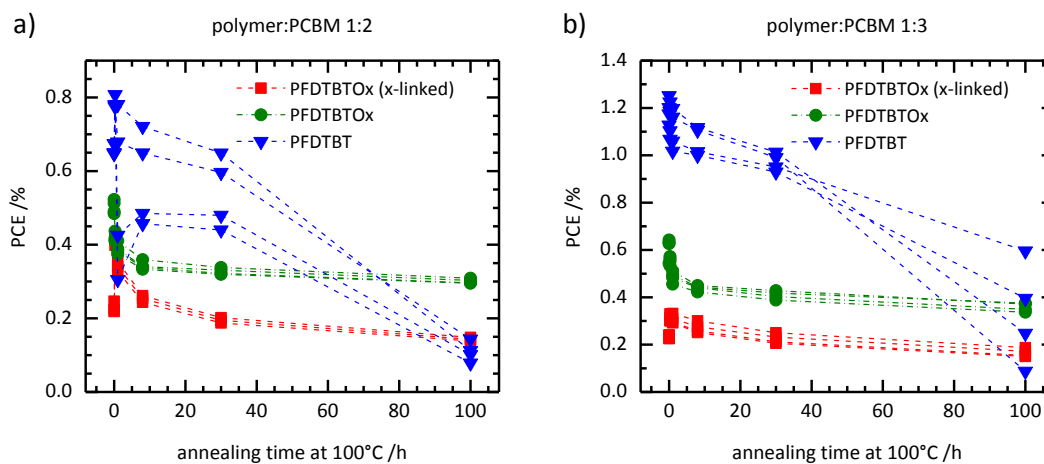


**Figure 49.** PCE for the crosslinked PFDTBTOx, not crosslinked PFDTBTOx and not crosslinkable PFDTBT in a 1:2 blend ratio (a) and in a 1:3 blend ratio (b) with PCBM. On the left side the development of the PCE upon annealing for the first 60 minutes is shown. The development of the PCE up to 100 hours is shown on the right side. For each material combination four solar cells were measured.

In the beginning, the overall performance of PFDTBTOx is much lower compared to the PFDTBT reference. Thus, the initial values for the three systems are very different. Since the primary goal of this experiment is investigating the effect of crosslinking on the long term stability, the normalized graphs provide more valuable information. In Figure 50 the development of the normalized PCEs is shown. The PCE was normalized to the initial value before annealing. Very drastic changes are observed at short annealing times. Thus, the development of the PCE for the first 60 minutes is shown separately in Figure 50a and c.

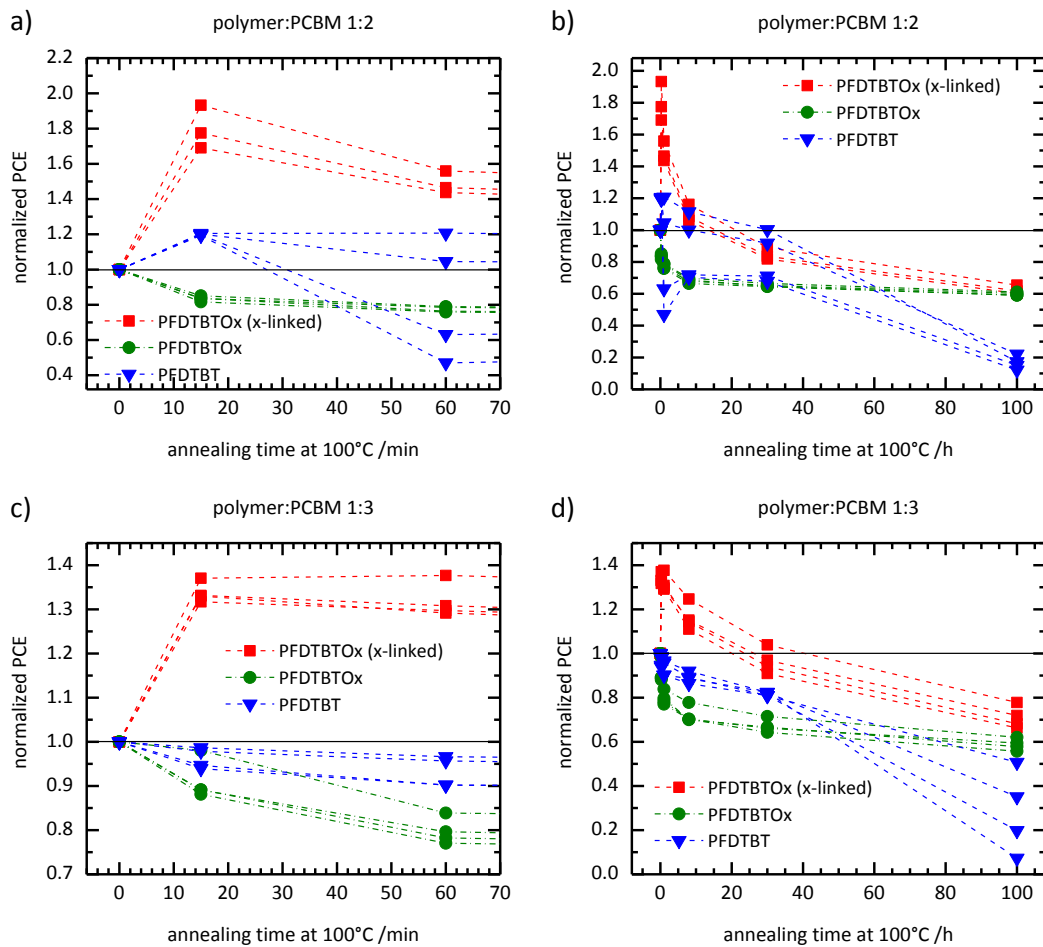


**Figure 50.** Normalized PCE (on the initial PCE before annealing) for the crosslinked PFDTBTOx, not crosslinked PFDTBTOx and non-crosslinkable PFDTBT in a 1:2 blend ratio (**a,b**) and in a 1:3 blend ratio (**c,d**) with PCBM. On the left side the development of the PCE upon annealing for the first 60 minutes is shown. The development of the PCE up to 100 hours is shown on the right side.

A significant change of the PCEs is visible after 15 minutes for both, the 1:2 and the 1:3 blends. For PFDTBTOx differences in PCE between the crosslinked and the non-crosslinked devices are observed. The PCE of the crosslinked devices increases, while the PCE of the non-crosslinked cells decreases. This trend is observed for the 1:2 blend as well as for the 1:3 blend. Looking at the development over the entire annealing time, the PCEs of the crosslinked devices reach their maxima and start to decrease afterwards. The initial PCE is reached after approximately 18 hours in the 1:2 blend and after approximately 30 hours with the 1:3 blend. After 100 hours of annealing at 100 °C, the crosslinked devices retain more than 60% of their initial efficiency. Similar experiments with oxetane functionalized low bandgap polymers are reported by Carlé *et al.* and Yau *et al.* In both cases the stability of crosslinked polymer:fullerene blend solar cells was investigated by accelerated aging experiments. The system of Yau *et al.* retained 80% of its initial PCE after a short annealing time of only 30 minutes at 150 °C.<sup>[203]</sup> In the study of Carlé *et al.* the impact of annealing at 100 °C for up to 50 hours was investigated. The efficiency of their crosslinked devices dropped to 50% of the initial value. The accelerated aging experiments performed in our

work exceed the tests of both studies providing insight into the influence of crosslinking on the device efficiency after thermal treatment for short as well as long times.

In the case of the non-crosslinked PFDTBTOx devices the most significant loss of efficiency happens within the first eight hours of annealing. At longer times the decay is slowed down, and the PCE saturates at around 60% of the starting value.

Compared with the PFDTBTOx based devices the solar cells comprising the PFDTBT reference polymer without crosslinkable oxetane groups behave differently. The PCE of the 1:3 blend device decays stepwise and no saturation is observed. Between 30 hours and 100 hours of annealing the most significant loss of efficiency is visible. Additionally, the values of the four investigated solar cells scatter severely at this point. The PCEs after 100 hours range from approximately 50% to below 20% of the initial value. On the contrary, in the 1:2 blend devices scattering sets in within the first 30 hours of the accelerated aging experiment. Again, the most significant decay is observed between 30 and 100 hours, and no saturation can be seen. After 100 hours of annealing, the PCE is approximately 20% of the starting value.

In summary, the PCEs of PFDTBT and PFDTBTOx blends behave differently upon annealing at 100°C. While the efficiencies of PFDTBT blends decays significantly to low efficiencies, the PCEs of PFDTBTOx blends seem to stabilize after 30 hours. For longer annealing times up to 100 hours only small changes can be observed. This behavior can be attributed to blend stabilization by crosslinking the polymer in the blend. The crosslinked polymer network lowers the diffusivity of the PCBM molecules<sup>[240]</sup> preventing the aggregation of PCBM. Consequently, the morphology of the bulk heterojunction is retained and the PCE is not further reduced.

Actually, this kind of stabilizing effect was expected for the crosslinked PFDTBTOx, but not for the non-crosslinked PFDTBTOx blends. In the first eight hours of this accelerated aging experiment the non-crosslinked PFDTBTOx devices showed the expected behavior. Here, a decrease in PCE was observed. However, at longer annealing times (30 to 100 hours) the PCE of the non-crosslinked blends remains constant, and no further decrease is observed. Strikingly, at these annealing times the PCE development is quite similar to the crosslinked PFDTBTOx. Obviously, the initially non-crosslinked PFDTBTOx seems to undergo thermal crosslinking after long times of more than 30 hours at 100 °C. From the optical micrographs of annealed blends discussed earlier in this section, the different behavior of the “non-crosslinked” PFDTBTOx and the non-crosslinkable PFDTBT samples is known. From solubility tests this can be attributed to a slow, thermally induced crosslinking of PFDTBTOx.

This explains the development of the PCEs of PFDTBT and PFDTBTOx blends and the similar behavior at the long annealing times of the crosslinked and initially non-crosslinked PFDTBTOx. In the case of PFDTBT no crosslinking can be observed, since this polymer does not contain any crosslinkable oxetane groups.

The scattering observed for single devices of PFDTBT 1:2 and 1:3 blends can be attributed to arbitrary PCBM aggregation in the not stabilized devices. If the morphology is frozen by

crosslinking and PCBM aggregation is slowed down, all measured solar cells show the same PCE and no scattering is observed.

Additionally, the data show an improvement of the PCE of the crosslinked PFDTBTOx blends within the first 15 minutes of annealing. This trend is not observed for the non-crosslinked PFDTBTOx and the PFDTBT blends. Such an improvement of the efficiency of crosslinked solar cells upon short annealing is known from other examples in the literature.<sup>[211]</sup> We assumed that this improvement might be observed for all devices from our experiment if more *J-V* characteristics would be measured within the first 15 minutes of annealing. In a densely crosslinked blend the morphology is frozen and the diffusion of PCBM is significantly reduced.<sup>[240]</sup> As a consequence, morphology changes much more slowly in a crosslinked sample. This might be the reason why the improvement of the PCE is visible after annealing for 15 minutes in the crosslinked devices, but not for the non-crosslinked PFDTBTOx and the non-crosslinkable PFDTBT.

The accelerated aging experiments showed that crosslinking of PFDTBTOx indeed results in more stable BHJ solar cells. Even if the share of crosslinkable polymer is low compared to PCBM, the stabilizing effect of crosslinking can be observed. The high amount of crosslinkable groups in PFDTBTOx is certainly helpful at this point. However, we experienced that the structural modification of PFDTBT by introducing oxetane groups reduces the solar cell performance. This is in accordance with comparable works from the literature dealing with crosslinkable low bandgap polymers.<sup>[203,207]</sup> To further develop this concept of stabilizing BHJ blends by crosslinking, polymers with a reduced amount of oxetane groups should be investigated. Certainly, it would be interesting to see if less oxetane groups would result in more efficient solar cells and the effect of stabilization would still be achieved. An indication that this might be possible comes from the crosslinking experiments with PFDTBTOx<sub>0.75</sub> and PFDTBTOx<sub>0.50-alt.</sub>. These materials contain less crosslinkable groups per repeat unit but still form insoluble films after very short crosslinking times.

Stabilization of BHJ solar cells by crosslinking the low bandgap polymer was reported by a few groups. Particularly interesting for this thesis are the studies of Carlé *et al.* and Yau *et al.*, since their low bandgap polymers are also modified with crosslinkable oxetane groups. Both materials are shown in Figure 51a and b. In these works the number of crosslinkable groups is distinctly lower (average 0.2 oxetanes per repeat unit) than in PFDTBTOx (2 oxetane groups in every repeat unit). Yau *et al.* chose the polymer with 20% of the crosslinkable comonomer for their accelerated aging tests because their PDTG-TPD-Ox<sub>100%</sub> showed a PCE of only 0.48%. The reduced number of oxetanes in PDTG-TPD-Ox<sub>20%</sub> resulted in an efficiency of 1.63%. We observed a similar trend that attaching oxetane groups resulted in a PCE of 0.64% for the PFDTBTOx:PCBM 1:3 blend. With the reference PFDTBT an efficiency of 1.35% was achieved. Furthermore, Yau *et al.* compared the efficiencies of crosslinked and non-crosslinked PDTG-TPD-Ox<sub>20%</sub> solar cells. They observed a loss in efficiency upon crosslinking of about 15%. In our PFDTBTOx a comparable effect became obvious. However, in our system the loss during crosslinking exceeds 50%. This might be attributed to the higher number of oxetanes and thus a higher degree of crosslinking.

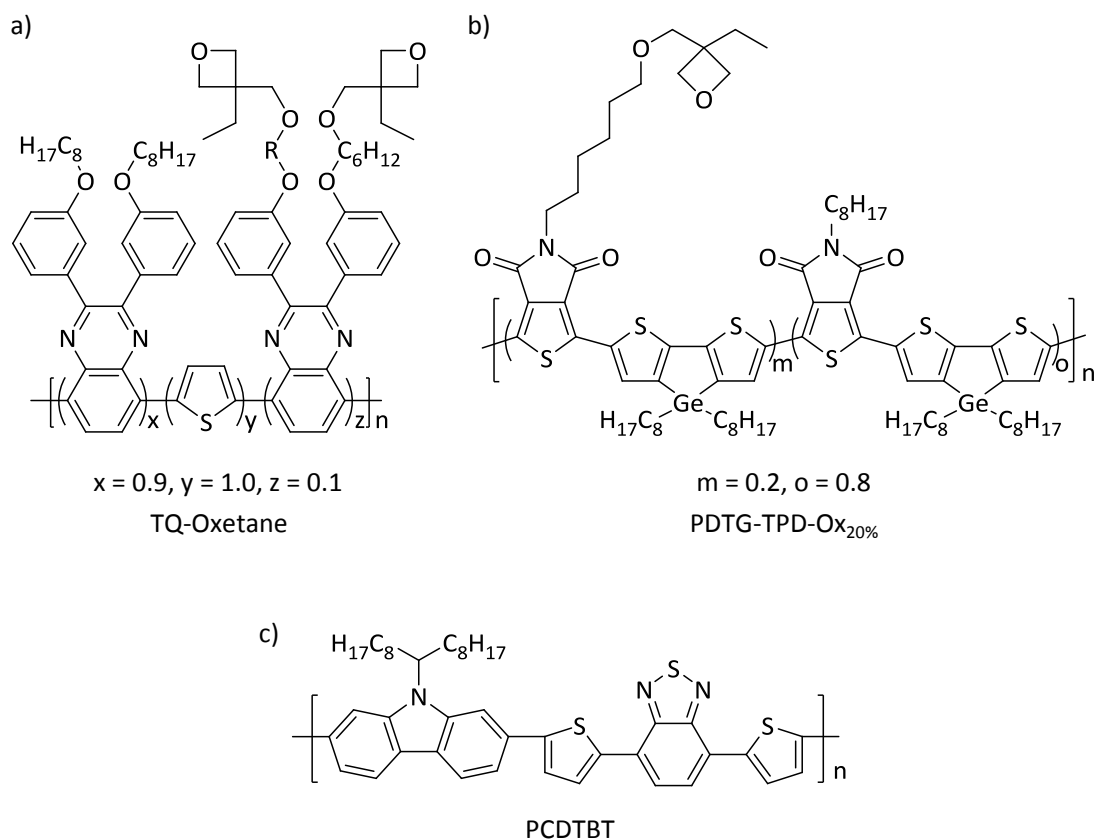


**Figure S1.** Examples from the literature for stabilization of BHJ solar cells by crosslinking of the low bandgap polymer. **a)** TQ-Oxetane by Carlé *et al.* crosslinked via PAG<sup>[207]</sup>. **b)** PDTG-TPD-Ox<sub>20%</sub> by Yau *et al.* This polymer is crosslinked by exposure to TFA vapor.<sup>[203]</sup> **c)** PCDTBT stabilizes BHJ blends by crosslinking *via* carbazoyl radicals.<sup>[241]</sup>

In this work, we conducted extensive studies concerning the blend ratio for the crosslinkable PFDTBTOx and the non-crosslinkable reference PFDTBT. We found a trend that increasing the share of PCBM resulted in improved PCEs. In addition to the solar cell experiments, the stabilizing effect of crosslinking was visualized by optical microscopy. From this experiments we saw that crosslinking PFDTBTOx prevents the formation of  $\mu\text{m}$ -sized PCBM aggregates during 100 hours of annealing at 100 °C. This was observed even in the PFDTBTOx:PCBM 1:3 blends. The high number of crosslinkable groups enables even a rather small portion of PFDTBTOx to stabilize a BHJ blend within the time of our experiment. In comparison with Carlé *et al.* (polymer:PCBM 1:1) and Yau *et al.* (polymer:PCBM 1:2) we could show the stabilizing effect with a lower amount of crosslinkable polymer. Yau *et al.* annealed their crosslinked devices for 30 minutes at 120 °C. Over this short time they observed a steady decay and their devices retained 80% of the initial efficiency. Longer times were investigated by Carlé *et al.* In their study, annealing was performed at 100 °C for 50 hours. After 50 hours the crosslinked solar cells lost about 50% of their PCE. However, in the report of Carlé instead of absolute efficiencies only normalized values are provided. We ran the accelerated aging experiment at 100 °C for a total time of 100 hours and covered both, short and long annealing times. Neither Carlé nor Yau observed an increase in PCE of the crosslinked devices after short annealing.

In addition, our crosslinked PFDTBTOx:PCBM 1:3 blend still retained its initial efficiency after 30 hours of thermal treatment. The devices studied by Carlé *et al.* and Yau *et al.* showed a steady downward trend in the accelerated aging experiment. Ultimately, our system retained 60% of the initial efficiency after 100 hours at 100 °C. This exceeds the value from Carlé *et al.*, who ended up with 50% after only 50 hours. The higher number of oxetane groups and the resulting crosslinking density might be the reason for the better stabilization of our system.

Interestingly, we also observed a stabilizing effect in the initially non-crosslinked PFDTBTOx:PCBM blends. This was attributed to thermally induced crosslinking of the oxetane groups of PFDTBTOx over long annealing times. The effect of stabilizing a polymer:PCBM blend by “unintentional” crosslinking was recently described by Tournebize *et al.* for PCDTBT (Figure 51c).<sup>[241]</sup> They proposed that photoinduced cleavage of the alkyl group leads to carbazolyl radicals. Subsequently, these polymer radicals undergo reactions with other polymer chains or with the electron acceptor PCBM which leads to the formation of a network.<sup>[241]</sup> In the case of our PFDTBTOx, the “unintentional” crosslinking is induced by thermal activation of the oxetane groups.



## 5 Patterning of low bandgap polymers by imprinting

In the field of organic solar cells basically two concepts exist for arranging the electron donor and electron acceptor materials in the active layer. Both materials can be aligned in separate layers on top of each other, the so-called bilayer or flat heterojunction structure. Alternatively, both materials are mixed together in a bulk heterojunction. Each of these approaches comes along with certain benefits and drawbacks. They are summarized in Figure 52. Patterning of active layer materials *via* nanoimprint lithography might be an approach towards a novel architecture of the active layer, combining the benefits of both established concepts. The basic idea of a nanostructured active layer is also displayed in Figure 52.

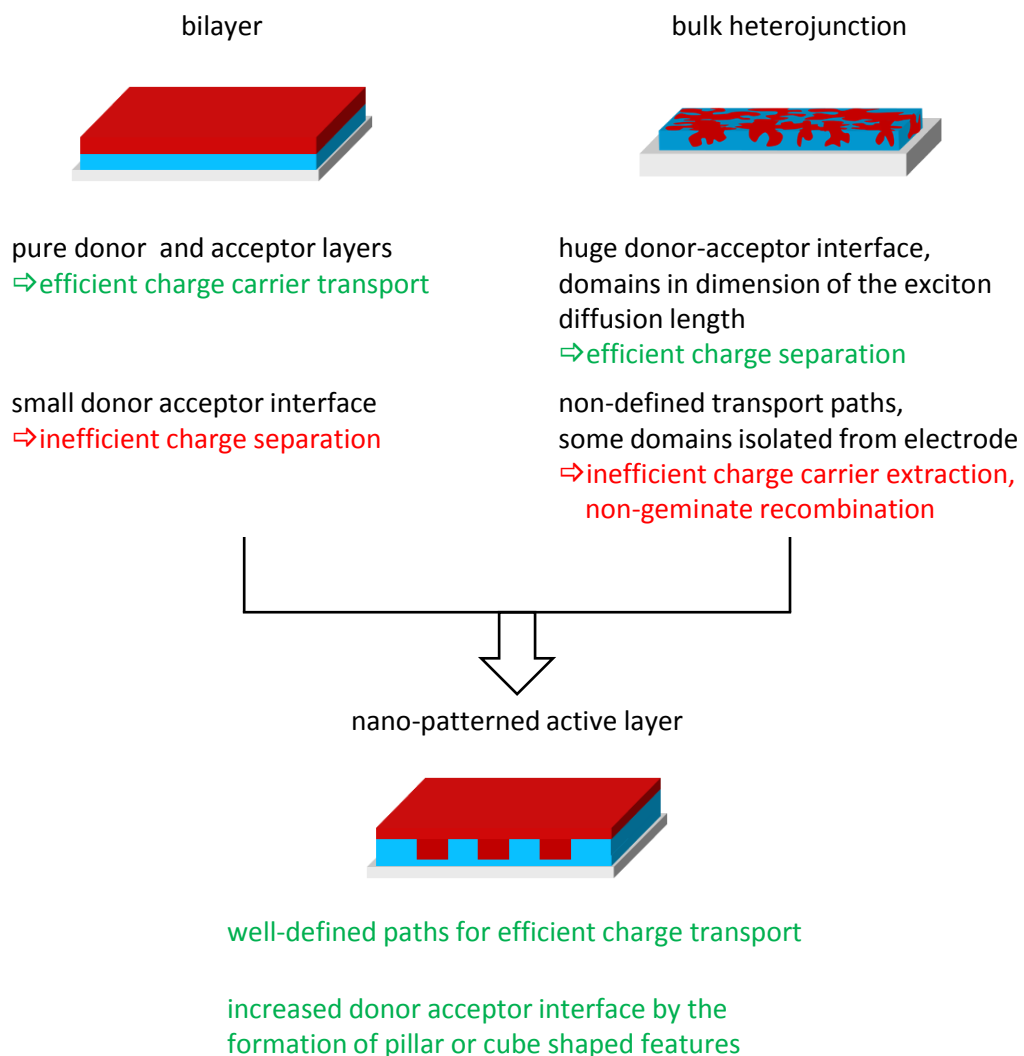


**Figure 52.** Motivation for nano-patterned active layers. This concept combines the benefits of the bilayer and the bulk heterojunction architecture.

Bilayer devices comprise pure layers of donor and acceptor material. Charge carriers are transported efficiently through the neat electron and hole conducting materials towards the electrodes. However, this concept lacks from the small interfacial area between the horizontally aligned materials. Thus, the majority of excitons will decompose before they reach the interface between donor and acceptor material where free charges can be generated. On the other side, the bulk heterojunction provides a huge interface between the intermixed donor and acceptor materials and, ideally, domains in the size of about twice the exciton diffusion length. The highly efficient exciton separation is the big advantage of this system. Weak spots of the BHJ concept become obvious when it comes to extraction of charge carriers. Non-geminate recombination is a major concern for such a structure. Due to the small domain sizes the transport paths for electrons and holes are very close to each other and recombination becomes dominant. Furthermore, there are some domains of donor or acceptor material which are not directly linked to an electrode. Charge carriers generated in such areas are trapped and cannot contribute to the photocurrent.

A nanostructured donor acceptor interface addresses the issues of bilayer and bulk heterojunction solar cells at the same time. Structures, such as bars, pillars, or columns, provide a significantly increased donor acceptor interface compared to a bilayer. Additionally, pure layers of both materials are achieved. This guarantees defined pathways for charge carrier transport towards the electrodes.

A few processes towards such nanometer sized structures in organic semiconductors are described in the literature.<sup>[219,221]</sup> For instance, P3HT films are patterned with aluminium oxide stamps<sup>[223]</sup> or by solvent assisted nanoimprint lithography.<sup>[226]</sup> Those examples are described more in detail in chapter 1.6. The challenge of all approaches towards nanostructured organic solar cells is the very small features size that is necessary for really efficient devices. Structures with lateral dimensions in the range of 20 nm or below are still hard to achieve.

In this work patterning of the crosslinkable low bandgap polymers PFDTBTO<sub>x</sub> and PFDTBTO<sub>x0.75</sub> was investigated. A soft polydimethylsiloxane (PDMS) stamp with features in the size of 1 μm to 10 μm was used for those preliminary tests. The steps of the patterning process by imprint lithography are shown in Figure 53. Polymer films with a thickness of roughly 80 nm are fabricated by spin coating from chlorobenzene solutions. After drying, the samples are placed on a hot plate. The hot plate is set to a temperature above the glass transition temperature ( $T_g$ ) of the polymers. In this particular case the temperature was 150 °C. After warming the samples to 150 °C, the stamp was applied either by gentle pressure or by putting a low weight (approximately 7 g) on top for the whole imprinting time of 15 minutes. During heating an argon atmosphere prevented oxidation. The samples were cooled to room temperature and the stamp was removed. Characterization of the formed patterns was done by optical and by scanning electron microscopy (SEM).

By using crosslinkable materials the process can be extended to steps 6 and 7. Crosslinking by the established exposure to TFA vapor renders the polymer insoluble. On top of the patterned and crosslinked low bandgap polymer an electron acceptor, such as PCBM, can be applied from solution without destroying the imprinted structures. Thus, the combination of imprinting and crosslinking can provide an interesting approach towards organic solar cells with defined donor acceptor heterojunctions.

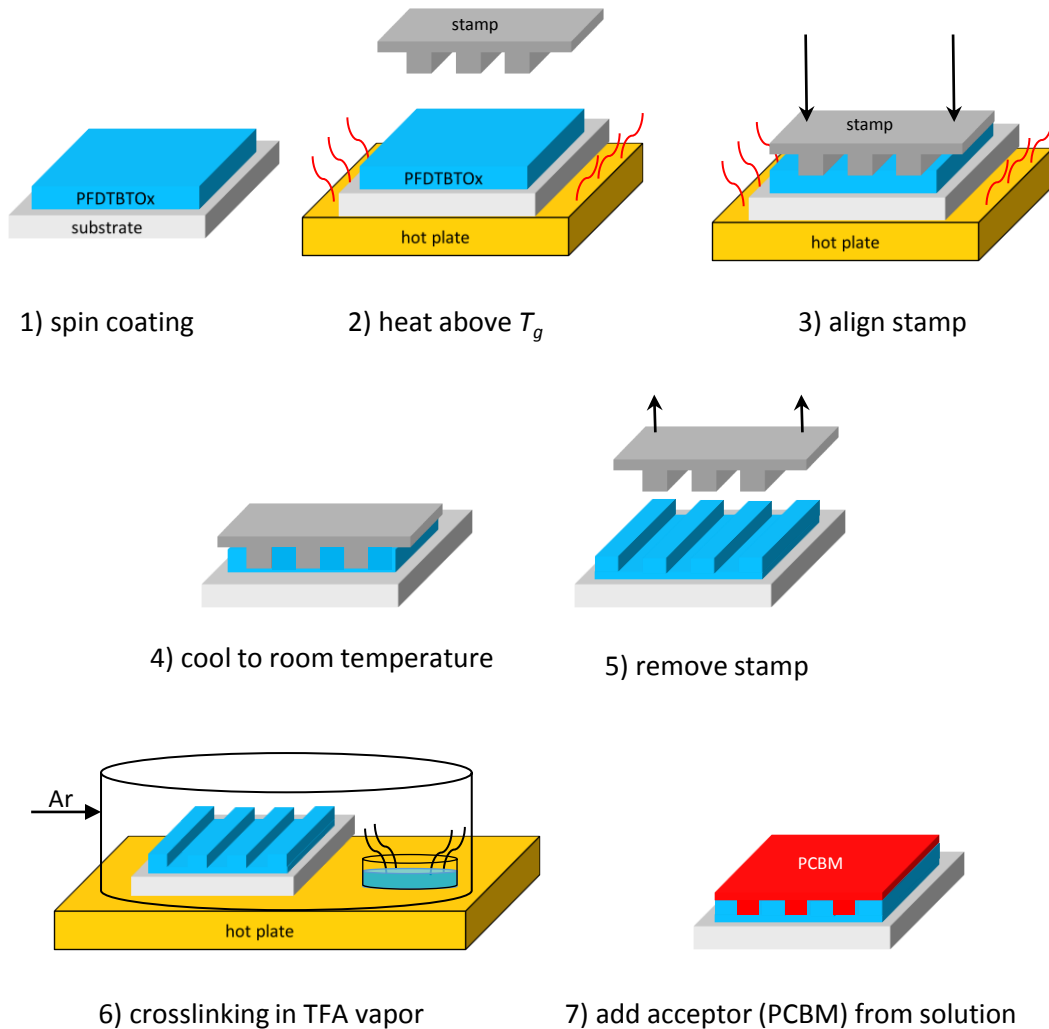


**Figure 53.** Overview of the sequence of steps for patterning a crosslinkable low bandgap polymer by imprint lithography. If the polymer is crosslinked after the imprinting process, the acceptor layer can be applied from solution.

In the following, SEM micrographs from imprinted PFDTBTO<sub>0.75</sub> films are shown and discussed. Figure 54a shows an overview of one series of patterns. The patterns are L-shaped lines. Lines with thicknesses of 1.0  $\mu\text{m}$ , 1.5  $\mu\text{m}$ , 2.0  $\mu\text{m}$ , 2.5  $\mu\text{m}$ , 5.0  $\mu\text{m}$ , and 10.0  $\mu\text{m}$  are transferred from the stamp to the low bandgap polymer (Figure 54b). Every bunch of lines consists of 10 single lines. The numbers next to the lines represent the thickness of the lines in micrometer.

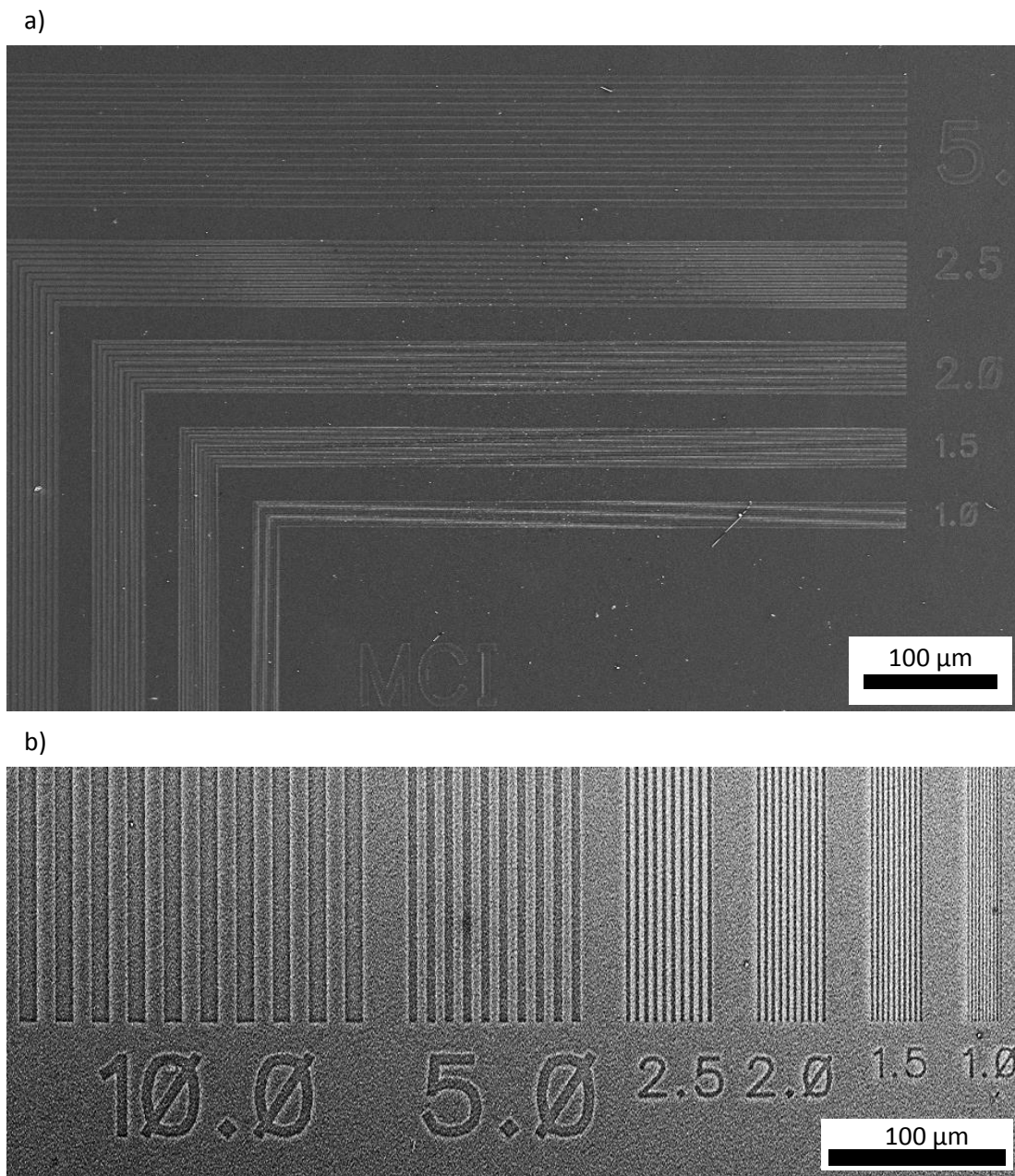


**Figure 54.** SEM micrographs of imprinted PFDTBTO<sub>x0.75</sub> films. **a)** Overview of the L-shaped bar patterns. **b)** Lines with thicknesses of 1.0  $\mu\text{m}$ , 1.5  $\mu\text{m}$ , 2.0  $\mu\text{m}$ , 2.5  $\mu\text{m}$ , 5.0  $\mu\text{m}$ , and 10.0  $\mu\text{m}$  are achieved. The numbers represent the line width in  $\mu\text{m}$ .

An important attribute for the quality of the imprinted structures is whether the feature sizes of the stamp are transferred to the polymer film accurately. This was determined by the SEM. The size determinations of the 10  $\mu\text{m}$  and the 2  $\mu\text{m}$  lines are shown in Figure 55a and Figure 55b.

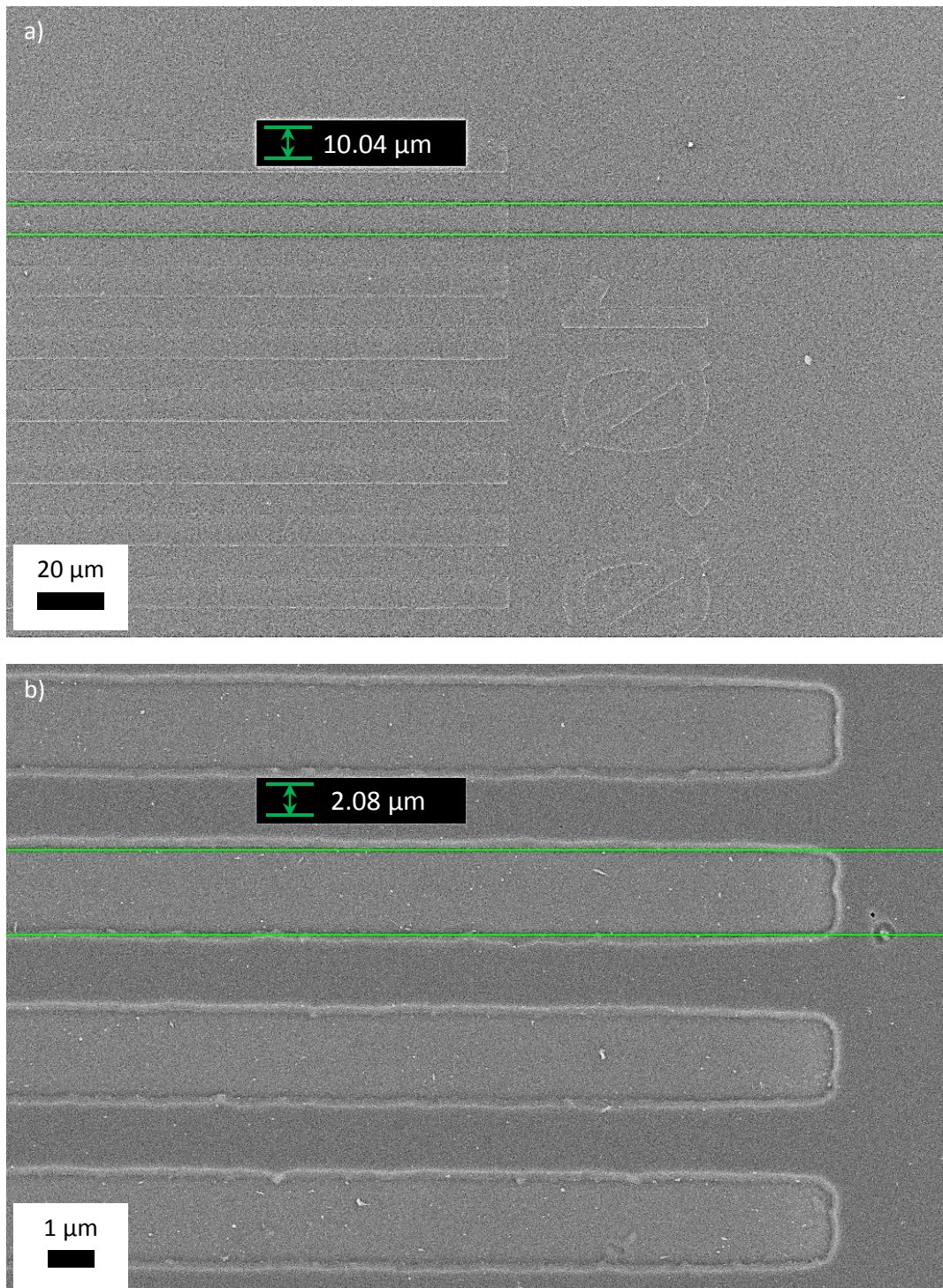


**Figure 55.** Determination of the line width. **a)** 10 μm lines, **b)** 2 μm lines. The line width of 10.04 μm and 2.08 μm represents the distance between the two green lines.

In both cases, the determined thickness of the lines is in very good agreement with the sizes of the stamp. At the magnification of Figure 55b some roughness becomes visible at the line edges.

There are two kinds of patterns produced by the stamp. Both are schematically drawn in Figure 56 for the example of the 1  $\mu\text{m}$  structures. In Figure 56a the 1  $\mu\text{m}$  lines are cavities in the stamp. During the imprinting process the voids of the stamp are filled with polymer. The resulting lines are elevated compared to the original polymer film. In the second case, shown in Figure 56b, the 1  $\mu\text{m}$  lines stand out from the stamp. Now, the stamp pushes the polymer aside, resulting in the corresponding dents in the polymer film.

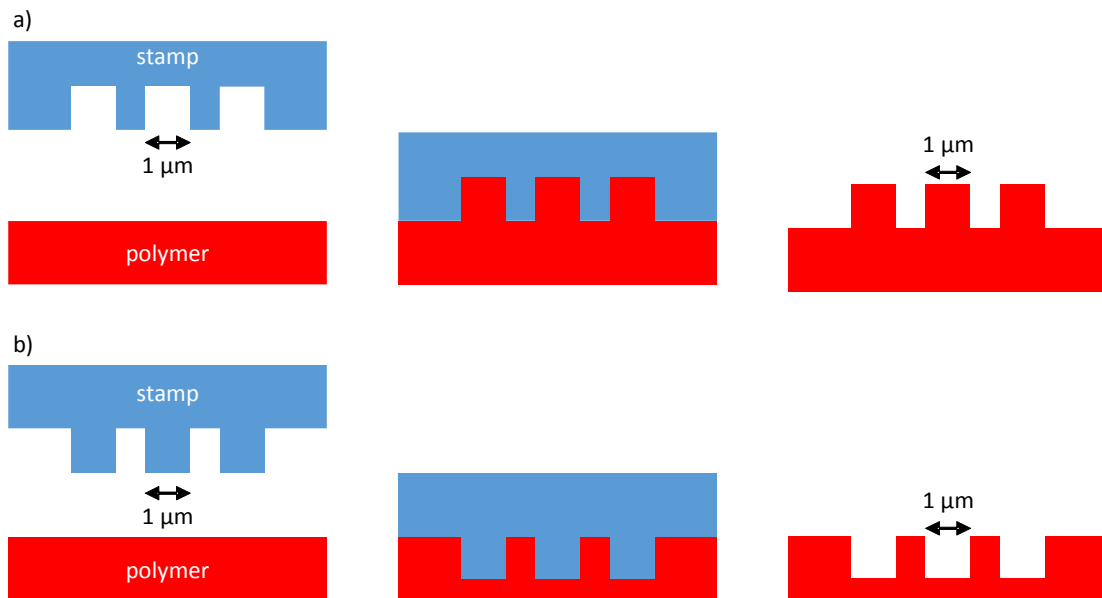


**Figure 56.** Positive and negative patterns formed by imprinting.

Both kinds of structures are formed in PFDTBTOx by imprinting in good quality for line widths as small as 1  $\mu\text{m}$ . From the SEM micrographs it might at times be hard to distinguish elevated from dented structures. Looking at tilted samples in the SEM gives better insight into the topography. In this case, the imprinted films were viewed from a 45° angle. Figure 57 shows micrographs of 1.5  $\mu\text{m}$  lines. The area around the rectangular corners of the lines is displayed. In Figure 57a elevated lines are depicted, dented lines are shown in Figure 57b.

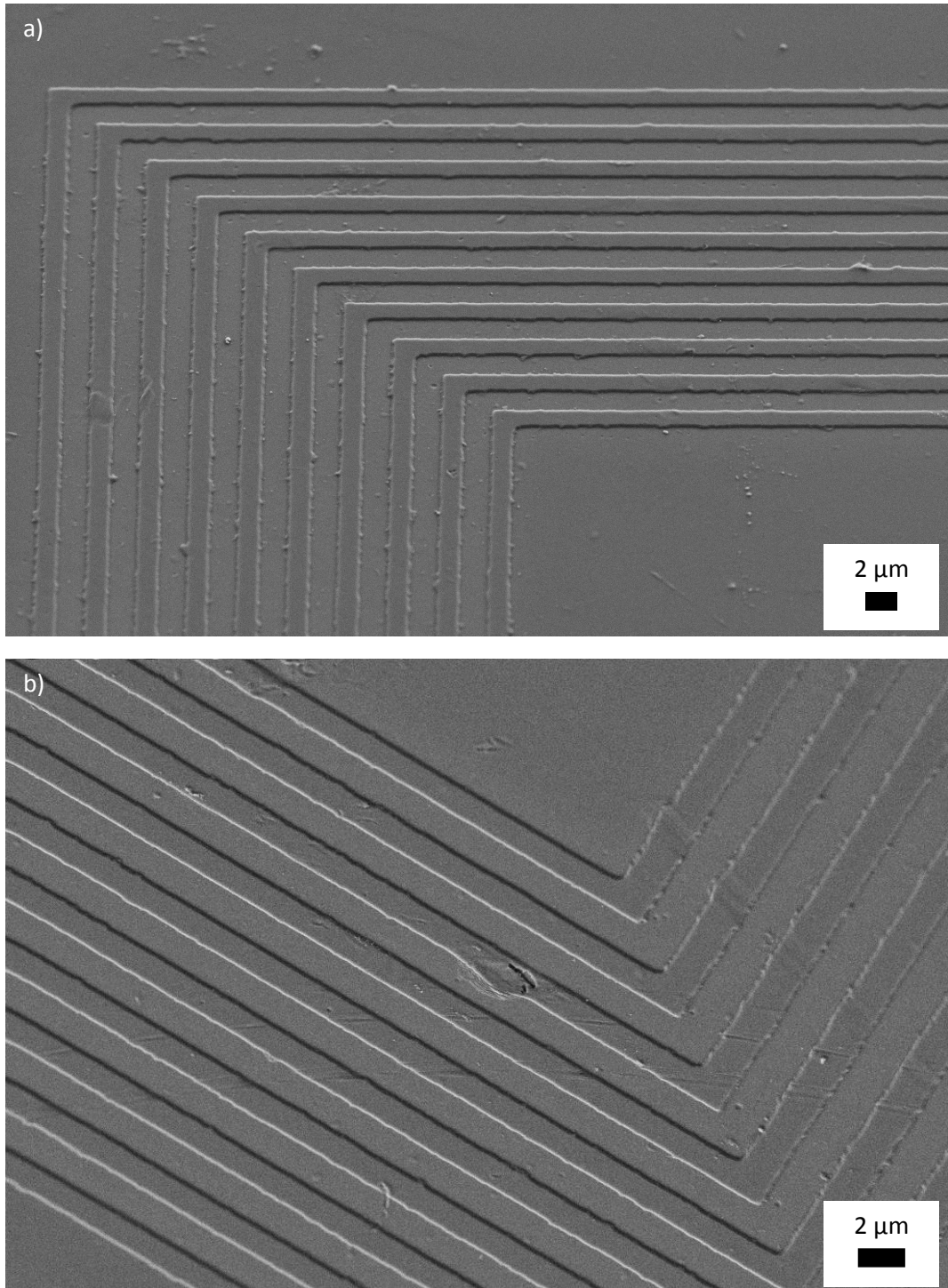


**Figure 57.** SEM micrographs of 1.5  $\mu\text{m}$  lines taken at a tilt angle of 45°. **a)** Elevated lines, **b)** dented lines.

Furthermore, this technique provides a perspective of the edges of elevated 1  $\mu\text{m}$  lines. This is displayed in Figure 58. The stamp with 1  $\mu\text{m}$  wide cavities is schematically illustrated. This micrograph shows that features with sizes down to 1  $\mu\text{m}$  can be achieved in good quality by imprinting.

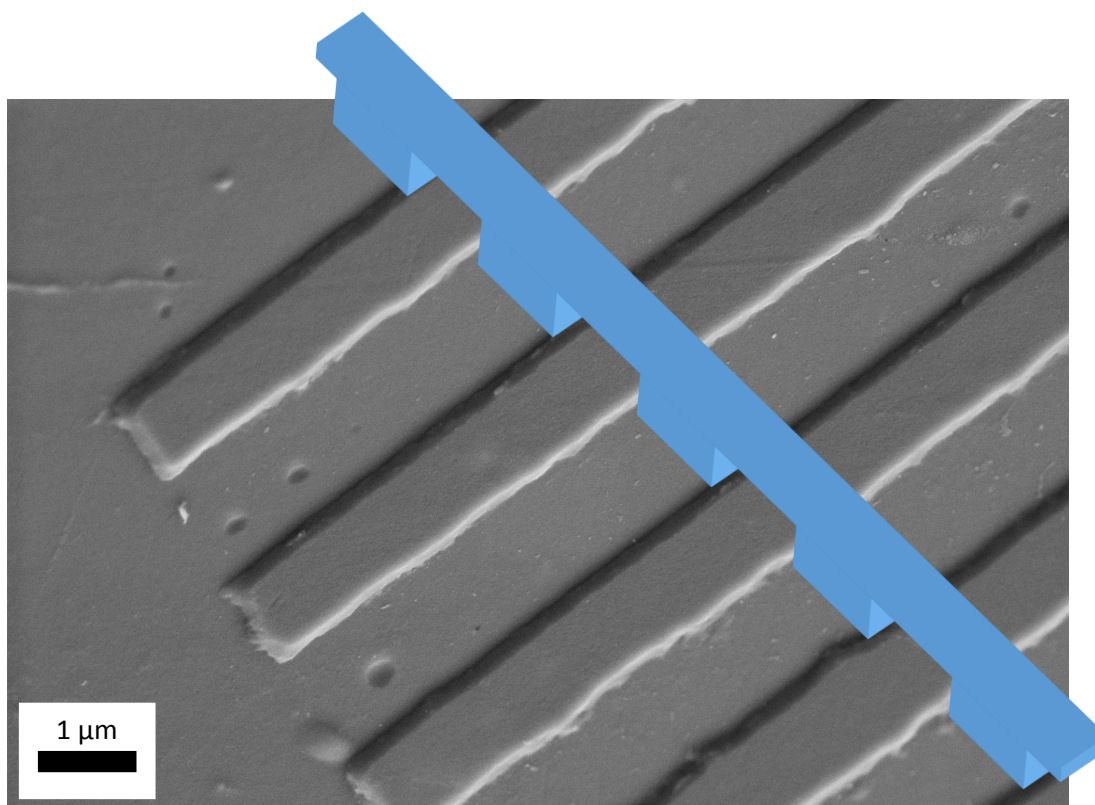


**Figure 58.** Elevated 1  $\mu\text{m}$  lines in PFDTBTO $_{x0.75}$ . A schematic drawing of the stamp is added as the light blue feature.

This set of preliminary results indicates that the synthesized low bandgap polymers can be patterned by imprinting. From the soft PDMS stamps used in this experiment all structures are transferred to the polymer film successfully. The films are structured with L-shaped lines with thicknesses from 10  $\mu\text{m}$  down to 1  $\mu\text{m}$ . Elevated as well as dented structures can be found. These results are an encouraging first step towards the fabrication of defined structures in low bandgap polymers. However, for an application in organic solar cells this processes requires further development. The achieved patterns in the dimension of micrometers are of course too large for being used in organic solar cells. For patterning low bandgap polymers for a structured active layer features in the size of 50 nm and below are required. Furthermore, this bar pattern is not the ideal structure for organic solar cells. Pillars or columns provide a much larger surface area compared to bars. Ultimately, a stamp with such nanometer sized structures has to be used for this purpose.





## 6 Summary

Long term stability is a persistent problem for organic solar cells. The sensitivity of the materials towards oxygen or moisture is one concern. Furthermore, photochemical degradation of the active layer materials is an issue. In the case of bulk heterojunction (BHJ) cells, the most popular device architecture, the stability of the morphology of the donor acceptor blend is yet another factor limiting the efficiency on a long time scale. Crosslinking is known as an approach towards more stable polymer:fullerene blends. In this work a series of crosslinkable low bandgap polymers was synthesized and their crosslinking behavior was thoroughly studied. The solar cell performance of the novel materials was tested and the beneficial effect of crosslinking on the long term stability of bulk heterojunction solar cells was shown. Furthermore, preliminary tests on imprinting as a method for achieving patterned films of the crosslinkable low bandgap polymer were performed.

Crosslinkable derivatives of the known low bandgap polymer PFDTBT (poly(2,7-(9,9-dialkylfluorene)-*alt*-(5,5-(4',7'-di-2-thienyl-2',1',3'-benzothiadiazole))) were synthesized by palladium catalyzed Suzuki polycondensation. An overview of the polymers from this work is given in Figure 59.

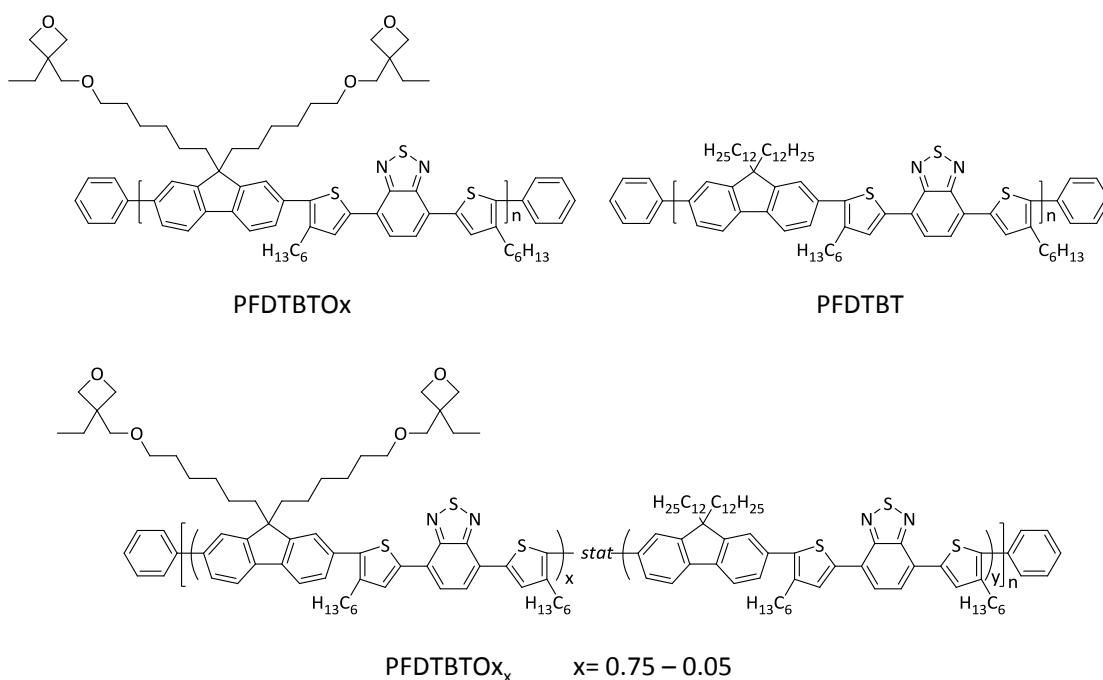


**Figure 59.** Low bandgap polymers synthesized within this work. Above: The crosslinkable PFDTBTOx with two oxetane groups per repeat unit and the non-crosslinkable reference polymer PFDTBT. Below: Series of copolymers with lower amounts of crosslinkable groups.

Oxetane groups for crosslinking were attached to the solubilizing side chains of the fluorene building block. For the synthesis of the functionalized alkyl chains, 1,6-dibromohexane was reacted with 3-ethyl-3-oxetanemethanol in an etherification. 2,7-dibromofluorene was substituted at 9-position with the oxetane terminated C6-chains. The crucial step of the synthetic route was the introduction of boronic acid ester groups to the crosslinkable 2,7-dibromofluorene. For a polycondensation extremely pure monomers are required. Thus, special care was taken at this point. Two or more chromatography runs were applied to achieve very pure fluorene monomers for the Suzuki polycondensation. The acceptor monomer 4,7-bis(5-bromo-4-hexyl-2-thienyl)-2,1,3-benzothiadiazole was commercially available in excellent purity. Suzuki polycondensation was carried out in a biphasic mixture of toluene and water with Pd(PPh<sub>3</sub>)<sub>4</sub> as the catalyst and Na<sub>2</sub>CO<sub>3</sub> as the base yielding the crosslinkable low bandgap polymer PFDTBTOx. As a reference material the non-crosslinkable PFDTBT was synthesized in analogous fashion. Here, dodecyl chains were attached to the fluorene. The dodecyl chain was chosen because it contains the same number of carbon atoms as the oxetane functionalized C6 chain. Both materials were characterized by SEC, TGA, NMR, UV-Vis, and fluorescence spectroscopy. The molecular weight is in the range of  $\overline{M}_n$  15,000 g mol<sup>-1</sup>, thermal and optical properties of both materials are similar. Thus, no detrimental effect of the oxetane groups on the polymerization and the mentioned properties was observed

The density of crosslinkable groups in PFDTBTOx is very high, with two oxetanes in each repeating unit. From Suzuki polycondensations using both, the crosslinkable and the non-crosslinkable fluorene monomer, statistic copolymers with reduced amounts of oxetane groups were obtained. The ratio of both fluorene building blocks in the polymers was determined from <sup>1</sup>H NMR spectra. It was in good agreement with the monomer feed ratio.

The crosslinking behavior of the synthesized materials was studied. Therefore, 80 nm thin films of the low bandgap polymers were fabricated. The success of a crosslinking method was checked by solubility tests before and after crosslinking. If every polymer chain of a sample is incorporated into a network, an entirely insoluble film is achieved.

Organic semiconductors equipped with oxetane groups are usually crosslinked by photoacid generators. This was successful for PFDTBTOx only with 5wt% of photoacid. However, with lower concentrations only partially insoluble films were achieved. An alternative concept was exposing the crosslinkable polymers to the vapor of trifluoroacetic acid (TFA). In this case insoluble films were obtained after very short exposure times at 100 °C. Even at milder conditions (80 °C) the crosslinking is complete within two minutes. The vapor of TFA penetrates the thin films and initiates the crosslinking reaction. With the series of polymers with varying amounts of crosslinkable groups solubility tests were performed after different TFA exposure times. Insoluble films are achieved immediately from polymers with high oxetane amounts (PFDTBTOx, PFDTBTOx<sub>0.75</sub>, PFDTBTOx<sub>0.50-alt</sub>). The statistic copolymer PFDTBTOx<sub>0.50</sub> formed insoluble

films after 20 minutes of treatment with TFA vapor at 80 °C. Partially insoluble films were obtained from PFDTBTO<sub>x0.25</sub>.

Furthermore, PFDTBTO<sub>x</sub> could also be crosslinked in blends with PCBM under these conditions. This was the key result from the crosslinking test with respect to the fabrication of BHJ solar cells.

Bulk heterojunction solar cells were fabricated from PFDTBTO<sub>x</sub> and the non-crosslinkable reference polymer PFDTBT. In preliminary experiments with PFDTBT a strong correlation between the power conversion efficiency (PCE) and the PCBM loading was observed (Figure 60a). Changing the blend ratio from PFDTBT:PCBM 1:1 to 1:3 lead to a significant increase in PCE from 0.11% to 1.35%. The solvent additive 1,8-diiodooctane (DIO) did not improve the efficiency of PFDTBT:PCBM blend devices. For the crosslinkable PFDTBTO<sub>x</sub> increasing the amount of PCBM did not influence the device performance as significantly as experienced from PFDTBT. The PCE of the 1:1 blend was 0.22%, the efficiency of the 1:3 blend only 0.65%. The efficiency of the crosslinked PFDTBTO<sub>x</sub>:PCBM blends was around 0.25% in any ratio. Nevertheless, the effect of crosslinking on the long term stability became obvious in an accelerated aging experiment (Figure 60b).

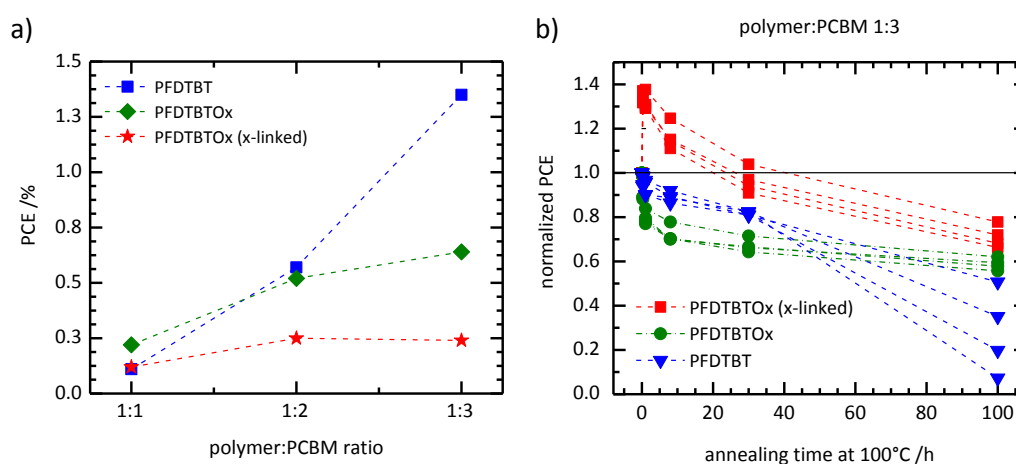


**Figure 60.** Results from OSC studies. **a)** Influence of polymer:PCBM ratio and crosslinking on the device efficiency. **b)** Accelerated aging experiment: Stabilization of BHJ blends by crosslinking of PFDTBTO<sub>x</sub>.

In this accelerated aging experiment BHJ solar cells were annealed at 100 °C for a total of 100 hours. During this experiment the solar cells were characterized after several time steps. Devices with the crosslinked PFDTBTO<sub>x</sub> were compared to “non-crosslinked” PFDTBTO<sub>x</sub> and the reference PFDTBT. The stabilizing effect of crosslinking was clearly shown in the crosslinked PFDTBTO<sub>x</sub>:PCBM devices. By crosslinking the initial efficiency was retained for 30 hours. After 100 hours about 70% of the PCE was retained. In contrast, the efficiency of devices with the non-crosslinkable PFDTBT steadily decayed upon thermal treatment. Ultimately, the efficiency dropped to 20% after 100 hours. Strikingly, the initially non-crosslinked PFDTBTO<sub>x</sub> devices behaved differently: After a loss of efficiency during the first hours of annealing, the efficiency did not decay further. This effect was

attributed to a slow, thermally induced crosslinking of PFDTBTOx. Thus, crosslinking with TFA vapor during device fabrication and thermally induced crosslinking both result in stabilized BHJ blends. Even if the amount of crosslinkable polymer is low compared to PCBM, as in the 1:3 blends, the stabilizing effect of crosslinking could be observed. The high amount of crosslinkable groups in PFDTBTOx is certainly helpful at this point. However, we experienced that the structural modification of PFDTBT by introducing oxetane groups reduces the solar cell performance. To further develop this concept of stabilizing BHJ blends by crosslinking, polymers with a reduced amount of oxetane groups should be investigated.

In preliminary experiments micrometer sized structures were successfully imprinted into low bandgap polymer films. This can be regarded as a proof of principle that the synthesized materials can be patterned by this technique.

## 7 Zusammenfassung

Auf dem Gebiet organischer Solarzellen ist die Langzeitstabilität der Bauteile nach wie vor verbesserungswürdig. Probleme stellen die Empfindlichkeit der Materialien gegenüber Sauerstoff und Feuchtigkeit sowie deren photochemische Stabilität dar. Die meist verbreitete Bauweise organischer Solarzellen ist die Bulk Heterojunction (BHJ). In diesem Fall wird die Langzeitstabilität, zusätzlich zu den vorher genannten Faktoren, auch noch von der Stabilität der Morphologie des Blends aus Donor- und Akzeptor-Material begrenzt. Vernetzung ist ein Ansatz, um Polymer:Fulleren-Blends zu stabilisieren. Im Rahmen dieser Arbeit wurde eine Serie vernetzbarer Low Bandgap Polymere synthetisiert. Das Vernetzungsverhalten wurde eingehend untersucht. Darüber hinaus wurden die Materialien in organischen Solarzellen getestet und der Einfluss der Vernetzung auf die Langzeitstabilität von Bulk Heterojunction Solarzellen gezeigt. Außerdem wurden in Vorversuchen Filme der Low Bandgap Polymere mittels Imprinting strukturiert.

Es wurden vernetzbare Derivate des bekannten low bandgap polymers PFDTBT (Poly(2,7-(9,9-dialkylfluoren)-*alt*-(5,5-(4',7'-di-2-thienyl-2',1',3'-benzothiadiazol))) mittels Palladium-katalysierter Suzuki Polykondensation hergestellt (Abbildung 59). Als vernetzbare Einheiten wurden Oxetan-Gruppen in die Seitenketten des Fluorens integriert.

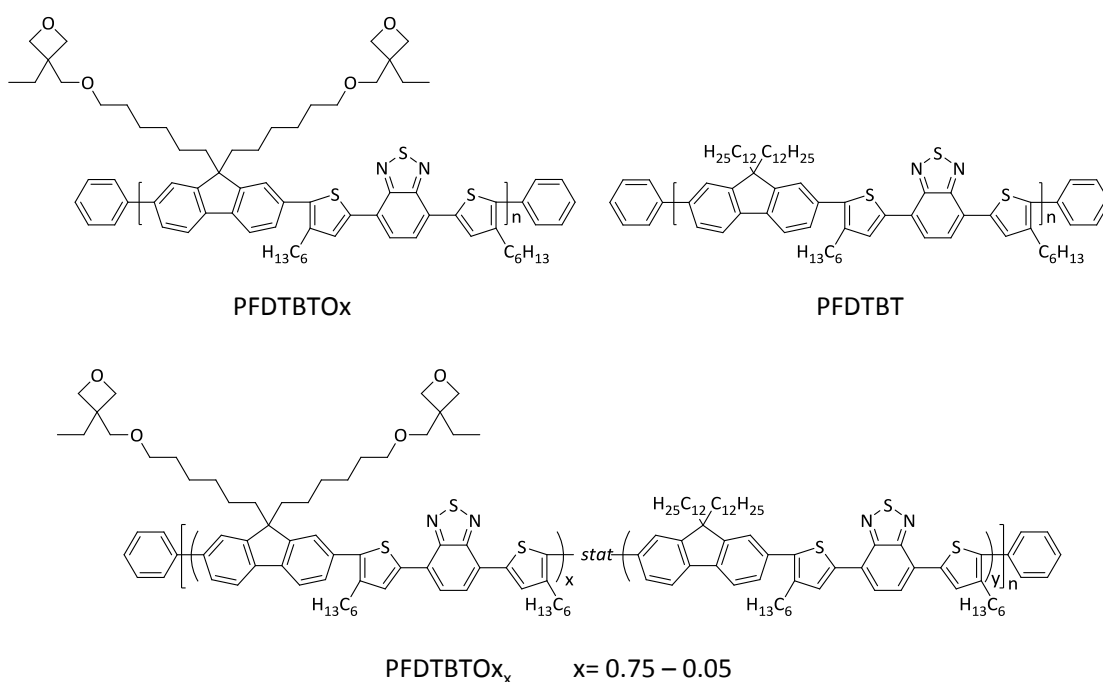


**Abbildung 59.** Low Bandgap Polymere aus dieser Arbeit. Oben: Vernetzbares PFDTBTOx mit zwei Oxetan-Gruppen in jeder Wiederholungseinheit und das nicht vernetzbare Referenzpolymer PFDTBT. Unten: Serie von Copolymeren mit geringerem Anteil an vernetzbaren Gruppen.

Um die funktionalisierte Alkylkette zu erhalten, wurde 1,6-Dibromhexan mit 3-Ethyl-3-oxetanmethanol in einer Veresterung umgesetzt. Die Alkylketten mit den Oxetan-Gruppen wurden an die 9-Position des 2,7-Dibromfluorens angebracht. Der entscheidende Schritt in der Synthese des Fluorenmonomers war die Umsetzung zum Diboronsäureester. Für die Polykondensation werden Monomere von extrem hoher Reinheit benötigt. Folglich wurde besonderes Augenmerk auf die Aufreinigung der Fluorenmonomere gelegt. Das zweite Comonomer, 4,7-Bis(5-brom-4-hexyl-2-thienyl)-2,1,3-benzothiadiazol, war in exzellenter Reinheit kommerziell verfügbar. Die Suzuki Polykondensationen wurden in einem zweiphasigen Gemisch aus Toluol und Wasser mit  $\text{Pd}(\text{PPh}_3)_4$  als Katalysator und  $\text{Na}_2\text{CO}_3$  als Base durchgeführt. Als Referenzmaterial wurde ein PFDTBT ohne vernetzbare Gruppen synthetisiert. Alle Polymere wurden mittels GPC, TGA, NMR, UV/Vis- und Fluoreszenzspektroskopie charakterisiert. Die Molekulargewichte lagen im Bereich von  $\overline{M}_n$  15,000  $\text{g mol}^{-1}$ , die thermischen sowie die optischen Eigenschaften der Materialien sind ähnlich. Folglich wurde an dieser Stelle kein negativer Einfluss der Oxetan-Gruppen auf die Polymerisation und die oben genannten Materialeigenschaften beobachtet.

Das Vernetzungsverhalten der synthetisierten Polymere wurde an dünnen Filmen untersucht. Verschiedene Vernetzungsstrategien wurden getestet. Über Löslichkeitstest wurde überprüft, ob ein Vernetzungsexperiment erfolgreich war.

In der Regel werden organische Halbleiter mit Oxetan-Gruppen durch die Zugabe von kationischen Photoinitiatoren vernetzt. Für PFDTBTOx war dieser Ansatz nur mit 5 wt% erfolgreich. Bei geringeren Konzentrationen wurden nur teilweise unlösliche Filme erhalten. Eine Alternative ist, das vernetzbare Polymer Trifluoressigsäure (TFA)-Dampf auszusetzen. Hierbei wurden nach sehr kurzen Zeiten im TFA-Dampf bei 100 °C vollständig unlösliche Filme erhalten. Auch bei nur 80 °C wurden innerhalb von zwei Minuten unlösliche Filme erhalten. Im Folgenden wurde der Einfluss der Zahl der vernetzbaren Gruppen im Polymer auf die Vernetzung untersucht. Polymere mit einem hohen Gehalt an Oxetan-Gruppen (PFDTBTOx, PFDTBTOx<sub>0.75</sub>, PFDTBTOx<sub>0.50-alt.</sub>) bilden bereits innerhalb von zwei Minuten vollständig unlösliche Filme. Das statistische Copolymer PFDTBTOx<sub>0.50</sub> bildet nach 20 Minuten im TFA-Dampf bei 80 °C unlösliche Filme. Mit PFDTBTOx<sub>0.25</sub> wurden unter diesen Bedingungen nur teilweise unlösliche Filme erhalten.

Weiterhin wurde gezeigt, dass PFDTBTOx auch in Gegenwart von PCBM vernetzt werden kann. Dieses war ein entscheidendes Zwischenergebnis im Hinblick auf die Herstellung von Solarzellen mit vernetzten Polymer:PCBM-Blends.

Bulk Heterojunction Solarzellen wurden mit dem vernetzbaren PFDTBTOx und dem Referenzpolymer PFDTBT hergestellt. In Vorversuchen mit PFDTBT wurde eine starke Abhängigkeit des Wirkungsgrades vom PCBM-Anteil festgestellt (Abbildung 60a). Durch die Erhöhung des PCBM-Gehaltes von 1:1 zu 1:3 wurde die Effizienz der Solarzellen von 0,11 % auf 1,35 % gesteigert. Keine Verbesserung bewirkte in diesem Fall der Einsatz von

1,8-Diiodoctan. Die Effizienzen des vernetzbaren PFDTBTOx sind geringer als die des Referenzpolymers. Durch das Vernetzen wird die Effizienz wiederum verringert.

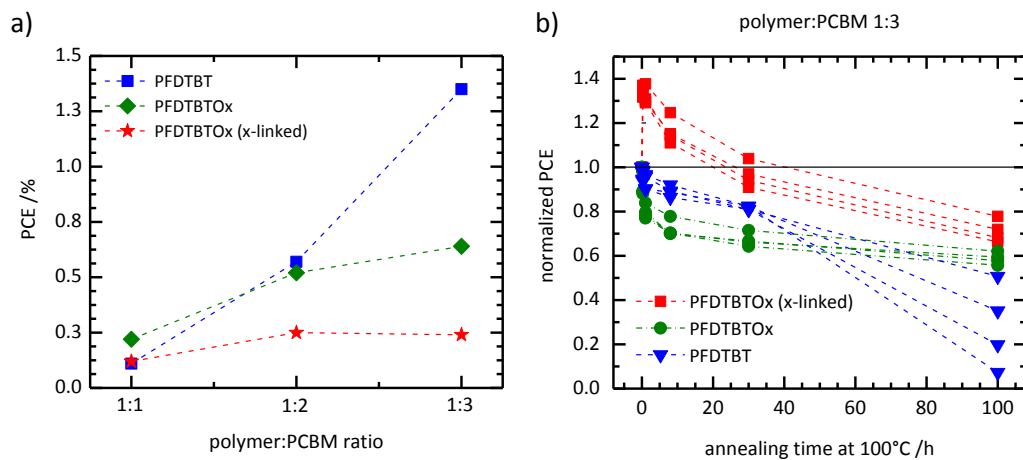


**Abbildung 60.** Ergebnisse der Solarzellen-Experimente. **a)** Einfluss des Polymer:PCBM-Verhältnisses und der Vernetzung auf den Wirkungsgrad der Solarzellen. **b)** Langzeit-Test der Solarzellen: Stabilisierung durch Vernetzung des low bandgap polymers PFDTBTOx.

Dessen ungeachtet zeigen die Langzeit-Experimente klar den stabilisierenden Effekt der Vernetzung. Hierzu wurden Solarzellen bei 100 °C für insgesamt 100 Stunden thermisch behandelt. Die Kenndaten der Solarzellen wurden zu bestimmten Zeitintervallen aufgenommen. Hierbei wurde die Entwicklung von Solarzellen mit dem vernetzten PFDTBTOx mit nicht vernetztem PFDTBTOx und der PFDTBT-Referenz verglichen (Abbildung 60b). Die Solarzellen mit dem vernetzten PFDTBTOx:PCBM-Blend konnten die Effizienz vom Beginn des Experiments bis zu 30 Stunden aufrechterhalten. Nach 100 Stunden blieben etwa 70 % der ursprünglichen Effizienz erhalten. Im Gegensatz dazu verloren die Solarzellen mit der nicht vernetzbaren Referenz PFDTBT über den gesamten Zeitraum stets an Effizienz. Nach 100 Stunden war diese auf 20 % des Ausgangswertes gesunken. Unerwartet war das Verhalten des nicht vernetzten PFDTBTOx: Anfangs sank auch hier die Effizienz durch die thermische Behandlung. Im weiteren Verlauf fiel diese jedoch nicht weiter ab und stabilisierte sich bei etwa 60 % des ursprünglichen Wertes. Wir konnten diesen Effekt mit einer langsamen thermischen Vernetzung der Oxetan-Gruppen erklären. Folglich können PFDTBTOx:PCBM-Blends durch zwei Arten der Vernetzung stabilisiert werden: Zum einen durch Vernetzung im TFA-Dampf während der Herstellung der Solarzellen und zum anderen durch thermische Vernetzung.

Mit PFDTBTOx können auch Blends stabilisiert werden, in denen der Anteil des vernetzbaren Polymers gering ist, wie hier im 1:3-Blend. Dies wird durch die große Zahl der vernetzbaren Gruppen begünstigt. Dennoch erwies sich dieser hohe Oxetan-Gehalt an anderer Stelle als hinderlich: Der Eingriff in die Polymerstruktur durch das Anbringen von Oxetan-Gruppen führt zu einer geringeren Effizienz in Solarzellen. Für weitere Arbeiten mit diesem Konzept wäre die Verwendung vernetzbarer Low Bandgap Polymere mit geringerem Anteil an Oxetan-Gruppen ratsam.

In Vorversuchen wurde gezeigt, dass die synthetisierten Low Bandgap Polymere durch Imprinting strukturiert werden können. Es wurden Linienstrukturen in Größen von 1  $\mu\text{m}$  bis 10  $\mu\text{m}$  erhalten. Dies kann als ein erster Schritt für die Herstellung organischer Solarzellen mit einer definierten Grenzfläche zwischen Donor- und Akzeptormaterial angesehen werden.





## 8 Experimental

### 8.1 Materials and methods

The reagents were purchased from ABCR (2,7-dibromofluorene, 3-ethyl-3-oxetanemethanol), Acros Organics (Aliquat 336, benzyltriethylammonium chloride, bromobenzene, *n*-butyllithium, 2-isopropoxy-4,4,5,5-tetramethyl-1,3,2-dioxaborolane, Pd(PPh<sub>3</sub>)<sub>4</sub>), Fluka (phenylboronic acid, tetrabutylammonium chloride), Hedinger (NaOH), Carl Roth (Na<sub>2</sub>SO<sub>4</sub>, Na<sub>2</sub>CO<sub>3</sub>, tetrabutylammonium bromide) and Sigma Aldrich (1,6-dibromohexane, 1,7-dibromo-heptane, 1-dodecylbromide) and used as received. Dry solvents were purchased from Acros Organics. The monomer 4,7-bis(5-bromo-4-hexyl-2-thienyl)-2,1,3-benzothiadiazole was purchased from SunaTech Inc. and used without further purification.

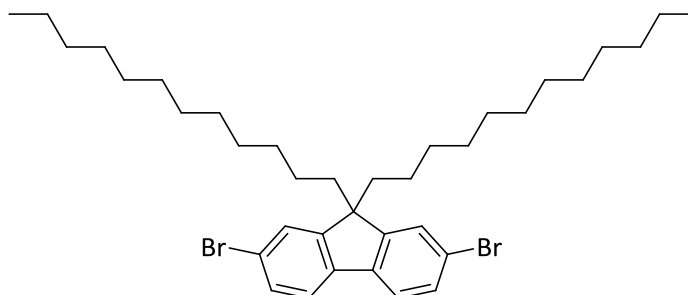
Chloroform and diethylether were purchased from Sigma Aldrich, DMSO was purchased from Fisher Scientific, and methanol was purchased from VWR. Other solvents were distilled once before use, tetrahydrofuran was distilled over KOH. Reactions were performed in oven-dried glassware under an inert atmosphere of argon. Argon was provided from Linde (Argon 4.8) and dried over molecular sieves (3 Å) and potassium on aluminium oxide.

<sup>1</sup> H NMR	Spectra were recorded on a Bruker AC spectrometer (300 MHz) at room temperature using CDCl <sub>3</sub> as solvent and internal standard. Chemical shifts are reported in ppm relative to residual protons in the deuterated solvent (CHCl <sub>3</sub> δ = 7.26 ppm), the coupling constants <i>J</i> are given in Hz. Multiplicities are denoted with m (multiplet), s (singlet), d (doublet), t (triplet), q (quartet), qui (quintet)
<sup>13</sup> C NMR	Spectra were recorded on a Bruker AC spectrometer (75 MHz) at room temperature using CDCl <sub>3</sub> as solvent and internal standard. Chemical shifts are reported in ppm relative to residual protons in the deuterated solvent (CHCl <sub>3</sub> δ = 77.4 ppm).
Mass spectrometry	Mass spectra (MS) were recorded on a FINNIGAN MAT 8500 instrument using electron spray ionization (EI).
IR spectroscopy	Infrared (IR) spectra were recorded on a PerkinElmer Spectrum 100 FT-IR spectrometer equipped with an universal ATR unit.

Polymer SEC	Size exclusion chromatography (SEC) was performed using a Waters 515-HPLC pump with stabilized THF as the eluent at a flow rate of 0.5 ml min <sup>-1</sup> . The array of columns consisted of a guard column (Varian, 50 × 0.75 cm, ResiPore particle size 3 μm) and two separation columns (Varian, 300 × 0.75 cm, ResiPore particle size 3 μm). The compounds were monitored using a Waters UV detector at 254 nm. As an internal standard 1,2-dichlorobenzene was added. Number average ( $\overline{M}_n$ ) and weight average ( $\overline{M}_w$ ) molecular weights were calculated based on a calibration with a polystyrene standard.
TGA	Thermogravimetric analysis (TGA) measurements were performed on a Mettler Toledo TGA/SDTA 851e at a heating rate of 10 K min <sup>-1</sup> under nitrogen flow.
UV/vis spectroscopy	UV/Vis spectra of solutions (THF, concentration 10 <sup>-3</sup> mg ml <sup>-1</sup> ) and thin films were recorded on a JASCO V-670 spectrophotometer at room temperature. UV/Vis spectra of thin films were also recorded on a ASH Scan 530 by Analytik Jena.
PL spectroscopy	Photoluminescence (PL) spectra were collected from a JASCO FP-8600 spectrofluorometer from solutions (THF, concentration 10 <sup>-3</sup> mg ml <sup>-1</sup> ) and thin films with nitrogen as purge gas. Photoluminescence quantum efficiency was measured using an Ulbricht sphere purged with nitrogen.
TLC	Thin-layer chromatography (TLC) was used to monitor the progress of reactions and to check the purity of products and educts. Polygram SIL G/UV 254 plates from Macherey Nagel with 0.2 mm silica gel and fluorescence indicator and TLC aluminium foil with silica gel 60, F <sub>254</sub> from Merk were used.
Flash chromatography	Flash chromatography was executed with silica gel as stationary phase (silica gel 60M, particle size 0.04 to 0.063 mm/230 to 400 mesh from Macherey Nagel).
MPLC	Medium pressure liquid chromatography (MPLC) was conducted on a Büchi Sepacore Flash System X50 with two pump modules C-605, UV-Vis detector C-640 and fraction collector C-660. Glass columns were filled with silica gel 60, particle size 0.025 to 0.04 mm from Macherey Nagel.
Film fabrication	Thin films were fabricated by spin-coating on a Siemens Coros OP15 with a CONVAC 1001 and by doctorblading.
Film thickness	The thickness of polymer thin films was measured on a Dektak 3030 ST surface profilometer from Sloan Technologies and on a Veeco Dektak 150.

Photoelectron spectroscopy	Photoelectron spectroscopy was conducted on a Riken Keiki photoelectron spectrometer AC 2 (at Evonik Creavis, Marl).
Electron microscopy	Scanning electron microscope (SEM) micrographs were taken with a Zeiss 1530 FESEM. Electron micrographs were recorded with a Phenom Pro from Phenom-World BV.
Polarized light microscopy	Polarized light microscopy was performed using a Nikon DIAPHOT 300 optical microscope. Optical micrographs were recorded by a Nikon ACT-1 software using a Nikon DMX1200 digital camera.

## 8.2 Syntheses of the monomers

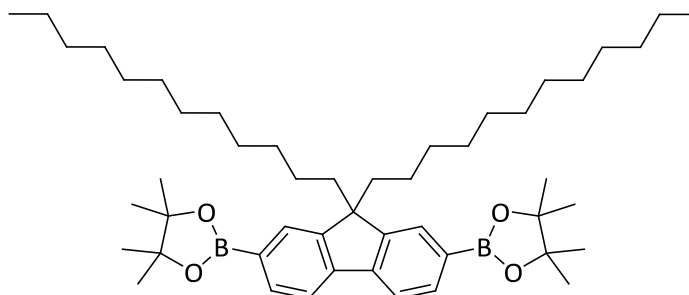
**2,7-Dibromo-9,9-didodecylfluorene**

A solution of 2,7-dibromofluorene (2.00 g, 6.17 mmol) and the phase-transfer catalyst benzyltriethylammonium chloride (0.10 g, 0.43 mmol) in DMSO (85 ml) was flushed with argon for 30 minutes. Under argon a 50% NaOH solution (25 ml) was added dropwise. After stirring for 20 minutes, 1-bromododecane (4.61 g, 18.51 mmol) was added dropwise. The mixture was heated to reflux for 20 hours. After cooling to room temperature, the mixture was poured into ice water and extracted with diethyl ether. The combined ether phases were washed with water and dried over sodium sulfate. The solvent was removed, and the crude product was purified by flash chromatography (eluent hexane) yielding 2,7-dibromo-9,9-didodecylfluorene (3.64 g, 5.53 mmol, 90%) as a colorless solid.

## Characterization

**EI-MS** ( $m/z$ , %): calculated for  $C_{37}H_{56}Br_2$  660.65; found 660 ( $M^+$ , 100%), 323 ( $M^+ - 2x C_{12}H_{25}$ , 30%)

**$^1H$  NMR** (300 MHz,  $CDCl_3$ ,  $\delta$  in ppm): 0.50 – 0.65 (bs, 4H, Ar- $CH_2$ - $\underline{CH_2}$ ), 0.87 (t,  $J = 6.8$  Hz, 6H, - $CH_3$ ) 0.97 – 1.34 (m, 36H, - $CH_2$ -), 1.84 – 1.95 (m, 4H, Ar- $CH_2$ -), 7.40 – 7.55 (m, 6H, Ar-H)

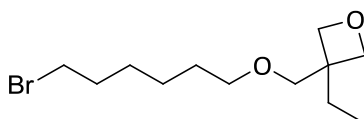
**2,7-Bis(4,4,5,5-tetramethyl-1,3,2-dioxaborolane)-9,9-didodecylfluorene**

A solution of 2,7-dibromo-9,9-didodecylfluorene (1.49 g, 2.26 mmol) in dry THF (50 ml) was cooled to  $-78\text{ }^{\circ}\text{C}$ . At  $-78\text{ }^{\circ}\text{C}$  *n*-butyllithium (1.6 M solution in hexane, 3.10 ml, 4.96 mmol) was added slowly. The solution was stirred at  $-78\text{ }^{\circ}\text{C}$  for 30 minutes before 2-isopropoxy-4,4,5,5-tetramethyl-1,3,2-dioxaborolane (1.01 g, 5.42 mmol) was added slowly. The reaction mixture was kept at  $-78\text{ }^{\circ}\text{C}$  for another hour and was allowed to warm to room temperature overnight. It was poured into ice water and extracted with diethyl ether. The combined ether phases were washed with a saturated NaCl solution and dried over sodium sulfate. The solvent was removed, and the crude product was purified by flash chromatography (eluent hexane/ethyl acetate 20:1) yielding 2,7-bis(4,4,5,5-tetramethyl-1,3,2-dioxaborolane)-9,9-didodecylfluorene (1.22 g, 1.62 mmol, 72%) as a colorless solid.

**Characterization**

**EI-MS** (*m/z*, %): calculated for  $\text{C}_{49}\text{H}_{80}\text{B}_2\text{O}_2$  754.78; found 754 ( $\text{M}^+$ , 100%), 585 ( $\text{M}^+ - \text{C}_{12}\text{H}_{25}$ , 80%), 417 ( $\text{M}^+ - 2 \times \text{C}_{12}\text{H}_{25}$ , 10%)

**$^1\text{H}$  NMR** (300 MHz,  $\text{CDCl}_3$ ,  $\delta$  in ppm): 0.45 – 0.60 (bs, 4H, Ar- $\text{CH}_2$ - $\text{CH}_2$ ), 0.85 (t,  $J = 6.8$  Hz, 6H,  $-\text{CH}_3$ ), 0.94 – 1.32 (m, 36H,  $-\text{CH}_2-$ ), 1.39 (s, 24H,  $-\text{CH}_3$ ), 1.93 – 2.04 (m, 4H, Ar- $\text{CH}_2$ ), 7.69 – 7.83 (m, 6H, Ar-H)

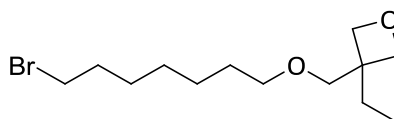
**3-(6-Bromohexyloxymethyl)-3-ethyloxetane**

The reactants 3-ethyl-3-oxetanemethanol (5.81 g, 50.00 mmol) and 1,6-dibromohexane (36.60 g, 150.00 mmol), and the phase-transfer catalyst tetrabutylammonium bromide (0.80 g, 2.50 mmol) were dissolved in hexane (200 ml). After addition of a 45% NaOH (28 ml), the mixture was heated to reflux for 16 hours. The solution was poured into ice water and extracted with hexane. The combined hexane phases were washed with water and dried over magnesium sulfate. After removal of the solvent, the crude product was purified by column chromatography (gradient hexane  $\rightarrow$  THF). Excess 1,6-dibromohexane was eluted with hexane before the product was eluted with THF. The solvent was removed, and 3-(6-bromohexyloxymethyl)-3-ethyloxetane (11.13 g, 39.86 mmol, 80%) was obtained as a colorless liquid.

## Characterization

**EI-MS** ( $m/z$ , %): calculated for  $C_{12}H_{23}BrO_2$  279.21; found 248 ( $M^+ - C_2H_5$ , 40%), 219 (60%), 163 ( $M^+ - C_6H_{11}O_2$ , 90%)

**$^1H$  NMR** (300 MHz,  $CDCl_3$ ,  $\delta$  in ppm): 0.86 (t,  $J=7.5$  Hz, 3H,  $-CH_3$ ), 1.32 – 1.50 (m, 4H,  $-CH_2-$ ), 1.58 (qui,  $J=6.6$  Hz, 2H,  $-CH_2-CH_2-O$ ), 1.72 (q,  $J=7.5$  Hz, 2H,  $-CH_2-CH_3$ ), 1.85 (qui,  $J=6.6$  Hz, 2H,  $Br-CH_2-CH_2-$ ), 3.36 – 3.47 (m, 4H,  $Br-CH_2-...-CH_2-O$ ), 3.51 (s, 2H,  $-O-CH_2-$ oxetane), 4.36, 4.43 (2 d,  $J=5.8$  Hz,  $2 \times 2H$  oxetane  $CH_2$ )

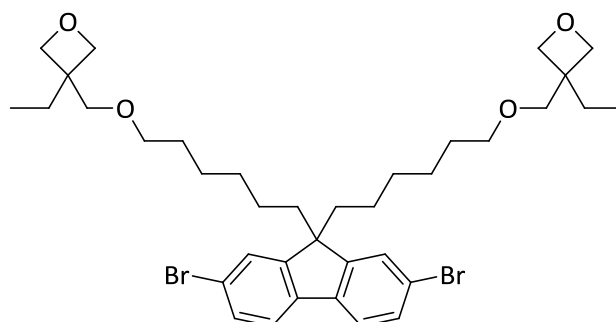
**3-(7-Bromoheptyloxymethyl)-3-ethyloxetane**

The reactants 3-ethyl-3-oxetanemethanol (5.91 g, 50.90 mmol) and 1,7-dibromoheptane (39.40 g, 152.72 mmol), and the phase-transfer catalyst tetrabutylammonium bromide (0.80 g, 2.50 mmol) were dissolved in hexane (200 ml). After addition of a 45% NaOH (28 ml), the mixture was heated to reflux for 22 hours. The solution was poured into ice water and extracted with hexane. The combined hexane phases were washed with water and dried over magnesium sulfate. After removal of the solvent, the crude product was purified by column chromatography (gradient hexane  $\rightarrow$  THF). Excess 1,7-dibromoheptane was eluted with hexane before the product was eluted with THF. The solvent was removed, and 3-(7-bromoheptyloxymethyl)-3-ethyloxetane (14.54 g, 49.58 mmol, 97%) was obtained as a colorless liquid.

**Characterization**

**EI-MS** ( $m/z$ , %): calculated for  $C_{13}H_{25}BrO_2$  292.10; found 263 ( $M^+ - C_2H_5$ , 15%), 234 (20%), 97 (60%), 86 (60%), 69 (50%), 56 (100%), 42 (60%)

**$^1H$  NMR** (300 MHz,  $CDCl_3$ ,  $\delta$  in ppm): 0.87 (t,  $J=7.5$  Hz, 3H,  $-CH_3$ ), 1.27 – 1.45 (m, 6H,  $-CH_2-$ ), 1.50 – 1.61 (m, 2H,  $-CH_2-CH_2-O$ ), 1.72 (q,  $J=7.5$  Hz, 2H,  $-CH_2-CH_3$ ), 1.80 – 1.90 (m, 2H, Br- $CH_2-CH_2-$ ), 3.34 – 3.47 (m, 4H, Br- $CH_2-\dots-CH_2-O$ ), 3.50 (s, 2H,  $-O-CH_2-$ oxetane), 4.37, 4.44 (2 d,  $J=5.8$  Hz,  $2 \times 2H$  oxetane  $CH_2$ )

**2,7-Dibromo-9,9-bis(hexyl-6,1-diyl)bis(oxymethyl-3-ethyloxetane)-fluorene**

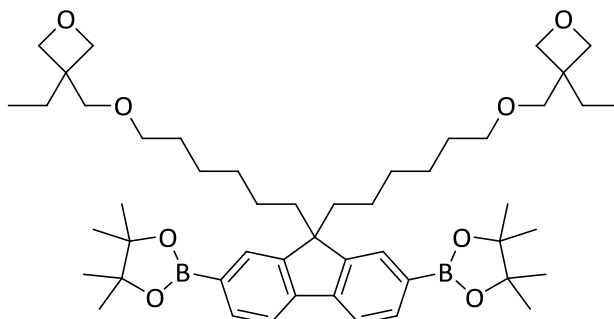
A solution of 2,7-dibromofluorene (2.00 g, 6.17 mmol) and the phase-transfer catalysts benzyltriethylammonium chloride (0.06 g, 0.35 mmol) and tetrabutylammonium chloride (0.07 g, 0.35 mmol) in DMSO (45 ml) was flushed with argon for 30 minutes. Under argon 20 ml of a 50% NaOH solution were added dropwise. After stirring for 20 minutes, 3-(6-bromohexyloxymethyl)-3-ethyloxetane (5.24 g, 18.51 mmol) was added dropwise. The mixture was heated to reflux for 20 hours. After cooling to room temperature, the solution was poured into ice water and extracted with diethyl ether. The combined ether phases were washed with water and dried over sodium sulfate. The solvent was removed, and the crude product was purified by flash chromatography (eluent hexane/ethyl acetate 3:1) yielding 2,7-dibromo-9,9-bis(hexyl-6,1-diyl)bis(oxymethyl-3-ethyloxetane)-fluorene (3.10 g, 4.30 mmol, 70%) as a yellowish oil.

## Characterization

**EI-MS** ( $m/z$ , %): calculated for  $C_{37}H_{52}Br_2O_4$  720.61; found 720 ( $M^+$ , 100%), 690 ( $M^+ - OCH_2$ , 15%), 622 ( $M^+ - C_6H_{11}O_2$ , 15%), 323 ( $M^+ - 2 \times C_{12}H_{23}O_2$ , 30%)

**$^1H$  NMR** (300 MHz,  $CDCl_3$ ,  $\delta$  in ppm): 0.48 – 0.64 (bs, 4H, Ar- $CH_2$ - $\underline{CH_2}$ -), 0.84 (t,  $J=7.5$  Hz,  $-CH_3$ ), 1.00 – 1.16 (m, 8H,  $-CH_2-$ ), 1.32 – 1.45 (m, 4H,  $-CH_2-$ ), 1.70 (q,  $J=7.5$  Hz, 2H,  $-\underline{CH_2}$ - $CH_3$ ), 1.87 – 1.96 (m, 4H, Ar- $CH_2-$ ), 3.33 (t,  $J=6.5$  Hz, 4H,  $-CH_2-O-$ ), 3.46 (s, 4H,  $-O-\underline{CH_2}$ -oxetane), 4.35, 4.41 (2 d,  $J=5.8$  Hz,  $2 \times 4H$ , oxetane  $CH_2$ ), 7.41 – 7.56 (m, 6H, Ar-H)

**2,7-Bis(4,4,5,5-tetramethyl-1,3,2-dioxaborolane)-9,9-bis(hexyl-6,1-diyl)bis-(oxymethyl-3-ethyloxetane)-fluorene**

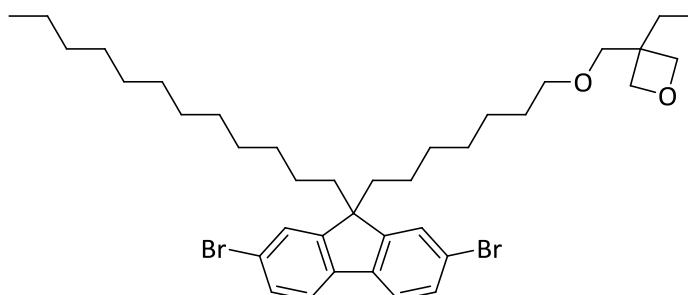


A solution of 2,7-dibromo-9,9-bis(hexyl-6,1-diyl)bis(oxymethyl-3-ethyloxetane)-fluorene (0.98 g, 1.36 mmol) in dry THF (30 ml) was cooled to  $-78\text{ }^{\circ}\text{C}$ . At  $-78\text{ }^{\circ}\text{C}$  *n*-butyllithium (1.6 M solution in hexane, 1.87 ml, 2.99 mmol) was added slowly. The solution was stirred at  $-78\text{ }^{\circ}\text{C}$  for 30 minutes before 2-isopropoxy-4,4,5,5-tetramethyl-1,3,2-dioxaborolane (0.61 g, 3.26 mmol) was added slowly. The reaction mixture was kept at  $-78\text{ }^{\circ}\text{C}$  for another hour and was allowed to warm to room temperature overnight. It was poured into ice water and extracted with diethyl ether. The combined ether phases were washed with a saturated NaCl solution and dried over magnesium sulfate. The solvent was removed, and the crude product was purified by MPLC (eluent hexane/ethyl acetate 3:2) yielding 2,7-bis(4,4,5,5-tetramethyl-1,3,2-dioxaborolane)-9,9-bis(hexyl-6,1-diyl)bis(oxymethyl-3-ethyloxetane)-fluorene (0.63 g, 0.78 mmol, 57%) as colorless solid.

Characterization

**EI-MS** (*m/z*, %): calculated for  $\text{C}_{49}\text{H}_{76}\text{B}_2\text{O}_8$  814.74; found 814 ( $M^+$ , 100%), 99 (20%), 83 (35%)

**$^1\text{H NMR}$**  (300 MHz,  $\text{CDCl}_3$ ,  $\delta$  in ppm): 0.46 – 0.62 (bs, 4H, Ar- $\text{CH}_2\text{-CH}_2\text{-}$ ), 0.83 (t,  $J = 7.5$  Hz, 6H, oxetane- $\text{CH}_2\text{-CH}_3$ ), 0.98 – 1.10 (m, 8H,  $\text{-CH}_2\text{-}$ ), 1.30 – 1.39 (m, 4H,  $\text{-CH}_2\text{-CH}_2\text{-O}$ ), 1.39 (s, 24H,  $\text{-CH}_3$ ), 1.68 (q,  $J = 7.5$  Hz, 4H, oxetane- $\text{CH}_2\text{-CH}_3$ ), 1.94 – 2.05 (m, 4H, Ar- $\text{CH}_2\text{-}$ ), 3.29 (t,  $J = 6.6$  Hz, 4H,  $\text{-CH}_2\text{-O}$ ), 3.44 (s, 4H,  $\text{-O-CH}_2\text{-oxetane}$ ), 4.38, 4.33 (2 d,  $J = 5, 8$  Hz,  $2 \times 4\text{H}$ , oxetane  $\text{CH}_2$ ), 7.70 – 7.83 (m, 6H, Ar-H)

**2,7-Dibromo-9-(1-dodecyl)-9-(heptyl-7,1-diyl-oxymethyl-3-ethyloxetane)-fluorene**

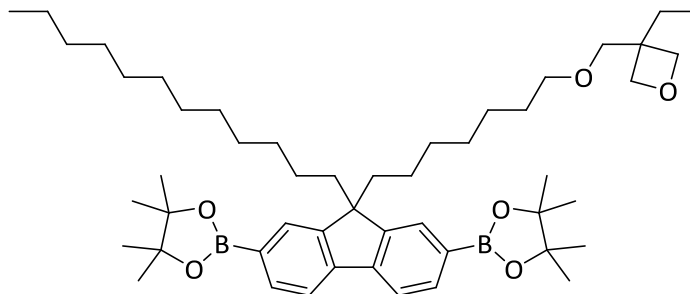
A solution of 2,7-dibromofluorene (1.00 g, 3.09 mmol) and the phase-transfer catalyst benzyltriethylammonium chloride (0.05 g, 0.22 mmol) in DMSO (50 ml) was flushed with argon for 30 minutes. Under argon a 50% NaOH solution (15 ml) was added dropwise. After stirring for 20 minutes, a mixture of 1-bromododecane (1.16 g, 4.64 mmol) and 3-(7-bromoheptyloxymethyl)-3-ethyloxetane (1.37 g, 4.64 mmol) was added dropwise. The solution was heated to reflux for 20 hours. After cooling to room temperature, it was poured into ice water and extracted with diethyl ether. The combined ether phases were washed with water and dried over sodium sulfate. The solvent was removed, and the crude product was purified by flash chromatography (eluent hexane/THF 5:1) yielding 2,7-dibromo-9-(1-dodecyl)-9-(heptyl-7,1-diyl-oxymethyl-3-ethyloxetane)-fluorene (0.91 g, 1.29 mmol, 42%) as a colorless oil.

## Characterization

**EI-MS** ( $m/z$ ): calculated for  $C_{38}H_{56}Br_2O_2$  704.66; found 704 ( $M^+$ , 100%), 674 ( $M^+ - C_2H_5$ , 10%), 323 ( $M^+ - [C_{12}H_{25}; C_{13}H_{25}O_2]$ , 40%)

**$^1H$  NMR** (300 MHz,  $CDCl_3$ ,  $\delta$  in ppm): 0.48 – 0.64 (bs, 4H, Ar- $CH_2-CH_2-$ ), 0.80 – 0.90 (m, 6H,  $-CH_3$ ), 0.98 – 1.32 (m, 24H,  $-CH_2-$ ), 1.40 – 1.51 (m, 2H,  $-CH_2-$ ), 1.71 (q,  $J = 7.6$  Hz, 2H, oxetane- $CH_2-CH_3$ ), 1.85 – 1.96 (m, 4H, Ar- $CH_2-$ ), 3.36 (t,  $J = 6.6$  Hz, 2H,  $-CH_2-O$ ), 3.48 (s, 2H,  $-O-CH_2-$  oxetane), 4.35, 4.42 (2 d,  $J = 5.8$  Hz,  $2 \times 2H$ , oxetane  $CH_2$ ), 7.41 – 7.54 (m, 6H, Ar-H)

**2,7-Bis(4,4,5,5-tetramethyl-1,3,2-dioxaborolane)-9-(1-dodecyl)-9-(heptyl-7,1-diyl-oxymethyl-3-ethyloxetane)-fluorene**



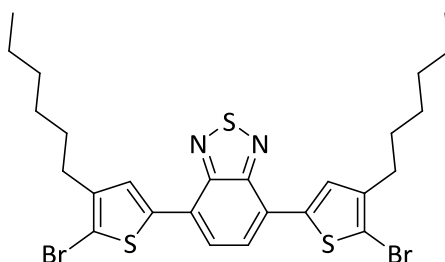
A solution of 2,7-dibromo-9-(1-dodecyl)-9-(heptyl-7,1-diyl-oxymethyl-3-ethyloxetane)-fluorene (1.00 g, 1.42 mmol) in dry THF (30 ml) was cooled to  $-78\text{ }^{\circ}\text{C}$ . At  $-78\text{ }^{\circ}\text{C}$  *n*-butyllithium (1.6 M solution in hexane, 1.95 ml, 3.12 mmol) was added slowly. The solution was stirred at  $-78\text{ }^{\circ}\text{C}$  for 30 minutes before 2-isopropoxy-4,4,5,5-tetramethyl-1,3,2-dioxaborolane (0.63 g, 3.40 mmol) was added slowly. The reaction mixture was kept at  $-78\text{ }^{\circ}\text{C}$  for another hour and was allowed to warm to room temperature overnight. It was poured into ice water and extracted with diethyl ether. The combined ether phases were washed with a saturated NaCl solution and dried over magnesium sulfate. The solvent was removed, and the crude product was purified by MPLC (eluent hexane/ethyl acetate 5:1) yielding 2,7-bis(4,4,5,5-tetramethyl-1,3,2-dioxaborolane)-9-(1-dodecyl)-9-(heptyl-7,1-diyl-oxymethyl-3-ethyloxetane)-fluorene (0.31 g, 0.39 mmol, 27%) as slightly yellowish solid.

**Characterization**

**EI-MS** (*m/z*, %): calculated for  $\text{C}_{50}\text{H}_{80}\text{B}_2\text{O}_6$  798.79; found 798 ( $\text{M}^+$ , 100%), 585 ( $\text{M}^+ - \text{C}_{13}\text{H}_{25}\text{O}_2$ , 45%), 83 (50%)

**$^1\text{H NMR}$**  (300 MHz,  $\text{CDCl}_3$ ,  $\delta$  in ppm): 0.46 – 0.63 (bs, 4H, Ar- $\text{CH}_2\text{-CH}_2\text{-}$ ), 0.78 – 0.90 (m, 6H,  $-\text{CH}_3$ ), 0.95 – 1.30 (m, 26H,  $-\text{CH}_2\text{-}$ ), 1.38 (s, 24H,  $-\text{CH}_3$ ), 1.69 (q,  $J = 7.5\text{ Hz}$ , 2H, oxetane- $\text{CH}_2\text{-CH}_3$ ), 1.94 – 2.06 (m, 4H, Ar- $\text{CH}_2\text{-}$ ), 3.34 (t,  $J = 6.6\text{ Hz}$ , 2H,  $-\text{CH}_2\text{-O-}$ ), 3.46 (s, 2H,  $-\text{O-CH}_2\text{-Oxetane}$ ), 4.34, 4.40 (2 d,  $J = 5.8\text{ Hz}$ ,  $2 \times 2\text{H}$ , oxetane  $\text{CH}_2$ ), 7.68 – 7.85 (m, 6H, Ar-H)

### 4,7-Bis(5-bromo-4-hexyl-2-thienyl)-2,1,3-benzothiadiazole



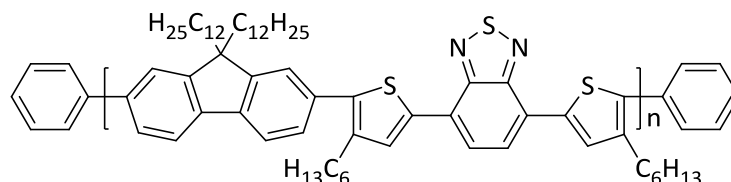
The acceptor monomer 4,7-bis(5-bromo-4-hexyl-2-thienyl)-2,1,3-benzothiadiazole was commercially available and purchased in excellent purity from SunaTech Inc.

#### Characterization

**EI-MS** ( $m/z$ , %): calculated for  $C_{26}H_{30}Br_2N_2S_3$  626.53; found 626 ( $M^+$ , 100%)

**$^1H$  NMR** (300 MHz,  $CDCl_3$ ,  $\delta$  in ppm): 0.90 (t,  $J = 7.0$  Hz, 6H,  $-CH_3$ ), 1.25 – 1.46 (m, 12H,  $-CH_2-$ ), 1.67 (qui,  $J = 7.6$  Hz, 4H, thiophene- $CH_2$ - $CH_2$ -), 2.64 (t,  $J = 7.7$  Hz, 4H, thiophene- $CH_2$ -), 7.74 (s, 2H, Ar-H), 7.76 (s, 2H, Ar-H)

## 8.3 Syntheses of the polymers

**PFDTBT**

Equimolar amounts of the monomers 2,7-bis(4,4,5,5-tetramethyl-1,3,2-dioxaborolane)-9,9-didodecylfluorene (233.37 mg, 0.309 mmol) and 4,7-bis(5-bromo-4-hexyl-2-thienyl)-2,1,3-benzothiadiazole (193.60 mg, 0.309 mmol) were dissolved in toluene (10 ml). A few drops of the phase-transfer catalyst Aliquat 336 and a 2 M solution of  $\text{Na}_2\text{CO}_3$  (12 ml) were added, and the mixture was degassed by three freeze-pump-thaw-cycles. After addition of the catalyst  $\text{Pd}(\text{PPh}_3)_4$  (0.015 eq., 5.40 mg,  $4.63 \times 10^{-3}$  mmol), another freeze-pump-thaw cycle was applied. The reaction mixture was heated to reflux under vigorous stirring. After four days, bromobenzene and phenylboronic acid (0.309 mmol each) were added to endcap the polymer. The organic phase was separated, concentrated, and precipitated from methanol. After drying, 265 mg (0.273 mmol, 88%) of the crude polymer were obtained. Soxhlet extraction with the sequence acetone, hexane and toluene was applied, and the fractions were concentrated and precipitated from methanol.

## Characterization

$^1\text{H NMR}$  (300 MHz,  $\text{CDCl}_3$ ,  $\delta$  in ppm): 0.58 – 0.96 (m, 16H,  $-\text{CH}_3$  + fluorene- $\text{CH}_2$ - $\text{CH}_2$ -), 1.00 – 1.48 (m, 45H,  $-\text{CH}_2$ -), 1.66 – 1.85 (m, 4H, thiophene- $\text{CH}_2$ - $\text{CH}_2$ -), 1.91 – 2.20 (m, 4H, fluorene- $\text{CH}_2$ -), 2.67 – 2.93 (m, 4H, thiophene- $\text{CH}_2$ -), 7.46 – 8.11 (m, 10H, Ar-H)

**Polymer SEC** (THF, PS calibration):

acetone fraction:  $\overline{M}_n$  800  $\text{g mol}^{-1}$ ,  $\overline{M}_w$  1,500  $\text{g mol}^{-1}$ , D 1.99 (22 mg)

hexane fraction:  $\overline{M}_n$  11,500  $\text{g mol}^{-1}$ ,  $\overline{M}_w$  24,400  $\text{g mol}^{-1}$ , D 2.11 (196 mg)

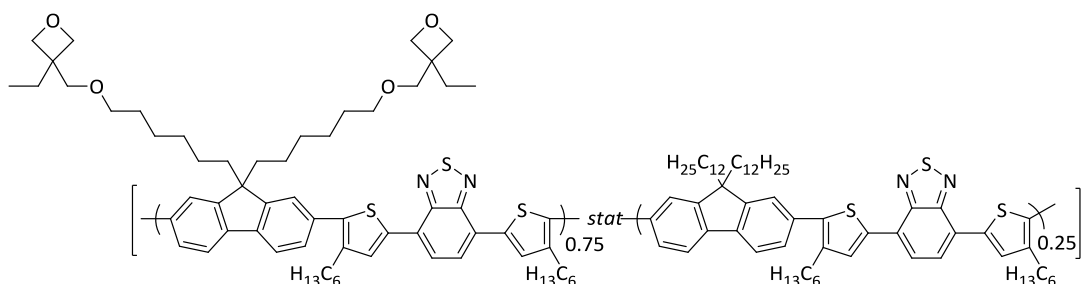
toluene fraction:  $\overline{M}_n$  24,500  $\text{g mol}^{-1}$ ,  $\overline{M}_w$  37,500  $\text{g mol}^{-1}$ , D 1.53 (35 mg)

**TGA** (10  $\text{K min}^{-1}$ ,  $\text{N}_2$ ): 1% weight loss at 282  $^\circ\text{C}$ , 5% weight loss at 420  $^\circ\text{C}$

**UV/Vis absorption** (THF,  $10^{-3}$   $\text{mg ml}^{-1}$ ):  $\lambda_{\text{max}}$ : 365 nm, 511 nm,  $\lambda_{\text{onset}}$ : 587 nm,  $E_{\text{opt}} \approx 2.10$  eV

**PL** (THF,  $10^{-3}$   $\text{mg ml}^{-1}$ ):  $\lambda_{\text{max}}$ : 639 nm



PFDTBTO<sub>x0.75</sub>

The monomers 2,7-bis(4,4,5,5-tetramethyl-1,3,2-dioxaborolane)-9,9-bis(hexyl-6,1-diyl)bis(oxymethyl-3-ethyloxetane)-fluorene (190.09 mg, 0.233 mmol), 2,7-bis(4,4,5,5-tetramethyl-1,3,2-dioxaborolane)-9,9-didodecylfluorene (58.87 mg, 0.078 mmol) and 4,7-bis(5-bromo-4-hexyl-2-thienyl)-2,1,3-benzothiadiazole (195.48 mg, 0.312 mmol) were dissolved in toluene (10 ml). A few drops of the phase-transfer catalyst Aliquat 336 and a 2 M solution of Na<sub>2</sub>CO<sub>3</sub> (12 ml) were added, and the mixture was degassed by three freeze-pump-thaw-cycles. After addition of the catalyst Pd(PPh<sub>3</sub>)<sub>4</sub> (0.015 eq., 5.40 mg, 4.68 × 10<sup>-3</sup> mmol) another freeze-pump-thaw cycle was applied. The reaction mixture was heated to reflux under vigorous stirring. After four days, bromobenzene and phenylboronic acid (0.312 mmol each) were added to endcap the polymer. The organic phase was separated, concentrated, and precipitated from methanol. After drying, 274 mg (0.271 mmol, 87%) of PFDTBTO<sub>x0.75</sub> were obtained.

## Characterization

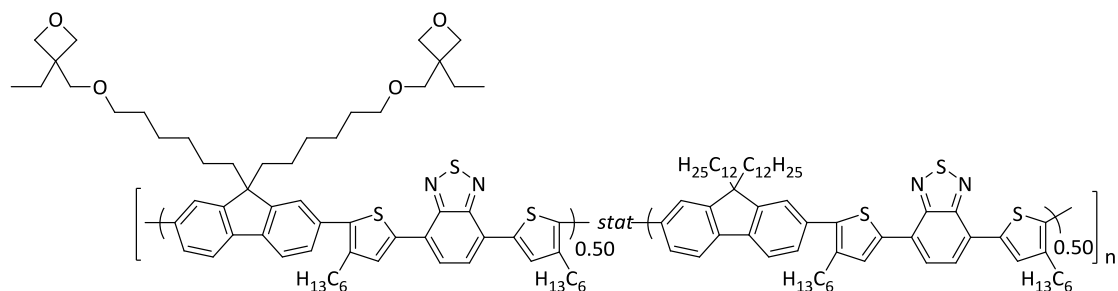
<sup>1</sup>H NMR (300 MHz, CDCl<sub>3</sub>, δ in ppm): 0.62 – 0.96 (m, 16H, -CH<sub>3</sub> + fluorene-CH<sub>2</sub>-CH<sub>2</sub>-), 1.02 – 1.50 (m, 31H, -CH<sub>2</sub>-), 1.62 – 1.85 (m, 7H, thiophene-CH<sub>2</sub>-CH<sub>2</sub>- + oxetane-CH<sub>2</sub>-CH<sub>3</sub>), 1.92 – 2.21 (m, 4H, fluorene-CH<sub>2</sub>-), 2.67 – 2.91 (m, 4H, thiophene-CH<sub>2</sub>-), 3.34 (t, *J* = 6.6 Hz, 3H, -CH<sub>2</sub>-O-), 3.45 (s, 3H, -O-CH<sub>2</sub>-oxetane), 4.32 + 4.39 (2d, *J* = 5.8 Hz, 2 × 3H, oxetane CH<sub>2</sub>), 7.50 – 8.10 (m, 10H, Ar-H)

**Polymer SEC** (THF, PS calibration):  $\overline{M}_n$  14,200 g mol<sup>-1</sup>,  $\overline{M}_w$  33,400 g mol<sup>-1</sup>, D 2.35

**TGA** (10 K min<sup>-1</sup>, N<sub>2</sub>): 1% weight loss at 368 °C, 5% weight loss at 426 °C

**UV/Vis absorption** (THF, 10<sup>-3</sup> mg ml<sup>-1</sup>):  $\lambda_{max}$ : 365 nm, 510 nm,  $\lambda_{onset}$ : 584 nm,  $E_{opt} \approx 2.10$  eV

**PL** (THF, 10<sup>-3</sup> mg ml<sup>-1</sup>):  $\lambda_{max}$ : 634 nm

PFDTBTO<sub>0.50</sub>

The monomers 2,7-bis(4,4,5,5-tetramethyl-1,3,2-dioxaborolane)-9,9-bis(hexyl-6,1-diyl)bis(oxymethyl-3-ethyloxetane)-fluorene (129.95 mg, 0.160 mmol), 2,7-bis(4,4,5,5-tetramethyl-1,3,2-dioxaborolane)-9,9-didodecylfluorene (120.39 mg, 0.160 mmol) and 4,7-bis(5-bromo-4-hexyl-2-thienyl)-2,1,3-benzothiadiazole (200.00 mg, 0.320 mmol) were dissolved in toluene (10 ml). A few drops of the phase-transfer catalyst Aliquat 336 and a 2 M solution of Na<sub>2</sub>CO<sub>3</sub> (12 ml) were added, and the mixture was degassed by three freeze-pump-thaw-cycles. After addition of the catalyst Pd(PPh<sub>3</sub>)<sub>4</sub> (0.015 eq., 5.55 mg, 4.78 × 10<sup>-3</sup> mmol), another freeze-pump-thaw cycle was applied. The reaction mixture was heated to reflux under vigorous stirring. After four days, bromobenzene and phenylboronic acid (0.320 mmol each) were added to endcap the polymer. The organic phase was separated, concentrated, and precipitated from methanol. After drying, 314 mg (0.315 mmol, 98%) of PFDTBTO<sub>0.50</sub> were obtained.

## Characterization

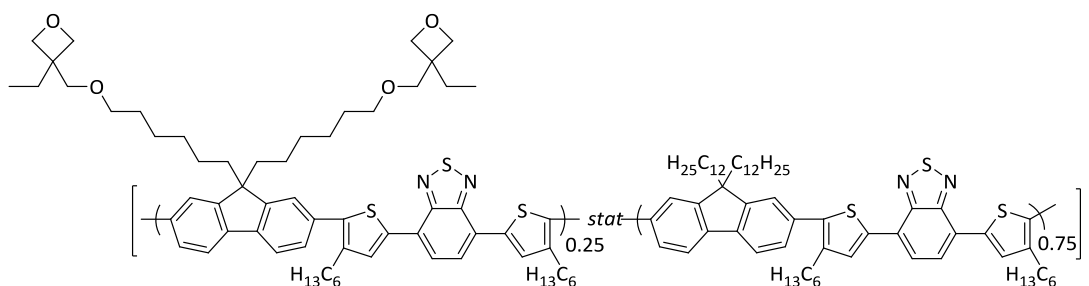
<sup>1</sup>H NMR (300 MHz, CDCl<sub>3</sub>, δ in ppm): 0.61 – 0.95 (m, 16H, -CH<sub>3</sub> + fluorene-CH<sub>2</sub>-CH<sub>2</sub>-), 1.01 – 1.48 (m, 40H, -CH<sub>2</sub>-), 1.63 – 1.85 (m, 6H, thiophene-CH<sub>2</sub>-CH<sub>2</sub>- + oxetane-CH<sub>2</sub>-CH<sub>3</sub>), 1.91 – 2.18 (m, 4H, fluorene-CH<sub>2</sub>-), 2.66 – 2.89 (m, 4H, thiophene-CH<sub>2</sub>-), 3.28 – 3.38 (m, 2H, -CH<sub>2</sub>-O-), 3.45 (s, 2H, -O-CH<sub>2</sub>-oxetane), 4.30 – 4.43 (m, 4H, oxetane CH<sub>2</sub>), 7.48 – 8.13 (m, 10H, Ar-H)

**Polymer SEC** (THF, PS calibration):  $\overline{M}_n$  6,200 g mol<sup>-1</sup>,  $\overline{M}_w$  13,200 g mol<sup>-1</sup>, D 2.15

**TGA** (10 K min<sup>-1</sup>, N<sub>2</sub>): 1% weight loss at 361 °C, 5% weight loss at 402 °C

**UV/Vis absorption** (THF, 10<sup>-3</sup> mg ml<sup>-1</sup>): λ<sub>max</sub>: 361 nm, 507 nm, λ<sub>onset</sub>: 584 nm, E<sub>opt</sub> ≈ 2.10 eV

**PL** (THF, 10<sup>-3</sup> mg ml<sup>-1</sup>): λ<sub>max</sub>: 633 nm

PFDTBTO<sub>x0.25</sub>

The monomers 2,7-bis(4,4,5,5-tetramethyl-1,3,2-dioxaborolane)-9,9-bis(hexyl-6,1-diyl)bis(oxymethyl-3-ethyloxetane)-fluorene (68.36 mg, 0.084 mmol), 2,7-bis(4,4,5,5-tetramethyl-1,3,2-dioxaborolane)-9,9-didodecylfluorene (190.00 mg, 0.252 mmol) and 4,7-bis(5-bromo-4-hexyl-2-thienyl)-2,1,3-benzothiadiazole (210.51 mg, 0.336 mmol) were dissolved in toluene (10 ml). A few drops of the phase-transfer catalyst Aliquat 336 and a 2 M solution of Na<sub>2</sub>CO<sub>3</sub> (12 ml) were added, and the mixture was degassed by three freeze-pump-thaw-cycles. After addition of the catalyst Pd(PPh<sub>3</sub>)<sub>4</sub> (0.015 eq., 5.82 mg, 5.04 × 10<sup>-3</sup> mmol), another freeze-pump-thaw cycle was applied. The reaction mixture was heated to reflux under vigorous stirring. After four days, bromobenzene and phenylboronic acid (0.336 mmol each) were added to endcap the polymer. The organic phase was separated, concentrated, and precipitated from methanol. After drying, 303 mg (0.308 mmol, 92%) of PFDTBTO<sub>x0.25</sub> were obtained.

## Characterization

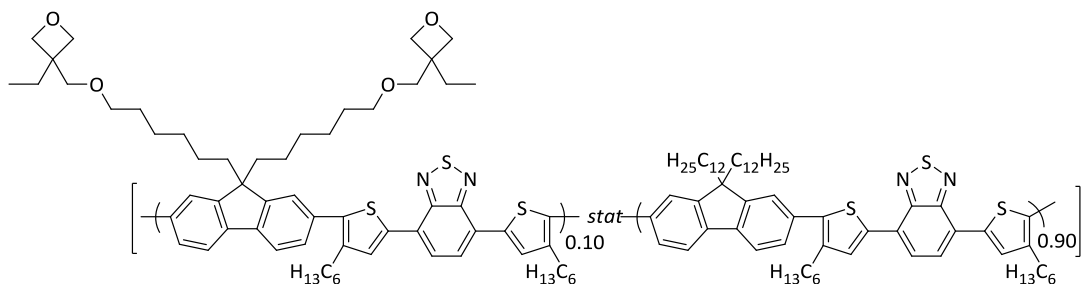
<sup>1</sup>H NMR (300 MHz, CDCl<sub>3</sub>, δ in ppm): 0.62 – 0.94 (m, 16H, -CH<sub>3</sub> + fluorene-CH<sub>2</sub>-CH<sub>2</sub>-), 0.99 – 1.47 (m, 42H, -CH<sub>2</sub>-), 1.60 – 1.83 (m, 5H, thiophene-CH<sub>2</sub>-CH<sub>2</sub>- + oxetane-CH<sub>2</sub>-CH<sub>3</sub>), 1.92 – 2.19 (m, 4H, fluorene-CH<sub>2</sub>-), 2.65 – 2.90 (m, 4H, thiophene-CH<sub>2</sub>-), 3.26 – 3.36 (m, 1H, -CH<sub>2</sub>-O-), 3.43 (s, 1H, -O-CH<sub>2</sub>-oxetane), 4.27 – 4.41 (m, 2H, oxetane CH<sub>2</sub>), 7.40 – 8.10 (m, 10H, Ar-H)

**Polymer SEC** (THF, PS calibration):  $\overline{M}_n$  12,500 g mol<sup>-1</sup>,  $\overline{M}_w$  22,500 g mol<sup>-1</sup>, D 1.80

**TGA** (10 K min<sup>-1</sup>, N<sub>2</sub>): 1% weight loss at 251 °C, 5% weight loss at 395 °C

**UV/Vis absorption** (THF, 10<sup>-3</sup> mg ml<sup>-1</sup>):  $\lambda_{max}$ : 364 nm, 509 nm,  $\lambda_{onset}$ : 584 nm,  $E_{opt} \approx 2.10$  eV

**PL** (THF, 10<sup>-3</sup> mg ml<sup>-1</sup>):  $\lambda_{max}$ : 633 nm

PFDTBTO<sub>x</sub>0.10

The monomers 2,7-bis(4,4,5,5-tetramethyl-1,3,2-dioxaborolane)-9,9-bis(hexyl-6,1-diyl)bis(oxymethyl-3-ethyloxetane)-fluorene (24.44 mg, 0.030 mmol), 2,7-bis(4,4,5,5-tetramethyl-1,3,2-dioxaborolane)-9,9-didodecylfluorene (203.79 mg, 0.270 mmol) and 4,7-bis(5-bromo-4-hexyl-2-thienyl)-2,1,3-benzothiadiazole (187.96 mg, 0.300 mmol) were dissolved in toluene (10 ml). A few drops of the phase-transfer catalyst Aliquat 336 and a 2 M solution of Na<sub>2</sub>CO<sub>3</sub> (12 ml) were added, and the mixture was degassed by three freeze-pump-thaw-cycles. After addition of the catalyst Pd(PPh<sub>3</sub>)<sub>4</sub> (0.015 eq., 5.20 mg, 4.50 × 10<sup>-3</sup> mmol), another freeze-pump-thaw cycle was applied. The reaction mixture was heated to reflux under vigorous stirring. After four days, bromobenzene and phenylboronic acid (0.300 mmol each) were added to endcap the polymer. The organic phase was separated, concentrated, and precipitated from methanol. Soxhlet extraction with the sequence acetone, hexane and toluene was applied, and the fractions were concentrated and precipitated from methanol. The cumulative weight of the fractions was 230 mg (0.234 mmol, 78%).

## Characterization

<sup>1</sup>H NMR (300 MHz, CDCl<sub>3</sub>, δ in ppm): 0.61 – 0.96 (m, 16H, -CH<sub>3</sub> + fluorene-CH<sub>2</sub>-CH<sub>2</sub>-), 1.02 – 1.49 (m, 46H, -CH<sub>2</sub>-), 1.62 – 1.85 (m, 4.5H, thiophene-CH<sub>2</sub>-CH<sub>2</sub>- + oxetane-CH<sub>2</sub>-CH<sub>3</sub>), 1.90 – 2.19 (m, 4H, fluorene-CH<sub>2</sub>-), 2.67 – 2.93 (m, 4H, thiophene-CH<sub>2</sub>-), 3.29 – 3.37 (m, 0.5H, -CH<sub>2</sub>-O-), 3.45 (s, 0.5H, -O-CH<sub>2</sub>-oxetane), 4.30 – 4.43 (m, 0.8H, oxetane CH<sub>2</sub>), 7.48 – 8.13 (m, 10H, Ar-H)

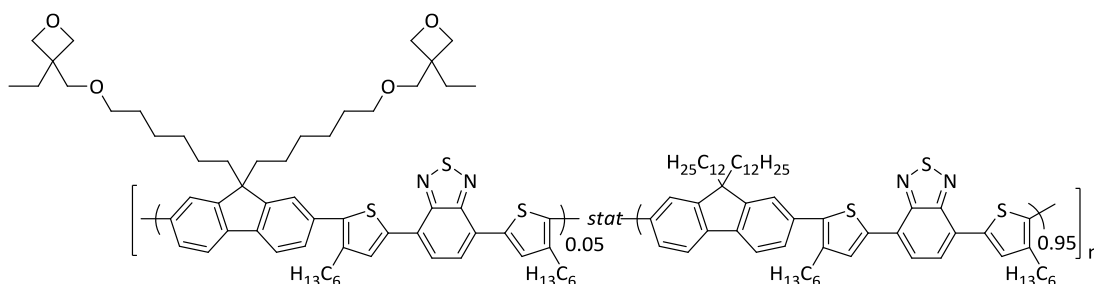
## Polymer SEC (THF, PS calibration):

hexane fraction  $\overline{M}_n$  11,800 g mol<sup>-1</sup>,  $\overline{M}_w$  24,000 g mol<sup>-1</sup>, D 2.03

TGA (10 K min<sup>-1</sup>, N<sub>2</sub>): 1% weight loss at 344 °C, 5% weight loss at 419 °C

UV/Vis absorption (THF, 10<sup>-3</sup> mg ml<sup>-1</sup>): λ<sub>max</sub>: 361 nm, 505 nm, λ<sub>onset</sub>: 584 nm, E<sub>opt</sub> ≈ 2.10 eV

PL (THF, 10<sup>-3</sup> mg ml<sup>-1</sup>): λ<sub>max</sub>: 633 nm

PFDTBTO<sub>x0.05</sub>

The monomers 2,7-bis(4,4,5,5-tetramethyl-1,3,2-dioxaborolane)-9,9-bis(hexyl-6,1-diyl)bis(oxymethyl-3-ethyloxetane)-fluorene (9.70 mg, 0.012 mmol), 2,7-bis(4,4,5,5-tetramethyl-1,3,2-dioxaborolane)-9,9-didodecylfluorene (170.99 mg, 0.226 mmol) and 4,7-bis(5-bromo-4-hexyl-2-thienyl)-2,1,3-benzothiadiazole (149.36 mg, 0.238 mmol) were dissolved in toluene (10 ml). A few drops of the phase-transfer catalyst Aliquat 336 and a 2 M solution of Na<sub>2</sub>CO<sub>3</sub> (12 ml) were added, and the mixture was degassed by three freeze-pump-thaw-cycles. After addition of the catalyst Pd(PPh<sub>3</sub>)<sub>4</sub> (0.015 eq., 4.13 mg, 3.57 × 10<sup>-3</sup> mmol), another freeze-pump-thaw cycle was applied. The reaction mixture was heated to reflux under vigorous stirring. After four days, bromobenzene and phenylboronic acid (0.238 mmol each) were added to endcap the polymer. The organic phase was separated, concentrated, and precipitated from methanol. After drying, 224 mg (0.227 mmol, 95%) of PFDTBTO<sub>x0.10</sub> were obtained.

## Characterization

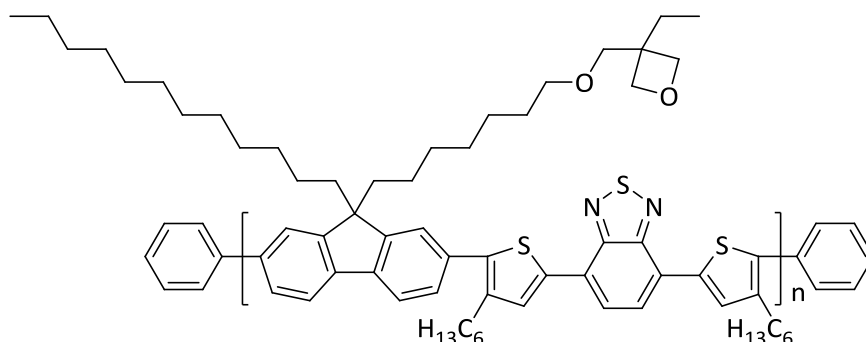
<sup>1</sup>H NMR (300 MHz, CDCl<sub>3</sub>, δ in ppm): 0.59 – 0.95 (m, 16H, -CH<sub>3</sub> + fluorene-CH<sub>2</sub>-CH<sub>2</sub>-), 0.99 – 1.49 (m, 46H, -CH<sub>2</sub>-), 1.64 – 1.82 (m, 4.4H, thiophene-CH<sub>2</sub>-CH<sub>2</sub>- + oxetane-CH<sub>2</sub>-CH<sub>3</sub>), 1.91 – 2.20 (m, 3H, fluorene-CH<sub>2</sub>-), 2.66 – 2.94 (m, 3H, thiophene-CH<sub>2</sub>-), 3.32 (s, 0.2H, -O-CH<sub>2</sub>-oxetane), 3.40 – 3.50 (m, 0.2H, -CH<sub>2</sub>-O-), 4.30 – 4.41 (m, 0.4H, oxetane CH<sub>2</sub>), 7.42 – 8.14 (m, 10H, Ar-H)

**Polymer SEC** (THF, PS calibration):  $\overline{M}_n$  11,000 g mol<sup>-1</sup>,  $\overline{M}_w$  21,100 g mol<sup>-1</sup>, D 1.91

**TGA** (10 K min<sup>-1</sup>, N<sub>2</sub>): 1% weight loss at 201 °C, 5% weight loss at 256 °C

**UV/Vis absorption** (THF, 10<sup>-3</sup> mg ml<sup>-1</sup>): λ<sub>max</sub>: 363 nm, 509 nm, λ<sub>onset</sub>: 586 nm, E<sub>opt</sub> ≈ 2.10 eV

**PL** (THF, 10<sup>-3</sup> mg ml<sup>-1</sup>): λ<sub>max</sub>: 634 nm

**PFDTBTO<sub>x0.50 alt.</sub>**

Equimolar amounts of the monomers 2,7-bis(4,4,5,5-tetramethyl-1,3,2-dioxaborolane)-9-(1-dodecyl)-9-(heptyl-7,1-dioxymethyl-3-ethyloxetane)-fluorene (159.19 mg, 0.199 mmol) and 4,7-bis(5-bromo-4-hexyl-2-thienyl)-2,1,3-benzothiadiazole (124.86 mg, 0.199 mmol) were dissolved in toluene (10 ml). A few drops of the phase-transfer catalyst Aliquat 336 and a 2 M solution of Na<sub>2</sub>CO<sub>3</sub> (12 ml) were added, and the mixture was degassed by three freeze-pump-thaw-cycles. After addition of 0.015 equivalents of the catalyst Pd(PPh<sub>3</sub>)<sub>4</sub>, another freeze-pump-thaw cycle was applied. The reaction mixture was heated to reflux under vigorous stirring. After four days bromobenzene and phenylboronic acid were added to endcap the polymer. The organic phase was separated and precipitated from methanol. The dried product was re-dissolved and washed with brine. The organic phase was concentrated and precipitated from methanol, again. After drying, 184 mg (0.182 mmol, 91%) of PFDTBTO<sub>x0.50 alt.</sub> were obtained as a red solid.

**Characterization**

**<sup>1</sup>H NMR** (300 MHz, CDCl<sub>3</sub>, δ in ppm): 0.60 – 0.95 (m, 16H, -CH<sub>3</sub> + fluorene-CH<sub>2</sub>-CH<sub>2</sub>-), 1.00 – 1.52 (m, 42H, -CH<sub>2</sub>-), 1.63 – 1.85 (m, 6H, thiophene-CH<sub>2</sub>-CH<sub>2</sub>- + oxetane-CH<sub>2</sub>-CH<sub>3</sub>), 1.90 – 2.18 (m, 4H, fluorene-CH<sub>2</sub>-), 2.65 – 2.89 (m, 4H, thiophene-CH<sub>2</sub>-), 3.35 (t, *J* = 6.5 Hz, 2H, -CH<sub>2</sub>-O-), 3.45 (s, 2H, -O-CH<sub>2</sub>-oxetane), 4.28 + 4.43 (m, 4H, oxetane CH<sub>2</sub>), 7.40 – 8.14 (m, 10H, Ar-H)

**Polymer SEC** (THF, PS calibration):  $\overline{M}_n$  11,500 g/mol,  $\overline{M}_w$  23,900 g/mol, D 2.07

**TGA** (10 K min<sup>-1</sup>, N<sub>2</sub>): 1% weight loss at 327 °C, 5% weight loss at 402 °C

**UV/Vis absorption** (THF, 10<sup>-3</sup> mg ml<sup>-1</sup>): λ<sub>max</sub>: 360nm, 510 nm, λ<sub>onset</sub>: 590 nm, E<sub>opt</sub> ≈ 2.10 eV

**PL** (THF, 10<sup>-3</sup> mg ml<sup>-1</sup>): λ<sub>max</sub>: 640 nm

## 8.4 Crosslinking experiments

Crosslinking experiments were run using a photoacid generator (PAG) or trifluoroacetic acid (TFA) vapor as initiator. To monitor the progress of crosslinking, solubility tests were executed.

The photoacid generator DPI-109 was purchased from Midori Kagaku Co. Ltd. and used without purification. Trifluoroacetic acid was purchased from Acros Organics.

For crosslinking with PAG films with a thickness of about 80 nm were prepared by doctor blading on glass substrates. To dichlorobenzene solutions of the low bandgap polymers ( $20 \text{ mg ml}^{-1}$ ) the photoacid generator DPI-109 (chemical structure in Figure 31a) was added in 5 wt% and 1 wt% with respect to the polymer. Before doctor blading, the solutions were filtered through  $0.20 \text{ }\mu\text{m}$  Teflon filters. The films were dried in an inert nitrogen atmosphere at  $80 \text{ }^\circ\text{C}$  for 10 minutes and at  $130 \text{ }^\circ\text{C}$  for 15 minutes. Before crosslinking, UV/vis absorption spectra of the films were recorded. The crosslinking steps were executed under an inert nitrogen atmosphere in a glovebox. In the first step the samples were exposed to light of a 50 W xenon lamp (op502, manufacturer: Opcoms) for five to 15 minutes. For the postbake the samples were placed on a hot plate at  $100 \text{ }^\circ\text{C}$  to  $150 \text{ }^\circ\text{C}$  for five to 30 minutes. Following the crosslinking process, UV/vis spectra of the films were recorded. The films were rinsed with THF for 30 seconds and dried in air. UV/vis spectra were recorded afterwards.

For crosslinking in TFA vapor films with a thickness of about 80 nm were prepared by spin coating on glass substrates. Polymer solutions ( $15 \text{ mg ml}^{-1}$ ) and solutions of polymer:PCBM (1:2 by weight,  $30 \text{ mg ml}^{-1}$ ) in chlorobenzene were filtered through  $0.20 \text{ }\mu\text{m}$  Teflon filters. After spin coating, the films were dried in vacuum at  $60 \text{ }^\circ\text{C}$ . UV/vis absorption spectra were recorded before crosslinking. For crosslinking the samples were placed on a hot plate equipped with a glass cover, which was flushed with argon, and a glass dish, where trifluoroacetic acid (2 ml) was added. Crosslinking experiments were performed at  $80 \text{ }^\circ\text{C}$  and  $100 \text{ }^\circ\text{C}$  for five to 60 minutes. Residual TFA was removed from the samples by storage in vacuum for 30 to 60 minutes. Afterwards, UV/vis absorption spectra were recorded. The films were rinsed with THF for 30 seconds and dried in air. Ultimately, UV/vis absorption spectra were recorded.

## 8.5 Fabrication and characterization of organic solar cells

Bulk heterojunction organic solar cell devices were fabricated on structured glass substrates coated with indium tin oxide (ITO). To avoid edge effects, a circular active area ( $7.07 \text{ mm}^2$ ) was defined on top of the ITO layer using a photoresist (AZ 1518, supplier: Microchemicals).<sup>[242]</sup> On the active area, a 15 nm thick layer of  $\text{MoO}_3$  (Sigma Aldrich) was added by vacuum evaporation. The  $\text{MoO}_3$  layer ensures a low dark current and a good diode behavior.

The active layer was applied by spin coating. From chlorobenzene solutions ( $20 \text{ mg ml}^{-1}$ ) 80 nm thick layers of the polymer:PCBM blends were cast. PCBM (99.5% purity, Sigma Aldrich) was used as acceptor in the blend. PCBM and polymer solutions ( $20 \text{ mg ml}^{-1}$ ) were produced separately, filtered through a  $0.4 \mu\text{m}$  Teflon filter and mixed in 1:1, 1:2, and 1:3 ratios. The layer thicknesses of the blends for each polymer were controlled with a Dektak (Veeco) profilometer directly on the device. Optionally, crosslinking in TFA vapor was performed in an argon glovebox at  $80 \text{ }^\circ\text{C}$  for 20 minutes (5 minutes heating up, 15 minutes exposure to TFA vapor). The not crosslinked reference blend solar cells were annealed for the same time and temperature (20 minutes,  $80 \text{ }^\circ\text{C}$ ) in TFA vapor free nitrogen atmosphere for comparability purpose. Finally, a 100 nm thick aluminium cathode was vacuum evaporated. To avoid contact of the not crosslinked reference devices with the TFA vapor resulting from outgassing of the crosslinked devices while evacuating the evaporation chamber, devices were coated with aluminium separately. First the not crosslinked devices, then the crosslinked devices were put under vacuum in the evaporation chamber for 10 hours at  $10^{-7}$  mbar until the evaporation was started.

Current-voltage characteristics under AM1.5 sun light condition were measured with a Newport sun simulator and an appropriate vacuum condition sample holder to prevent oxygen degradation of the device during the measurement. For solar cell measurements a Keithley 238 source-measure-unit was used.

Accelerated aging was realized by annealing the solar cells at  $100 \text{ }^\circ\text{C}$  on a hot plate in a nitrogen glovebox. Prior to the first annealing step, the efficiencies of all devices were measured. After every annealing timestep, all devices were measured again and brought back to the hot plate in the glovebox. The annealing times given in the text are total annealing times, respectively. Using the vacuum condition sample holder, an oxygen free transport of the devices from the glovebox to the sun simulator was guaranteed.

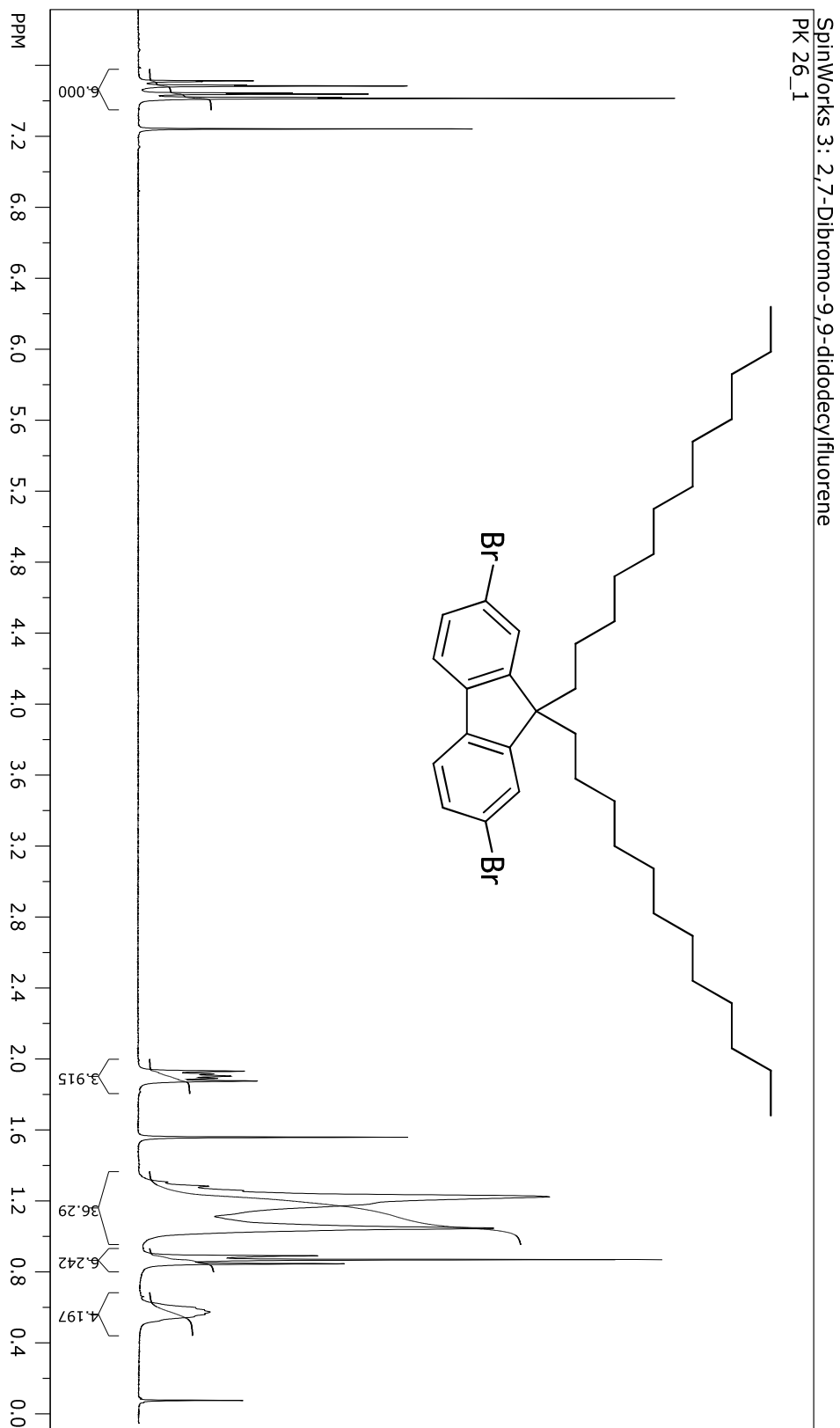
## 8.6 Imprinting

Films with a thickness of about 80 nm were prepared by spin coating on glass substrates. Polymer solutions ( $15 \text{ mg ml}^{-1}$ ) in chlorobenzene were filtered through  $0.20 \text{ }\mu\text{m}$  Teflon filters before. The films were dried in vacuum at  $60 \text{ }^\circ\text{C}$ . For imprinting the samples were put on a hot plate equipped with a glass cover, which was flushed with argon. At  $150 \text{ }^\circ\text{C}$  the soft stamp was placed on top of the film. After 15 minutes, the samples were cooled to room temperature, and the stamp was removed. Micrographs of the films were taken with a SEM.

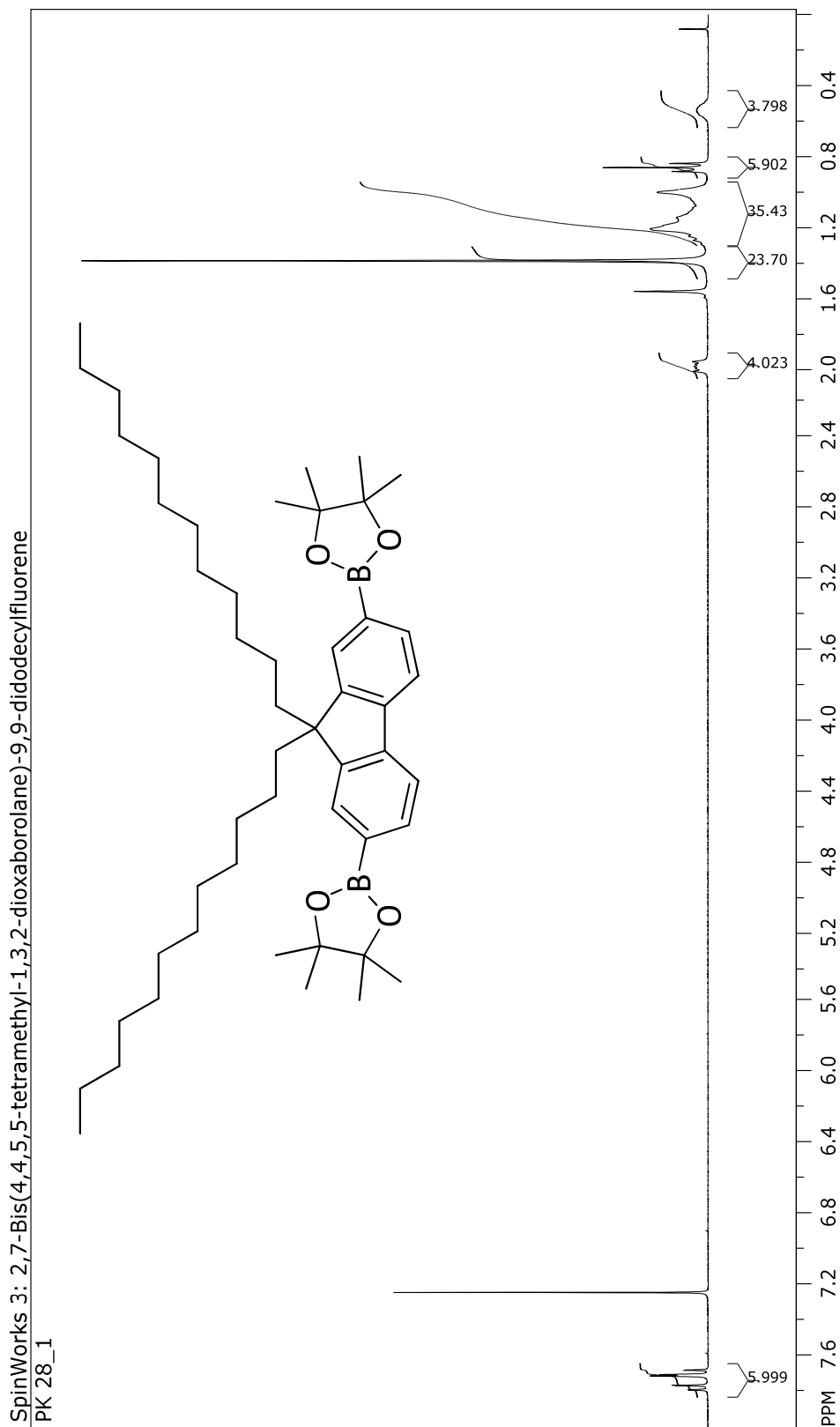


## 9 Appendix

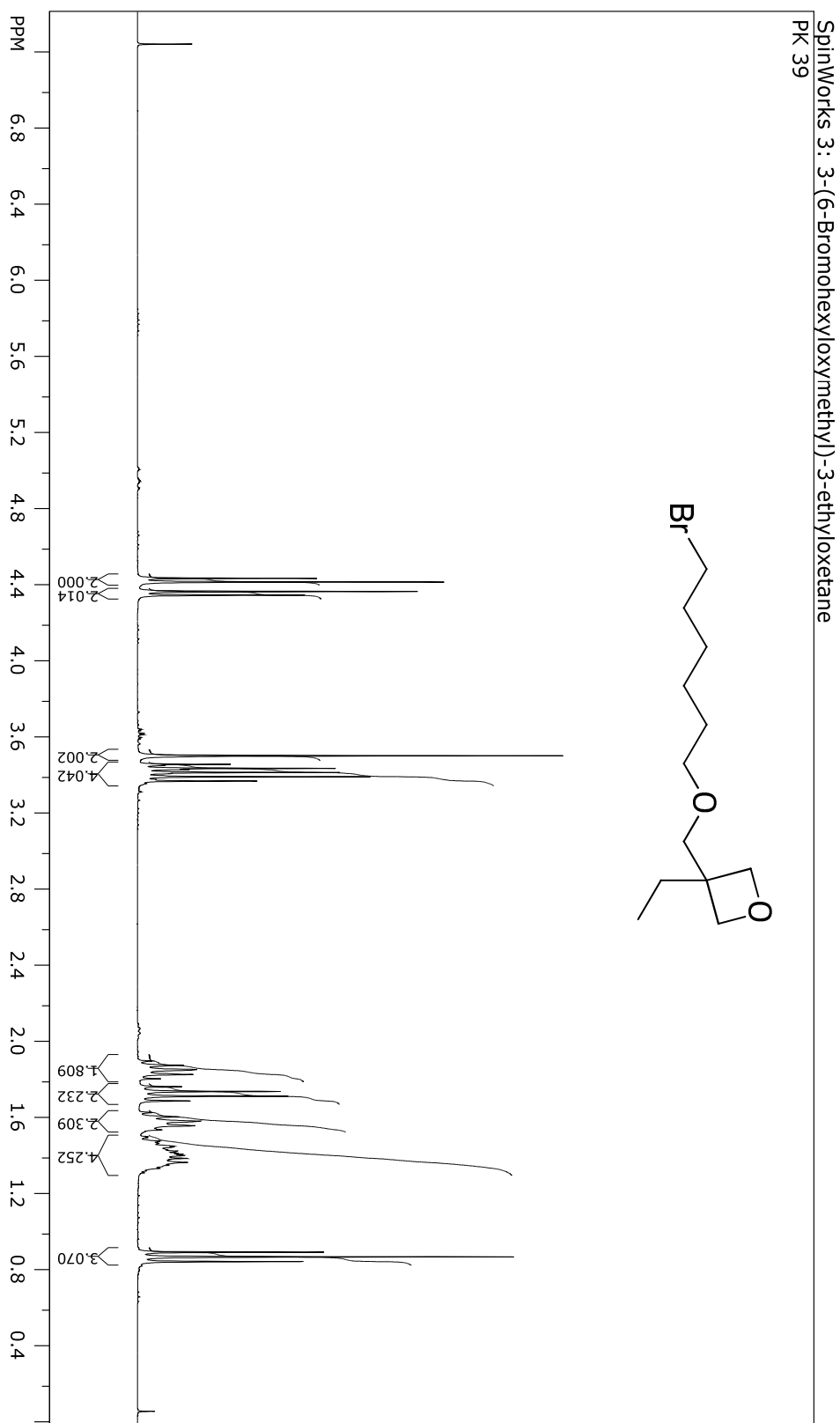
## 2,7-Dibromo-9,9-didodecylfluorene



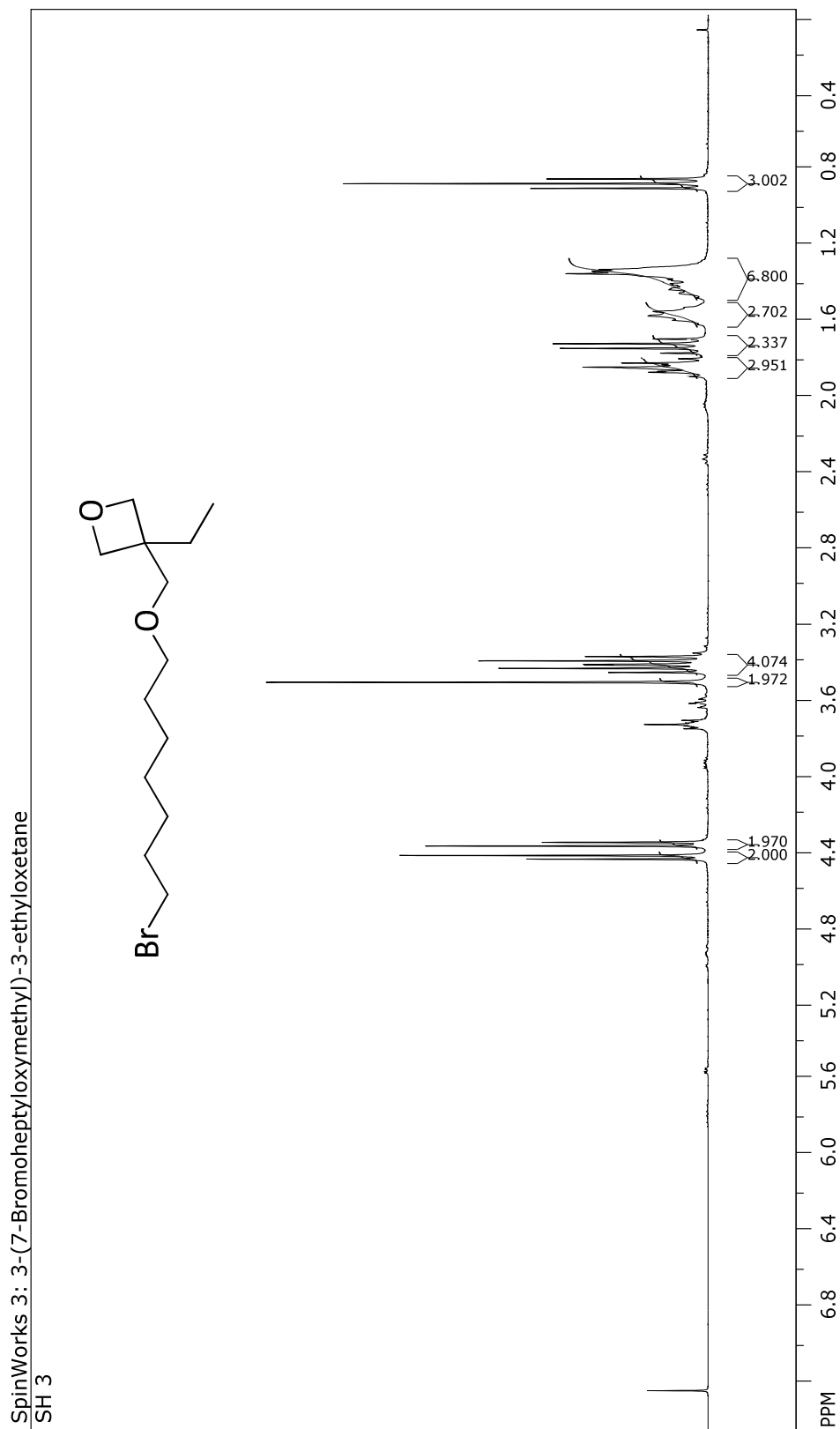
## 2,7-Bis(4,4,5,5-tetramethyl-1,3,2-dioxaborolane)-9,9-didodecylfluorene

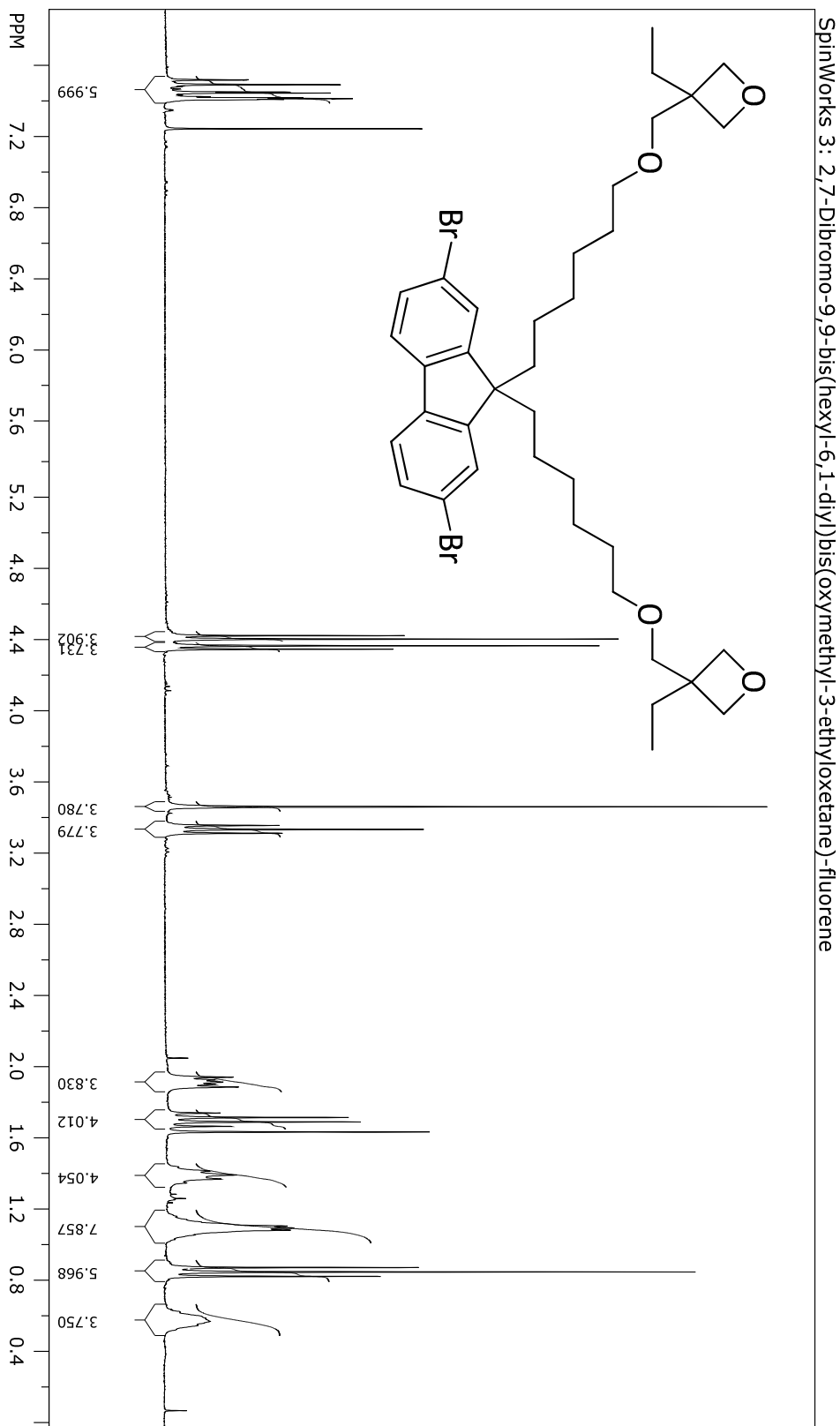


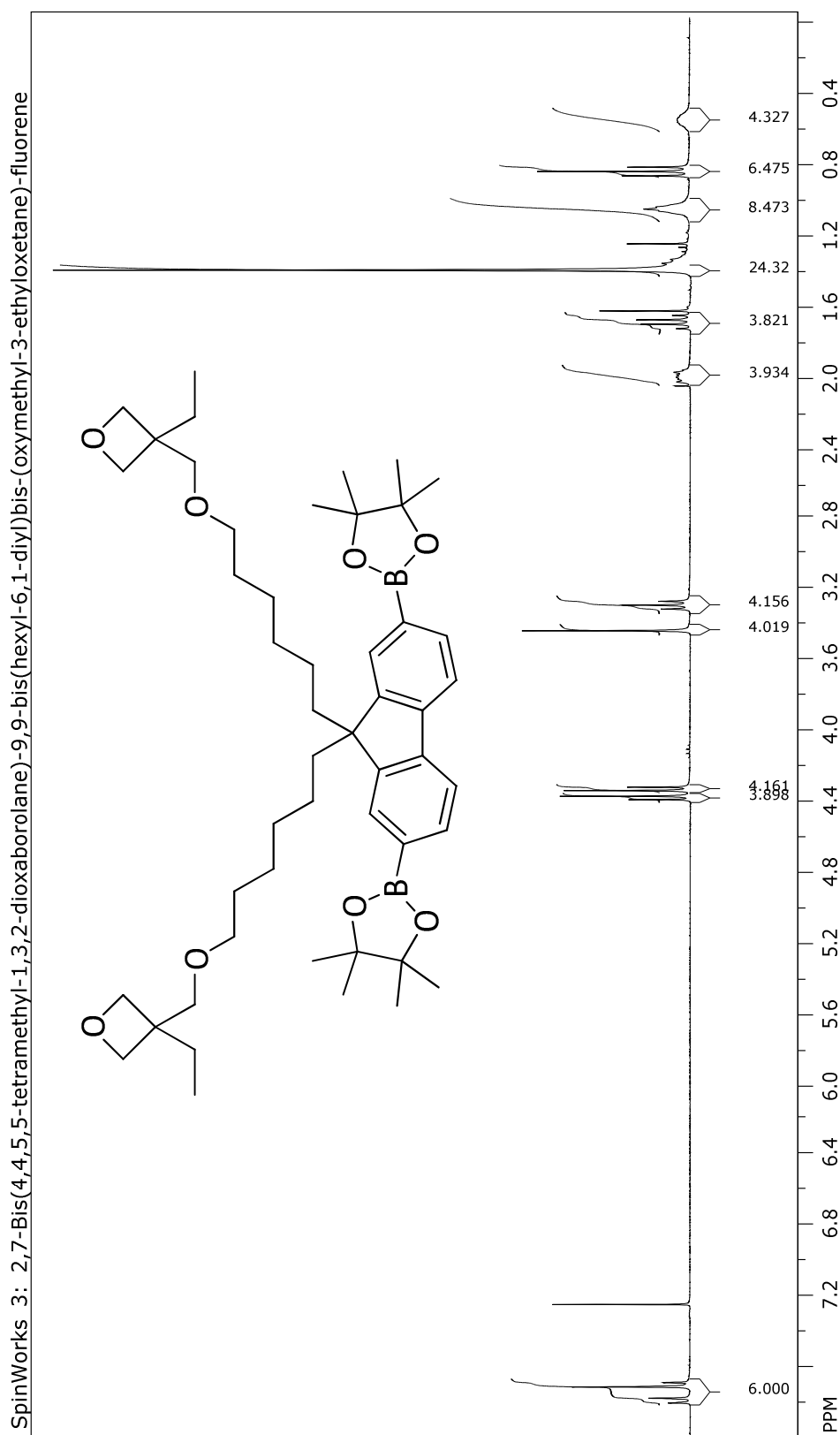
## 3-(6-Bromohexyloxymethyl)-3-ethyloxetane

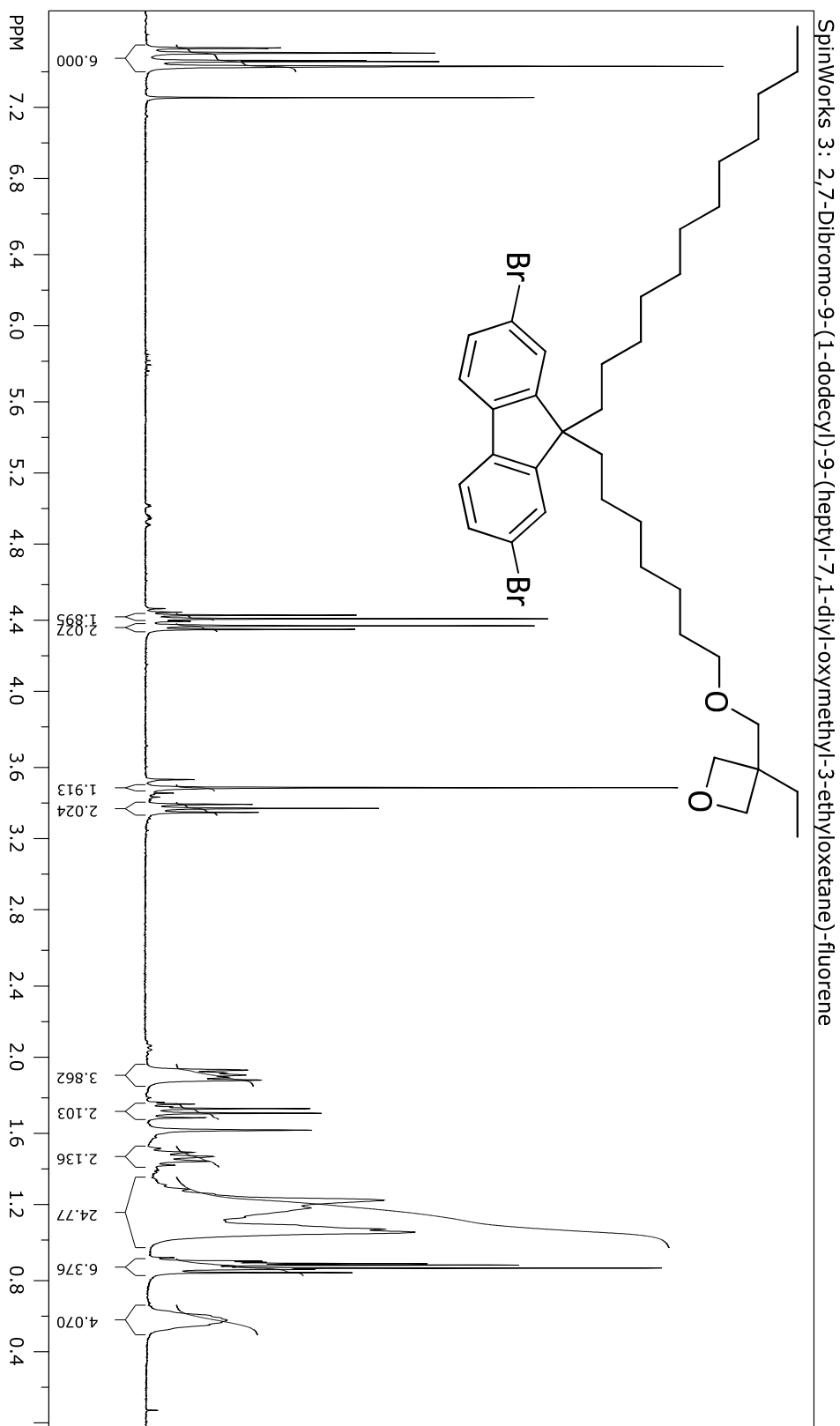


## 3-(7-Bromoheptyloxymethyl)-3-ethyloxetane

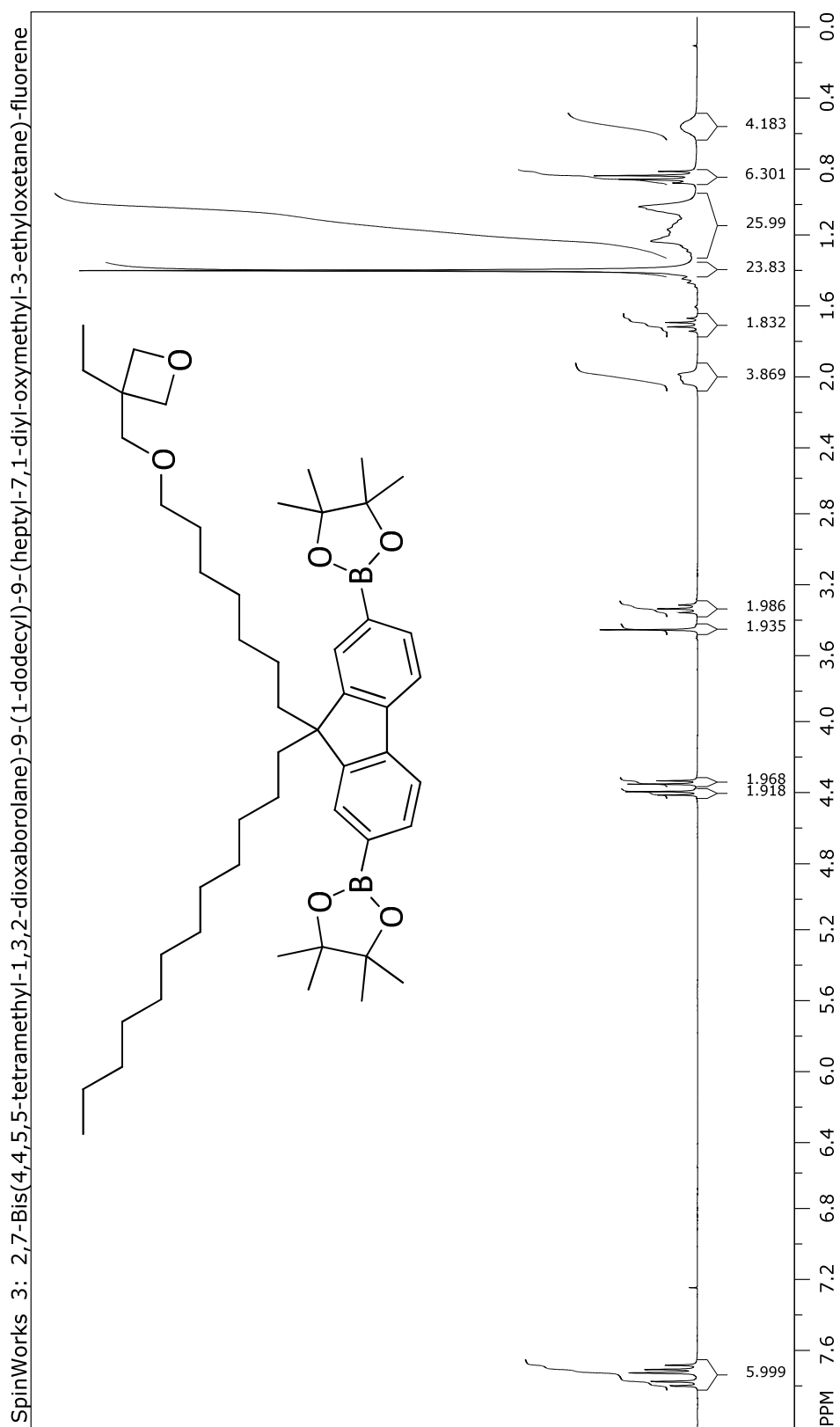


**2,7-Dibromo-9,9-bis(hexyl-6,1-diyl)bis(oxyethyl-3-ethoxy)fluorene**

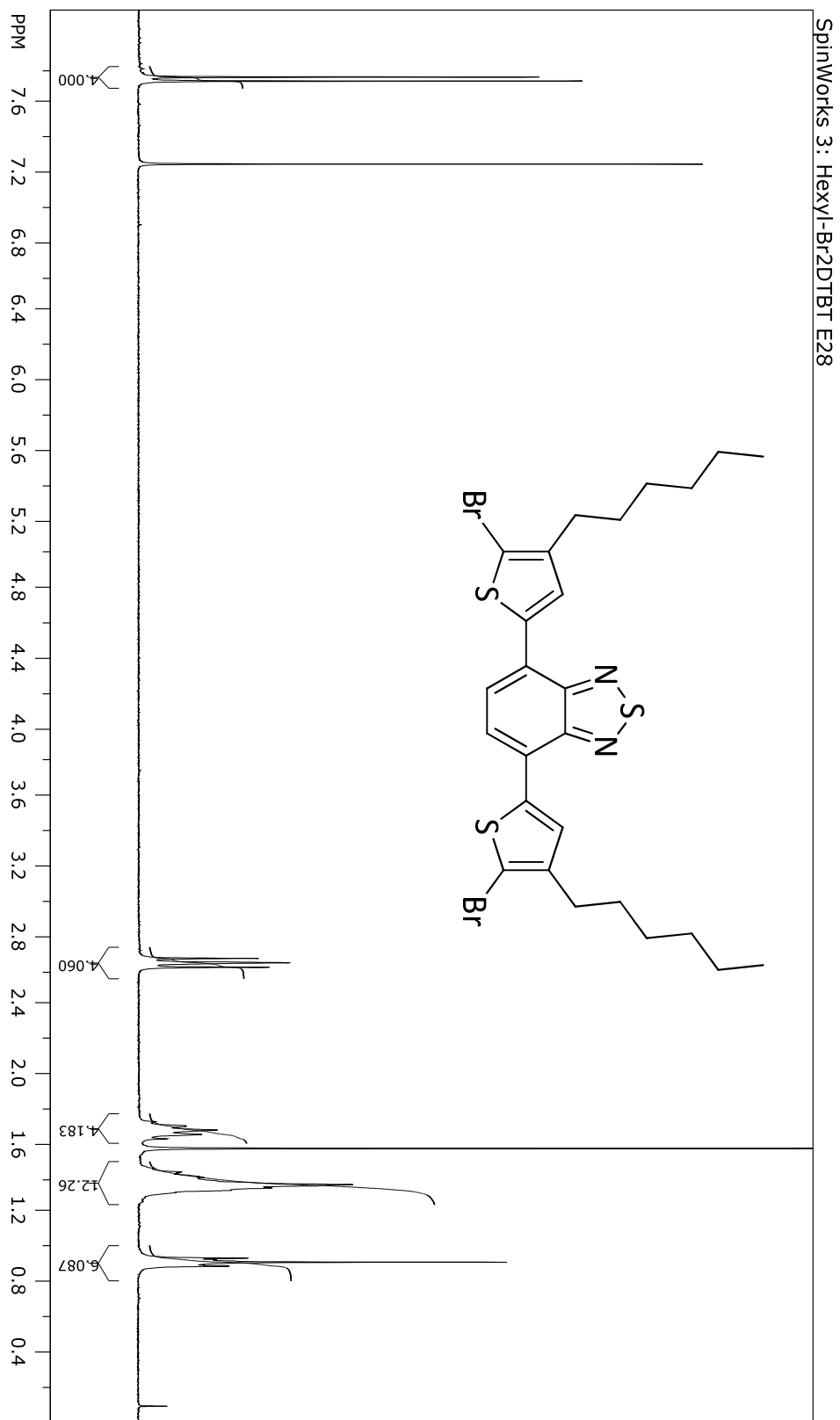
**2,7-Bis(4,4,5,5-tetramethyl-1,3,2-dioxaborolane)-9,9-bis(hexyl-6,1-diyl)bis-(oxymethyl-3-ethyloxetane)-fluorene**

**2,7-Dibromo-9-(1-dodecyl)-9-(heptyl-7,1-diyl-oxymethyl-3-ethyloxetane)-fluorene**

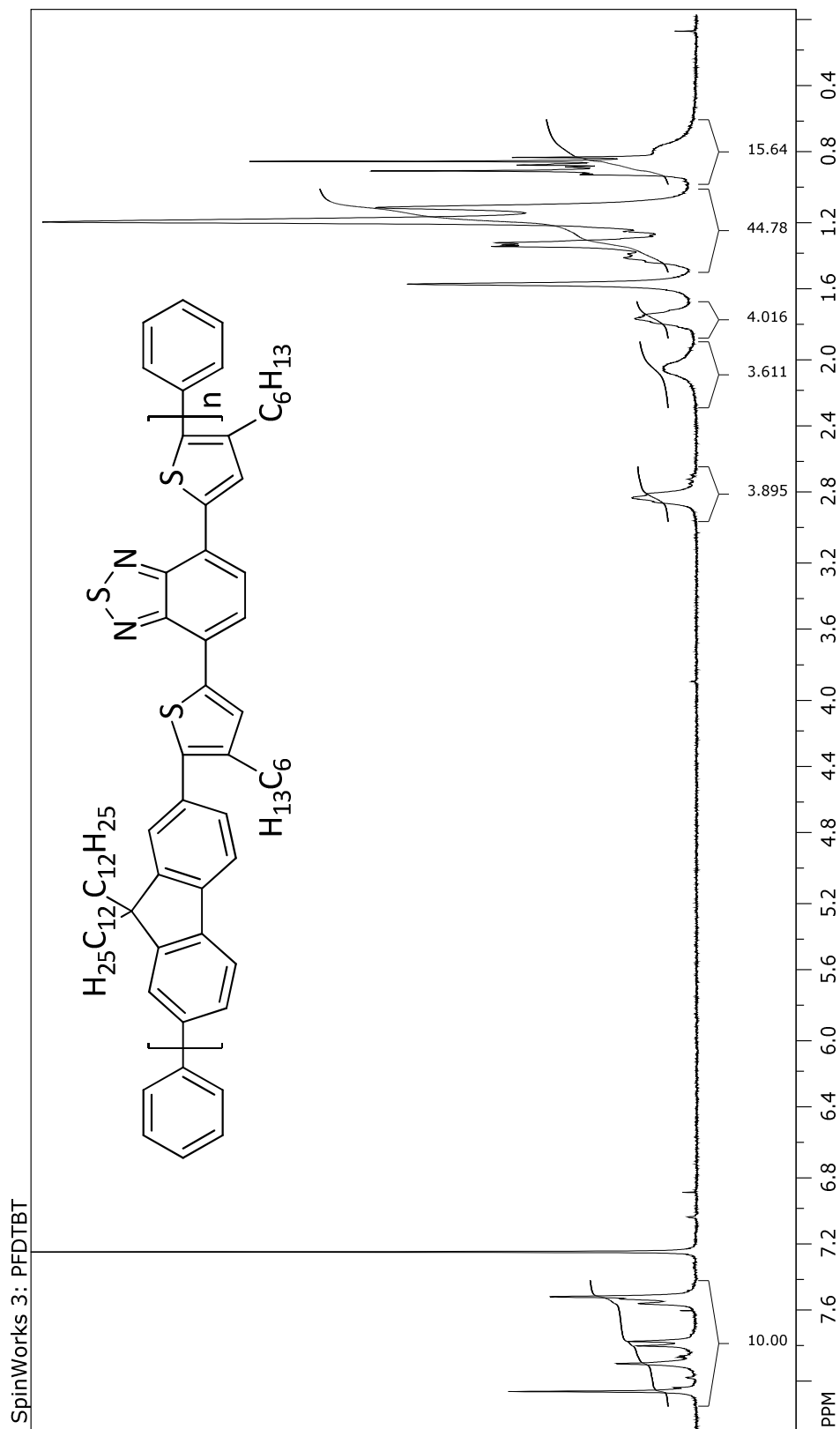
**2,7-Bis(4,4,5,5-tetramethyl-1,3,2-dioxaborolane)-9-(1-dodecyl)-9-(heptyl-7,1-diyloxyethyl-3-ethyloxetane)-fluorene**



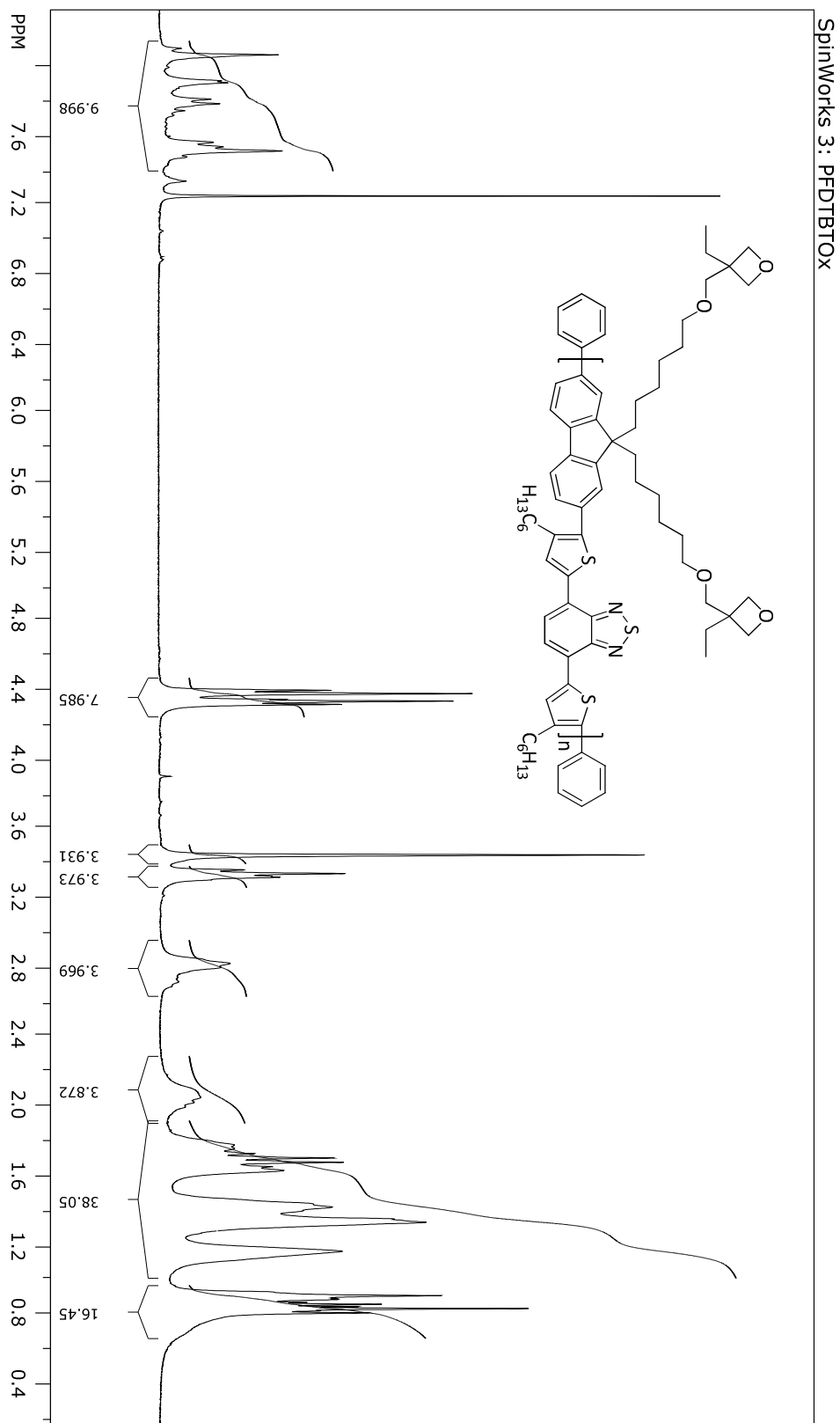
## 4,7-bis(5-bromo-4-hexyl-2-thienyl)-2,1,3-benzothiadiazole



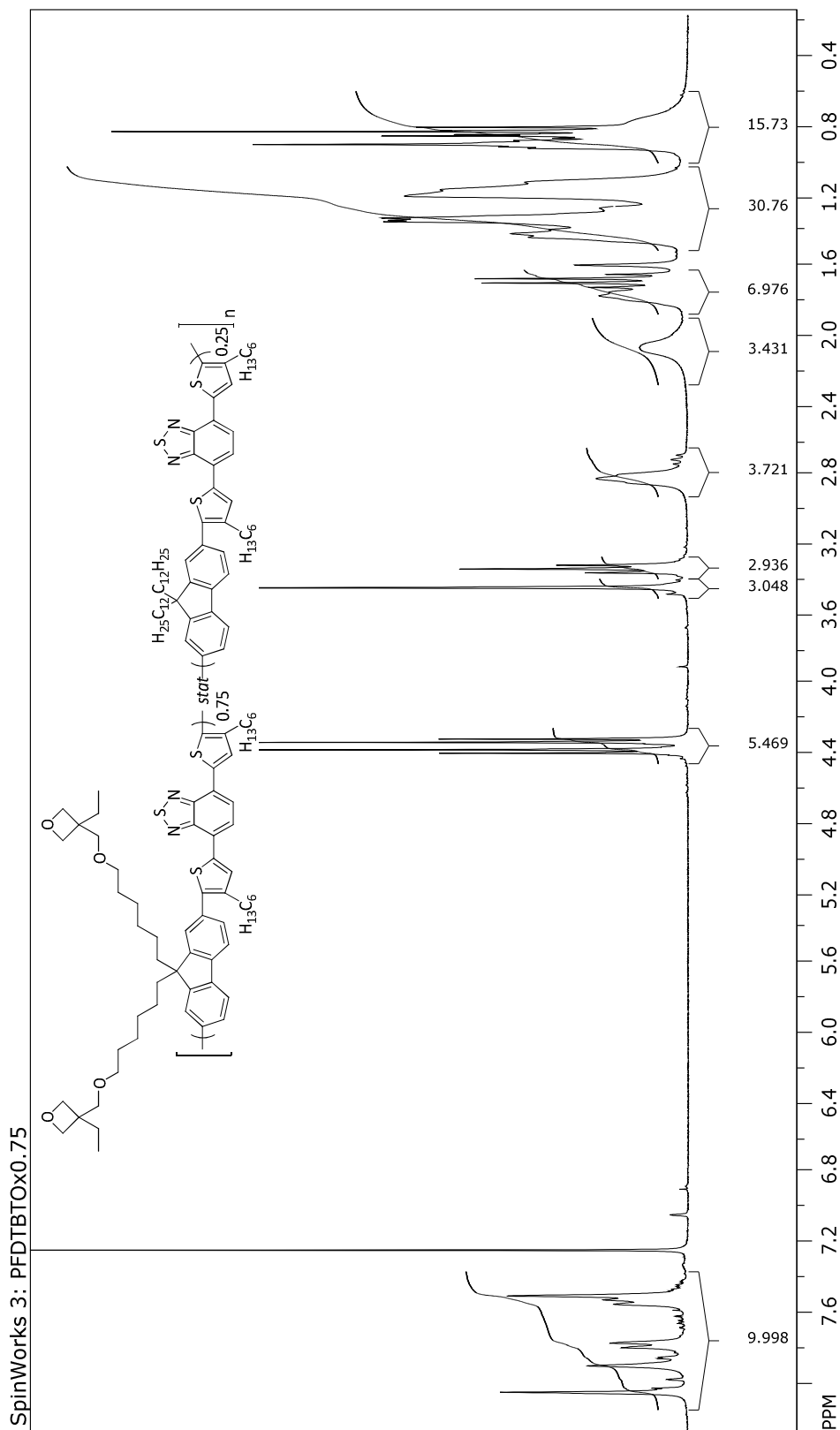
## PFDTBT



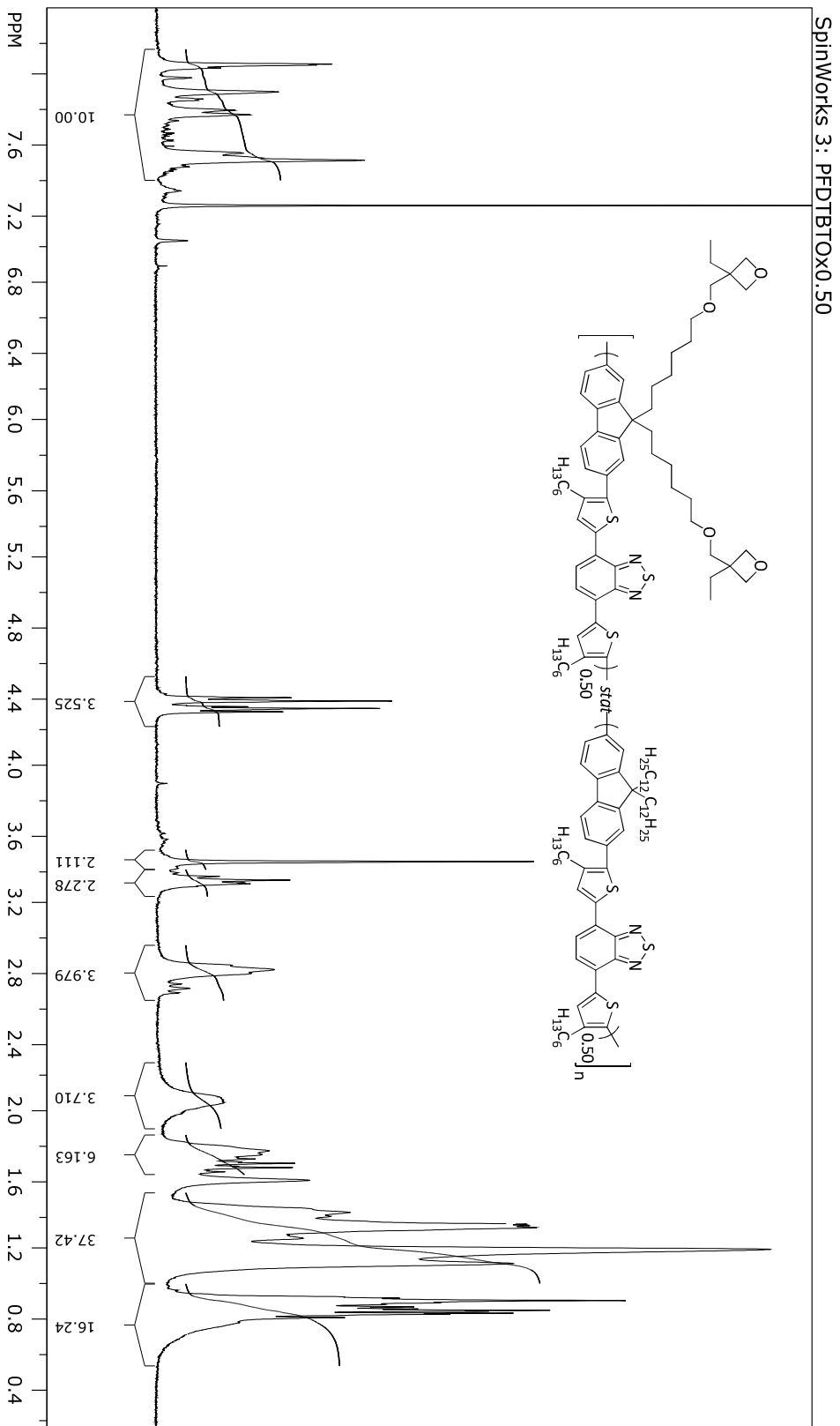
## PFDTBTOx



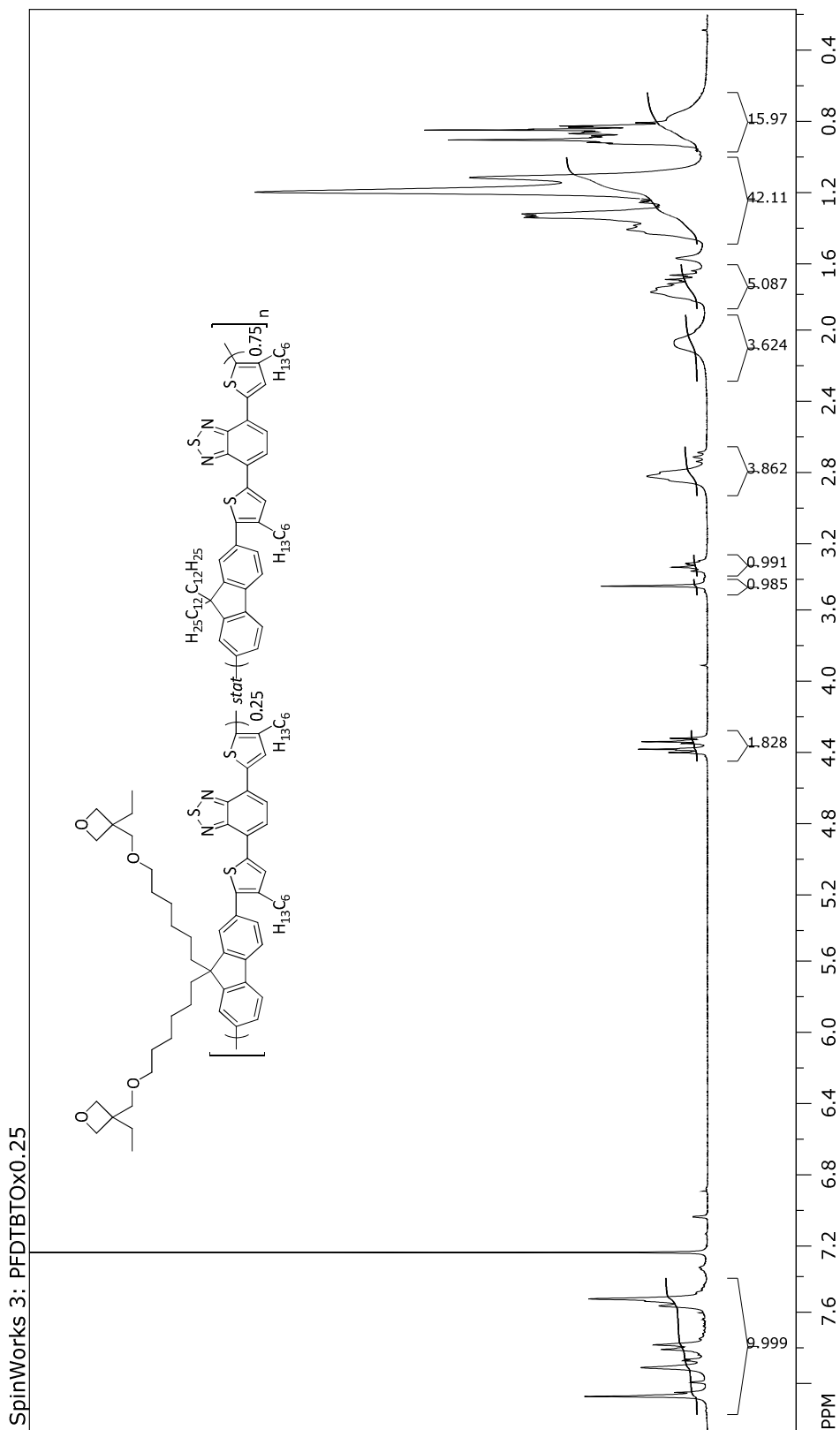
## PFDTBTOx0.75



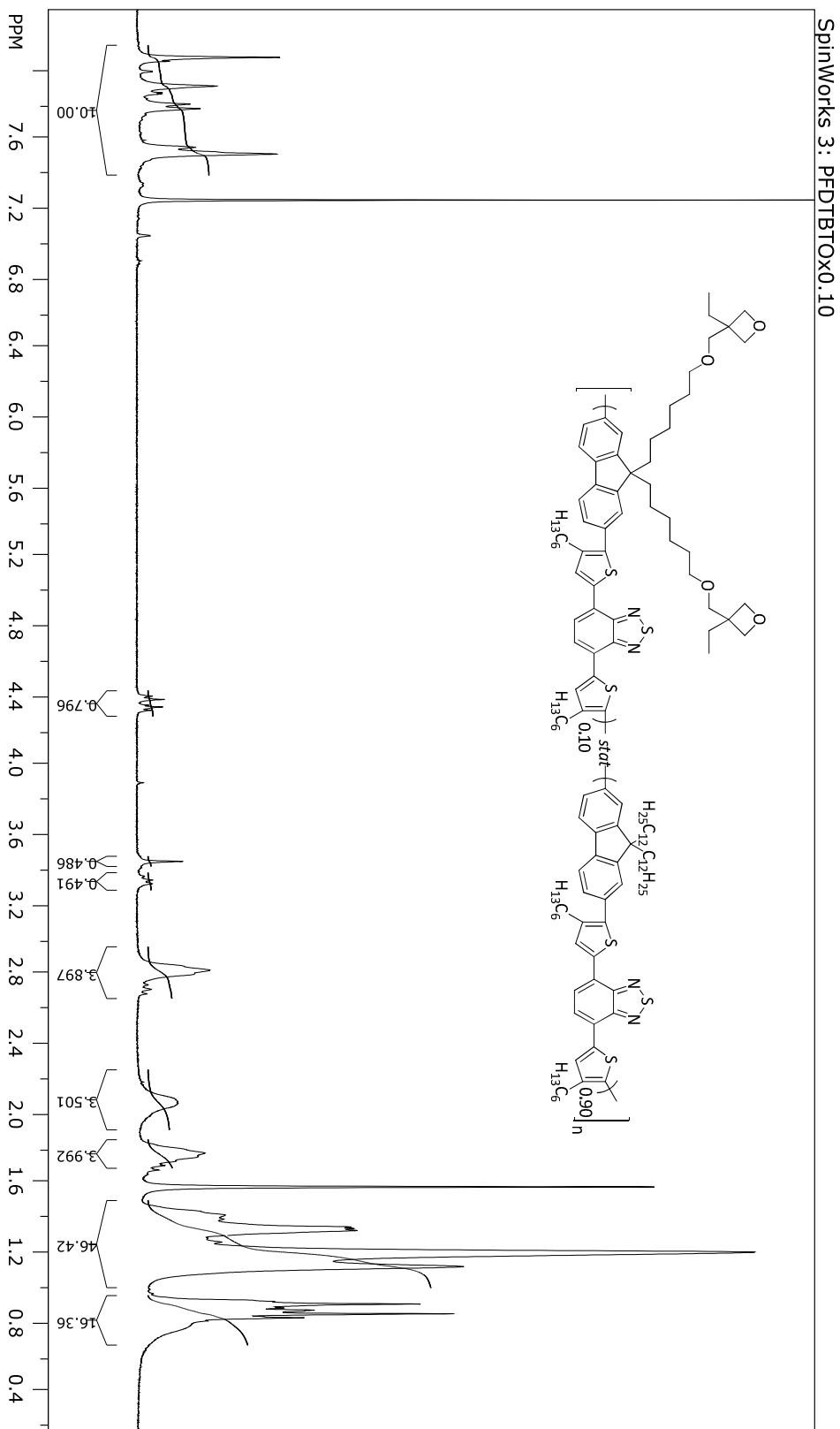
PFDTBTO<sub>x0.50</sub>



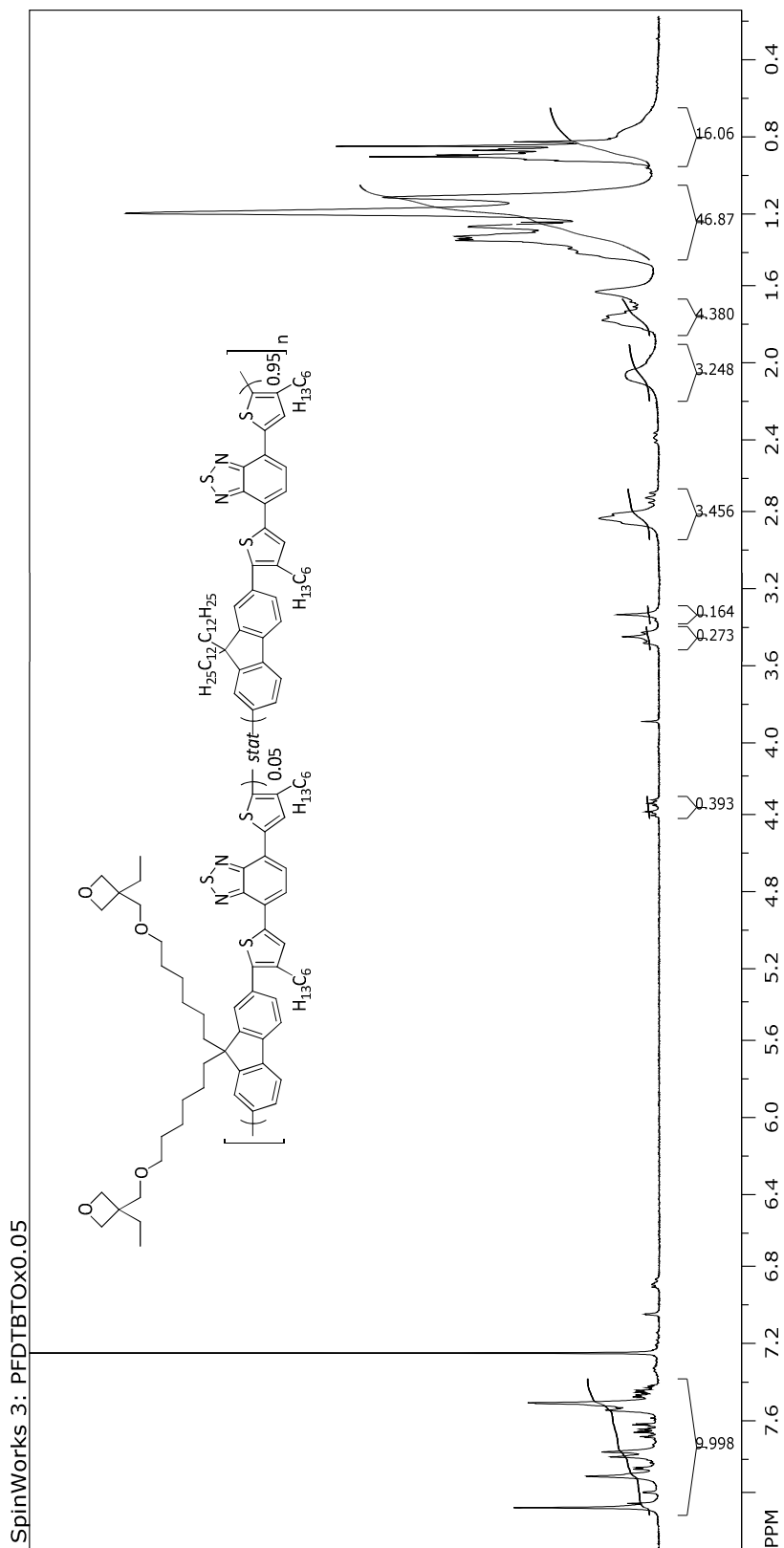
## PFDTBTOx0.25

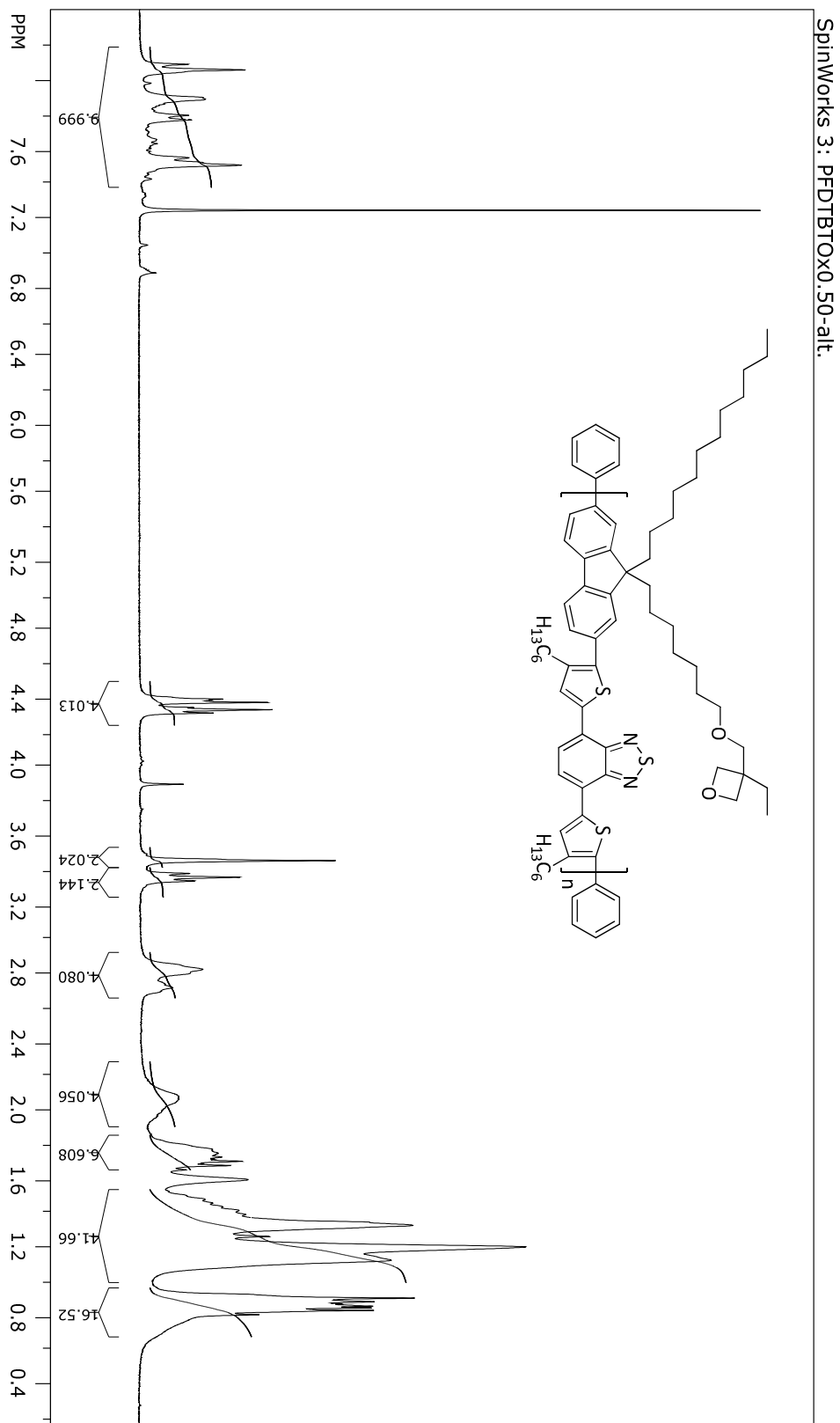


PFDTBTO<sub>x</sub>0.10



PFDTBTOx0.05



PFDTBTOx<sub>0.50</sub>-alt.





## 10 References

- [1] Bundesministerium für Wirtschaft und Energie (BMWi), *Erneuerbare Energien in Zahlen: Nationale und internationale Entwicklung im Jahr 2014*, Berlin **2015**.
- [2] B. Kippelen, J.-L. Brédas, *Energy Environ. Sci.* **2009**, *2*, 251.
- [3] Fraunhofer ISE, *Photovoltaics Report, November 2015*.
- [4] G. Nisato, J. Hauch, in *Organic Photovoltaics: Materials, Device Physics, and Manufacturing Technologies* (Eds.: C. Brabec, U. Scherf, V. Dyakonov), Wiley-VCH Verlag GmbH & Co. KGaA **2014**, p. 587.
- [5] A. Jäger-Waldau, in *Solar Cells (Second Edition)* (Eds.: A. McEvoy, L. Castañer, T. Markvart), Elsevier **2013**, p. 565.
- [6] S. Xiao, S. Xu, in *High-Efficiency Solar Cells*, Vol. 190 (Eds.: X. Wang, Z. M. Wang), Springer International Publishing. Cham **2014**, p. 1.
- [7] Y. Yang, F. Wudl, *Adv. Mater.* **2009**, *21*, 1401.
- [8] S. P. Economopoulos, G. Itskos, P. A. Koutentis, S. A. Choulis, in *Organic Photovoltaics: Materials, Device Physics, and Manufacturing Technologies* (Eds.: C. Brabec, U. Scherf, V. Dyakonov), Wiley-VCH Verlag GmbH & Co. KGaA **2014**, p. 3.
- [9] R. R. Søndergaard, N. Espinosa, M. Jørgensen, F. C. Krebs, *Energy Environ. Sci.* **2014**, *7*, 1006.
- [10] Heliatek GmbH, *EU Commissioner very impressed by her visit to Heliatek* **2012**, <http://www.heliatek.com/en/press/press-releases/details/eu-commissioner-very-impressed-by-her-visit-to-heliatek>. Accessed 27 October 2015.
- [11] Heliatek GmbH, *Heliatek reaches efficiency record with 40% transparent organic solar cells* **2015**, <http://www.heliatek.com/en/press/press-releases/details/heliatek-reaches-efficiency-record-with-40-transparent-organic-solar-cells>. Accessed 27 October 2015.
- [12] Heliatek GmbH, *Heliatek announces successful start of pilot project for energy self-sufficient air dome using HeliaFilm®* **2015**, <http://www.heliatek.com/en/press/press-releases/details/heliatek-announces-successful-start-of-pilot-project-for-energy-self-sufficient-air-dome-using-heliafilm>. Accessed 27 October 2015.
- [13] Heliatek GmbH, *Concrete facades with solar films* **2015**, <http://www.heliatek.com/en/press/downloads>. Accessed 27 October 2015.
- [14] Heliatek GmbH, *Transparent Solar Films for Windows* **2015**, <http://www.heliatek.com/en/press/downloads>. Accessed 27 October 2015.
- [15] F. C. Krebs, N. Espinosa, M. Hösel, R. R. Søndergaard, M. Jørgensen, *Adv. Mater.* **2014**, *26*, 29.
- [16] C. W. Tang, *Appl. Phys. Lett.* **1986**, *48*, 183.
- [17] C. Deibel, V. Dyakonov, *Rep. Prog. Phys.* **2010**, *73*, 96401.
- [18] R. Kersting, U. Lemmer, M. Deussen, H. J. Bakker, R. F. Mahrt, H. Kurz, V. I. Arkhipov, H. Bässler, E. O. Göbel, *Phys. Rev. Lett.* **1994**, *73*, 1440.
- [19] M. C. Scharber, N. S. Sariciftci, *Progress in polymer science* **2013**, *38*, 1929.

- [20] D. Hertel, H. Bässler, *ChemPhysChem* **2008**, *9*, 666.
- [21] Y. Tamai, H. Ohkita, H. Benten, S. Ito, *J. Phys. Chem. Lett.* **2015**, *6*, 3417.
- [22] G. Yu, J. Gao, J. C. Hummelen, F. Wudl, A. J. Heeger, *Science* **1995**, *270*, 1789.
- [23] J. J. M. Halls, C. A. Walsh, N. C. Greenham, E. A. Marseglia, R. H. Friend, S. C. Moratti, A. B. Holmes, *Nature* **1995**, *376*, 498.
- [24] N. S. Sariciftci, L. Smilowitz, A. J. Heeger, F. Wudl, *Science* **1992**, *258*, 1474.
- [25] I.-W. Hwang, D. Moses, A. J. Heeger, *J. Phys. Chem. C* **2008**, *112*, 4350.
- [26] C. Deibel, T. Strobel, V. Dyakonov, *Adv. Mater.* **2010**, *22*, 4097.
- [27] T. M. Clarke, J. R. Durrant, *Chem. Rev.* **2010**, *110*, 6736.
- [28] E. L. Frankevich, A. A. Lymarev, I. Sokolik, F. E. Karasz, S. Blumstengel, R. H. Baughman, H. H. Hörhold, *Phys. Rev. B* **1992**, *46*, 9320.
- [29] L. Onsager, *Phys. Rev.* **1938**, *54*, 554.
- [30] C. L. Braun, *J. Chem. Phys.* **1984**, *80*, 4157.
- [31] L. J. A. Koster, E. C. P. Smits, V. D. Mihailetschi, P. W. M. Blom, *Phys. Rev. B* **2005**, *72*, 85205.
- [32] A. Köhler, H. Bässler, in *Electronic Processes in Organic Semiconductors*, Wiley-VCH Verlag GmbH & Co. KGaA **2015**, p. 307.
- [33] V. D. Mihailetschi, J. Wildeman, P. W. M. Blom, *Phys. Rev. Lett.* **2005**, *94*, 126602.
- [34] K. Emery, in *Handbook of photovoltaic science and engineering, 2nd Edition* (Eds.: A. Luque, S. Hegedus), Wiley **2010**, p. 701.
- [35] V. Shrotriya, G. Li, Y. Yao, T. Moriarty, K. Emery, Y. Yang, *Adv. Funct. Mater.* **2006**, *16*, 2016.
- [36] C. A. Gueymard, D. Myers, K. Emery, *Solar Energy* **2002**, *73*, 443.
- [37] K. Neumann, *Triphenylamine based semiconducting polymers for organic/hybrid photovoltaics and sensors*, Dissertation Universität Bayreuth, Bayreuth **2014**.
- [38] J. J. M. Halls, K. Pichler, R. H. Friend, S. C. Moratti, A. B. Holmes, *Appl. Phys. Lett.* **1996**, *68*, 3120.
- [39] A. Haugeneder, M. Neges, C. Kallinger, W. Spirkel, U. Lemmer, J. Feldmann, U. Scherf, E. Harth, A. Gügel, K. Müllen, *Physical Review B* **1999**, *59*, 15346.
- [40] B. O'Regan, M. Grätzel, *Nature* **1991**, *353*, 737.
- [41] A. Yella, H.-W. Lee, H. N. Tsao, C. Yi, A. K. Chandiran, M. K. Nazeeruddin, E. W.-G. Diau, C.-Y. Yeh, S. M. Zakeeruddin, M. Grätzel, *Science* **2011**, *334*, 629.
- [42] N. Cai, S.-J. Moon, L. Cevey-Ha, T. Moehl, R. Humphry-Baker, P. Wang, S. M. Zakeeruddin, M. Grätzel, *Nano Lett.* **2011**, *11*, 1452.
- [43] J. Burschka, A. Dualeh, F. Kessler, E. Baranoff, N.-L. Cevey-Ha, C. Yi, M. K. Nazeeruddin, M. Grätzel, *J. Am. Chem. Soc.* **2011**, *133*, 18042.
- [44] A. Kojima, K. Teshima, Y. Shirai, T. Miyasaka, *J. Am. Chem. Soc.* **2009**, *131*, 6050.
- [45] K. Neumann, M. Thelakkat, *RSC Adv.* **2014**, *4*, 43550.
- [46] H. J. Snaith, *J. Phys. Chem. Lett.* **2013**, *4*, 3623.
- [47] National Renewable Energy Laboratory NREL, *Best Research-Cell Efficiencies: accessed 10-21-2015* **2015**,

- [http://www.nrel.gov/ncpv/images/efficiency\\_chart.jpg](http://www.nrel.gov/ncpv/images/efficiency_chart.jpg). Accessed 21 October 2015.
- [48] U. Bach, *Nature chemistry* **2015**, *7*, 616.
- [49] X. Huang, Z. Zhao, L. Cao, Y. Chen, E. Zhu, Z. Lin, M. Li, A. Yan, A. Zettl, Y. M. Wang, X. Duan, T. Mueller, Y. Huang, *Science* **2015**, *348*, 1230.
- [50] L. G. Kaake, D. Moses, A. J. Heeger, *J. Phys. Chem. Lett.* **2013**, *4*, 2264.
- [51] F. Wudl, P.-M. Allemand, G. Srdanov, Z. Ni, D. McBranch, in *Materials for Nonlinear Optics*, Vol. 455, American Chemical Society **1991**, p. 683.
- [52] J. C. Hummelen, B. W. Knight, F. LePeq, F. Wudl, J. Yao, C. L. Wilkins, *J. Org. Chem.* **1995**, *60*, 532.
- [53] I. Osaka, R. D. McCullough, in *Conjugated polymer synthesis: Methods and reactions* (Ed.: Y. Chujo), Wiley-VCH **2010**, p. 59.
- [54] C. L. Chochos, S. A. Choulis, *Progress in polymer science* **2011**, *36*, 1326.
- [55] C. J. Brabec, N. S. Sariciftci, J. C. Hummelen, *Adv. Funct. Mater.* **2001**, *11*, 15.
- [56] A. J. Heeger, *Adv. Mater.* **2014**, *26*, 10.
- [57] A. R. Campbell, J. M. Hodgkiss, S. Westenhoff, I. A. Howard, R. A. Marsh, C. R. McNeill, R. H. Friend, N. C. Greenham, *Nano Lett.* **2008**, *8*, 3942.
- [58] G. R. Strobl, *The physics of polymers* **2007**, Springer, p. 122-124.
- [59] L. Lu, T. Zheng, Q. Wu, A. M. Schneider, D. Zhao, L. Yu, *Chem. Rev.* **2015**, *115*, 12666.
- [60] S. H. Park, A. Roy, S. Beaupré, S. Cho, N. Coates, J. S. Moon, D. Moses, M. Leclerc, K. Lee, A. J. Heeger, *Nature Photonics* **2009**, *3*, 297.
- [61] M. A. Ruderer, S. Guo, R. Meier, H.-Y. Chiang, V. Körstgens, J. Wiedersich, J. Perlich, S. V. Roth, P. Müller-Buschbaum, *Adv. Funct. Mater.* **2011**, *21*, 3382.
- [62] R. Kokubu, Y. Yang, *Phys. Chem. Chem. Phys.* **2012**, *14*, 8313.
- [63] L. Zhang, X. Xing, L. Zheng, Z. Chen, L. Xiao, B. Qu, Q. Gong, *Scientific reports* **2014**, *4*, 5071.
- [64] Y. Zhao, G. Yuan, P. Roche, M. Leclerc, *Polymer* **1995**, *36*, 2211.
- [65] G. Li, V. Shrotriya, J. Huang, Y. Yao, T. Moriarty, K. Emery, Y. Yang, *Nature materials* **2005**, *4*, 864.
- [66] D. Chirvase, J. Parisi, J. C. Hummelen, V. Dyakonov, *Nanotechnology* **2004**, *15*, 1317.
- [67] J. K. Lee, W. L. Ma, C. J. Brabec, J. Yuen, J. S. Moon, J. Y. Kim, K. Lee, G. C. Bazan, A. J. Heeger, *J. Am. Chem. Soc.* **2008**, *130*, 3619.
- [68] S. J. Lou, J. M. Szarko, T. Xu, L. Yu, T. J. Marks, L. X. Chen, *J. Am. Chem. Soc.* **2011**, *133*, 20661.
- [69] M. R. Hammond, R. J. Kline, A. A. Herzing, L. J. Richter, D. S. Germack, H.-W. Ro, C. L. Soles, D. A. Fischer, T. Xu, L. Yu, M. F. Toney, D. M. Delongchamp, *ACS nano* **2011**, *5*, 8248.
- [70] T. Erb, U. Zhokhavets, G. Gobsch, S. Raleva, B. Stühn, P. Schilinsky, C. Waldauf, C. J. Brabec, *Adv. Funct. Mater.* **2005**, *15*, 1193.

- [71] N. C. Miller, E. T. Hoke, M. D. McGehee, in *Organic Photovoltaics: Materials, Device Physics, and Manufacturing Technologies* (Eds.: C. Brabec, U. Scherf, V. Dyakonov), Wiley-VCH Verlag GmbH & Co. KGaA **2014**, p. 421.
- [72] W. L. Rance, A. J. Ferguson, T. McCarthy-Ward, M. Heeney, D. S. Ginley, D. C. Olson, G. Rumbles, N. Kopidakis, *ACS nano* **2011**, *5*, 5635.
- [73] A. Facchetti, in *Organic Photovoltaics: Materials, Device Physics, and Manufacturing Technologies* (Eds.: C. Brabec, U. Scherf, V. Dyakonov), Wiley-VCH Verlag GmbH & Co. KGaA **2014**, p. 239.
- [74] H. Yan, Z. Chen, Y. Zheng, C. Newman, J. R. Quinn, F. Dötz, M. Kastler, A. Facchetti, *Nature* **2009**, *457*, 679.
- [75] J. A. Love, C. M. Proctor, J. Liu, C. J. Takacs, A. Sharenko, van der Poll, Thomas S., A. J. Heeger, G. C. Bazan, T.-Q. Nguyen, *Adv. Funct. Mater.* **2013**, *23*, 5019.
- [76] Y. Sun, G. C. Welch, W. L. Leong, C. J. Takacs, G. C. Bazan, A. J. Heeger, *Nature materials* **2012**, *11*, 44.
- [77] A. K. K. Kyaw, D. H. Wang, V. Gupta, J. Zhang, S. Chand, G. C. Bazan, A. J. Heeger, *Adv. Mater.* **2013**, *25*, 2397.
- [78] A. K. Ko Kyaw, D. Gehrig, J. Zhang, Y. Huang, G. C. Bazan, F. Laquai, T.-Q. Nguyen, *J. Mater. Chem. A* **2015**, *3*, 1530.
- [79] P. B. Amaresh Mishra, in *Organic Photovoltaics: Materials, Device Physics, and Manufacturing Technologies* (Eds.: C. Brabec, U. Scherf, V. Dyakonov), Wiley-VCH Verlag GmbH & Co. KGaA **2014**, p. 139.
- [80] R. Fitzner, E. Reinold, A. Mishra, E. Mena-Osteritz, H. Ziehlke, C. Körner, K. Leo, M. Riede, M. Weil, O. Tsaryova, A. Weiß, C. Urich, M. Pfeiffer, P. Bäuerle, *Adv. Funct. Mater.* **2011**, *21*, 897.
- [81] M. Riede, T. Mueller, W. Tress, R. Schueppel, K. Leo, *Nanotechnology* **2008**, *19*, 424001.
- [82] Heliatek GmbH, *Neuer Weltrekord für organische Solarzellen: Heliatek behauptet sich mit 12 % Zelleffizienz als Technologieführer* **2013**, <http://www.heliatek.com/de/presse/pressemitteilungen/details/neuer-weltrekord-fuer-organische-solarzellen-heliatek-behauptet-sich-mit-12-zelleffizienz-als-technologiefuehrer>. Accessed 22 October 2015.
- [83] H. Zhou, Y. Zhang, C.-K. Mai, S. D. Collins, T.-Q. Nguyen, G. C. Bazan, A. J. Heeger, *Adv. Mater.* **2014**, *26*, 780.
- [84] J. Roncali, *Accounts of chemical research* **2009**, *42*, 1719.
- [85] B. C. Thompson, J. M. J. Fréchet, *Angew. Chem. Int. Ed.* **2008**, *47*, 58.
- [86] Y. Liu, J. Zhao, Z. Li, C. Mu, W. Ma, H. Hu, K. Jiang, H. Lin, H. Ade, H. Yan, *Nature communications* **2014**, *5*, 5293.
- [87] C. Duan, C. Zhong, F. Huang, Y. Cao, in *Progress in High-Efficient Solution Process Organic Photovoltaic Devices*, Vol. 130 (Eds.: Y. Yang, G. Li), Springer **2015**, p. 191.
- [88] R. Po, C. Carbonera, A. Bernardi, N. Camaioni, *Energy Environ. Sci.* **2011**, *4*, 285.
- [89] L.-M. Chen, Z. Xu, Z. Hong, Y. Yang, *J. Mater. Chem.* **2010**, *20*, 2575.

- [90] K. W. Wong, H. L. Yip, Y. Luo, K. Y. Wong, W. M. Lau, K. H. Low, H. F. Chow, Z. Q. Gao, W. L. Yeung, C. C. Chang, *Appl. Phys. Lett.* **2002**, *80*, 2788.
- [91] V. Shrotriya, G. Li, Y. Yao, C.-W. Chu, Y. Yang, *Appl. Phys. Lett.* **2006**, *88*, 73508.
- [92] S. Hu, C. Zhong, H. Wu, Y. Cao, in *Conjugated Polyelectrolytes* (Eds.: B. Liu, G. C. Bazan), Wiley-VCH Verlag GmbH & Co. KGaA **2012**, p. 345.
- [93] D. Y. Kim, J. Subbiah, G. Sarasqueta, F. So, H. Ding, Irfan, Y. Gao, *Appl. Phys. Lett.* **2009**, *95*, 93304.
- [94] H.-L. Yip, A. K.-Y. Jen, *Energy Environ. Sci.* **2012**, *5*, 5994.
- [95] C. J. Brabec, S. E. Shaheen, C. Winder, N. S. Sariciftci, P. Denk, *Appl. Phys. Lett.* **2002**, *80*, 1288.
- [96] H. Ma, H.-L. Yip, F. Huang, A. K.-Y. Jen, *Adv. Funct. Mater.* **2010**, *20*, 1371.
- [97] Y. Zhao, Z. Xie, C. Qin, Y. Qu, Y. Geng, L. Wang, *Solar Energy Materials and Solar Cells* **2009**, *93*, 604.
- [98] Q. Wei, T. Nishizawa, K. Tajima, K. Hashimoto, *Adv. Mater.* **2008**, *20*, 2211.
- [99] J. Y. Kim, S. H. Kim, H.-H. Lee, K. Lee, W. Ma, X. Gong, A. J. Heeger, *Adv. Mater.* **2006**, *18*, 572.
- [100] J. K. Lee, N. E. Coates, S. Cho, N. S. Cho, D. Moses, G. C. Bazan, K. Lee, A. J. Heeger, *Appl. Phys. Lett.* **2008**, *92*, 243308.
- [101] A. K. K. Kyaw, D. H. Wang, D. Wynands, J. Zhang, T.-Q. Nguyen, G. C. Bazan, A. J. Heeger, *Nano letters* **2013**, *13*, 3796.
- [102] J. W. Rumer, I. McCulloch, *Materials Today* **2015**, *18*, 425.
- [103] E. Bundgaard, F. C. Krebs, *Solar Energy Materials and Solar Cells* **2007**, *91*, 954.
- [104] P. A. Tipler, G. Mosca, in *Physik* (Eds.: P. A. Tipler, G. Mosca, J. Wagner), Springer **2015**, p. 1287.
- [105] J.-L. Bredas, *Mater. Horiz.* **2014**, *1*, 17.
- [106] C. Deibel, D. Mack, J. Gorenflot, A. Schöll, S. Krause, F. Reinert, D. Rauh, V. Dyakonov, *Phys. Rev. B* **2010**, *81*.
- [107] Z. Zhang, J. Wang, *J. Mater. Chem.* **2012**, *22*, 4178.
- [108] Y. Li, Y. Zou, *Adv. Mater.* **2008**, *20*, 2952.
- [109] Y.-J. Cheng, S.-H. Yang, C.-S. Hsu, *Chem. Rev.* **2009**, *109*, 5868.
- [110] L. Yang, H. Zhou, A. C. Stuart, W. You, in *Organic Photovoltaics: Materials, Device Physics, and Manufacturing Technologies* (Eds.: C. Brabec, U. Scherf, V. Dyakonov), Wiley-VCH Verlag GmbH & Co. KGaA **2014**, p. 61.
- [111] L. Bian, E. Zhu, J. Tang, W. Tang, F. Zhang, *Progress in polymer science* **2012**, *37*, 1292.
- [112] H. Zhou, L. Yang, W. You, *Macromolecules* **2012**, *45*, 607.
- [113] M. García-Melchor, A. A. C. Braga, A. Lledós, G. Ujaque, F. Maseras, *Accounts of chemical research* **2013**, *46*, 2626.
- [114] N. Miyaura, A. Suzuki, *Chem. Rev.* **1995**, *95*, 2457.
- [115] K. C. Nicolaou, P. G. Bulger, D. Sarlah, *Angew. Chem. Int. Ed.* **2005**, *44*, 4442.
- [116] N. Miyaura, K. Yamada, A. Suzuki, *Tetrahedron Lett.* **1979**, *36*, 3437.

- [117] N. Miyaura, A. Suzuki, *J. Chem. Soc. Chem. Commun.* **1979**, 8, 866.
- [118] J. Hassan, M. Sévignon, C. Gozzi, E. Schulz, M. Lemaire, *Chem. Rev.* **2002**, 102, 1359.
- [119] C. D. Varnado, C. W. Bielawski, in *Polymer Science: A Comprehensive Reference* (Eds.: A. D. Schlüter, C. J. Hawker, J. Sakamoto), Elsevier **2012**, p. 175.
- [120] G. B. Smith, G. C. Dezeny, D. L. Hughes, A. King, T. R. Verhoeven, *J. Org. Chem.* **1994**, 59, 8151.
- [121] U. Christmann, R. Vilar, *Angew. Chem. Int. Ed.* **2005**, 44, 366.
- [122] J. Tsuji, *Palladium Reagents and Catalysts*, John Wiley & Sons, Ltd **2004**.
- [123] J. Sołoducho, K. Olech, A. Świst, D. Zając, J. Cabaj, *Advances in Chemical Engineering and Science* **2013**, 03, 19.
- [124] S. D. Walker, T. E. Barder, J. R. Martinelli, S. L. Buchwald, *Angew. Chem. Int. Ed.* **2004**, 43, 1871.
- [125] R. Martin, S. L. Buchwald, *Accounts of chemical research* **2008**, 41, 1461.
- [126] F. Bellina, A. Carpita, R. Rossi, *Synthesis* **2004**, 2004, 2419.
- [127] A. F. Littke, C. Dai, G. C. Fu, *J. Am. Chem. Soc.* **2000**, 122, 4020.
- [128] M. Rehahn, A.-D. Schlüter, G. Wegner, W. Feast, *Polymer* **1989**, 30, 1060.
- [129] A. D. Schlüter, *Journal of Polymer Science: Part A: Polymer Chemistry* **2001**, 39, 1533.
- [130] Y. Sangvikar, K. Fischer, M. Schmidt, A. D. Schlüter, J. Sakamoto, *Organic letters* **2009**, 11, 4112.
- [131] W. H. Carothers, *Trans. Faraday Soc.* **1936**, 32, 39.
- [132] M. D. Lechner, K. Gehrke, E. H. Nordmeier, *Makromolekulare Chemie*, Springer **2014**.
- [133] J. Sakamoto, A. D. Schlüter, in *Synthesis of polymers*, Vol. 2 (Eds.: A. D. Schlüter, C. J. Hawker, J. Sakamoto), Wiley-VCH Verlag GmbH & Co. KGaA **2012**, p. 627.
- [134] A. J. J. Lennox, G. C. Lloyd-Jones, *Chemical Society reviews* **2014**, 43, 412.
- [135] J. P. Parrish, Y. C. Jung, R. J. Floyd, K. W. Jung, *Tetrahedron Letters* **2002**, 43, 7899.
- [136] M. Jayakannan, van Dongen, Joost L. J., R. A. J. Janssen, *Macromolecules* **2001**, 34, 5386.
- [137] O. Navarro, H. Kaur, P. Mahjoor, S. P. Nolan, *J. Org. Chem.* **2004**, 69, 3173.
- [138] J. Sakamoto, M. Rehahn, G. Wegner, A. D. Schlüter, *Macromol. Rapid Commun.* **2009**, 30, 653.
- [139] M. Inbasekaran, W. Wu, E. P. Woo, *WO 9920675A1* **1999**.
- [140] C. R. Towns, R. O'Dell, *WO 0053656 A1 (2000)* **2000**.
- [141] C. Liu, A. Repoley, B. Zhou, *J. Polym. Sci. A Polym. Chem.* **2008**, 46, 7268.
- [142] J. Murage, J. W. Eddy, J. R. Zimbalist, T. B. McIntyre, Z. R. Wagner, F. E. Goodson, *Macromolecules* **2008**, 41, 7330.
- [143] K. T. Nielsen, K. Bechgaard, F. C. Krebs, *Macromolecules* **2005**, 38, 658.
- [144] F. E. Goodson, T. I. Wallow, B. M. Novak, *Macromolecules* **1998**, 31, 2047.

- [145] A. J. McNeil, E. L. Lanni, in *Synthesis of polymers*, Vol. 1 (Eds.: A. D. Schlüter, C. J. Hawker, J. Sakamoto), Wiley-VCH Verlag GmbH & Co. KGaA **2012**, p. 475.
- [146] T. Yokozawa, A. Yokoyama, *Progress in polymer science* **2007**, *32*, 147.
- [147] C. S. Fischer, M. C. Baier, S. Mecking, *J. Am. Chem. Soc.* **2013**, *135*, 1148.
- [148] T. Yokozawa, H. Kohno, Y. Ohta, A. Yokoyama, *Macromolecules* **2010**, *43*, 7095.
- [149] A. Yokoyama, T. Yokozawa, *Macromolecules* **2007**, *40*, 4093.
- [150] T. Yokozawa, Y. Ohta, *Chem. Commun.* **2013**, *49*, 8281.
- [151] T. Yokozawa, Y. Nanashima, Y. Ohta, *ACS Macro Lett.* **2012**, *1*, 862.
- [152] U. Scherf, E. J. W. List, *Adv. Mater.* **2002**.
- [153] M. Svensson, F. Zhang, O. Inganäs, M. R. Andersson, *Synthetic Metals* **2003**, *135-136*, 137.
- [154] M. Svensson, F. Zhang, S. C. Veenstra, W. Verhees, J. C. Hummelen, J. M. Kroon, O. Inganäs, M. R. Andersson, *Adv. Mater.* **2003**, *15*, 988.
- [155] S. Janietz, H. Krueger, H.-F. Schleiermacher, U. Würfel, M. Niggemann, *Macromol. Chem. Phys.* **2009**, *210*, 1493.
- [156] O. Inganäs, M. Svensson, A. Gadisa, F. Zhang, N. K. Persson, X. Wang, M. R. Andersson, *Applied Physics A: Materials Science & Processing* **2004**, *79*, 31.
- [157] C. M. Björström Svanström, J. Rysz, A. Bernasik, A. Budkowski, F. Zhang, O. Inganäs, M. R. Andersson, K. O. Magnusson, J. J. Benson-Smith, J. Nelson, E. Moons, *Adv. Mater.* **2009**, *21*, 4398.
- [158] C. M. Björström, A. Bernasik, J. Rysz, A. Budkowski, S. Nilsson, M. Svensson, M. R. Andersson, K. O. Magnusson, E. Moons, *J. Phys.: Condens. Matter* **2005**, *17*, L529-L534.
- [159] L. M. Andersson, F. Zhang, O. Inganäs, *Appl. Phys. Lett.* **2007**, *91*, 71108.
- [160] S. Admassie, O. Inganäs, W. Mammo, E. Perzon, M. R. Andersson, *Synthetic Metals* **2006**, *156*, 614.
- [161] O. Inganäs, F. Zhang, M. R. Andersson, *Accounts of chemical research* **2009**, *42*, 1731.
- [162] S. De, T. Pascher, M. Maiti, K. G. Jespersen, T. Kesti, F. Zhang, O. Inganäs, A. Yartsev, V. Sundström, *J. Am. Chem. Soc.* **2007**, *129*, 8466.
- [163] K. Vandewal, K. Tvingstedt, A. Gadisa, O. Inganäs, J. V. Manca, *Nature materials* **2009**, *8*, 904.
- [164] J.-H. Kim, H. U. Kim, D. Mi, S.-H. Jin, W. S. Shin, S. C. Yoon, I.-N. Kang, D.-H. Hwang, *Macromolecules* **2012**, *45*, 2367.
- [165] M.-H. Chen, J. Hou, Z. Hong, G. Yang, S. Sista, L.-M. Chen, Y. Yang, *Adv. Mater.* **2009**, *21*, 4238.
- [166] A. Calabrese, G. Schimperia, R. Po, T. Yohannes, S. E. Debebe, F. Tinti, N. Camaioni, *J. Appl. Phys.* **2011**, *110*, 113106.
- [167] L. H. Slooff, S. C. Veenstra, J. M. Kroon, D. J. D. Moet, J. Sweelssen, M. M. Koetse, *Appl. Phys. Lett.* **2007**, *90*, 143506.
- [168] L.-F. Yu, C.-W. Ge, J.-T. Wang, X. Xiang, W.-S. Li, *Polymer* **2015**, *59*, 57.

- [169] H. Zhou, L. Yang, S. Xiao, S. Liu, W. You, *Macromolecules* **2010**, *43*, 811.
- [170] L. Yang, H. Zhou, W. You, *J. Phys. Chem. C* **2010**, *114*, 16793.
- [171] Q. Hou, Q. Zhou, Y. Zhang, W. Yang, R. Yang, Y. Cao, *Macromolecules* **2004**, *37*, 6299.
- [172] C. Shi, Y. Yao, Yang, Q. Pei, *J. Am. Chem. Soc.* **2006**, *128*, 8980.
- [173] C. R. McNeill, J. J. M. Halls, R. Wilson, G. L. Whiting, S. Berkebile, M. G. Ramsey, R. H. Friend, N. C. Greenham, *Adv. Funct. Mater.* **2008**, *18*, 2309.
- [174] C. R. McNeill, A. Abrusci, J. Zaumseil, R. Wilson, M. J. McKiernan, J. H. Burroughes, J. J. M. Halls, N. C. Greenham, R. H. Friend, *Appl. Phys. Lett.* **2007**, *90*, 193506.
- [175] H. Wong, P. Wang, A. Abrusci, M. Svensson, M. R. Andersson, N. C. Greenham, *J. Phys. Chem. C* **2007**, *111*, 5244.
- [176] D. Mori, H. Benten, H. Ohkita, S. Ito, *Adv. Energy Mater.* **2015**, *5*, 1500304.
- [177] M. Sommer, H. Komber, S. Huettnner, R. Mulherin, P. Kohn, N. C. Greenham, W. T. S. Huck, *Macromolecules* **2012**, *45*, 4142.
- [178] Z.-K. Tan, K. Johnson, Y. Vaynzof, A. A. Bakulin, L.-L. Chua, P. K. H. Ho, R. H. Friend, *Adv. Mater.* **2013**, *25*, 4131.
- [179] R.-Q. Png, P.-J. Chia, J.-C. Tang, B. Liu, S. Sivaramakrishnan, M. Zhou, S.-H. Khong, H. S. O. Chan, J. H. Burroughes, L.-L. Chua, R. H. Friend, P. K. H. Ho, *Nature materials* **2010**, *9*, 152.
- [180] B. J. Kim, Y. Miyamoto, B. Ma, J. M. J. Fréchet, *Adv. Funct. Mater.* **2009**, *19*, 2273.
- [181] C.-Y. Nam, Y. Qin, Y. S. Park, H. Hlaing, X. Lu, B. M. Ocko, C. T. Black, R. B. Grubbs, *Macromolecules* **2012**, *45*, 2338.
- [182] R. Penterman, S. I. Klink, H. de Koning, G. Nisato, D. J. Broer, *Nature* **2002**, *417*, 55.
- [183] S. Miyanishi, K. Tajima, K. Hashimoto, *Macromolecules* **2009**, *42*, 1610.
- [184] C. D. Müller, A. Falcou, N. Reckefuss, M. Rojahn, V. Wiederhirn, P. Rudati, H. Frohne, O. Nuyken, H. Becker, K. Meerholz, *Nature* **2003**, *421*, 829.
- [185] G. Griffini, J. D. Douglas, C. Piliago, T. W. Holcombe, S. Turri, J. M. J. Fréchet, J. L. Mynar, *Adv. Mater.* **2011**, *23*, 1660.
- [186] K. A. Murray, A. B. Holmes, S. C. Moratti, G. Rumbles, *J. Mater. Chem.* **1999**.
- [187] G. Wantz, L. Derue, O. Dautel, A. Rivaton, P. Hudhomme, C. Dagron-Lartigau, *Polym. Int.* **2014**, *63*, 1346.
- [188] A. E. A. Contoret, S. R. Farrar, M. O'Neill, J. E. Nicholls, G. J. Richards, S. M. Kelly, A. W. Hall, *Chem. Mater.* **2002**, *14*, 1477.
- [189] H. Thiem, M. Jandke, D. Hanft, P. Strohriegl, *Macromol. Chem. Phys.* **2006**, *207*, 370.
- [190] E. Scheler, P. Strohriegl, *J. Mater. Chem.* **2009**, *19*, 3207.
- [191] J. V. Crivello, J. H. W. Lam, *Macromolecules* **1977**, *10*, 1307.
- [192] J. V. Crivello, J. H. W. Lam, *J. Polym. Sci. Part A: Polym. Chem.* **1979**, *17*, 977.
- [193] K. Meerholz, C. D. Müller, O. Nuyken, in *Organic light-emitting devices: Synthesis, properties, and applications* (Eds.: K. Müllen, U. Scherf), Wiley-VCH Verlag GmbH & Co. KGaA **2006**, p. 293.

- [194] S. Feser, K. Meerholz, *Chem. Mater.* **2011**, *23*, 5001.
- [195] M. C. Gather, A. Köhnen, A. Falcou, H. Becker, K. Meerholz, *Adv. Funct. Mater.* **2007**, *17*, 191.
- [196] G. Brotas, J. Farinhas, Q. Ferreira, R. Rodrigues, I. L. Martins, J. Morgado, A. Charas, *J. Polym. Sci. Part A: Polym. Chem.* **2014**, *52*, 652.
- [197] P. S. Rudati, D. C. Mueller, K. Meerholz, *Procedia Chemistry* **2012**, *4*, 216.
- [198] A. Charas, H. Alves, J. M. Martinho, L. Alcácer, O. Fenwick, F. Cacialli, J. Morgado, *Synthetic Metals* **2008**, *158*, 643.
- [199] A. Charas, L. Alcácer, A. Pimentel, J. P. Conde, J. Morgado, *Chemical Physics Letters* **2008**, *455*, 189.
- [200] A. Charas, Q. Ferreira, J. Farinhas, M. Matos, L. Alcácer, J. Morgado, *Macromolecules* **2009**, *42*, 7903.
- [201] J. Farinhas, Q. Ferreira, R. E. Di Paolo, L. Alcácer, J. Morgado, A. Charas, *J. Mater. Chem.* **2011**, *21*, 12511.
- [202] G. Brotas, J. Farinhas, Q. Ferreira, J. Morgado, A. Charas, *Synthetic Metals* **2012**, *162*, 2052.
- [203] C. P. Yau, S. Wang, N. D. Treat, Z. Fei, Tremolet de Villers, Bertrand J., M. L. Chabiny, M. Heeney, *Adv. Energy Mater.* **2015**, *5*, 1401228.
- [204] A. J. Moulé, K. Meerholz, *Adv. Funct. Mater.* **2009**, *19*, 3028.
- [205] M. Jørgensen, K. Norrman, S. A. Gevorgyan, T. Tromholt, B. Andreasen, F. C. Krebs, *Adv. Mater.* **2012**, *24*, 580.
- [206] E. Wang, L. Hou, Z. Wang, S. Hellström, F. Zhang, O. Inganäs, M. R. Andersson, *Adv. Mater.* **2010**, *22*, 5240.
- [207] J. E. Carlé, B. Andreasen, T. Tromholt, M. V. Madsen, K. Norrman, M. Jørgensen, F. C. Krebs, *J. Mater. Chem.* **2012**, *22*, 24417.
- [208] X. Chen, L. Chen, Y. Chen, *J. Polym. Sci. Part A: Polym. Chem.* **2013**, *51*, 4156.
- [209] F. Ouhib, M. Tomassetti, J. Manca, F. Piersimoni, D. Spoltore, S. Bertho, H. Moons, R. Lazzaroni, S. Desbief, C. Jerome, C. Detrembleur, *Macromolecules* **2013**, *46*, 785.
- [210] C.-Z. Li, H.-L. Yip, A. K.-Y. Jen, *J. Mater. Chem.* **2012**, *22*, 4161.
- [211] Y.-J. Cheng, C.-H. Hsieh, P.-J. Li, C.-S. Hsu, *Adv. Funct. Mater.* **2011**, *21*, 1723.
- [212] H. J. Kim, A.-R. Han, C.-H. Cho, H. Kang, H.-H. Cho, M. Y. Lee, J. M. J. Fréchet, J. H. Oh, B. J. Kim, *Chem. Mater.* **2012**, *24*, 215.
- [213] M. S. Ryu, J. Jang, *Solar Energy Materials and Solar Cells* **2010**, *94*, 1384.
- [214] D. He, X. Du, W. Zhang, Z. Xiao, L. Ding, *J. Mater. Chem. A* **2013**, *1*, 4589.
- [215] S. M. Lindner, S. Hüttner, A. Chiche, M. Thelakkat, G. Krausch, *Angew. Chem. Int. Ed.* **2006**, *45*, 3364.
- [216] H. J. Snaith, G. L. Whiting, B. Sun, N. C. Greenham, W. T. S. Huck, R. H. Friend, *Nano letters* **2005**, *5*, 1653.
- [217] E. Scheler, E. Betthausen, P. Strohriegl, *Macromol. Chem. Phys.* **2010**, *211*, 2081.
- [218] A. J. C. Kuehne, M. Kaiser, A. R. Mackintosh, B. H. Wallikewitz, D. Hertel, R. A. Pethrick, K. Meerholz, *Adv. Funct. Mater.* **2011**, *21*, 2564.

- [219] J. Weickert, R. B. Dunbar, H. C. Hesse, W. Wiedemann, L. Schmidt-Mende, *Adv. Mater.* **2011**, *23*, 1810.
- [220] H.-C. Scheer, T. Glinsner, M. Wissen, R. Pelzer, in *Microlithography 2004* (Ed.: R. S. Mackay), SPIE **2004**, p. 203.
- [221] Y. Yang, K. Mielczarek, M. Aryal, A. Zakhidov, W. Hu, *ACS nano* **2012**, *6*, 2877.
- [222] M. Aryal, F. Buyukserin, K. Mielczarek, X.-M. Zhao, J. Gao, A. Zakhidov, W. Hu, *Journal of Vacuum Science & Technology B* **2008**, *26*, 2562.
- [223] M. Aryal, K. Trivedi, W. W. Hu, *ACS nano* **2009**, *3*, 3085.
- [224] W. Wiedemann, L. Sims, A. Abdellah, A. Exner, R. Meier, K. P. Musselman, J. L. MacManus-Driscoll, P. Müller-Buschbaum, G. Scarpa, P. Lugli, L. Schmidt-Mende, *Appl. Phys. Lett.* **2010**, *96*, 263109.
- [225] X. He, F. Gao, G. Tu, D. Hasko, S. Hüttner, U. Steiner, N. C. Greenham, R. H. Friend, W. T. S. Huck, *Nano letters* **2010**, *10*, 1302.
- [226] X. He, F. Gao, G. Tu, D. G. Hasko, S. Hüttner, N. C. Greenham, U. Steiner, R. H. Friend, W. T. S. Huck, *Adv. Funct. Mater.* **2011**, *21*, 139.
- [227] S. Jungermann, N. Riegel, D. Müller, K. Meerholz, O. Nuyken, *Macromolecules* **2006**, *39*, 8911.
- [228] M. Ranger, D. Rondeau, M. Leclerc, *Macromolecules* **1997**, *30*, 7686.
- [229] F. Lemasson, N. Berton, J. Tittmann, F. Henrich, M. M. Kappes, M. Mayor, *Macromolecules* **2012**, *45*, 713.
- [230] S. Goswami, R. W. Winkel, K. S. Schanze, *Inorganic chemistry* **2015**, *54*, 10007.
- [231] S. Telitel, F. Ouhib, J.-P. Fouassier, C. Jerome, C. Detrembleur, J. Lalevée, *Macromol. Chem. Phys.* **2014**, *215*, 1514.
- [232] J.-C. Li, H.-Y. Lee, S.-H. Lee, K. Zong, S.-H. Jin, Y.-S. Lee, *Synthetic Metals* **2009**, *159*, 201.
- [233] F. Lombeck, R. Matsidik, H. Komber, M. Sommer, *Macromolecular rapid communications* **2015**, *36*, 231.
- [234] E. Scheler, P. Strohhriegl, *Liquid Crystals* **2007**, *34*, 667.
- [235] F. C. Krebs, J. Alstrup, H. Spanggaard, K. Larsen, E. Kold, *Solar Energy Materials and Solar Cells* **2004**, *83*, 293.
- [236] G. Dennler, C. Lungenschmied, H. Neugebauer, N. S. Sariciftci, M. Latrèche, G. Czeremuszkin, M. R. Wertheimer, *Thin Solid Films* **2006**, *511-512*, 349.
- [237] S. Sarkar, J. H. Culp, J. T. Whyland, M. Garvan, V. Misra, *Organic Electronics* **2010**, *11*, 1896.
- [238] M. Manceau, E. Bundgaard, J. E. Carlé, O. Hagemann, M. Helgesen, R. Søndergaard, M. Jørgensen, F. C. Krebs, *J. Mater. Chem.* **2011**, *21*, 4132.
- [239] W. R. Mateker, J. D. Douglas, C. Cabanetos, I. T. Sachs-Quintana, J. A. Bartelt, E. T. Hoke, A. El Labban, P. M. Beaujuge, J. M. J. Fréchet, M. D. McGehee, *Energy Environ. Sci.* **2013**, *6*, 2529.
- [240] F. Fischer, T. Hahn, H. Bäessler, I. Bauer, P. Strohhriegl, A. Köhler, *Adv. Funct. Mater.* **2014**, *24*, 6172.

- [241] A. Tournebize, A. Rivaton, J.-L. Gardette, C. Lombard, B. Pépin-Donat, S. Beaupré, M. Leclerc, *Adv. Energy Mater.* **2014**, *4*, n/a-n/a.
- [242] C. Schwarz, H. Bässler, I. Bauer, J.-M. Koenen, E. Preis, U. Scherf, A. Köhler, *Adv. Mater.* **2012**, *24*, 922.



## 11 List of publications and presentations

### Publications

Parts of this work have been published in *Proceedings of SPIE*:

Peter Strohriegl, **Philipp Knauer**, Christina Saller, Esther Scheler  
„Patternable Conjugated Polymers for Organic Solar Cells“  
Proceedings of SPIE, **2013**, 8830, Organic Photovoltaics XIV, 8830P  
DOI: 10.1117/12.2023899

A paper on the stabilization of organic solar cells by crosslinking will be published in the near future:

**Philipp Knauer**, Tobias Hahn, Anna Köhler, Peter Strohriegl  
Insight into the stabilization of bulk heterojunction solar cells by crosslinking

During the time of my thesis, I worked on perlyne bisimides. Results from this work are not included in this thesis but published in *ChemPhysChem*:

Andrew O. F. Jones, **Philipp Knauer**, Roland Resel, Andreas Ringk, Peter Strohriegl, Oliver Werzer, Michele Sferrazza  
„Thermal Stability and Molecular Ordering of Organic Semiconductor Monolayers: Effect of an Anchor Group“  
*ChemPhysChem* **2015**, 16, 1712-1718

### Conference Talk

“Crosslinkable conjugated polymers for organic solar cells”  
at *Gordon Research Seminar: Electronic Processes in Organic Materials*  
Barga, Italy, May 2014

Poster Presentations

“Patternable Conjugated Polymers for Organic Solar Cells”

at *Light Harvesting Processes*

Bad Staffelstein, Germany, April 2013

“Patternable Low bandgap Polymers for Organic Solar Cells”

at *Bayreuther Polymer Symposium*

Bayreuth, Germany, September 2013

“Crosslinkable conjugated polymers for organic solar cells”

at *Gordon Research Conference: Electronic Processes in Organic Materials*

Barga, Italy, May 2014

“Crosslinkable conjugated polymers for organic photovoltaics”

at the *12<sup>th</sup> International Symposium on Functional  $\pi$ -Electron Systems*

Seattle, USA, July 2015

“Crosslinking of low bandgap polymers for organic solar cells”

at *Bayreuther Polymer Symposium*

Bayreuth, Germany, September 2015

## Danksagung

Zum Ende dieser Arbeit möchte ich mich bei allen bedanken, die in welcher Weise auch immer dazu beigetragen haben, dass diese Doktorarbeit entstanden ist.

Allen voran danke ich Prof. Dr. Peter Strohriegl für die Möglichkeit zur Promotion und für die Bereitstellung dieses abwechslungsreichen und interessanten Themas. Besonders für seine Hilfsbereitschaft zu jeder Zeit möchte ich mich ausdrücklich bedanken.

Ein Dank geht an den gesamten Lehrstuhl MC I für die Zusammenarbeit. Dem Lehrstuhlinhaber Prof. Dr. Hans-Werner Schmidt danke ich für die Bereitstellung eines ausgezeichnet ausgestatteten Laborarbeitsplatzes.

Ganz herzlich danke ich meinen 595ern für die gute Stimmung, die harmonische Zusammenarbeit und die gegenseitige Hilfe bei allem, was das Laborleben zu bieten hat. Danke, Andreas, Christina, Daniel, Irene und Julia! Bei Andreas möchte ich mich auf das Schärfste bedanken, dass er mich während der Bachelorarbeit hier aufgenommen und mich bis zur Doktorarbeit begleitet hat. Für das Korrekturlesen dieser Arbeit danke ich Christina, Daniel und Julia. Irene danke ich für die Hilfe im Labor und bei einzelnen Synthesen. Danke für deine Geduld und dass du immer für Probleme jeder Art und Größe ein offenes Ohr und ein gutes Wort übrig hattest.

Ich danke der Gruppe um Prof. Dr. Anna Köhler vom Lehrstuhl EP II für die Zusammenarbeit an organischen Solarzellen. Besonders danke ich meinem Kooperationspartner Tobias Hahn für seinen Einsatz, seine Ideen und die zahlreichen Messungen und Auswertungen. Danke an Frank-Julian Kahle und Steffen Tscheuschner für Diskussionen und Hilfestellungen. Irene Bauer und Frank Schirmer möchte ich für die Herstellung der unzähligen Solarzellen-Substrate und die Hilfe bei vielen anderen kleinen Dingen danken.

Danke an Florian Wieberger, Tristan Kolb und Christian Neuber für die Diskussionen und Hilfen rund ums Thema Photoacid Generators. Tristan danke ich außerdem sehr für die Herstellung des Stempels für die Imprinting-Experimente.

Vielen Dank an Martina Heider für die Aufnahmen am Elektronenmikroskop und an Hannes Welz für die Phenom-Aufnahmen.

Für die vielen GPC-Messungen möchte ich mich bei Katharina Neumann, Klaus Kreger, Paul Reichstein, Robin Pettau und Tina Weller bedanken.

Vielen Dank auch an Tina Weller, Ferdinand Seibold, Sven Hafke, Thomas Krapfl, Christian Goldhahn, Daniel Schmidmeier, Florian Dresel und Lina Mayr für die Synthesen und Messungen während ihrer Praktika oder Bachelorarbeiten.

Danke an die Sekretärinnen Petra Weiß, Christina Wunderlich und Claudia Geier für ihre Hilfe bei allen möglichen organisatorischen Sachen.

Danke an Alexander Kern und Jonas Mayer für die Hilfe bei den diversen Computerfragen.

Ich danke allen meinen Bayreuther Chemiefreunden, den Leuten von der CSG und den Fußballer von der CSB und den Weißbierbrasilianern für viele schöne Erlebnisse. Danke an die MC I-Freunde für diverse Grillingers, Kochingers, Dillingers und Feierabendbiere und all die großartigen Aktionen außerhalb des Labors.

Schließlich möchte ich mich bei meinen Weidhäuser Freunden bedanken, dass sie mich auch während meines Studiums begleitet haben. Danke für eure Geduld und euer Verständnis, wenn ich wieder einmal wegen einer Prüfung oder der Arbeit in Bayreuth geblieben oder vorzeitig gegangen bin. Danke, dass ich durch euch immer wieder daran erinnert wurde, dass sich die Welt auch mal ohne Chemie weiter dreht.

Danke möchte ich auch meiner Familie für die Unterstützung sagen. Der größte Dank geht an meine Eltern und meine Schwester. Danke, dass ihr immer für mich da seid und mich während des gesamten Studiums und besonders in der Zeit dieser Arbeit auf jede Weise unterstützt habt.

**DANKE.**





## Erklärung

nach der Promotionsordnung der BayNAT in der Fassung vom 20. März 2014

(§ 8 S. 2 Nr. 6 PromO)

Hiermit erkläre ich mich damit einverstanden, dass die elektronische Fassung meiner Dissertation unter Wahrung meiner Urheberrechte und des Datenschutzes einer gesonderten Überprüfung hinsichtlich der eigenständigen Anfertigung der Dissertation unterzogen werden kann.

(§ 8 S. 2 Nr. 8 PromO)

Hiermit erkläre ich eidesstattlich, dass ich die Dissertation selbstständig verfasst und keine anderen als die von mir angegebenen Quellen und Hilfsmittel benutzt habe.

(§ 8 S. 2 Nr. 9 PromO)

Ich habe diese Dissertation nicht bereits zur Erlangung eines akademischen Grades anderweitig eingereicht und habe auch nicht bereits diese oder eine gleichartige Doktorprüfung endgültig nicht bestanden.

(§ 8 S. 2 Nr. 10 PromO)

Hiermit erkläre ich, dass ich keine Hilfe von gewerblichen Promotionsberatern bzw. -vermittlern in Anspruch genommen habe und auch künftig nicht nehmen werde.

Bayreuth, 24. März 2016

---

Philipp Knauer



*It ain't over till it's over.*

R. Balboa